UNIVERSITY OF SOUTHAMPTON

FACULTY OF ENGINEERING AND THE ENVIRONMENT

Aeronautics, Astronautics and Computational Engineering Unit

An Investigation on Structure-Vibration Isolator Interactions for Particular Performance

by

Khairiah Kamilah binti Turahim

Thesis for the degree of Doctor of Philosophy

December 2017

UNIVERSITY OF SOUTHAMPTON

ABSTRACT

FACULTY OF ENGINEERING AND THE ENVIRONMENT

Computational Engineering Design group

Thesis for the degree of Doctor of Philosophy

AN INVESTIGATION ON STRUCTURE-VIBRATION ISOLATOR INTERACTIONS FOR PARTICULAR PERFORMANCE

Khairiah Kamilah binti Turahim

In engineering, particularly in certain application of vibration isolation, there is a need to achieve a special low or high supporting stiffness. There are two methods found to be effective in providing these particular performances mainly nonlinear vibration isolation and/or active vibration isolation. To assess the efficiency of a nonlinear isolator, interaction analysis is necessary, as for the structure control interactions, the dynamic characteristics of both structure and control system affect each other. There have been fewer publications that consider or discuss the interactions between a structure and a nonlinear vibration isolator, and between a structure and an active isolator. This thesis presents the study of the interaction between a beam and a nonlinear isolator and between a beam and an active isolator for low and high supporting stiffness.

For the beam- nonlinear isolator , the system consists of an elastic beam- like structure and a geometrically nonlinear isolation system in which a horizontal degree provides a physical approach for realising the required horizontal force. The generalised dynamic equations of the proposed interaction system are derived, from which three reduced models can be obtained by introducing the related conditions into the generalised model. The modal summation method is used to analyse the beam. The nonlinear dynamic behaviour on equilibria and stabilities of the system are investigated. The dynamic interaction mechanism between the nonlinear isolation system and the elastic structure is revealed. The beam-nonlinear isolator design for low stiffness support and high stiffness support is discussed. Then the interaction between the beam and the active isolator is found, theoretical design strategies of the active vibration isolation system are developed, and two cases are investigated; an active isolator with low suspension frequency and an active isolator with high suspension frequency.

It is found that the beam provides additional mass, stiffness and force to the nonlinear vibration isolator and to the active isolator. For the beam-nonlinear isolator and beam- active isolator with low stiffness support, the requirement to perform ground vibration test whereby the rigid mode of the beam must be less than one third of the first elastic natural frequency of the free-free beam has been satisfied. The condition to achieve high stiffness support has also been satisfied. Nonlinear dynamical behaviour of the beam-nonlinear isolator indicates that period doubling bifurcation occurs when the excitation force is 1 and excitation frequency is 0.5Hz. Poincare maps reveals that the system form closed loops and no chaotic behaviour is observed. Perfomance analysis in terms of force transmissibility of the nonlinear isolator shows that the nonlinear isolator performs better than a linear isolator and also performs better than a hardening HSLDS mount. For the conceptual design of the beam-active isolator, the dynamic response of the system was done using Simulink Simscape blockset and is found to be similar to the dynamic response found using Simulink alone. The investigated system in the thesis can provide extremely low or high supporting stiffness and frequencies to satisfy special engineering applications for high precision vibration isolation.

Table of Contents

Table of Contents i
List of Tables v
List of Figures vii
List of Symbols xiii
DECLARATION OF AUTHORSHIP xv
Acknowledgements xvii
Definitions and Abbreviations xix
Chapter 1: Introduction 1
1.1 Problem Statement and Motivation 1
1.1.1 Engineering background 1
1.1.2 Science background 2
1.2 Aim and objectives 4
1.3 Outline of thesis 5
Chapter 2: Literature review 7
2.1 Vibration Isolation 7
2.1.1 Passive vibration isolation 9
2.1.2 Semi-active vibration isolation 10
2.1.3 Limitation of linear passive vibration isolation 11
2.2 Active Vibration Isolation 12
2.2.1 Active systems with low suspension frequency 13
2.2.2 Active systems with high suspension frequency 14
2.2.3 Active control strategies to realize low and high suspension frequency 14
2.2.4 Active vibration isolation of flexible structures 15
2.3 Nonlinear Vibration Isolation 15
2.3.1 Negative stiffness mechanism 16
2.3.2 Quasi-zero-stiffness mechanism 17
2.3.3 High static low dynamic stiffness mount 19

2.3.4 Using beams 21
2.3.5 Other techniques involving nonlinear isolation 22
2.3.6 Nonlinear dynamical behaviour 23
2.4 Effects of support conditions on modal frequencies 23
2.5 Contribution of this study 24

Chapter 3: Fundamental theory 27

3.1 Beam dynamics 27
3.1.1 Lateral vibration of beams 27
3.1.2 Natural vibrations 29
3.1.3 Orthogonality of natural modes 30
3.1.4 Mode shapes 32
3.2 Modal summation method 33
3.3 Nonlinear Dynamics 36
3.3.1 General formulation equation in state space 36
3.3.2 Stability of Equilibrium states 36
3.3.3 Bifurcation and Chaos 41
3.3.4 Methods used to solve nonlinear differential equations 44
3.4 Nonlinear passive vibration isolator 49
3.4.1 Example of a nonlinear vibration isolator 49
3.5 Active vibration control 51
3.5.1 Controller strategies used in active vibration control 53
3.5.2 Actuators and sensors used in active vibration control 53

Chapter 4: Beam-nonlinear isolator interaction 55

4.1 Introduction 55
4.2 Model of a general nonlinear beam isolation interaction system 55
4.2.1 Governing equations of integrated interaction system 57
4.2.2 Non- dimensional dynamic equations 60
4.2.3 Integrated coupling matrix equation 61
4.3 Nonlinear behaviour of integrated coupling system 62

4.3.1 Equilibrium points 62
4.3.2 Stability and frequency of small vibrations about equilibrium points 65
4.3.3 Bifurcation 70
4.4 Interaction analysis 74
4.4.1 Equation governing the influence of beam motions on nonlinear suspension system 74
4.4.2 Phase trajectories of nonlinear isolator 86
4.4.3 Equation governing the influence of nonlinear suspension unit on beam motions 87
4.5 Beam-nonlinear isolator design 88
4.5.1 Low stiffness support 88
4.5.2 High stiffness support 100
4.6 Special cases of the generalised interaction system 103
4.6.1 Case I: A rigid mass supported by a nonlinear suspension unit 103
4.6.2 Case II: Simplified nonlinear suspension unit with fixed points A and B 104
4.6.3 Case III: Simplified nonlinear suspension unit with two rigid springs $\boldsymbol{k}$. 104
4.7 Performance Analysis 105
4.8 Summary 109

Chapter 5: Beam- active vibration isolator interaction 111

5.1 Introduction 111
5.2 Beam-active isolator with low suspension frequency 111
5.2.1 Mathematical model of an integrated active isolator-structure interaction 112
5.2.2 Interaction analysis of beam-active isolator with low suspension frequency 113
5.3 Controller design for beam-active isolator with low suspension frequency 118
5.3.1 Suitable negative feedback for a low suspension frequency 118

5.3.2 Applying active control 124
5.4 Beam-active isolator with high suspension frequency 126
5.4.1 Mathematical model and governing equations 126
5.4.2 Dynamic equilibrium equation of the active suspension system 127
5.4.3 Interaction analysis of beam-active isolator with high suspension frequency 127
5.5 Controller design for beam-active isolator with high suspension frequency 128
5.5.1 Suitable negative feedback gains for a high suspension frequency 128
5.5.2 Applying active control 129
5.6 Summary 132
Chapter 6: Beam-active vibration isolator design for low and high suspension frequency 135
6.1 Introduction 135
6.2 Conceptual design of beam-active isolator for low and high frequency support 135
6.3 Design of active isolation system 136
6.3.1 Electric system equation 137
6.4 Active vibration isolation design in Simulink 138
6.4.1 Supporting system with low supporting frequency 139
6.4.2 Suspension system with high suspension frequency 143
6.5 Summary 145
Chapter 7: Conclusion and recommendation 149
7.1 Conclusion 149
7.2 Recommendation 151
List of References 153
Papers and conferences 159

List of Tables

Table 3.1 Numerical values of $(\beta nl)^2$ for typical end conditions (Thomson, 1996) 30

Table 3.2 Four values of the 4th-order Runge-Kutta method (Thomson, 1996) 48

Table 4.1 The equilibrium points (β =1,2,3) of the system 62

Table 4.2 The values of added parameters affected by retained mode number of the beam on the nonlinear suspension unit ($\bar{m}_b = \frac{m_b}{\bar{M}_{11}}, \xi_0 = 1$) 75

Table 4.3 The values of added parameters affected by a unit dynamic response mode *n* of the beam on the nonlinear suspension unit 75

Table 4.4 Parameter values for low stiffness support 90

Table 4.5 Natural frequencies of beam supported on the nonlinear support at equilibrium point (3) 91

Table 4.6 Natural frequency of the free-free beam 91

Table 4.7 Natural frequency error for modes *n* =1...5 92

Table 4.8 Mode shape error for modes, *n* =1...5 92

Table 4.9 List of parameters used for high stiffness support 100

Table 4.10 Natural frequencies of fixed- free beam 101

Table 4.11 Natural frequencies of beam on nonlinear vibration isolator with high stiffness support 101

Table 4.12 Error between natural frequency of fixed - free beam to beam on nonlinear isolator with high stiffness support for modes, *n*= 1...5 102

Table 4.13 Error between mode shape of fixed - free beam to beam on nonlinear isolator with high stiffness support for modes, *n*= 1...5 102

Table 5.1 The values of added parameters affected by retained mode number *N* of the beam on the active suspension unit, $(\xi_0 = 1)$. 115

Table 5.2 The values of added parameters affected by a unit dynamic response mode *n* of the beam on the active suspension unit. 115

Table 5.3 Beam frequency at modes 1 to 5 when there is support but no feedback control119

Table 5.4 Value of g_d and k_1 that produces a minimum dynamic stiffness 120

Table 5.5 Beam frequency at modes 1 to 5 when there is support and feedback control .121

Table 5.6 Error between natural frequency of free - free beam to beam on active isolator with low stiffness support for modes, *n*= 1...5.....122

Table 5.7 Error between mode shape of free - free beam to beam on active isolator with low stiffness support for modes, *n*= 1...5.....122

Table 5.8 The values of added parameters affected by a unit dynamic response mode *n* of the beam on the active suspension unit 128

Table 5.9 The values of added parameters affected by retained mode number *N* of the beam on the active suspension unit.....128

Table 5.10 Values of g_d and k_1 that produces a maximum dynamic stiffness at the rigid mode 129

List of Figures

Figure 1.1 EADS Sogerma (European Aerospace & Defence System) (Bordeaux, France, www.fabreeka.com) 3

Figure 1.2 A three-spring model of a QZS mechanism (Kovacic et al, 2008) 4

Figure 1.3 An active vibration isolator built at the ULB (Université libre de Bruxelles, 2004) 4

Figure 2.1 Schematic diagrams of vibration isolation systems: (a) vibration isolation where motion u is imposed at the foundation and motion x is transmitted to the equipment; (b) vibration isolation where force F is applied by the equipment and force F_T is transmitted to the foundation (Crede & Ruzicka, 1976) 8

Figure 2.2 Theoretical transmissibility of a system (Yu. L et al., 2009) 8

Figure 2.3 (a) Passive vibration isolation, (b) Active vibration isolation, (c) Semi -active vibration isolation (Unsal, 2006) 9

Figure 2.4 (a) Design I and (b) Design II (Yilmaz & Kikuchi, 2006) 10

Figure 2.5 Configuration of an MR damper with an inner bypass (Bai et al., 2015) 11

Figure 2.6 Comparison of negative stiffness mechanism and conventional spring (Platus, 1992) 16

Figure 2.7 Schematic representation of the simplest system which can exhibit quasi-zero stiffness (Carrella et al., 2007) 17

Figure 2.8 Zero dynamic stiffness system schematic (Yang et al., 2012) 18

Figure 2.9 (a) SD oscillator (Hao & Cao, 2014), (b)Dynamical model of a nonlinear supporting system with stable QZS (SQZS) system (Cao et al., 2006) 19

Figure 2.10 Schematic of the HSLDS isolator consisting of mechanical springs providing a positive stiffness and the attracting magnets (Carrella et al.,2008) 20

Figure 3.1 Element of the beam (Thomson, 1996) 27

Figure 3.2 Symmetric and antisymmetric modes of the free-free beam (Han & Benaroya, 2002) 33

Figure 3.3 Classification of equilibrium points (Rao, 2011) 41

Figure 3.4 Phase plane of Equation (3.68) (Rao, 2011) 43

Figure 3.5 Poincare map of Equation (3.69) (Rao, 2011) 43

Figure 3.6 Distortion of phase plane (Rao, 2011) 44

Figure 3.7 A schematic of a nonlinear vibration isolator (Yang et al., 2013) 49

Figure 3.8 Active vibration isolation system (Rao, 2011) 52

Figure 4.1 An integrated interaction system consisting of an elastic beam and a generalised nonlinear isolation unit (Xing, 2013) 56

Figure 4.2 The circle governing the static equilibrium points 63

Figure 4.3 (a) Equilibrium position 1, (b) Equilibrium position 2, (c) Equilibrium position 3 of the system 64

Figure 4.4 Free vibration time series and phase plots 70

Figure 4.5 Time series and phase plots of the system using ODE45 function 71

Figure 4.6 Time series and phase plots of the system using RK4 with time step, h= 0.01 .. 72

Figure 4.7 Time series and phase plots of the system using RK4 with time step, h=0.001. 73

Figure 4.8 Time series and phase plots of the system using RK4 with time step, h=0.000173

Figure 4.9 Graph of additional mass mb with respect to retained mode number 76

Figure 4.10 Graph of force factor with respect to retained mode number 77

Figure 4.11 Graph of added mass for a unit dynamic response with respect to mode number 77

Figure 4.12 Graph of added stiffness for a unit dynamic response with respect to mode number. 78

Figure 4.13 Horizontal nonlinear stiffness force affected by k_b 79

Figure 4.14 Vertical nonlinear stiffness force when k_b = 0 80

Figure 4.15 Vertical nonlinear stiffness force when k_b = 67.99 80

Figure 4.16 Vertical nonlinear stiffness force when k_b = 1443.4 81

Figure 4.17 Vertical nonlinear stiffness force when k_b = 8908 81

Figure 4.18 Vertical nonlinear stiffness force when k_b = 30787 82

Figure 4.19 Potential energy for position q at the static position q_{10} = 0.6471 83

Figure 4.20 Potential energy for position q at the static position q_{10} = 0.6471 84

Figure 4.21 Potential energy for position q at the static position q_{10} = 0.6471 84

Figure 4.22 Potential energy for position q at the static position q_{10} = 0.6471 85

Figure 4.23 Potential energy for position q at the static position q_{10} = 0.6471 85

Figure 4.24 Undamped phase trajectories of the nonlinear unit affected by elastic beam . 86

Figure 4.25 Damped phase trajectories of the nonlinear unit affected by elastic beam with c1=0.01, c=0.2. 87

Figure 4.26 Mode shapes of the beam affected by the nonlinear isolator at equilibrium point (3) for mode, n=1 to 5 91

Figure 4.27 Mode shapes of the free-free beam 91

Figure 4.28 Change in frequency when k is varied 93

Figure 4.29 Change in frequency when $\Omega 0$ is varied 93

Figure 4.30 Simulink programme using the Differential Equation Editor block 94

Figure 4.31 Phase plane plot when $F0 = 0.01$, $\Omega 0$=0.5 95

Figure 4.32 Phase plane plot when $F0 = 1$,$\Omega 0$=0.5 95

Figure 4.33 Phase plane plot when $F0 = 6$,$\Omega 0$=0.5 96

Figure 4.34 Phase plane plot when $F0 = 12$,$\Omega 0$=0.5 96

Figure 4.35 Phase plane plot when $F0 = 18$,$\Omega 0$=0.5 97

Figure 4.36 Poincare' maps of the system when $F0 = 20$ and
(a)Ω_0=0.1Hz,(b)Ω_0=0.3Hz,(c)Ω_0=0.6Hz,(d)Ω_0=1.1Hz,
(e)Ω_0=3.3Hz,(f)Ω_0=5Hz,(g)Ω_0=10Hz,(h)Ω_0=30Hz,
(i)Ω_0=40Hz,(j)Ω_0=50Hz,(k)Ω_0=100Hz 99

Figure 4.37 Mode shapes of the fixed-free beam 101

Figure 4.38 Mode shapes of beam on nonlinear isolator for modes n=1 to 5 101

Figure 4.39 Mode shapes with varying supporting frequency, fs 103

Figure 4.40 Force transmissibility of nonlinear isolator compared to a linear isolator.....106

Figure 4.41 Force transmissibility of nonlinear isolator with different initial conditions 107

Figure 4.42 Force transmissibility of nonlinear isolator with varying damping coefficients108

Figure 4.43 Force transmissibility of nonlinear isolator with varying stiffness 108

Figure 4.44 Force transmissibility of nonlinear isolator compared with HSLDS isolator .109

Figure 5.1 An integrated system consisting of an elastic beam and an active isolator unit.112

Figure 5.2 Graph of additional mass with respect to retained mode number 116

Figure 5.3 Graph of force factor with respect to retained mode number 116

Figure 5.4 Graph of added stiffness for a unit dynamic response with respect to mode number 117

Figure 5.5 Graph of added mass for a unit dynamic response with respect to mode number 117

Figure 5.6 Mode shapes of beam when there is support but no feedback control 120

Figure 5.7 Mode shapes of beam when there is support and feedback control is applied 121

Figure 5.8 Effect of α on the suspension frequency using k=19620 and k_1=0 to 1000 123

Figure 5.9 Suspension frequency VS k with different values of k_1.....123

Figure 5.10 Suspension frequency VS k1 with different values of k.....124

Figure 5.11 Simulink block diagram of the active suspension system.....125

Figure 5.12 Displacement of mass and beam $(M + mb(\varphi n))$ using different values of gd126

Figure 5.13 A suspension system with a high suspension stiffness (Xing et al., 2005).....127

Figure 5.14 Effect of α on the suspension frequency using k=200 and k_1=0 to 1000.....129

Figure 5.15 Simulink block diagram of the active suspension system.....130

Figure 5.16 Excitation signal given to the system.....131

Figure 5.17 Displacement of mass and beam for high support frequency using gd = -560131

Figure 5.18 Displacement of mass and beam using different values of g_d.....132

Figure 6.1 An active vibration isolation system including a mass-spring-damper unit modelling a practical actuator (Xing et al., 2005)....136

Figure 6.2 Equivalent diagram of the electric circuit of the electromagnetic actuator....138

Figure 6.3 Displacement of $(M + mb(\varphi n))$ using Simulink and using Simscape....140

Figure 6.4 Design of active isolator in Simulink using the Simcape blockset for low suspension frequency....141

Figure 6.5 Displacement of mass and beam using different values of g_d....143

Figure 6.6 Dynamic response for high suspension frequency using Simscape and Simulink144

Figure 6.7 Dynamic response for high suspension frequency with varying g_d....144

Figure 6.8 Design of active isolator in Simulink using the Simcape blockset for high suspension frequency....147

List of Symbols

C : Damping coefficient of the damper connected along the vertical axis

C_1 : Damping coefficient of the damper connected to the cart

E : Elastic modulus of the beam

f_{bs} : Reaction force from the lumped mass to the beam

f_{sb} : Reaction force from beam to the lumped mass

f_b : Force factor at which the excitation force is added to the lumped mass

F_0 : Force applied symmetrically to the beam

$\boldsymbol{F}_R$: Components of stiffness forces

g : Gravity

I : Area moment of inertia of the beam

k : Stiffness of inclined spring

k_b : Additional stiffness added to the nonlinear suspension system by the beam

K_1 : Stiffness of horizontal spring

K : Stiffness of spring connected along the vertical axis

l : Non stretched length of the inclined spring

L_1 : Non stretched length of horizontal spring

m : Mass of cart

m_b : Additional mass added to the nonlinear suspension system by the beam

M : Lumped mass connected to the beam

M : Bending moments

O : Middle point of the beam

$p(x)$: The loading per unit length of the beam

S : Span length of the beam

t : Time

V : Shear forces

w_n : Natural frequency

y : Vertical axis of the system

Y : Beam deflection

$Y_n(\xi)$: Non dimensional symmetrical mode function

Δ_1 : Static extension of horizontal spring

λ : Non dimensional frequency

ξ : Beam material point

ξ_0 : Point on the beam where the harmonic force is applied

Π : Potential energy

ρ : Mass density per unit length of the beam

T : Kinetic energy

φ_n : Generalised coordinate corresponding to mode *n*

Ψ : Bending stiffness of the beam

Ω_0 : Frequency of the force applied symmetrically to the beam

$\hat{\Omega}_n$: N^{th} natural frequency

DECLARATION OF AUTHORSHIP

I, Khairiah Kamilah binti Turahim

declare that this thesis and the work presented in it are my own and has been generated by me as the result of my own original research.

An Investigation on Structure-Vibration Isolator Interactions for Particular Performance

I confirm that:

1. This work was done wholly or mainly while in candidature for a research degree at this University;
2. Where any part of this thesis has previously been submitted for a degree or any other qualification at this University or any other institution, this has been clearly stated;
3. Where I have consulted the published work of others, this is always clearly attributed;
4. Where I have quoted from the work of others, the source is always given. With the exception of such quotations, this thesis is entirely my own work;
5. I have acknowledged all main sources of help;
6. Where the thesis is based on work done by myself jointly with others, I have made clear exactly what was done by others and what I have contributed myself;
7. Parts of this work have been published as in the Papers and Conferences section;

Signed: .....

Date: 22/12/2017

Acknowledgements

Alhamdulillah praise be to Allah the Almighty for giving me the ability to complete this PhD thesis. I would like to express my sincere gratitude to my supervisors Dr Kamal Djidjeli and Prof. Jing Tang Xing for the continuous support throughout my PhD study and research, for their patience, motivation, enthusiasm, and immense knowledge. Their guidance helped me throughout this research and writing of this thesis.

I would like to thank the Ministry of Higher Education (MOHE) Malaysia and International Islamic University Malaysia (IIUM) for providing financial support during my study. I would also like to thank my internal and external examiners for their criticisms, comments, corrections and suggestions in improving my work.

Special thanks to Arina Kamarudin who helped me start my life in Southampton and to *Keluarga* Soton for making my days in Southampton feel like home. I would like to thank my friends in Boldrewood, Nu Rhahida Arini, Firdaus Tasnim and Ikhwan Syafiq for helping me print and submit this thesis . Deepest appreciation goes to my Haluan UKE friends Dr Siti Fadhilah Ishak, Dr Zainab Kasim, Nurul Ainain, Dr Rosnia Masruki, Amnani Shamjuddin, Asma Lailee Mohd Nor, Fazlinil Irma Mohamed Aki, Wan Nur Wan Mansor, Siti Farhana Lokman, Nik Fatihah and Safiah Zulkifli for organizing programs to fulfil my spiritual needs.

I would also like to thank Dr Nabilah Ramli for giving me a more clearer understanding of MATLAB, Dr. Fadly Jashi Darsivan for the knowledge on vibration, Dr Faried Hasbullah for the mathematical knowledge and my desk mate Sarah A'fifah Abdullah Sani for always being available to discuss any doubts that I faced. I would also like to thank my friends Zuraidah Zainudin, Najwa Nasuha Mahzan, Amnani Abdullah Akhili and many others for the advice and comfort given in times I needed them most.

Finally, I dedicate this thesis to my family for their unconditional love, sacrifice, support and prayers: my parents, Norlia Sudin and Turahim Abdul Hamid, my husband Muhammad Zubair Hazni, my son Abdurrahman, my mother in law Shariffah Ismail, my in laws and my siblings; Mashitah Aminah, Zarreen Nadhirah, Abdullah Azzam, Tasnim, Muhammad and Tariq. To my husband, thank you for being a great companion.

I pray that the Almighty will repay the kindness from everyone that contributed directly or indirectly to this PhD with many more great things to come.

Definitions and Abbreviations

GVT	: Ground vibration test
NASA	: National Aeronautics and Space Administration
EADS	: European Aerospace and Defence System
SDOF	: Single degree of freedom
DVA	: Dynamic vibration absorber
DOF	: Degree of freedom
MR	: Magneto-rheological
NSM	: Negative stiffness mechanism
QZS	: Quasi-zero-stiffness
HSLDS	: High-static-low-dynamic stiffness
FE	: Finite element
FRCs	: Frequency response curves
HBM	: Harmonic balance method
OFRF	: Output frequency response function
SUT	: Structure under test
ULB	: Université libre de Bruxelles
PID	: Proportional integral-derivative
IMSC	: Independent modal space control
KAFB	: Kalman-based active feedforward-feedback controller
LQR	: Linear Quadratic Regulator

Chapter 1: Introduction

1.1 Problem Statement and Motivation

1.1.1 Engineering background

A vibration isolation system can be used either to protect an object from vibration transmitted to it from its supporting structure or to prevent the transmission of vibration generated by machines from being transmitted to the surrounding environment (Thomson, 1996). Vibration isolation systems with particular low or high supporting frequencies are of great importance in scientific and industrial fields.

For ground vibration tests (GVT) of very large civil aircrafts, the supporting frequency required is less than 1/3 of the system's fundamental frequency (Green, 1945). The aim of GVT is to simulate an aircraft in a free-free state on the ground so that information on the dynamic characteristics of an aircraft can be obtained. For large thin-wing aircraft with fundamental frequencies below 1 Hz, some further development in methods of support is necessary. A method that has attracted scientists and engineers is by using nonlinear spring system and one such system is found capable of providing supporting frequencies less than 0.25 Hz for a limited range of movement (Molyneux,1958). GVT has widely been applied around the world; at the National Aeronautics and Space Administration (NASA) Dryden Flight Research Center, at the European Aerospace and Defence System (EADS) in Sogerma-Bordeaux, France as illustrated in Figure 1.1, and the Embraer in Sao Paolo, Brazil (Xing, 2012).

A low supporting frequency is also needed for vibration isolation of high precision positioning system which can be achieved by magnetic levitation used in the semiconductor industry (Zhang et al., 2015) and also for high precision optical instruments used in spacecrafts such as for gravitational wave detection (Winterflood, 2001).

In laboratory vibration tests, a rigid boundary condition of the foundation is often assumed, which requires the dynamic supporting stiffness to be very high up to infinity (Wagg & Nield, 2010). Many engineering structures experience large temperature changes which lead to an extreme thermal stress/deformation and activate structural failure. Examples can be found in aero-spatial applications, where temperature differences between sunny and shady sides of structures can be more than 150 °C. Such temperature differences can cause the distortion of space antennas and supports of space cameras which affect the function and precision of aero-

spatial equipment greatly. To suppress such failures, materials used to manufacture the structure are expected to have a low thermal expansion coefficient (α). However, most of the astronautic equipment also needs to have enough stiffness in order to carry mechanical loads. Wang et al. (2011) developed a new bi-objective structural topology optimization formulation which aims at design of structures composed of two materials with differing Young's modulus and thermal expansion coefficients to achieve low thermal directional expansion and high stiffness.

Traditional linear passive isolation units cannot realise these particular supporting performances. Active isolation unit and / or nonlinear passive isolation system provide possible solutions for these particular vibration isolation performance requirements.

1.1.2 Science background

Currently there is a growing interest in the study of nonlinear isolators due to the benefits of nonlinearity and the fact that many practical isolators exhibit nonlinear behaviour (Kovacic et al. 2008). Linear passive vibration isolators are only effective if the excitation frequency is larger than $\sqrt{2}$ times the natural frequency. The lower the static stiffness of a system and hence the lower the natural frequency, the wider the isolation region. However, a low static stiffness causes a large static deflection. This can be overcome by adding oblique springs as shown in Figure 1.2 to obtain a high static stiffness, small static displacement, small dynamic stiffness and hence low natural frequency (Rivin, 2003). Nonlinearity becomes important in the study of an isolator when large deflections occur due to the effects of equipment weight and sustained acceleration. These effects are encountered in the behaviour of suspensions of high-speed vehicles and mounts for sensitive instruments (Ibrahim, 2008) .

Active vibration isolation systems are usually more complex and expensive compared to passive systems. An active vibration isolator built at the Université libre de Bruxelles (ULB) is shown in Figure 1.3. The advantages of active isolation which justify their increased cost and complexity are mainly better static stability of the supported equipment and better performance especially at low frequencies. Active systems can also be used to minimise vibrations at critical locations on a flexible support structure at some distance from the isolator attachment point. Active systems also have the ability of adjusting to changes in machine operating conditions without any outside intervention. Another important advantage is that they can dissipate energy as well as supply it, although a major disadvantage in addition to cost and complexity is the requirement of an external power source and in many cases the need for

numerous sensors as well as actuators, which could have durability problems (Hansen et al., 2012).

Practical isolation units have to be connected on to the supported structures, hence the structure vibration behaviour and the isolation dynamic characteristics will affect each other. Therefore, the practical system is a structure-isolation unit interaction system. To design an accurate practical isolation system, the interaction analysis is necessary. This research will consider the structure and isolation unit as an integrated interaction system to investigate its vibration behaviours using a numerical approach. The importance of this study is to provide an effective approach to improve the practical performance of particular vibration isolation systems. A new contribution of the presented work consists of investigating, first, the interaction between a structure and a nonlinear isolator and second, between a structure an active isolator. For both systems, a particular low stiffness support condition and high stiffness support condition will be investigated.

Figure 1.1 EADS Sogerma (European Aerospace & Defence System) (Bordeaux, France, www.fabreeka.com)

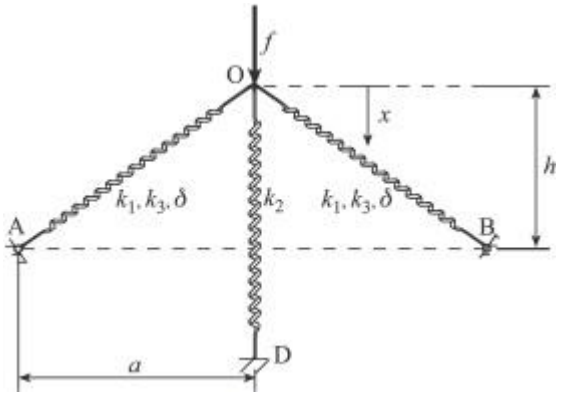

Figure 1.2 A three-spring model of a QZS mechanism (Kovacic et al, 2008)

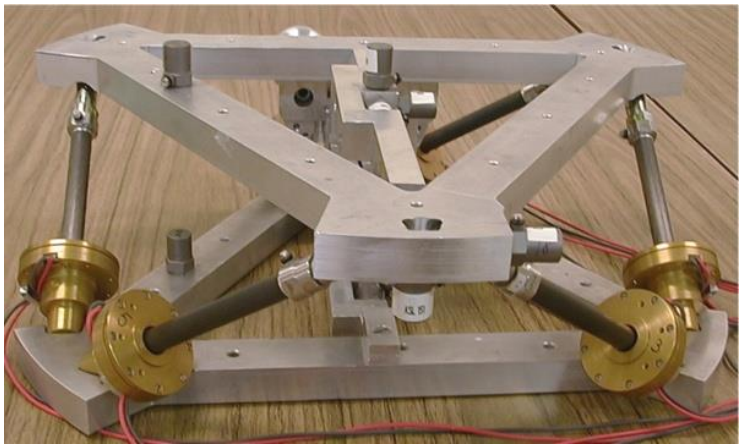

Figure 1.3 An active vibration isolator built at the ULB (Université libre de Bruxelles, 2004)

1.2 Aim and objectives

The aim of this research is to investigate the interaction between a structure and a passive nonlinear isolator and between a structure and an active isolator for special low and high stiffness support.

In this thesis, to achieve the above aim, we consider a beam-nonlinear isolator interaction system and a beam-active isolator interaction system; the following objectives will be fulfilled.

1. To establish the mathematical model describing the interaction dynamics of the integrated system (beam-nonlinear isolator and beam-active isolator).
2. To analyse the equilibrium and stabilities about them of the integrated nonlinear system and the dynamic response and possible nonlinear phenomena such as chaos and bifurcation.

3. To perform a numerical study of the natural frequencies in small vibration of the system around the chosen stable equilibrium point to reveal the interaction characteristics of the integrated nonlinear system.
4. To design a controller and find the dynamic response for the beam- active isolator for low stiffness support and high stiffness support.
5. To apply active control for low stiffness support and high stiffness support of the beam-active isolator interaction system.
6. To design a suitable beam- isolator system that can provide particular low and high stiffness support.

1.3 Outline of thesis

In Chapter 2, literature review on nonlinear vibration isolation, passive and active vibration isolation will be presented. Chapter 3 will discuss some fundamental theory including beam dynamics, nonlinear dynamical system and active vibration isolation. In Chapter 4, the interaction between a beam and a nonlinear vibration isolator will be discussed. Chapter 5 will present the interaction between a beam and an active vibration isolator for low and high suspension frequency. In Chapter 6, a conceptual design of a practical active vibration isolator system that can provide particular low and high stiffness support will be presented. Chapter 7 concludes the thesis and outlines the recommendation for future work.

Chapter 2: Literature review

2.1 Vibration Isolation

Vibration is a phenomenon that results from the movement or oscillation of a mechanical system or occurs naturally from phenomenon such as earthquakes and human activities. Vibration can be useful in some applications such as in a loudspeaker or for musical instruments. In many other areas, vibration is undesirable as it can cause damage to a system, wastes energy and creates unwanted noise. Since vibration cannot be eliminated, many efforts have been made by scientists and engineers to reduce or mitigate the effects of vibration. Vibration isolation is one of the methods widely used to isolate an object or a system from unwanted vibration and reduces transmission of vibration from one body or structure to another. It is used to protect human, machine or systems from a vibration source. Vibration isolation is closely related to dealing with the source, which aims at minimizing the incoming disturbing excitation. Vibration isolation may be located in between the source and the mechanical structure. The mechanical structure is said to be isolated from the source (and vice versa) when the transmission of vibration between them is considerably reduced (Holterman, 2002).

There are two classes of problems in which vibration isolation is necessary; first is to isolate a vibrating body such as a machine from a receiving structure, such as a car body, ship hull, aircraft fuselage or building and second is to isolate a body such as sensitive equipment or a railway car from vibrations imposed by another source such as ground vibrations or railway track unevenness. This situation corresponds to, for example, a telescope in a spacecraft, a precision machine tool in a workshop, or a passenger seated in a car. In both classes of problem, the source of the vibrations may be either deterministic (i.e. having a perfectly predictable waveform) or random (i.e. having a waveform that is not perfectly predictable) (Fuller et al. , 1996).

Figure 2.1 illustrates the concept of a single degree of freedom vibration isolation system. The system consists of an equipment represented as a rigid body connected to a foundation by an isolator having elastic and energy-dissipating characteristics. The body is constrained to move only in the vertical direction (Crede & Ruzicka, 1976).

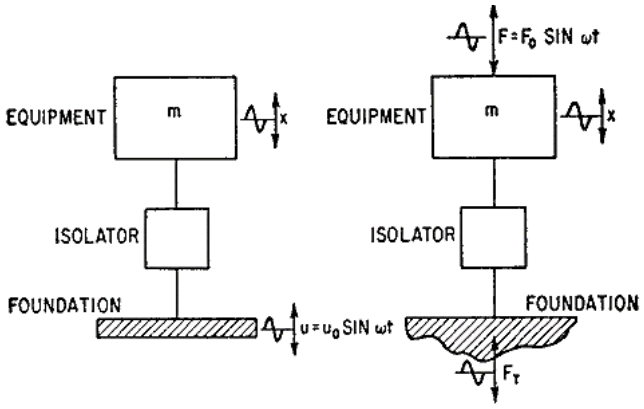

(a) (b)

Figure 2.1 Schematic diagrams of vibration isolation systems: (a) vibration isolation where motion u is imposed at the foundation and motion x is transmitted to the equipment; (b) vibration isolation where force F is applied by the equipment and force F_T is transmitted to the foundation (Crede & Ruzicka, 1976)

The efficiency of a vibration isolator varies with frequency. The natural frequency of an isolation system is the frequency at which it will vibrate when it is not disturbed by an external force. This is a function of the stiffness of the isolation system, as well as the mass being supported by the system. Figure 2.2 shows a transmissibility curve. Transmissibility is defined as the ratio of the magnitude of force transmitted to that of exciting force (Rao, 2011). If the ratio is greater than one, vibration is amplified, and if the ratio is less than one, vibration is reduced, or attenuated. The maximum transmissibility occurs at the natural frequency of the isolation system.

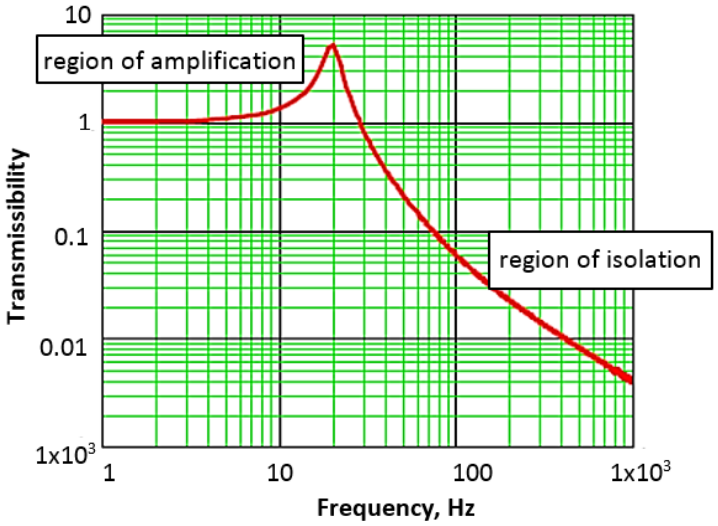

Figure 2.2 Theoretical transmissibility of a system (Yu. L et al., 2009)

From Figure 2.2, it is seen that there is a region where vibrations are amplified and a region where vibrations are reduced, or isolated. Attention must be given in selecting the natural frequency of the isolation system to be well below the driving frequency of concern. If the natural frequency of the isolation system coincides with the driving frequency, amplification will occur, which is known as resonance. Transmissibility also varies with damping in the isolation system (Yu. L et al., 2009).

The theory of linear vibration isolation has been widely covered by many authors (Hartog,1985 ; de Silva, 2006 ; Inman, 2007 ; Rao, 2011). Linear vibration isolation can be categorized according to three control schemes; passive vibration isolation, semi-active vibration isolation and active vibration isolation as shown in Figure 2.3.

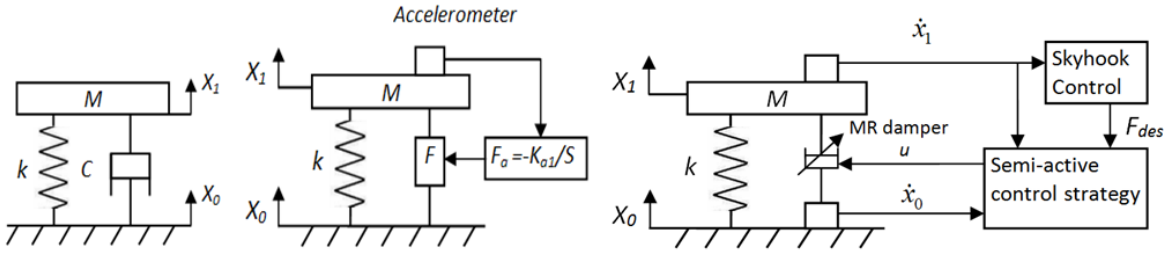

(a) (b) (c)

Figure 2.3 (a) Passive vibration isolation, (b) Active vibration isolation, (c) Semi -active vibration isolation (Unsal, 2006)

2.1.1 Passive vibration isolation

Passive isolation is a classical approach to vibration isolation that uses a passive system of dampers and springs. Passive vibration isolation systems consist of a mass supported on a soft spring. The spring can be made of air, metal, or rubberized materials. The spring and associated damping will absorb vibrations above the resonance of the spring. As vibrations enter a passive system, they are passed through, amplified, or reduced.

Yilmaz & Kikuchi (2006) analysed and designed a passive band-stop filter-type vibration isolator for low frequency applications. The bandwidths of two systems which are the single degree of freedom (SDOF) Dynamic Vibration Absorber (DVA) equipped systems and lever-type anti-resonant vibration isolators were formulated. Two different types of anti-resonant vibration isolators were analysed; Type I and Type II isolators. In a Type I isolator, the pivot attached to the base is nearer to the isolator mass and in a Type II isolator, the pivot attached to the load is nearer to the isolator mass. Then, a two degree of freedom (DOF) DVA system was developed and this system managed to increase the applicability range of passive vibration

isolation systems in the low-frequency range. Figure 2.4 shows two different 2 DOF anti-resonant vibration isolator that were designed. In Design I, the lower stage is equipped with a Type I isolator and the upper stage is equipped with a Type II isolator. In Design II, the lower stage is equipped with a Type II isolator and the upper stage is equipped with a Type I isolator.

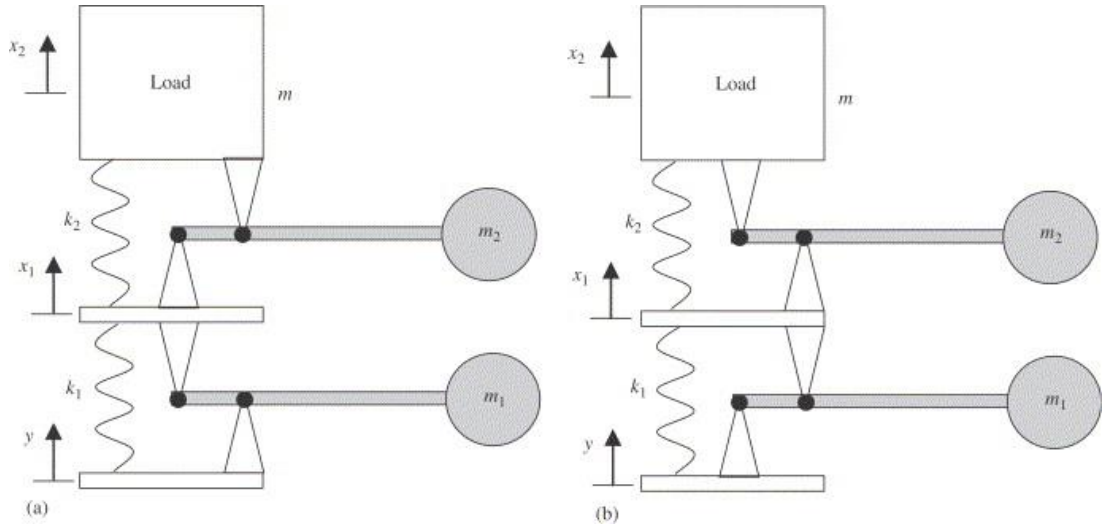

Figure 2.4 (a) Design I and (b) Design II (Yilmaz & Kikuchi, 2006)

In a study by Hosseinloo & Yap (2011) , a new passive isolation design is proposed that caters for the requirements to support a static load where the vibration excitation is random and undeterministic. The new design integrates a linear isolation subsystem with a bilinear softening one to isolate the system in both absence and presence of sustained acceleration also known as G-loading. The linear subsystem caters for the situation when there is no G-loading on the system while the bilinear softening subsystem together with the linear one, cater for vibration isolation of the payload when subjected to the G-loading. Design optimization problem of the isolation system is defined, and it is shown that the optimized new isolator has better performance than a linear or a simple hardening or softening isolator.

2.1.2 Semi-active vibration isolation

Semi-active vibration isolation systems fill the gap between passive and active systems, delivering the flexibility and adaptability of fully active systems, by using a small amount of energy to change system parameters such as damping and stiffness. Semi-active vibration isolation consists of passive devices with controllable properties. Examples include the magneto-rheological (MR) fluid damper and piezoelectric transducers with switched electrical networks (Preumont & seto,2008) .

Bai et al. (2015) investigated a SDOF semi-active vibration control system based on a MR damper with an inner bypass. The MR damper is designed by using a pair of concentric tubes, between which the inner bypass is formed as shown in Figure 2.5. MR fluids are then energized to provide large dynamic range and damping force range. The damping force performance of the MR damper is modelled using phenomenological model and experimentally verified.

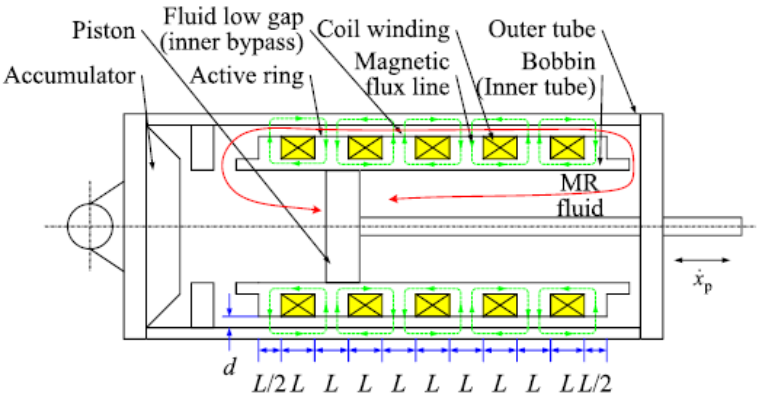

Figure 2.5 Configuration of an MR damper with an inner bypass (Bai et al., 2015)

2.1.3 Limitation of linear passive vibration isolation

Linear passive vibration isolation has found to have its limitation, according to (Inman,2007) where there arises the issue of static deflection. A passive vibration isolator can perform very well when the systems natural frequency is decreased, which will increase its isolation frequency bandwidth. Unfortunately, a low natural frequency, which means having a low supporting stiffness, will result in a large static deflection which is undesirable. To overcome this limitation, there have been two approaches found to be effective. First is to adapt active vibration isolation, and second is to use nonlinear passive vibration isolation. The first approach uses sensors and actuators to modify the characteristics of the passive isolator (Fuller et al., 1996), (Xing et al., 2005) , and requires external energy which might be a bit expensive for certain applications. Nonlinear isolators carries the benefit of possessing softening stiffness behaviour which make it possible to achieve, on one side a high static stiffness and small static displacements, and on another side a low dynamic stiffness and a wide frequency range of vibration isolation (Carrella et al., 2007).

Current advances in engineering and industrial fields have seen demands in applications that require very low or very high vibration suspension stiffness. Aircrafts that undergo ground vibration tests must satisfy requirements for accurate aircraft flutter analysis. To achieve this, the suspension frequency of the assumed rigid aircraft on the supporting system must be lower than one third of its first elastic natural frequency. A large aircraft possess a huge weight,

however, its first elastic natural frequency is quite low, therefore the stiffness of the supporting system must have a high static stiffness to support the large weight and a low dynamic stiffness to have a low supporting frequency (Molyneux, 1958; Xing, 1975). A fundamental standard for effective vibration isolation also requires a low supporting frequency (Harris & Crede, 1976; Rivin, 2004) for example in application of high precision optical instruments used in space, such as for gravitational wave detection (Winterflood et al., 2002). For dynamic tests of structures in laboratories, the structure is often fixed on a rigid foundation, thus to achieve this rigid foundation condition, the stiffness of the supporting system must be extremely high.

2.2 Active Vibration Isolation

Active vibration isolation is an isolation system that detects vibration levels through sensors that send signals into a feedback or feedforward controller, which then sends a signal to actuators to counteract the forces. In a feedback system, a sensor will detect vibrations affecting the payload and react to these vibrations via force transducers to reduce the vibration levels at the payload. In active vibration isolation system amongst the spring there is feedback circuit which consists of a piezoelectric accelerometer, an analog control circuit, and an electromagnetic transducer.

In a study by Wang et al. (2008) , an active landing gear system was investigated to reduce aircraft vibrations caused by landing impacts and runway excitations. The active system showed effectiveness over the passive system by reducing the magnitude of the displacement of the centre of gravity of the aircraft and the loads transmitted to the airframe by the landing gear during aircraft landing and taxiing. Furthermore, a reduction in the time length of responses to return to their static equilibrium positions is achieved, which will improve the performance of the landing gear, the fatigue life of the airframe and landing system, crew and passenger comfort, the pilot's ability to control the plane during ground operations and a reduction of the influence of runway unevenness.

Xing et al. (2009) developed a generalised mathematical model and analysis for integrated multi-channel vibration control–structure interaction systems. The introduction of an additional dynamic impedance matrix between structure and control system allows vibration structure–control interaction mechanisms to be investigated. To illustrate the general formulations developed and their applications, simple one- and two-channel systems are investigated using non-dimensional parameters.

2.2.1 Active systems with low suspension frequency

Heiland (1992) introduced and analysed the technology of using servo-control mechanisms with feedback and feedforward capabilities to further optimize isolation characteristics by decreasing natural frequencies to well below 0.5Hz. This can be achieved using an active vibration isolation system. Recent advancements that have improved the performance of active vibration isolation is by using the concept of adaptive control strategy whereby the system is able to adapt to changes in the payload or in the disturbance profile, resulting in superior performance of the effected equipment.

A compact stable active low frequency vibration isolation system was designed by Tang et al. (2014) to decrease the vibrational noise caused by the reflecting mirror of Raman beams in atom interferometry. By using field programmable gate array-based control subsystem, the vibration isolation system performed flexibly and accurately. When the feedback is on, the intrinsic resonance frequency of the system changed from 0.8 Hz to about 0.015 Hz. The vertical vibration (0.01–10 Hz) measured by the in-loop seismometer is reduced by an additional factor of up to 500 on the basis of a passive vibration isolation platform, and the performance has been proven by adding an additional seismometer as well as applying it in the atom interferometry experiment.

In the work of Liu et al. (2014) , a control method of an active vibration isolation system with parallel mechanism was proposed which is effective for disturbance suppression for space application. It is known that the characteristics of vibration in microgravity environment are to be of low frequency, small amplitude and randomness. The dynamic model of active vibration isolation system with payload is represented via Kane's method which is also known as Lagrange form of d'Alembert's principle. The system is then put into state space form. The step responses and system properties in open loop are first evaluated and then, observability and controllability of the system are checked using the state space equation developed earlier. To design the decoupling matrix, the state feedback decoupling with double-loop Proportional Integral-Derivative (PID) control strategy is implemented. A control system with H-infinity method is also designed and evaluated to improve the properties of the system. Using the H-infinity method, the control problem is first expressed as a mathematical optimization problem, then the controller that solves for this optimization is found. Simulation results show that both PID control and H-infinity control laws effectively attenuate the displacement and acceleration of the system.

2.2.2 Active systems with high suspension frequency

Mizuno et al. (2007) analytically and experimentally studied about an active vibration isolation system using zero-power magnetic suspension system. A zero-power magnetic suspension system behaves as if it has negative stiffness and when connected in series with a normal spring can generate infinite stiffness against disturbances acting on an isolation table. When two springs with spring constants $k_1$and k_2 are connected in series, the total stiffness k_c is given by

$$k_c = \frac{k_1 k_2}{k_1 + k_2} \tag{2.1}$$

If $k_1 = k_2$, $k_1$is the negative stiffness spring, k_2 is the normal spring

$$k_c = \infty \tag{2.2}$$

A simple model involving a single-axis apparatus was analysed which clarified the fundamental characteristics of the system. It was confirmed through experiment that combining a zero-power magnetic suspension with a normal spring generates high stiffness against static direct disturbances acting on an isolation table.

2.2.3 Active control strategies to realize low and high suspension frequency

Xing et al. (2005) demonstrated an extended study of parallel and series connections of an active spring with a mechanical spring to produce zero or infinite supporting stiffness to more generalised cases by examining the influence of dynamic modulus involving active-passive stiffness, damping and inertia forces. The extended study provides a theoretical basis to design an isolation system with infinite or zero modulus with the introduction of infinite or zero stiffness and damping.

In a study by Tjepkema et al. (2012), a feedback controller based on the sensor fusion of an acceleration at low frequency and a force signal at high frequency applied on active hard mounts is proposed. The objectives of the study are (1) to improve the performance of active vibration isolation of precision equipment by lowering the transmissibility of floor vibrations to make it comparable to soft mounts, (2) increasing the damping ratio of internal machine modes and (3) providing a stiff support to reduce the equipment's sensitivity for direct disturbances. Using sensor fusion has made it possible to achieve all three objectives simultaneously. The feedback strategy has shown to provide excellent performance through experiments conducted on a single-axis setup.

Kletz & Melcher (2013) described a technique that enables vibration reduction of a sensitive object while seismic base and direct force disturbances are simultaneously present. To suppress the vibration at those sensitive components effectively, a dual feed forward and a combined feed forward and feedback controller are introduced. The controller is experimentally shown to effectively supress vibrations at the payload. A vibration free exterior vehicle mirror can be realized using this technique since the proposed isolation interface can theoretically generate the needed infinite and infinitesimal stiffness at once.

2.2.4 Active vibration isolation of flexible structures

El-Sinawi (2004) studied the design and simulation of vibration isolation at any location on a flexible structure mounted on a flexible base using a Kalman-based active feedforward-feedback controller (KAFB) with non-collocated sensors and actuators. The control strategy is numerically shown to have high performance in terms of isolating any location on the structure from the vibration of the structure's elastic base, as well as its considerable robustness in the presence of process and measurement noise. Comparison between active feedforward only and active feedforward–feedback arrangements show that the latter is more effective in isolating the structure from the vibrating base.

An active vibration control of a flexible beam mounted on an elastic base was investigated by Chu et al. (2006) using a finite element approach. An independent modal space control (IMSC) is applied for modal decoupling of the system and design of a vibration controller. Optimal control principle is used to suppress excessive vibration of the beam subject to base excitation and also improves the system dynamic characteristics. It is demonstrated that the control strategy is effective for vibration suppression of the beam system under impulsive, pure tone, and sweeping excitations.

2.3 Nonlinear Vibration Isolation

Ibrahim (2008) comprehensively discussed about the recent advances in nonlinear passive vibration isolators in the absence of active control means. The basic characteristics of nonlinear isolators which include shifting of resonance frequency, jump phenomena, chaotic response and internal resonance have been described. Ultra-low-frequency isolators for specific applications were discussed which include the folded pendulum isolator, the X-pendulum isolator table and the conical pendulum.

2.3.1 Negative stiffness mechanism

The drawback of linear passive isolator is that they are limited by the mount stiffness that is used to support a static load. A way to overcome this is by using nonlinear mounts that have negative stiffness elements been configured in a way that the static stiffness is much more than the dynamic stiffness. The theory of negative stiffness mechanism (NSM) was developed by Platus (1992) whereby it is able to cancel the stiffness of a spring suspension. Various configurations of 6 DOF isolators and isolation systems were described and prototype systems of undamped vertical-motion system and damped and undamped horizontal-motion system were built and tested. The NSM is illustrated in Figure 2.6.

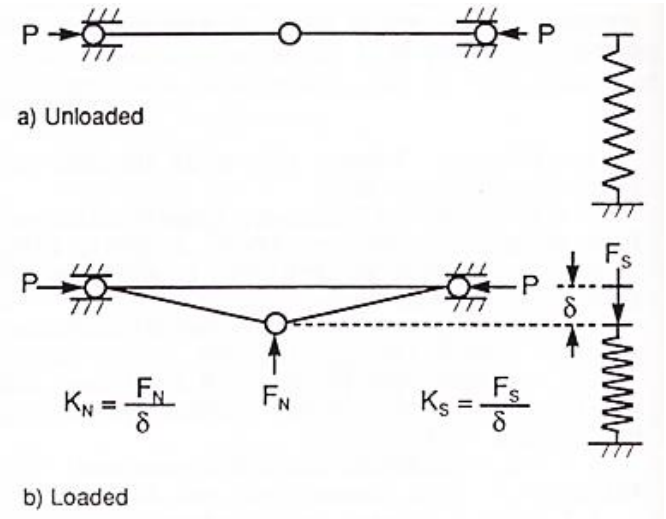

Figure 2.6 Comparison of negative stiffness mechanism and conventional spring (Platus, 1992)

Yang et al. (2013) demonstrated that adding a NSM to a linear isolator produces a much lower natural frequency compared to using the linear isolation alone. Furthermore, transmissibility curves obtained shows that the effective isolation frequency range is enlarged and the power input into the system around the resonance frequency of the corresponding linear isolator is greatly reduced. However, adding a NSM introduces a restriction on maximum deflection which should be considered in practical designs.

Under asymmetric excitation, using NSM may lead to period doubling bifurcation and eventually leads to chaos (Kovacic et al., 2008) . Cao et al.(2008) describes NSM as having complex, smooth, discontinuous dynamics. Apart from that, according to Ahn (2008) NSM also possess performance limit and nonlinear characteristics. Other issues related to nonlinearity have been found when using NSM, whereby it brings undesirable effects, reduces isolation capacity and may cause damage to a system (Yang et al., 2013) .

2.3.2 Quasi-zero-stiffness mechanism

Carrella et al.(2007) studied about a system that consists of a vertical spring in parallel with two oblique springs as shown in Figure 2.7. The figure shows the unloaded condition of the simplest system which can exhibit quasi-zero stiffness. When it is loaded with a suitably sized mass, the springs compress and the oblique springs, k_o moves to the horizontal position and the static load is taken by the vertical spring, k_v. This is the static equilibrium position, and it is the motion about this position that is of primary interest. When the system of springs is used in this way, the oblique springs act as a negative stiffness in the vertical direction counteracting the positive stiffness of the vertical spring. The stiffness and the geometry of the spring were configured in a way that results in a system with zero dynamic stiffness or also known as quasi-zero-stiffness (QZS) mechanism at the static equilibrium point. It is found that to achieve a large excursion from the static equilibrium position such that the stiffness of the system does not exceed a prescribed value, there is an optimum geometry and a corresponding optimum relationship between the stiffnesses. It has also been found that for the spring configuration studied, the oblique springs have to be inclined at an angle between approximately 48° and 57°. An approximate polynomial expression for the stiffness of the system has also been determined and the errors in this expression compared to the exact expression have been quantified.

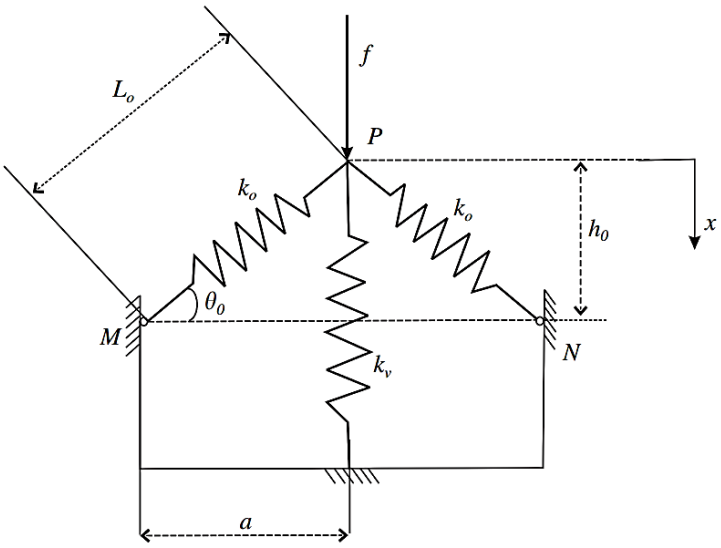

Figure 2.7 Schematic representation of the simplest system which can exhibit quasi-zero stiffness (Carrella et al., 2007)

In a study by Kovacic et al. (2008) , it was demonstrated how the use of nonlinear pre-stressed oblique springs can improve the static characteristics of a QZS mechanism. However, such a system under asymmetric excitation can exhibit period doubling bifurcations. A dynamical

analysis was done to characterise this behaviour with respect to the system parameters and the principal resonance, which led to a conclusion that the system period-doubling bifurcations are likely to happen within a specific frequency range that are characterised by regions with increasing periodicity of the response, resulting in chaotic behaviour. However, period doubling does not occur for some values of the system parameters.

Yang et al. (2012) designed a passive vibration isolator based on nonlinear passive vibration damping theory with a broad frequency field (zero dynamic stiffness system) as shown in Figure 2.8. The zero dynamic system is developed based on theoretical study and simulation analysis. An experimental validation of modal and frequency field has been acquired. The modal experiment showed that the natural frequency of the isolator dropped from 11.715 Hz to 2.5421 Hz because of importing negative stiffness mechanism. The result of the frequency field experiment is that the isolator has a better vibration reduction effect between 3Hz and 100 Hz.

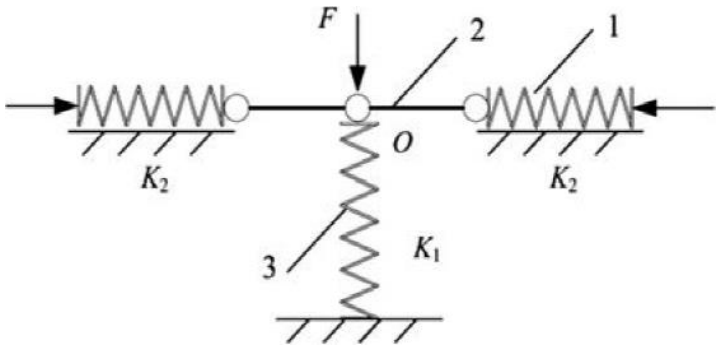

Figure 2.8 Zero dynamic stiffness system schematic (Yang et al., 2012)

A vertical QZS vibration isolator was presented by Araki et al. (2013) that comprises of a mechanism for adjusting restoring force to overcome the limitation of existing QZS vibration isolators. A difficulty in keeping the vibration reduction capability when the vibration isolated object is replaced, happens with existing QZS vibration isolator. Therefore, adjustment of the restoring force is necessary according to the weight of the newly placed object to be isolated. Thus, a mechanism that offers quick and easy adjustment of its nonlinear restoring force was proposed. A prototype of the simple mechanism shows that it was able to quickly and easily adjust when the mass of the isolated object is changed while keeping the peak response acceleration within the same tolerance. The ability of the proposed mechanism was demonstrated through shaking table tests and numerical simulations where the vibration isolator was excited with sine waves and scaled earthquake ground motions under different values of the mass of the isolated object.

Xu et al. (2013) made a study of a QZS isolator. A unique relationship between the geometry configuration and the stiffness of the spring elements is obtained to design the property of high-static-low-dynamic stiffness. Analytical solutions of the nonlinear QZS system are derived with the harmonic balance method for the characteristic analysis of the force transmissibility and critical conditions for occurring jump-down and jump-up phenomena. A series of experimental tests demonstrate that the QZS system greatly outperforms a corresponding linear isolation system. The former enables vibration to be attenuated at 0.5Hz, while the latter can only execute attenuation after 4.2Hz. The QZS system is especially effective for vibration isolation in the low-frequency range.

A novel dynamical model of a nonlinear supporting system with stable QZS (SQZS) system was proposed by Hao & Cao (2014) as shown in Figure 2.9 (a) which can be used for GVT of large scale aircraft and also for vibration isolation. The SQZS structure with low frequency is constructed by a vertical linear spring providing a high positive stiffness as a supporting component and a pair of inclined linear springs or SD oscillator (Cao et al., 2006) shown in Figure 2.9 (b) providing negative stiffness.

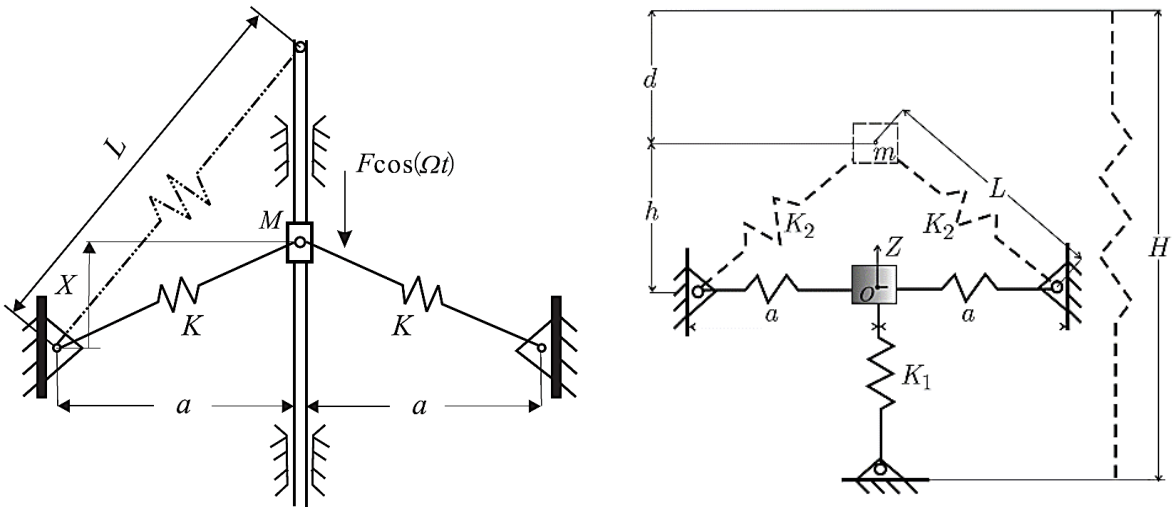

(a) (b)

Figure 2.9 (a) SD oscillator (Hao & Cao, 2014), (b)Dynamical model of a nonlinear supporting system with stable QZS (SQZS) system (Cao et al., 2006)

2.3.3 High static low dynamic stiffness mount

A theoretical and experimental study of a high-static-low-dynamic stiffness (HSLDS) mount was demonstrated by Carrella et al. (2008) as shown in Figure 2.10, which comprises of two

vertical mechanical springs with a permanent magnet at the outer edge of each spring, between which an isolated mass which is also a magnet is attached. The combination of the magnets acts as a negative stiffness that counteracts the positive stiffness of the springs. The transmissibility of this configuration is compared with a conventional mass-spring system that was realised by replacing the magnets with non-magnetic elements. Experimental results show that a reduction in the natural frequency of the system was achieved from 14Hz without using magnets to 7 Hz by using magnets. Furthermore, using the HSLDS mount, the static displacement of the system was reduced from 5mm to 1.5mm. The measured transmissibility from the measured displacement shows that the device behaved approximately linear when subjected to reasonably high base excitation levels (4mm).

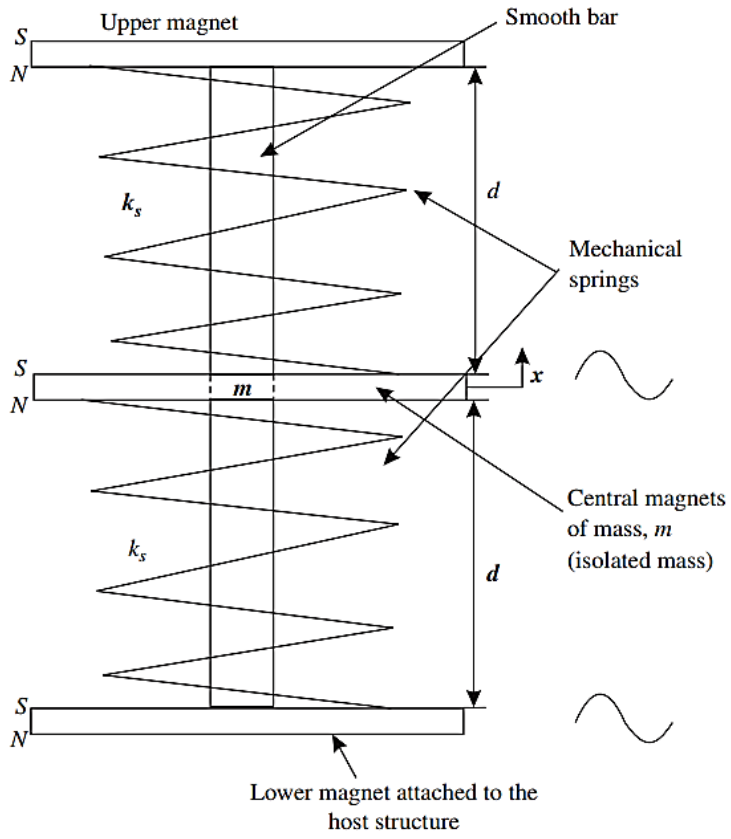

Figure 2.10 Schematic of the HSLDS isolator consisting of mechanical springs providing a positive stiffness and the attracting magnets (Carrella et al.,2008)

Friswell et al. (2012) addressed two significant problems with nonlinear HSLDS. Firstly, current approaches to realise the required nonlinear characteristics are often inconvenient, therefore various designs based on beam type structures were investigated. Secondly, the weight of the supported equipment, the environment, or the structural stiffness may change, which requires the mount to be semi-active and to tune its nonlinear characteristics.

2.3.4 Using beams

Winterflood et al. (2002) developed a new vertical suspension technique by utilising the properties of column springs in Euler buckling mode. The technique is most applicable for suspending constant loads under conditions of very small vibration. However, some inefficiencies have been identified which may allow even better performance to be obtained from spring material of a given yield strength.

A nonlinear isolator with asymmetric stiffness was modelled as a Duffing oscillator by Abolfathi (2012) . A study is presented for the case of a nonlinear isolator comprised of a curved beam. The high stiffness of the beam in extension causes impulsive behaviour in the transmitted force which is alleviated by the inclusion of a linear spring placed in series. It is shown that this combination significantly outperforms a linear isolator with the same static deflection.

Tsuji et al. (2014) proposed a nonlinear passive vibration isolator based on a post-buckled beam and investigated its characteristics and effectiveness using Finite element (FE) analysis. The system demonstrates the achievement of HSLDS and exhibits a correspondingly low fundamental resonance frequency. However, internal resonances of the isolator are also prominent in its frequency response.

The vibration isolation characteristics of a nonlinear isolator using Euler buckled beams as a negative stiffness corrector were studied analytically and experimentally by Huang et al. (2014a) . The performance of the nonlinear isolator is evaluated and compared to a linear isolator without the stiffness corrector. The study shows that the asymmetric SDOF nonlinear system can behave like a purely softening, a softening–hardening or a purely hardening system, depending on the magnitude of the excitation level. It is found that, by introducing the stiffness corrector, the starting frequency of isolation of the nonlinear isolator is lower than the linear one with the same support capacity. The proposed nonlinear isolator performs well in applications where the excitation amplitude is not too large. The same authors Huang et al. (2014b) presents a novel structured ultra-low frequency nonlinear passive isolator. The isolator is composed of a knife-edge supported sliding beam which offers negative stiffness and a vertical mechanical spring in parallel to obtain quasi-zero dynamic stiffness. Assuming light viscous damping, the dynamic behaviour is investigated and the response under harmonic excitation is derived using a simple approximation. Frequency response curves (FRCs), which exhibit complex double jump phenomenon, are obtained by harmonic balance method (HBM). The force transmissibility is derived and compared with an equivalent linear system with the

same damping ratio. The isolation performance of the nonlinear isolator is shown to outperform the linear system for providing a wider isolation region.

2.3.5 Other techniques involving nonlinear isolation

Zhang et al. (2004) developed a novel combined positive and negative stiffness isolator based on the analysis of the mechanism of negative stiffness, whose negative stiffness cancels much of the positive stiffness of the elastic element near the balance point. Experimental results show that the inherent frequency of the isolator can be adjusted from 10 Hz to 1 Hz. The isolation bandwidth of the isolator is widened, and the performance of isolation is distinctly enhanced.

A nonlinear interactive system was discussed by Xiong et al. (2005) whereby the system consists of equipment, nonlinear isolator and travelling flexible ship exited by waves. The study provided a theoretical approach to analyse power flow transmissions in a nonlinear system.

Peng et al. (2008) proposed and studied the concept of the Output Frequency Response Function (OFRF), which is applied to theoretically investigate the transmissibility of SDOF passive vibration isolators with a nonlinear anti-symmetric damping curve. The results indicate that nonlinear vibration isolators with an anti-symmetric damping characteristic have great potential to overcome the problem encountered in the design of passive linear vibration isolators, that is, increasing the level of damping to reduce the transmissibility at the resonance could increase the transmissibility over the range of higher frequencies.

An analysis of a magnetic levitation system for vibration isolation was presented by Robertson et al. (2009) . It is shown analytically that for cubical magnets the ratio of force to displacement is directly proportional to face area. The arrangement of magnets examined uses a negative stiffness element to reduce the natural frequency of the suspension. The vibration response of a system designed to satisfy these requirements is compared to an equivalent linear system and is shown to become increasingly nonlinear as the system moves towards instability.

Lu et al. (2013) investigated a configuration of a two-stage nonlinear vibration isolation system, in which the isolators contain hardening geometric stiffness nonlinearity and linear viscous damping. The force transmissibility of the system is used as a measure of the effectiveness of the isolation system. It is found that nonlinearity in the upper stage has very little effect and thus serves little purpose. The nonlinearity in the lower stage, however, has a profound effect, and can significantly improve the effectiveness of the isolation system. Furthermore, it is found that it is desirable to have high damping in the upper stage and very low damping in the lower stage.

2.3.6 Nonlinear dynamical behaviour

Several studies (Alabuzhev et al. 1989; Platus ,1992; Zhang et al. 2004; Carrella et al. 2007,2008 ; Kovacic et al. 2008; Ahn, 2008) have investigated the design, techniques and performance of nonlinear isolation systems. Recent publications about nonlinear dynamical behaviour on stabilities, bifurcations and chaos of nonlinear isolation systems were reported by Cao et al. (2008a, 2008b) and Liu et al.(2012) .

Ravindra & Mallik (1995) investigated the chaotic oscillations of a harmonically excited mass on a nonlinear isolator and showed that nonlinear damping can be used as a passive mechanism to suppress chaos.

Yu et al. (2008) discussed the bifurcation analysis of two-DOF nonlinear vibration isolation and the results of this work may be used to analyse the bifurcation problem in engineering by considering the constrained conditions of the physical parameters. They investigated the classical nonlinear behaviours and global bifurcation of a multi-degree-of-freedom nonlinear vibration isolation system subject to harmonic excitation. Three routes to chaos, including period-doubling route, quasi-period route and crisis route, were observed continuously with the increase of excitation amplitude.

2.4 Effects of support conditions on modal frequencies

When a structure is to be tested, it will be in contact with the instrument used for testing and there exist an interaction between the two.

An analysis on the beam-exciter interaction in modal analysis was studied by Han (1998) . From the experimental results obtained, it was shown that the natural frequency of the exciter and the vibration characteristics of the stinger changed according to different test conditions. This different vibration characteristic of the exciter and stinger should be considered to explain the reason why the structure-exciter interaction can significantly distort the actual vibration characteristics such as natural frequencies and mode shapes of the structure under test (SUT).

Varoto et al. (2002) studied the interaction between the electrodynamic exciter and the SUT. It was found that the shaker interacts significantly with the SUT and under some circumstances exciter dynamic effects can be accounted for in the process of improving measured data.

In the work of Carne et al.(2007), the effects of the support conditions on both the measured modal frequencies and damping factors were investigated. It has been determined that the

measured modal damping is significantly more sensitive to the support system (stiffness and damping) than the measured modal frequency.

2.5 Contribution of this study

From the literature survey, it is found that linear passive isolators possess certain limitations that cannot reach particular requirements, thus, nonlinear passive isolators and active isolators could be the solution to achieve this particular low or high stiffness support.

However, there have been fewer publications that consider or discuss about the interaction between a structure and a nonlinear vibration isolator, and between a structure and an active isolator, whereby the structure is modelled as an elastic beam. Other work have been discussed by Carrella (2008), Yang et al. (2013), Hao & Cao (2014) and Hao (2016) that considered a mass (instead of a structure) connected to a nonlinear isolator. In this work, the system is more complex as it includes the elastic beam. Therefore, suppose if the first two beam modes (one rigid mode and another one is the first beam natural mode) were considered, the system will be a 3 DOF system (vertical direction, horizontal direction and beam first elastic mode).

The work of Carella (2008), Hao & Cao (2014) and Hao (2016) considered a pair of oblique springs fixed at the end and a vertical spring to support the static weight of a mass. In this work, a general model of nonlinear vibration isolator was designed, that consists of two oblique springs, a vertical spring and two horizontal springs that were added at the left and right side for practical design. This general model can be reduced to reported models, for example when the stiffness of the horizontal springs is infinite, it will become a fixed point and this general model will be reduced to the model reported by Hao & Cao (2014) and Hao (2016). The different design in this work compared to others work is the additional horizontal springs.

The purpose of this study is to investigate the interaction that occurs between a structure and a nonlinear isolator and their nonlinear dynamic behaviour on stabilities, bifurcations and chaos and to investigate the interaction between a structure and an active isolator, so that an accurate design for the particular low and high stiffness support can be obtained.

The contribution of this work have been presented and published in conference proceedings as follows:

Turahim, K. K., Djidjeli, K., & Xing, J. T. (2016) An investigation on the effect of active vibration isolator on to a structure for low stiffness support. At 23*rd International Congress on Sound and Vibration (ICSV* 23*), Greece*. 10 - 14 *Jul* 2016*.* 7 pp.

Turahim, K. K., Djidjeli, K., & Xing, J. T. (2017) An investigation on the interaction analysis of beam- active isolator with low suspension frequency. At 12*th ICBEN congress on Noise as a Public Health Problem, Switzerland*. 18 - 22 *June* 2017. 10 pp.

Xing, J. T., Xiong, Y. P., Djidjeli, K., & Turahim, K. K. (2017) A Generalised Nonlinear Isolator-Elastic Beam Interaction Analysis for Extremely Low or High Supporting Frequency. At 9*th European Nonlinear Dynamics Conference (ENOC* 2017*), Hungary*. 25 - 30 *June* 2017. 10 pp.

Turahim, K. K., Djidjeli, K., & Xing, J. T. (2019) An investigation on the interaction analysis of beam- nonlinear isolator with low and high stiffness support, *Journal of Engineering and Technology*, 10(2), 1-25.

Chapter 3: Fundamental theory

3.1 Beam dynamics

3.1.1 Lateral vibration of beams

The elastic beam is analysed as a continuous system. The lateral vibration of beams is first derived. As shown in Figure 3.1, an element of the beam is considered. In this figure, the following notations are used:

M : bending moments

v : shear forces

$p(x)$: the loading per unit length of the beam

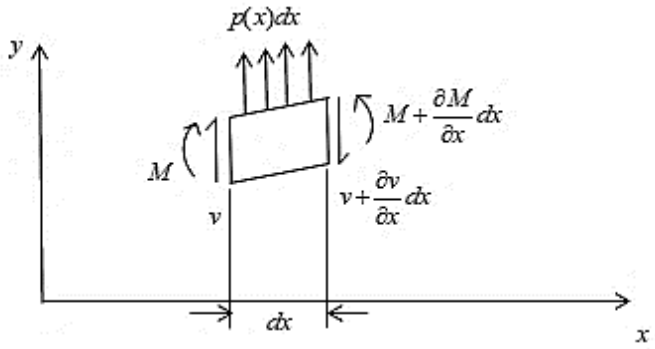

Figure 3.1 Element of the beam (Thomson, 1996)

By summing forces in the y - direction and summing moments about any point on the right face of the element, it follows that

$$\frac{\partial v}{\partial x} = p \tag{3.1}$$

$$\frac{\partial M}{\partial x} = v \tag{3.2}$$

where the term with (dx^2) is neglected.

Equation (3.1) states that the rate of change of shear along the length of the beam is equal to the loading per unit length and Equation (3.2) states that the rate of change of the moment along the beam is equal to the shear.

The bending moment is related to the curvature by the equation

$$M = EI\frac{\partial^2 y}{\partial x^2} \tag{3.3}$$

where *EI* is the flexural rigidity of the beam.

Substituting Equation (3.1) and (3.3) into Equation (3.2) we obtain

$$\frac{\partial^2}{\partial x^2}\left(EI\frac{\partial^2 y}{\partial x^2}\right) = P \tag{3.4}$$

For a beam vibrating about its static equilibrium position with an external force $\hat{f}(x,t)$ applied to it, the load *P* is equal to the sum of the external force $\hat{f}(x,t)$ and the inertial load (note the negative sign shows direction of gravity)

$$P = \hat{f}(x,t) - \rho\frac{\partial^2 y}{\partial t^2} \tag{3.5}$$

where ρ is mass per unit length of the beam.

Using this relation, the equation for the lateral vibration of the beam reduces to

$$\frac{\partial^2}{\partial x^2}\left[EI\frac{\partial^2 y}{\partial x^2}\right] + \rho\frac{\partial^2 y}{\partial t^2} = \hat{f}(x,t) \tag{3.6}$$

The boundary conditions are:

1. Free end

$$M = 0 \quad or \quad \frac{\partial^2 y}{\partial x^2} = 0 \tag{3.7}$$

$$v = 0 \quad or \quad \frac{\partial}{\partial x}\left(EI\frac{\partial^2 y}{\partial x^2}\right) = 0 \tag{3.8}$$

2. Clamped end

$$\begin{aligned} y &= 0 \\ \frac{\partial y}{\partial x} &= 0 \end{aligned} \tag{3.9}$$

3. An end with pin connection

$$\begin{matrix} y = 0 \\ M = 0 \quad or \quad \frac{\partial^2 y}{\partial x^2} = 0 \end{matrix} \tag{3.10}$$

3.1.2 Natural vibrations

To find the general solution of the beam, natural vibration is considered, that is when there are no external forces, $\hat{f} = 0$.

Here, a special case where the flexural rigidity EI is a constant is considered. Equation (3.6) may be written as

$$EI\frac{\partial^4 Y}{\partial x^4} \quad E + \rho\frac{\partial^2 Y}{\partial t^2} = 0 \tag{3.11}$$

which is the equation of natural vibration of a uniform beam. The solution of Equation (3.11) takes the form

$$y(x,t) = Y(x)e^{j\omega t} \tag{3.12}$$

which reduces Equation (3.11) to

$$\frac{d^4 Y}{dx^4} - \beta^4 Y = 0 \tag{3.13}$$

where

$$\beta^4 = \frac{\rho\omega^2}{EI} \tag{3.14}$$

The general solution of Equation (3.13) can be represented in the form

$$Y = A\cosh\beta x + B\sinh\beta x + C\cos\beta x + D\sin\beta x \tag{3.15}$$

where constants A, B, C and D are determined by using the boundary conditions of the problem.

The natural frequencies of vibration are found from Equation (3.14) to be

$$\omega_n = \beta_n^2 \sqrt{\frac{EI}{\rho}} = (\beta_n l)^2 \sqrt{\frac{EI}{\rho l^4}} \tag{3.16}$$

where the number β_n depends on the boundary conditions of the problem. A list of numerical values of $(\beta_n l)^2$ for typical end conditions is shown in Table 3.1.

Table 3.1 Numerical values of $(\beta_n l)^2$ for typical end conditions (Thomson, 1996)

Beam configuration	$(\boldsymbol{\beta_1 l})^2$ **Fundamental**	$(\boldsymbol{\beta_2 l})^2$ **2nd mode**	$(\boldsymbol{\beta_3 l})^2$ **3rd mode**
Simply supported	9.87	39.5	88.9
Cantilever	3.52	22.0	61.7
Free-free	22.4	61.7	121.0
Clamped-clamped	22.4	61.7	121.0
Clamped-hinged	15.4	50.0	104.0
Hinged-free	0	15.4	50.0

The natural modes corresponding to the natural vibrations given in Equation (3.16) can be obtained by Equation (3.15) in the form

$$Y_n = A \cosh \beta_n x + B \sinh \beta_n x + C \cos \beta_n x + D \sin \beta_n x \tag{3.17}$$

where $n = 1,2,3 \ldots, N$ is the mode number

3.1.3 Orthogonality of natural modes

In general cases, the natural modes of the beam satisfy the equation (Meirovitch, 1975)

$$\frac{\partial^2}{\partial x^2}\left[EI \frac{\partial^2 Y}{\partial x^2}\right] + \rho \omega^2 Y = 0 \tag{3.18}$$

and the corresponding boundary conditions given in Equation (3.7) and (3.8). Assume that ω_n , Y_n and ω_m , Y_m are two different natural modes with different natural frequencies $\omega_n \neq \omega_m$.

From Equation (3.18), it follows that

$$\frac{\partial^2}{\partial x^2}\left(EI\frac{\partial^2 Y_n}{\partial x^2}\right)-\rho\omega_n^2 Y_n=0 \tag{3.19}$$

$$\frac{\partial^2}{\partial x^2}\left(EI\frac{\partial^2 Y_m}{\partial x^2}\right)-\rho\omega_m^2 Y_m=0 \tag{3.20}$$

Multiplying Equation (3.19) by Y_m and integrating from 0 to l, we obtain

$$\int_0^l Y_m\frac{\partial^2}{\partial x^2}\left[EI\frac{\partial^2 Y_n}{\partial x^2}\right]dx=\omega_n^2\int_0^l \rho Y_m Y_n dx \tag{3.21}$$

An integration by parts for the left-hand integral in Equation (3.21) results in

$$\begin{aligned}&\int_0^l Y_m\frac{\partial^2}{\partial x^2}\left[EI\frac{\partial^2 Y_n}{\partial x^2}\right]dx \\ &=\left[Y_m\frac{\partial}{\partial x}\left(EI\frac{\partial^2 Y_n}{\partial x^2}\right)\right]\Bigg|_0^l-\int_0^l\frac{\partial Y_m}{\partial x}\frac{\partial}{\partial x}\left[EI\frac{\partial^2 Y_n}{\partial x^2}\right]dx \\ &=\left[Y_m\frac{\partial}{\partial x}\left(EI\frac{\partial^2 Y_n}{\partial x^2}\right)\right]\Bigg|_0^l-\left[\frac{\partial Y_m}{\partial x}EI\frac{\partial^2 Y_n}{\partial x^2}\right]\Bigg|_0^l+\int_0^l EI\frac{\partial^2 Y_m}{\partial x^2}\frac{\partial^2 Y_n}{\partial x^2}dx\end{aligned} \tag{3.22}$$

By using the boundary conditions in Equation (3.7) and (3.8) for free-free beam, this equation reduces to

$$\int_0^l Y_m\frac{\partial^2}{\partial x^2}\left(EI\frac{\partial^2 Y_n}{\partial x^2}\right)dx=\int_0^l EI\frac{\partial^2 Y_m}{\partial x^2}\frac{\partial^2 Y_n}{\partial x^2}dx \tag{3.23}$$

and Equation (3.21) becomes

$$\int_0^l EI\frac{\partial^2 Y_m}{\partial x^2}\frac{\partial^2 Y_n}{\partial x^2}dx=\omega_n^2\int_0^l \rho Y_m Y_n\,dx \tag{3.24}$$

Similarly, starting from Equation (3.20), we obtain

$$\int_0^l EI\frac{\partial^2 Y_n}{\partial x^2}\frac{\partial^2 Y_m}{\partial x^2}dx=\omega_m^2\int_0^l \rho Y_n Y_m\,dx \tag{3.25}$$

Subtracting Equation (3.25) from (3.24) gives

$$(\omega_n^2-\omega_m^2)\int_0^l \rho Y_n Y_m dx=0 \tag{3.26}$$

Since $\omega_n^2\neq\omega_m^2$, we obtain

$$\int_0^l \rho Y_n Y_m dx=\begin{cases}0, & m\neq n\\ M_n, & m=n\end{cases} \tag{3.27}$$

Furthermore, from Equation (3.25) it follows that

$$\int_0^l EI \frac{\partial^2 Y_n}{\partial x^2} \frac{\partial^2 Y_m}{\partial x^2} dx = \begin{cases} 0, & m \neq n \\ K_n, & m = n \end{cases} \tag{3.28}$$

Here M_n and K_n are the generalized mass and stiffness of the n-th natural mode of the beam respectively. Equations (3.27) and (3.28) are the orthogonality conditions of natural modes of the beam.

3.1.4 Mode shapes

The number of natural frequencies of vibration of any system is equal to the number of degrees of freedom, thus, any system having distributed parameters has an infinite number of natural frequencies. At a given time, such system usually vibrates with appreciable amplitude at a limited number of frequencies often at only one. With each natural frequency is associated a shape, called the normal or natural mode (Harris & Crede, 1976).

Due to symmetry of the problem, natural vibrations of a free-free beam can be split into two different sets of modes, symmetric (even) modes and anti-symmetric (odd) modes (Han & Benaroya, 2002).

For symmetric modes,

$$B = D = 0, \text{ so } Y_n = A \cosh \beta_n x + C \cos \beta_n x \tag{3.29}$$

By imposing boundary conditions at $x = L$

$$\begin{bmatrix} -\cos(\beta_n L) & \cosh(\beta_n L) \\ \sin(\beta_n L) & \sinh(\beta_n L) \end{bmatrix} \begin{bmatrix} A \\ C \end{bmatrix} = \begin{bmatrix} 0 \\ 0 \end{bmatrix} \tag{3.30}$$

For a non-trivial solution, one gets

$$\tan(\beta_n L) + \tanh(\beta_n L) = 0 \tag{3.31}$$

Symmetric natural modes can be written in normalized form as

$$Y_n(x) = \frac{1}{2}\left\{\frac{\cosh(\beta_n x)}{\cosh(\beta_n L)} + \frac{\cos(\beta_n x)}{\cos(\beta_n L)}\right\} \tag{3.32}$$

The free-sliding is the symmetric mode and the free-hinged is the anti-symmetric mode of the free-free beam, excluding the rigid body mode, as shown in Figure 3.2. The anti-symmetric (free-hinged) cases contain half the cycles in the free-free case. Therefore, the dimensionless wave numbers are also half of that of the free-free case.

It is important to note that in Figure 3.2 the cross-sectional areas of the beams are the same and the lengths of the free-sliding or free-hinged beams are half of the free-free beam. As long as the slenderness ratio of the free-free beam is twice that of the free-sliding or free-hinged beam, this analysis works. Therefore, more precisely we can say that the dimensionless wave numbers of the free-free beam with the slenderness ratio of S is twice the dimensionless numbers of the free-sliding or free-hinged case with the slenderness ratio of $S/2$ (Han & Benaroya, 2002).

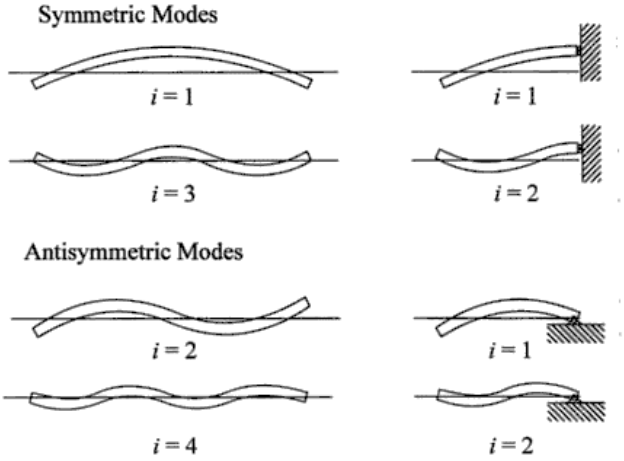

Figure 3.2 Symmetric and antisymmetric modes of the free-free beam (Han & Benaroya, 2002)

3.2 Modal summation method

Structures made up of beams are common in engineering. The structure creates its own system of degrees of freedom and can be analysed using the modal summation method (Thomson, 1996).

The technique in applying modal summation is done by expanding the deflection in terms of the normal modes of the system.

Consider, for example, the general motion of a beam loaded by a distributed force $p(x,t)$, whose equation of motion is

$$[EIy''(x,t)]'' + m(x)\ddot{y}(x,t) = p(x,t) \tag{3.33}$$

The normal modes $\varphi_i(x)$of such a beam must satisfy the equation

$$(EI\varphi_i'')'' - \omega_i^2 \quad m(x)\varphi_i = 0 \tag{3.34}$$

and its boundary conditions. As discussed in equations (3.27) and (3.28), the normal modes $\varphi_i(x)$ are also orthogonal functions satisfying the following relations

$$\int_0^l m(x)\,\varphi_i\varphi_j dx = \begin{cases} 0 & for j \neq i \\ M_i & for j = i \end{cases} \tag{3.35}$$

Here an orthogonal relation for K_i, similar to equation (3.35), used in equation (3.39), is needed.

By representing the solution to the general problem in terms of $\varphi_i(x)$

$$y(x,t) = \sum_i \varphi_i(x)\,q_i(t) \tag{3.36}$$

the generalized coordinate $q_i(t)$can be determined from Lagrange's equation by first establishing the kinetic and potential energies.

Recognizing the orthogonality relation from Equation (3.35), the kinetic energy is

$$\begin{aligned} T &= \frac{1}{2}\int_0^l \dot{y}^2(x,t)m(x)dx = \frac{1}{2}\sum_i\sum_j \dot{q}_i\,\dot{q}_j \int_0^l \varphi_i\varphi_j m(x)\,dx \\ &= \frac{1}{2}\sum_i M_i\dot{q}_i^2 \end{aligned} \tag{3.37}$$

where the generalized mass $M_i$is defined as

$$M_i = \int_0^l \varphi_i^2\,(x)m(x)dx \tag{3.38}$$

Similarly, the potential energy is

$$\begin{aligned} U &= \frac{1}{2}\int_0^l EIy''^2\,(x,t)dx = \frac{1}{2}\sum_i\sum_j q_i q_j \int_0^l EI\varphi_i''\varphi_j''\,dx \\ &= \frac{1}{2}\sum_i K_i q_i^2 = \frac{1}{2}\sum \omega_i^2\,M_i q_i^2 \end{aligned} \tag{3.39}$$

where the generalized stiffness is

$$K_i = \int_0^l EI[\varphi_i''(x)]^2\,dx \tag{3.40}$$

In addition to T and U, we need the generalized force Q_i, which is determined from the work done by the applied force $p(x,t)$ in the virtual displacement δq_i

$$\begin{aligned}\delta W &= \int_0^l p(x,t)\left(\sum_i \varphi_i \delta q_i\right) dx \\ &= \sum_i \delta q_i \int_0^l p(x,t)\,\varphi_i(x) dx\end{aligned} \tag{3.41}$$

where the generalized force is

$$Q_i = \int_0^l p(x,t)\varphi_i\,(x) dx \tag{3.42}$$

Substituting into Lagrange's equation (Thomson, 1996)

$$\frac{d}{dt}\left(\frac{\partial T}{\partial \dot{q}_i}\right) - \frac{\partial T}{\partial q_i} + \frac{\partial U}{\partial q_i} = Q_i \tag{3.43}$$

we find the equation for $q_i(t)$to be

$$\ddot{q}_i + \omega_i^2 q_i = \frac{1}{M_i}\int_0^l p(x,t)\varphi_i\,(x) dx \tag{3.44}$$

It is convenient at this point to consider the case when the loading per unit length $p(x,t)$ is separable in the form

$$p(x,t) = \frac{P_0}{l} p(x) f(t) \tag{3.45}$$

Equation (3.44) then reduces to

$$\ddot{q}_i + \omega_i^2 q_i = \frac{P_0}{M_i}\Gamma_{\mathrm{i}} f(t) \tag{3.46}$$

where

$$\Gamma_i = \frac{1}{l}\int_0^l p(x)\,\varphi_i(x) dx$$

is defined as the mode participation factor for mode *i.* Based on Thomson (1996), the solution of Equation (3.46) is then

$$\begin{aligned}q_i(t) = q_i(0)\cos\omega_i\, t + \frac{1}{\omega_i}\dot{q}_i(0)\sin\omega_i\,(t) \\ + \left(\frac{P_0\Gamma_{\mathrm{i}}}{M_i\omega_i^2}\right)\omega_i \int_0^t f(\xi)\sin\omega_i\,(t-\xi) d\xi\end{aligned} \tag{3.47}$$

Because the *i*th mode static deflection [with $\ddot{q}_i(t) = 0$] expanded in terms of $\varphi_i(x)$ is $P_0\Gamma_i/M_i\omega_i^2$, the quantity

$$D_i(t) = \omega_i \int_0^t f(\xi)\, sin\, \omega_i\, (t-\xi) d\xi \tag{3.48}$$

can be called the dynamic load factor for the *i* th mode.

3.3 Nonlinear Dynamics

Nonlinear dynamics is the study of the dynamical behaviour of a nonlinear system. A nonlinear system is a system whose time evolution equations are nonlinear; that is the dynamical variables describing the properties of the system (for example, position, velocity, acceleration, pressure etc.) appear in the equations in a nonlinear form. For nonlinear systems, a small change in a parameter can lead to sudden and dramatic changes in both the qualitative and quantitative behaviour of the system (Hilborn, 2000). By using the state space approach and studying the motion presented in the phase plane allows us to learn more about the behaviour of a nonlinear system (Thomson, 1996).

3.3.1 General formulation equation in state space

A system is said to be autonomous if the time, t does not appear explicitly in the differential equation of motion. For an autonomous system with the differential equation

$$\ddot{x} + f(x, \dot{x}) = 0 \tag{3.49}$$

where $f(x, \dot{x})$ can be a nonlinear function of x and $\dot{x}$. Using the state space approach, Equation (3.49) is expressed in terms of two first order equations:

$$\begin{aligned} \dot{x} &= y \\ \dot{y} &= -f(x, y) \end{aligned} \tag{3.50}$$

If x and y are Cartesian coordinates, the xy -plane is called the phase plane. The coordinate x and $y = \dot{x}$ are the state of the system and represent a point on the phase plane. The point on the phase plane moves as the state of the system changes, thereby generating a curve called a trajectory (Thomson, 1996).

3.3.2 Stability of Equilibrium states

Equilibrium points (also called fixed points or stationary points or critical points or singular points) in state space plays a key role in understanding the dynamics of a nonlinear system

(Hilborn, 2000). The equilibrium points are defined as the points in state space for which all the time derivatives of the state variables are 0. The equilibrium points correspond to a state of equilibrium of the system; the velocity $y = \dot{x}$ and the force $\ddot{x} = -f$ are zero at an equilibrium point (Thomson, 1996).

3.3.2.1 Stability Analysis

Consider a single degree of freedom nonlinear vibratory system described by two first order differential equations (Rao,2011)

$$\begin{aligned} \frac{dx}{dt} &= f_1(x, y) \\ \frac{dy}{dt} &= f_2(x, y) \end{aligned} \tag{3.51}$$

where f_1 and f_2 are nonlinear functions of x and $y = \dot{x} = \frac{dx}{dt}$. For this system, the slope of the trajectories in phase plane is given by

$$\frac{dy}{dx} = \frac{\dot{y}}{\dot{x}} = \frac{f_2(x, y)}{f_1(x, y)} \tag{3.52}$$

Let (x_0, y_0) be an equilibrium point so that

$$f_1(x_0, y_0) = f_2(x_0, y_0) = 0 \tag{3.53}$$

A study of Equation (3.51) in the neighbourhood of the equilibrium points provides us with answers as to the stability of equilibrium. We first note that there is no loss of generality if we assume that the equilibrium point is located at origin (0,0). This is because the slope $(dy)/(dx)$ of the trajectories does not vary with a translation of the coordinate axes x and y to $x'$and y':

$$\begin{aligned} x' &= x - x_0 \\ y' &= y - y_0 \\ \frac{dy}{dx} &= \frac{dy'}{dx'} \end{aligned} \tag{3.54}$$

Thus we assume that $(x = 0, y = 0)$ is an equilibrium point, so that

$$f_1(0,0) = f_2(0,0) = 0$$

if $f_1$and f_2 are expanded in terms of Taylor's series about the equilibrium point (0,0), we obtain

$$\begin{aligned} \dot{x} &= f_1(x, y) = a_{11}x + a_{12}y + \text{Higher order terms} \\ \dot{y} &= f_2(x, y) = a_{21}x + a_{22}y + \text{Higher order terms} \end{aligned} \tag{3.55}$$

where

$$a_{11} = \left.\frac{\partial f_1}{\partial x}\right|_{(0,0)}, \qquad a_{12} = \left.\frac{\partial f_1}{\partial y}\right|_{(0,0)}, \qquad a_{21} = \left.\frac{\partial f_2}{\partial x}\right|_{(0,0)}, \qquad a_{22} = \left.\frac{\partial f_2}{\partial y}\right|_{(0,0)}$$

In the neighbourhood of (0,0), x and y are small; $f_1$and f_2 can be approximated by linear terms only, so that Equation (3.55) can be written as

$$\begin{Bmatrix}\dot{x}\\ \dot{y}\end{Bmatrix} = \begin{bmatrix}a_{11} & a_{12}\\ a_{21} & a_{22}\end{bmatrix}\begin{Bmatrix}x\\ y\end{Bmatrix} \tag{3.56}$$

The solutions of Equation (3.56) are expected to be geometrically similar to those of Equation (3.51). We assume the solution of Equation (3.56) in the form

$$\begin{Bmatrix}x\\ y\end{Bmatrix} = \begin{Bmatrix}X\\ Y\end{Bmatrix} e^{\lambda t} \tag{3.57}$$

where X,Y and λ are constants. Substitution of Equation (3.57) into Equation (3.56) leads to the eigenvalue problem

$$\begin{bmatrix}a_{11}-\lambda & a_{12}\\ a_{21} & a_{22}-\lambda\end{bmatrix}\begin{Bmatrix}X\\ Y\end{Bmatrix} = \begin{Bmatrix}0\\ 0\end{Bmatrix} \tag{3.58}$$

The eigenvalues $\lambda_1$and λ_2 can be found by solving the characteristic equation

$$\begin{vmatrix}a_{11}-\lambda & a_{12}\\ a_{21} & a_{22}-\lambda\end{vmatrix} = 0$$

as

$$\lambda_1, \lambda_2 = \frac{1}{2}(p \pm \sqrt{p^2 - 4q}) \tag{3.59}$$

where $p = a_{11} + a_{22}$ and $q = a_{11}a_{22} - a_{12}a_{21}$. If

$$\begin{Bmatrix}X_1\\ Y_1\end{Bmatrix} \quad \text{and} \quad \begin{Bmatrix}X_2\\ Y_2\end{Bmatrix}$$

denote the eigenvectors corresponding to λ_1 and λ_2, respectively, the general solution of Equation (3.51) can be expressed as (assuming $\lambda_1 \neq 0$, $\lambda_2 \neq 0$, and $\lambda_1 \neq \lambda_2$):

$$\begin{Bmatrix}x\\ y\end{Bmatrix} = C_1\begin{Bmatrix}X_1\\ Y_1\end{Bmatrix} e^{\lambda_1 t} + C_2\begin{Bmatrix}X_2\\ Y_2\end{Bmatrix} e^{\lambda_2 t} \tag{3.60}$$

where C_1 and C_2 are arbitrary constants. We can note the following (Rao, 2011):

If $(p^2 - 4q) < 0$, the motion is oscillatory.

If $(p^2 - 4q) > 0$, the motion is aperiodic.

If $p > 0$, the system is unstable.

If $p < 0$, the system is stable.

3.3.2.2 Classification of equilibrium points

If we use the transformation

$$\begin{Bmatrix} x \\ y \end{Bmatrix} = \begin{bmatrix} X_1 & X_2 \\ Y_1 & Y_2 \end{bmatrix} \begin{Bmatrix} \alpha \\ \beta \end{Bmatrix} = [T] \begin{Bmatrix} \alpha \\ \beta \end{Bmatrix}$$

where $[T]$ is the modal matrix and α and β are the generalised coordinates, Equation (3.56) will be uncoupled:

$$\begin{Bmatrix} \dot{\alpha} \\ \dot{\beta} \end{Bmatrix} = \begin{bmatrix} \lambda_1 & 0 \\ 0 & \lambda_2 \end{bmatrix} \begin{Bmatrix} \alpha \\ \beta \end{Bmatrix} \text{ or } \dot{\alpha} = \lambda_1 \alpha, \ \dot{\beta} = \lambda_2 \beta \tag{3.61}$$

The solution of (3.61) can be expressed as

$$\begin{aligned} \alpha(t) &= e^{\lambda_1 t} \\ \beta(t) &= e^{\lambda_2 t} \end{aligned} \tag{3.62}$$

Depending on the values of λ_1 and λ_2 in (3.59), the equilibrium points can be classified as follows (Rao,2011)

3.3.2.2.1 Case 1: λ_1 and λ_2 are Real and Distinct ($p^2 > 4q$)

In this case Equation (3.62) gives

$$\alpha(t) = \alpha_0 e^{\lambda_1 t} \text{and } \beta(t) = \beta_0 e^{\lambda_2 t} \tag{3.63}$$

where α_0 and β_0 are initial values of α and β respectively.

If λ_1 and λ_2 have the same sign ($q > 0$) the equilibrium point is called a node. The phase plane diagram is shown in Figure 3.3(a) for the case when $\lambda_2 < \lambda_1 < 0$ (when λ_1 and λ_2 are real and negative or $p < 0$). In this case, Equation (3.63) shows that all the trajectories tend to the origin as $t \to \infty$ and hence the origin is called a stable node. If $\lambda_2 > \lambda_1 > 0$ ($p > 0$), the arrow heads change in direction and the origin is called an unstable node as shown in Figure 3.3(b). If λ_1 and λ_2 are real but of opposite signs ($q < 0$ irrespective of the sign of p) one solution tend to

the origin while the other tends to infinity. In this case the origin is called a saddle point and it corresponds to unstable equilibrium as shown in Figure 3.3(d).

3.3.2.2.2 Case 2: λ_1 and λ_2 are Real and Equal ($p^2 = 4q$)

In this case Equation (3.62) gives

$$\alpha(t) = \alpha_0 e^{\lambda_1 t} \text{and } \beta(t) = \beta_0 e^{\lambda_1 t} \tag{3.64}$$

The trajectories will be straight lines passing through the origin and the equilibrium point (origin) will be a stable node if $\lambda_1 < 0$ as shown in Figure 3.3(c) and an unstable node if $\lambda_1 > 0$.

3.3.2.2.3 Case 3: λ_1 and λ_2 are Complex Conjugates ($p^2 < 4q$)

Let $\lambda_1 = \theta_1 + i\theta_2$ and $\lambda_2 = \theta_1 + i\theta_2$ where θ_1 and θ_2 are real. Then Equation (3.61) gives

$$\dot{\alpha} = (\theta_1 + i\theta_2)\alpha \text{ and } \dot{\beta} = (\theta_1 + i\theta_2)\beta \tag{3.65}$$

This shows that α and β must also be complex conjugates. We can rewrite Equation (3.62) as

$$\alpha(t) = \left(\alpha_0 e^{\theta_1 t}\right)e^{i\theta_2 t}, \beta(t) = \left(\beta_0 e^{\theta_1 t}\right)e^{i\theta_2 t} \tag{3.66}$$

These equations represent logarithmic spirals. In this case the equilibrium point (origin) is called a focus or a spiral point. Since the factor $e^{i\theta_2 t}$ in $\alpha(t)$ represents a vector of unit magnitude rotating with angular velocity θ_2 in the complex plane, the magnitude of the complex vector $\alpha(t)$ and hence the stability of motion is determined by $e^{\theta_1 t}$. If $\theta_1 < 0$ the motion will be asymptotically stable and the focal point will be stable ($p < 0$ and $q > 0$). If $\theta_1 > 0$, the focal point will be unstable ($p > 0$ and $q > 0$). The sign of θ_2 gives the direction of rotation of the complex vector, counterclockwise for $\theta_2 > 0$ and clockwise for $\theta_2 < 0$. If $\theta_1 = 0$, the magnitude of the complex radius vector $\alpha(t)$ will be constant and the trajectories reduce to circles with the center as the equilibrium point (origin). The motion will be periodic and hence stable. The equilibrium point in this case is called a centre or vertex point and the motion is simply stable and not asymptotically stable. The stable focus, unstable focus and center are shown in Figure 3.3 (e) to (g) (Rao,2011).

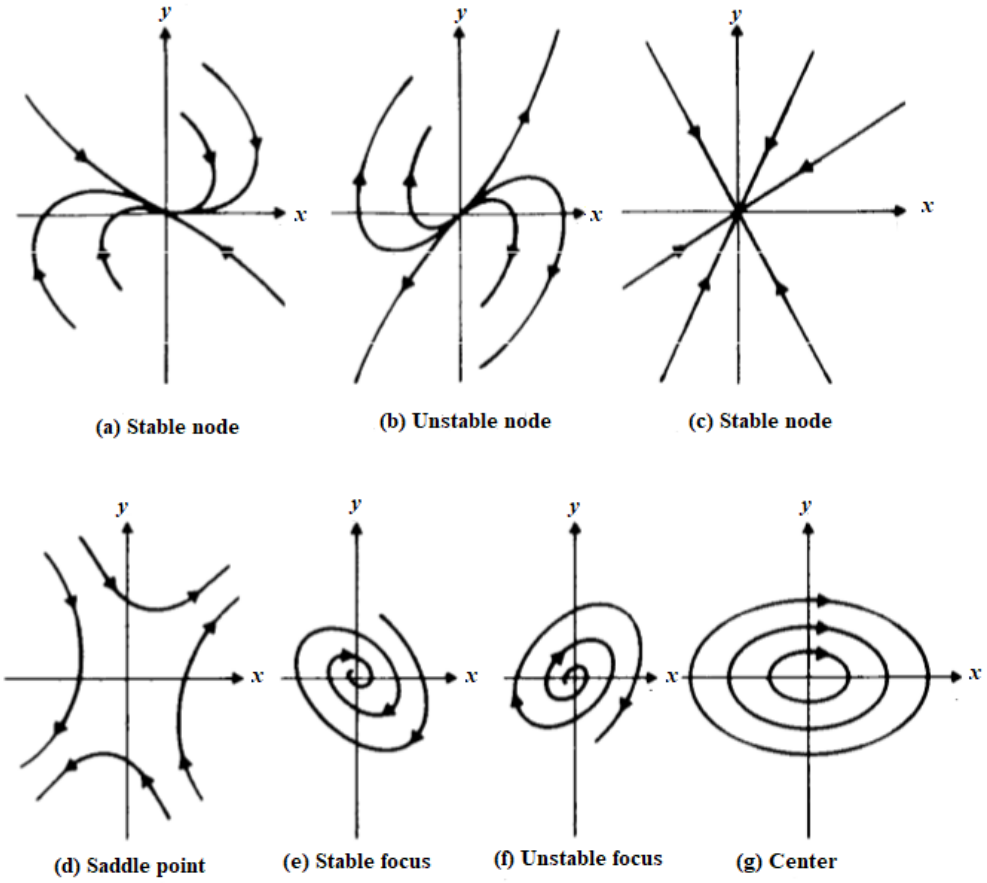

Figure 3.3 Classification of equilibrium points (Rao, 2011)

3.3.3 Bifurcation and Chaos

Bifurcation is used to describe a qualitative change that occurs in the features of a system when one or more parameters on which the system depends on are varied. Local bifurcation refers to the qualitative change that occurs in the neighbourhood of a fixed point or a periodic solution of the system, whilst any other qualitative change apart from the aforementioned is referred to as global bifurcation (Nayfeh & Balachandran, 1995).

Chaos is a complex behaviour that results from some sudden and dramatic change in nonlinear system. Chaos is defined as aperiodic long-term behaviour in a deterministic system that exhibits sensitive dependence on initial conditions (Strogatz, 1994).

1. "Aperiodic long-term behaviour" means that there are trajectories which do not settle down to equilibrium points, periodic orbits, or quasiperiodic orbits as $\rightarrow \infty$. For practical reasons, we should require that such trajectories are not too rare. For instance, we could insist that there be an open set of initial conditions leading to

aperiodic trajectories, or perhaps that such trajectories should occur with nonzero probability, given a random initial condition.

2. "Deterministic" means that the system has no random or noisy inputs or parameters. The irregular behaviour arises from the system's nonlinearity, rather than from noisy driving forces.
3. "Sensitive dependence on initial conditions" means that nearby trajectories separate exponentially fast, i.e., the system has a positive Lyapunov exponent.

An example of bifurcation and chaos can be studied from Duffing's equation with the forcing term (Rao, 2011). Consider a single degree of freedom system with a nonlinear spring and a harmonic forcing function. The equation of motion (Duffing's equation) can be expressed as

$$\ddot{x} + \mu\dot{x} - \alpha x + \beta x^3 = F_0 \cos \omega t \tag{3.67}$$

Using the value of $\mu = 0.2$ and $\alpha = \beta = 1$, within the forcing term, small changes in the frequency (ω) or the amplitude (F_0) can lead to chaos.

When ω is changed, for a fixed value of $F_0$the phase plane response of Equation (3.67) can be periodic or chaotic depending on the value of ω. For example, Figure 3.4 and Figure 3.5 indicate the two situations that are described by the equation

$$\ddot{x} + 0.2\dot{x} - x + x^3 = 0.3 \cos 1.4t \text{ (periodic, Figure 3.4)} \tag{3.68}$$

$$\ddot{x} + 0.2\dot{x} - x + x^3 = 0.3 \cos 1.29t \text{ (chaotic, Figure 3.5)} \tag{3.69}$$

where $F_0 = 0.3$ has been assumed. Figure 3.4 has been plotted using an approximate analysis known as the harmonic balance method (will be shown further in Section 3.3.4.1). Figure 3.5 represents a Poincare map which indicates points that occur at equal intervals of time $T_0, 2T_0, 3T_0, \ldots$ where T_0 is the fundamental period of excitation, $T_0 = \frac{2\pi}{\omega} = \frac{2\pi}{1.29}$.

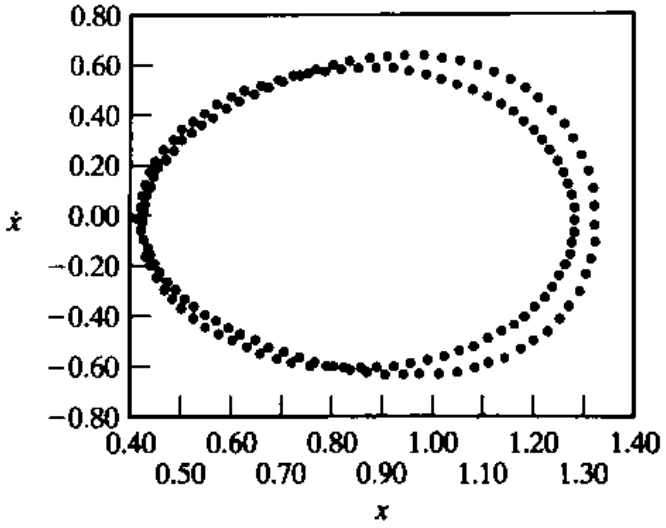

Figure 3.4 Phase plane of Equation (3.68) (Rao, 2011)

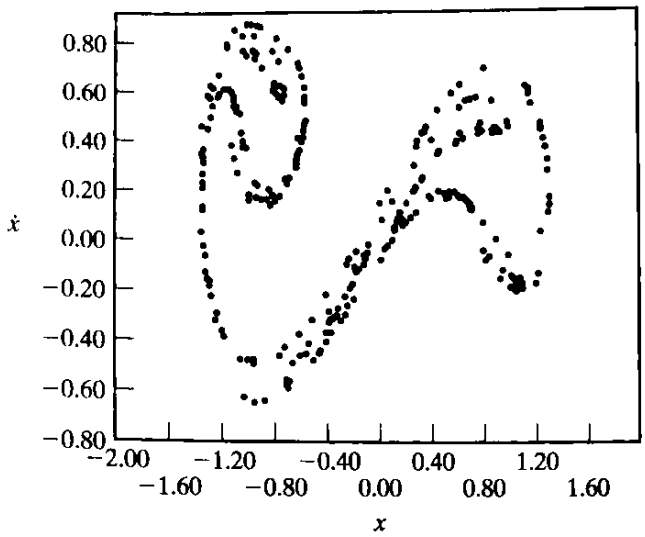

Figure 3.5 Poincare map of Equation (3.69) (Rao, 2011)

Chaos can also be observed when the amplitude, F_0 is changed. To illustrate this, consider the following equation

$$\ddot{x} + 0.168\dot{x} - 0.5x + 0.5x^3 = F_0 \sin \omega t = F_0 \sin t \tag{3.70}$$

For definiteness, we assume the initial conditions as $x_0 = 1$ and $\dot{x}_0 = 0$. When F_0 is sufficiently small, the response of the system will be a simple harmonic motion (that is, the phase plane will be an ellipse) about its static equilibrium position, $x = +1$. When F_0 is increased, additional harmonics beyond the fundamental are detected and the phase plane will be distorted from a simple ellipse as shown in Figure 3.6 (a) for $F_0 = 0.177$. The response is called a 1 period motion for $0 \leq F_0 \leq 0.177$, implying that the response oscillates through one period while the force oscillates through one period. For $F_0 = 0.178$, the phase plane is shown in

Figure 3.6 (b) which indicates that the response is a period 2 motion. Thus, for the response to oscillate through one period, the force must oscillate through two periods. This change from a 1 to a 2 period response as F_0 changes from 0.177 to 0.178 is called a bifurcation. When $F_0 = 0.197$, the response will be a 4 period motion as shown in Figure 3.6(c). As F_0 is increased, 8,16, … period motions occur and finally for $F_0 \geq 0.205$, chaos can be observed with no apparent periodicity as shown in Figure 3.6(d) (Rao, 2011).

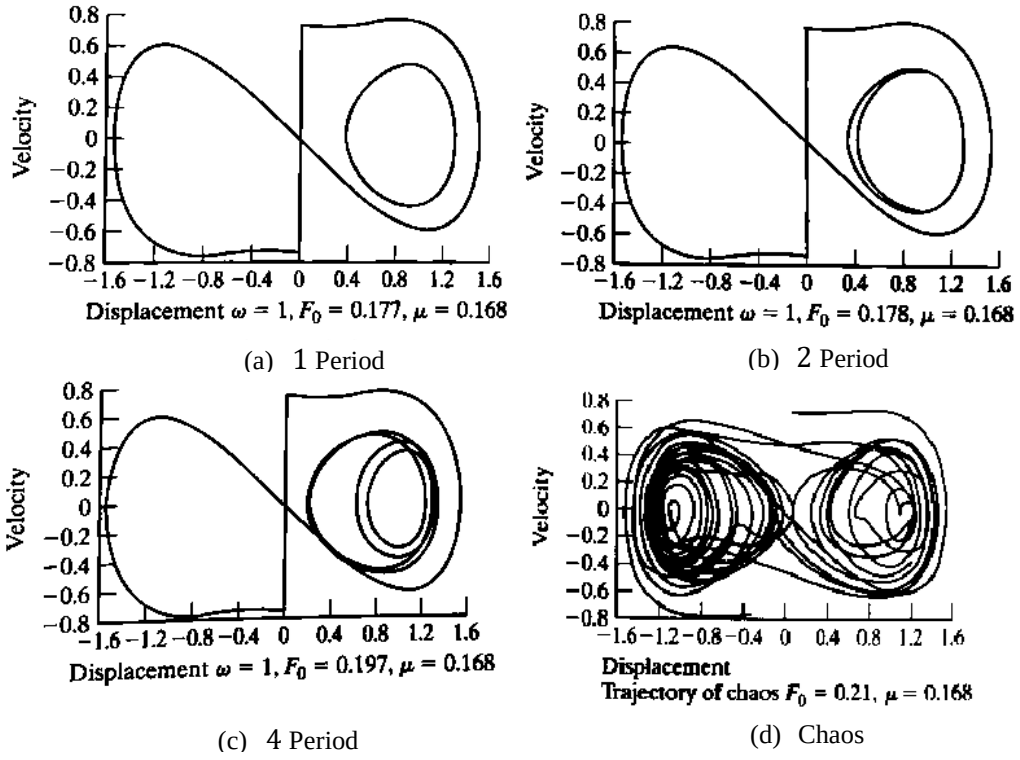

(a) 1 Period (b) 2 Period

(c) 4 Period (d) Chaos

Figure 3.6 Distortion of phase plane (Rao, 2011)

3.3.4 Methods used to solve nonlinear differential equations

Nonlinear systems can be solved either by exact method or by approximate methods. An exact solution can only be obtained for a relatively few nonlinear systems whose motion is governed by specific types of second order nonlinear differential equations. The solutions are exact in the sense that they are given either in closed form or in the form of an expression that can be numerically evaluated at any degree of accuracy. In the absence of exact solution, we wish to find at least an approximate solution for the nonlinear system. Although analytical and numerical methods are available for approximate solutions of nonlinear systems, the analytical methods are more desirable. This is because, once the analytical solution is obtained, any

desired numerical values can be substituted and the possible range of solutions can be investigated (Rao, 2011).

3.3.4.1 Approximate analytical methods

Some common approximation methods for solving nonlinear systems are the harmonic balance method and perturbation approximation methods.

For the Harmonic balance method, the idea is to assume the response of a nonlinear differential equation to be in the following form

$$x = \sum_{m=0}^{M} A_m \cos(m\Omega\tau + m\theta_0) \tag{3.71}$$

Then, substituting Equation (3.71) in the governing equation and equating the coefficient of each of the lowest $M + 1$ harmonics to zero, one obtains a system of $M + 1$ algebraic equation relating Ω and the A_m . Usually these equations are solved for $A_0, A_2, A_3, \ldots A_m$ and Ω in terms of A_1 . The accuracy of the resulting periodic solution depends on the value of A_1 and the number of harmonics in the assumed solution (Nayfeh & Mook, 2004). The harmonic balance method is further illustrated in the following example of the forced Duffing equation (Carrella, 2008).

Consider the unforced duffing equation

$$\ddot{x} + 2\xi\dot{x} + x + \alpha x^3 = F_o \cos(\Omega\tau) \tag{3.72}$$

Substituting the one term expansion

$$x = A_1 \cos(\Omega\tau + \theta_0) = A_1 \cos\phi \tag{3.73}$$

which implies

$$\dot{x} = -\Omega A_1 \sin\phi \qquad x = -\Omega^2 A_1 \cos\phi \tag{3.74}$$

Substituting Equation (3.73) and Equation (3.74) into Equation (3.72) yields

$$-\Omega^2 A_1 \cos\phi - 2\xi\Omega A_1 \sin\phi + A_1 \cos\phi + \alpha A_1^3 \cos^3\phi = F_o \cos(\Omega\tau) \tag{3.75}$$

By neglecting harmonics of order higher than 1, one can simplify the trigonometric identity

$$\cos^3\phi \equiv \frac{1}{4}(3\cos\phi + \cos 3\phi) \approx \frac{3}{4}\cos\phi \tag{3.76}$$

The forcing term can be rearranged as

$$F_o \cos(\Omega\tau) = F_o \cos(\phi - \theta_o) = F_o \cos\phi \cos\theta_o + F_o \sin\phi \sin\theta_o \tag{3.77}$$

Finally, inserting Equation (3.76)and Equation (3.77)into Equation (3.75) gives

$$\begin{aligned} &-\Omega^2 A_1 \cos\phi - 2\xi\Omega A_1 \sin\phi + A_1 \cos\phi + \frac{3}{4}\alpha A_1^3 \cos\phi \quad = \\ &F_o \cos\phi \cos\theta_o + F_o \sin\phi \sin\theta_o \end{aligned} \tag{3.78}$$

Equating the coefficients of similar functions yields the system of two coupled algebraic equations

$$\frac{3}{4}\alpha A_1^3 + (1-\Omega^2)\ A_1 = F_o \cos\theta_o \tag{3.79a}$$

$$-2\xi\Omega A_1 = F_o \sin\theta_o \tag{3.80b}$$

from which the two unknowns A_1 and θ_o can be determined. The relationship between the response amplitude and frequency of excitation which is known as the frequency response function can be calculated by squaring and adding both equations (3.79a) and (3.80b) which results in

$$\frac{9}{16}\alpha^2 A_1^6 + \frac{3}{2}(1-\Omega^2)\ \alpha A_1^4 + [(1-\Omega^2)^2 + 4\xi^2\Omega^2]A_1^2 = {F_o}^2 \tag{3.80}$$

Equation (3.80) can be seen either as a cubic in A_1^2 or a quadratic in Ω^2.

As for the perturbation method, it is applicable to problems in which a small parameter μ is associated with the nonlinear term of the differential equation. The solution is formed in terms of a series of the perturbation parameter μ, the result being a development in the neighbourhood of the solution of the linearized problem. If the solution of the linearized problem is periodic, and if μ is small, we can expect the perturbed solution to be periodic also. We can reason from the phase plane that the periodic solution must represent a closed trajectory. The period, which depends on the initial conditions is then a function of the amplitude of vibration (Thomson, 1996).

3.3.4.2 Numerical methods

Numerical methods are techniques by which mathematical problems are formulated so that they can be solved with arithmetic operations. Although there are many kinds of numerical methods, they have one common characteristic: they invariably involve large numbers of tedious arithmetic calculations (Chapra & Canale, 2015).

Numerical methods have been widely used to study the dynamic response characteristics of nonlinear systems. The benefit of using numerical approach compared to analytical approach is that it can be applied to study different types of steady state responses, e.g., periodic, quasi-periodic or chaotic motions. However, the disadvantage is that potentially significant errors can arise in numerical simulations and factors such as the time step size as well as the orders of accuracy should be carefully chosen.

The Runge-Kutta method is one of the numerical method used to solve nonlinear differential equations. The Runge-Kutta method is widely used as it is self-starting and results in good accuracy. A brief discussion of its basis is presented here (Thomson, 1996).

In the Runge-Kutta method, the second-order differential equation is first reduced to two first-order equations. As an example, consider the differential equation for the single-DOF system, which can be written as

$$\ddot{x} = \frac{1}{m}[f(t) - kx - c\dot{x}] = F(x, \dot{x}, t) \tag{3.81}$$

By letting $\dot{x} = y$ this equation is reduced to the following two first-order equations

$$\begin{aligned} \dot{x} &= y \\ \dot{y} &= F(x, y, t) \end{aligned} \tag{3.82}$$

Both *x* and *y* in the neighbourhood of x_1 and y_1 can be expressed in terms of the Taylor series. Letting the time increment be $h=\Delta t$, we have

$$\begin{aligned} x &= x_1 + \left(\frac{dx}{dt}\right)h + \left(\frac{d^2x}{dt^2}\right)\frac{h^2}{2} + \cdots \\ y &= y_1 + \left(\frac{dy}{dt}\right)h + \left(\frac{d^2y}{dt^2}\right)\frac{h^2}{2} + \ldots \end{aligned} \tag{3.83}$$

Instead of using these expressions, it is possible to replace the first derivative by an average slope and ignore higher-order derivatives

$$x_i + \left(\frac{dx}{dt}\right)_{1av} h \qquad (3.84)$$
$$y_i + \left(\frac{dy}{dt}\right)_{1av} h$$

If we used Simpson's rule, the average slope in the interval h becomes

$$\left(\frac{dy}{dt}\right)_{iav} = \frac{1}{6}\left[\left(\frac{dy}{dt}\right)_{t_i} + 4\left(\frac{dy}{dt}\right)_{t_i+h/2} + \left(\frac{dy}{dt}\right)_{t_i+h}\right] \qquad (3.85)$$

The 4th-order Runge-Kutta method, for example, is very similar to the preceding computations, except that the center term of the given equation is split into two terms and four values of *t, x, y,* and f are computed for each point *i* as shown in Table 3.2.

Table 3.2 Four values of the 4th-order Runge-Kutta method (Thomson, 1996)

$\boldsymbol{t}$	$\boldsymbol{x}$	$\boldsymbol{y = \dot{x}}$	$\boldsymbol{f = \dot{y} = \ddot{x}}$
$\boldsymbol{T_1 = t_i}$	$X_1 = x_i$	$Y_1 = y_i$	$F_1 = f(T_1, X_1, Y_1)$
$\boldsymbol{T_2 = t_i + \frac{h}{2}}$	$X_2 = x_i + Y_1\frac{h}{2}$	$Y_2 = y_i + F_1\frac{h}{2}$	$F_2 = f(T_2, X_2, Y_2)$
$\boldsymbol{T_3 = t_i + \frac{h}{2}}$	$X_3 = x_i + Y_2\frac{h}{2}$	$Y_3 = y_i + F_2\frac{h}{2}$	$F_3 = f(T_3, X_3, Y_3)$
$\boldsymbol{T_4 = t_i + h}$	$X_4 = x_i + Y_3 h$	$Y_4 = y_i + F_3 h$	$F_4 = f(T_4, X_4, Y_4)$

These quantities are then used in the following recurrence formula:

$$x_{i+1} = x_i + \frac{h}{6}(Y_1 + 2Y_2 + 2Y_3 + Y_4) \qquad (3.86)$$
$$y_{i+1} = y_i + \frac{h}{6}(F_1 + 2F_2 + 2F_3 + F_4)$$

where it is recognized that the four values of Y divided by 6 represent an average slope $\frac{dx}{dt}$ and the four values of F divided by 6 results in an average of $\frac{dy}{dt}$ as defined by equation (3.84). In the book by Xing (2015), a Matlab program using Runge-Kutta method to solve nonlinear dynamical equations is presented. In our numerical simulations the Runge-Kutta method is used.

3.4 Nonlinear passive vibration isolator

A nonlinear passive vibration isolator is an isolator that incorporates a nonlinear element or a nonlinear configuration of springs or dampers together with a linear spring and/or damper to achieve improved performance. The nonlinearity usually takes the form of either a nonlinear spring force or a nonlinear damping force (Ho & Billings, 2012) and may not be the result of physical properties of the material only, but also of geometry of the system; shape and dimensions of the body, type of laying, loading etc. (Cveticanin, 2014).

3.4.1 Example of a nonlinear vibration isolator

An example of a nonlinear vibration isolator design (Yang et al., 2013) developed from the one in Platus (1992) is illustrated in Figure 3.7.

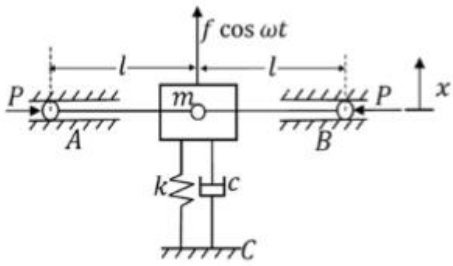

Figure 3.7 A schematic of a nonlinear vibration isolator (Yang et al., 2013)

It consists of a conventional linear mass–spring–damper system and a nonlinear negative stiffness mechanism (NSM). The linear part is made up of a mass m subject to harmonic excitation, a vertical linear spring of stiffness k and a viscous damper with a damping coefficient c. The NSM is created by two rigid massless bars of fixed length l, hinged together at one end with the mass while the other ends, subject to two equivalent compression forces P, are allowed to move freely in frictionless horizontal channels. It is assumed that the bars are horizontal when the unforced mass is in its static equilibrium position of $x = 0$.

3.4.1.1 Governing equations

The motion of the system is restricted to be in two-dimensional plane. As the system is symmetric, the mass only has vertical movement.

If the mass reaches $x = \pm l$, the bars will be vertical, and the motion cannot be maintained, so that situation should be avoided. When $-l < x < l$, the equation of motion is

$$m\ddot{x} + c\dot{x} + kx - 2P\frac{x}{\sqrt{l^2 - x^2}} = f\cos\omega t \tag{3.87}$$

where f and ω are the amplitude and frequency of the harmonic excitation force, respectively. Letting,

$$\omega_o = \sqrt{\frac{k}{m}} \quad , T = \omega_o t \quad , \xi = \frac{c}{2m\omega_o} \quad , \alpha = \frac{2P}{kl} \quad , X = \frac{x}{l} \quad , F = \frac{f}{kl} \quad , \Omega = \frac{\omega}{\omega_o}$$

we obtain a non-dimensional equation of motion:

$$X'' + 2\xi X' + X\left(1 - \frac{1}{\sqrt{1 - X^2}}\right) = F\cos\Omega t, |X| < 1 \tag{3.88}$$

where $(\ )'$ denotes a differentiation of $(\ )$ with respect to T.

The total non-dimensional restoring force from both the linear spring and NSM is given by

$$G(X) = X\left(1 - \alpha\frac{1}{\sqrt{1 - X^2}}\right), |X| < 1 \tag{3.89}$$

A differentiation of $G(X)$ with respect to X gives the following non-dimensional stiffness of the system:

$$H(X) = 1 - \frac{\alpha}{(1 - X^2)\sqrt{1 - X^2}}, \quad |X| < 1 \tag{3.90}$$

This equation shows that nonlinear stiffness is affected by a positive α and the displacement X through a negative nonlinear term $\alpha/(1 - X^2)\sqrt{1 - X^2}$. Its value decreases with an increase of α and deflection $|X|$.

3.4.1.2 Analysing the equilibrium points

The position $X = 0$ is a static equilibrium position, around which, for a small-amplitude vibration, Equation (3.89) can be expanded using a Taylor series:

$$G(X) = X\left(1 - \alpha\frac{1}{\sqrt{1 - X^2}}\right) = X(1 - \alpha) - \frac{\alpha}{2}X^3 + o(X^4) \tag{3.91}$$

where $o(X^4)$represents the higher-order terms.

The linearized stiffness of the system is $1-\alpha \quad (0<\alpha<1)$, and thus the linearized natural frequency of the system about the static equilibrium is given by

$$\Omega_n = \sqrt{1-\alpha} \tag{3.92}$$

When α is set close to 1, this frequency will be much lower than 1, which is the fundamental frequency of the linear isolator without NSM ($x = 0$). Linear vibration isolation theory would suggest a wider frequency range of effective vibration isolation. However, it may not be necessarily true for the cases with NSM, since the NSM is inherently nonlinear and undesirable nonlinear effects may arise from it.

To design this isolation system, it is necessary to determine the static equilibrium points of the damped system and investigate their corresponding stabilities to choose a suitable supporting position. These can be completed by using fundamental nonlinear dynamics theories.

Such investigation reveals a pitchfork bifurcation. When $0<\alpha<1$ there are two unstable equilibrium points $\left(\pm\sqrt{1-\alpha^2}, 0\right)$ and a stable point at (0,0). However, when $\alpha \geq 1$ there exists only an unstable point at (0,0) (Ahn, 2008). As a result, the range of $0<\alpha<1$ is used and the point (0,0) should be employed as the static supporting point for the nonlinear isolation system studied herein.

3.5 Active vibration control

A vibration isolation system is called active if it uses external power to perform its function. It consists of a servomechanism with a sensor, signal processor, and an actuator, as shown schematically in Figure 3.8. This system maintains a constant distance between the vibrating mass and the reference plane. As the force $F(t)$ applied to the mass varies, the distance l tends to vary. This change in l is sensed by the sensor and a signal, proportional to the magnitude of the excitation (or response) of the vibrating body, is produced. The signal processor produces a command signal to the actuator based on the sensor signal it receives. The actuator develops a motion or force proportional to the command signal. The actuator motion or force will control the base displacement such that the distance l is maintained at the desired constant value. Different types of sensors are available to create feedback signals based on the displacement, velocity, acceleration, jerk, or force. The signal processor may consist of a passive mechanism, such as a mechanical linkage, or an active electronic or fluidic network that can perform functions such as addition, integration, differentiation, attenuation, or amplification. The

actuator may be a mechanical system such as a rack-and-pinion or ball screw mechanism, a fluidic system, or piezoelectric and electromagnetic force generating system (Rao,2011).

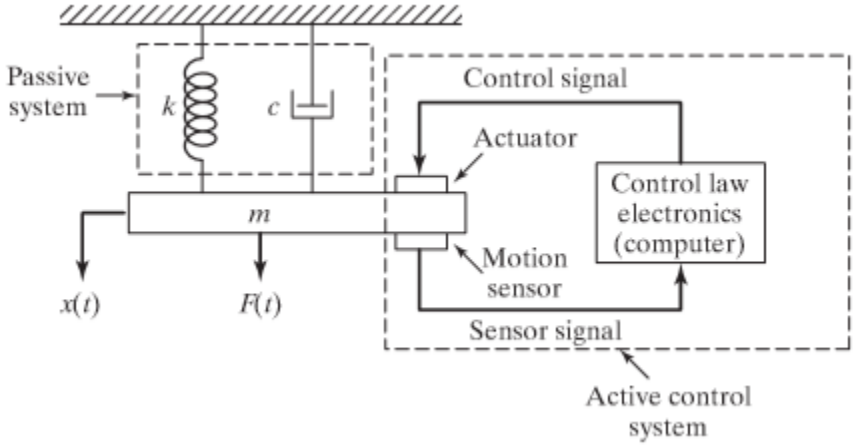

Figure 3.8 Active vibration isolation system (Rao, 2011)

Consider a single-degree-of-freedom system in which the mass m is subjected to an applied force $f(t)$ as shown in Figure 3.8. If we use an active control system to control the vibration of the mass m , the actuator will be designed to exert a control force so that the equation of motion of the system becomes

$$m\ddot{x} + c\dot{x} + kx = F(t) = f(t) + f_c(t) \tag{3.93}$$

Most commonly, the sensor measures the displacement x and the velocity $\dot{x}$ of the mass in real time and sends a signal to a computer. The computer computes the control force $f_c(t)$ necessary to control the motion and commands the actuator to exert the force $f_c(t)$ on the mass. Usually the computer is programmed to generate the control force proportional to the displacement $x(t)$ and the displacement derivative or velocity $\dot{x}(t)$ of the mass so that

$$f_c(t) = -g_p x - g_d \dot{x} \tag{3.94}$$

where g_p and g_d are constants whose values are to be determined and programmed into the computer by the designer. The constants g_p and g_d are known as control gains, with g_p denoting the proportional gain and g_d indicating the derivative or rate gain. The control algorithm in this case is known as the proportional and derivative (PD) control. By substituting Equation (3.94) into Equation (3.93), we obtain

$$m\ddot{x} + (c + g_d)\dot{x} + (k + g_p)x = f(t) \tag{3.95}$$

which shows that g_d acts like additional damping and g_p like additional stiffness. Equation (3.95), known as the closed-loop equation, can be solved to find the response characteristics of the system. For example, the new (effective) natural frequency is given by

$$\omega_n = \left(\frac{k + g_p}{m}\right)^{\frac{1}{2}} \tag{3.96}$$

and the new (effective) damping ratio by

$$\zeta = \frac{c + g_d}{2\sqrt{m(k + g_p)}} \tag{3.97}$$

The new (effective) time constant of the system, for $\zeta \leq 1$,is given by

$$\tau = \frac{2m}{c + g_d} \tag{3.98}$$

Thus the functioning of the active vibration control system can be described as follows: Given the values of m, c, and k, compute the control gains g_p and g_d to achieve the desired values of ω_n, ζ or τ. In practice, the response of the system is continuously monitored, the computations are done, and the actuator is made to apply the control force f_c to the mass in real time so that the response of the system lies within the stated limits. Note that the gains g_p and g_d can be positive or negative depending on the measured and desired responses (Rao, 2011).

3.5.1 Controller strategies used in active vibration control

There are many control strategies that have been applied for active vibration control by scientists and researchers. These include among others; linear control with displacement, velocity and acceleration feedback, Proportional-integral-derivitive (PID) controller, Linear Quadratic Regulator (LQR) controller, Fuzzy logic Robust control, Neurofuzzy, Quasi active, H2 or H-infinity, and Robust linear.

For linear control with displacement and velocity feedback, the effect of displacement feedback is to increase the structure stiffness, thus increasing the natural frequencies, whilst the effect of velocity feedback is to provide viscous damping (Meirovitch, 1990).

3.5.2 Actuators and sensors used in active vibration control

3.5.2.1 Actuators

The actuator is the heart of the control system. It is a device that converts electrical signal to a physical output and behaves as an artificial muscle that has a potential to affect the system in

an intelligent manner. This enables the command of arbitrary control forces by the active system (Lee & Clark, 1999)

Actuators that are commonly used in active vibration isolation include smart materials such as piezoelectric patches and magnetostrictive materials, and also electromagnetic and pneumatic actuators.

Piezoelectricity, defined literally as electricity generated from pressure is found naturally in many monocrystalline materials, such as, Rochelle salt, topaz, quartz and tourmaline. Piezoelectric patches are commonly used in the form of thin sheets that can be embedded in or bonded to composite structures. Their main function as actuator is to generate moment in flexible structures and is also available in the form of "stacks", where many layers of electrodes and materials are assembled together (Moheimani & Fleming, 2006). Magnetostrictive materials are generally defined as materials that go through a change in shape due to change in the magnetization state of the material. An electrodynamic or electromagnetic actuator consists of an electrical conductor, in the form of a coil that moves in a magnetic field. This will result in voltage being generated in the conductor (Rao, 2011). A pneumatic actuator is a device in which energy of compressed air is utilized for carrying out mechanical work (Funakubo, 1991).

3.5.2.2 Sensor

A sensor is a device that converts a physical parameter to an electrical output. An accelerometer is a type of sensor commonly used in an active vibration isolation system. The working principle of an accelerometer is the force caused by vibration or a change in motion (acceleration) causes the mass to squeeze the piezoelectric material inside the accelerometer producing an electrical charge proportional to the force exerted upon it. Since the charge is proportional to the force, and the mass is a constant, then the charge is also proportional to the acceleration.

Chapter 4: Beam-nonlinear isolator interaction

4.1 Introduction

In this chapter, first, a general model of the beam-nonlinear isolator interaction system is developed. Then, the solution method is discussed to obtain the equations to analyse the system. The modal summation method has been used to describe the beam model. Here, the corresponding modes of the beam are chosen, and mathematical transformation is done to obtain the numerical matrix equations. Then, the equilibrium points of the system are identified, and the stability of small vibrations at the equilibrium point is examined. The conditions for bifurcation and chaos are then investigated. From here, the interaction analysis will be done to see the effects of the beam on the isolator. Subsequently, the system will then be considered for real experiment by finding the dynamic response for two cases; (i) low frequency case, and (ii) High frequency or rigid case. Two sinusoidal vertical forces will be applied to the beam and vibration analysis will be done by observing the stability during the vibration excitation and detecting the conditions for bifurcation and chaos. These conditions will be analysed to obtain a stable system with no bifurcation and chaos to achieve a reliable design that can be used for real applications. Then, three special cases of the generalised interaction system will be presented. Lastly, performance analysis will be discussed by looking at the force transmissibility of the nonlinear isolator.

4.2 Model of a general nonlinear beam isolation interaction system

The investigated generalised nonlinear isolation system covers the published systems (such as the one in Figure 3.7 by Yang et al. (2013) which is a model for NSM and the one in Figure 2.9 (a) & (b) by Cao et al. (2006) and Hao & Cao (2014) which is a model for QZS system) that can be obtained by choosing suitable parameters of the generalised system. This general nonlinear system has two degrees of freedom in which a horizontal degree is introduced, which provides a means to physically realise the required horizontal forces investigated by Platus (1992) and Liu et al. (2012).

The integrated interaction system consists of an elastic structure which is supported by a nonlinear isolation unit as shown in Figure 4.1. The structure is considered as a uniform elastic free-free beam subject to two harmonic forces $F_0 \cos \Omega_0 t$ applied symmetrically at point ξ_0

under the beam coordinate system $O-\xi Y$ fixed at the middle point O of the beam. There is a lumped mass $2M$ connected at point O by a rigid rod of which the mass is included into $2M$. The beam is of span length $2S$, mass density ρ per unit length and bending stiffness $\Psi = EI$. Since the beam is elastic, its deflection $Y(\xi, t)$ is a function of beam material point ξ and time t. The lumped mass $2M$ is supported by a generalised nonlinear isolation system symmetrical to the vertical axis $o-y$, and therefore it moves in the y direction only. The two linear inclined massless springs of stiffness k and non-stretched length l are connected to the mass $2M$ with their other two ends being respectively connected to the two carts A and B of mass m allowing horizontal motions. There are two horizontal massless springs of stiffness K_1 and non-stretched length L_1 as well as two dampers of damping coefficient C_1 connected to carts A and B, respectively.

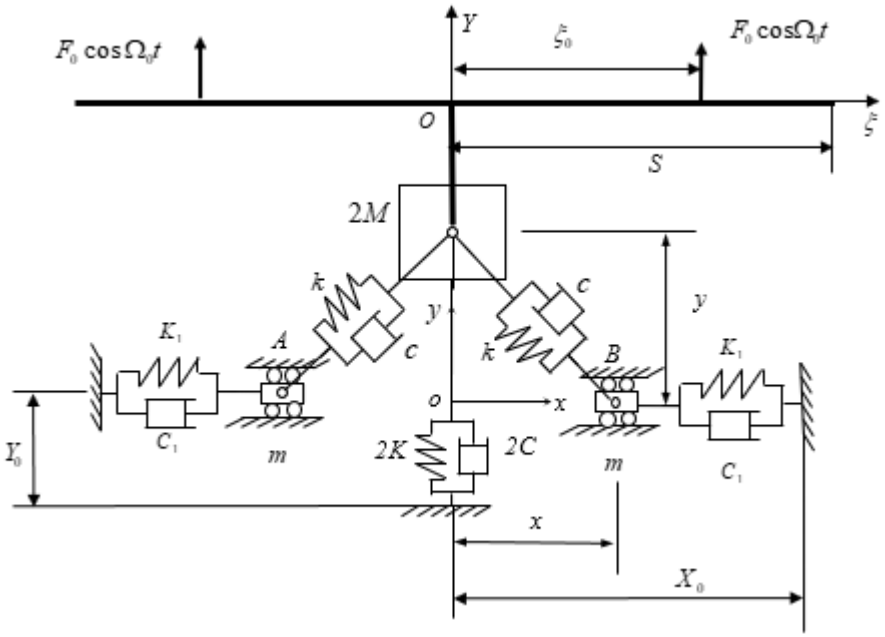

Figure 4.1 An integrated interaction system consisting of an elastic beam and a generalised nonlinear isolation unit (Xing, 2013)

Along the symmetrical axis $o-y$, a spring-damper set consisting of a spring of stiffness $2K$ and non-stretched length L and a damper of damping coefficient $2C$ is connected to the mass $2M$. The coordinate x can identify the positions of the two carts.

The model shown in Figure 4.1 is a generalised model of structure-nonlinear suspension interaction system. The arranged elements in this model are to realise practical designs for engineering applications. The horizontal spring-damper unit (K_1, C_1) aims to provide a means to realise the two horizontal forces added at the two carts to adjust the vertical dynamic stiffness of the total system. A suitable adjustment of the initial length L_1 of the spring K_1 results

in a pull or push force applied at the two carts A and B, which increases or decreases the vertical supporting stiffness of the system, respectively. The vertical spring-damper unit (K, C) supports the static weight of the mass $2M$ and the structure. The two spring-damper units (k, c) are the main elements with geometric nonlinear characteristics to adjust the dynamic supporting stiffness. The dampers in the system provide the adjusted parameters for the stability requirement of the system. Based on this generalised model, several simplified models (Platus, 1992), (Cao et al., 2008a,2008b), (Liu et al., 2012) can be obtained by introducing additional conditions or reducing some elements. The generalised system can be reduced to several simplified systems reported in the available references and is shown in Section 4.6 of this chapter.

4.2.1 Governing equations of integrated interaction system

Considering the symmetry of the system in Figure 4.1, the right-half part of the system was investigated to derive the governing equations. It would be convenient to choose origin O of coordinate system $o - xy$ and origin O of beam coordinate system $O - \xi Y$ respectively located at their corresponding positions in a static equilibrium state when the mass $2M$ and the two inclined springs k are on the horizontal axis o-x with mass m at x_o. To realise this, we can choose a suitable extension $\Delta = Y_0 - L$ of the vertical spring K by investigating the static equilibrium of the system subject to the gravity only, i.e.

$$\begin{array}{ll} K\Delta = -g(M + \rho S), & \Delta = -g(M + \rho S)/K, \\ (K_1 + k)x_0 - kl = K_1\Delta_1, & \Delta_1 = X_0 - L_1 \end{array} \tag{4.1}$$

4.2.1.1 Dynamic equilibrium equation and boundary conditions of beam structure

The dynamic equilibrium equation of the beam is

$$\Psi \frac{\partial^4 Y}{\partial \xi^4} + \rho \frac{\partial^2 Y}{\partial t^2} = \delta(\xi - \xi_0) F_0 \cos \Omega_0 t; \tag{4.2}$$

and the boundary conditions are: $Y'' = 0 = Y''', \xi = S; Y' = 0, \Psi Y'' = f_{bs}, \xi = 0$

Here, f_{bs} represents a dynamic shearing force acted on the beam section $\xi = 0$ by the rigid rod, $\delta()$denotes delta function.

The beam is considered as a linear elastic structure, so that its motion can be represented in its mode space using a mode superposition method (Thomson, 1996). In engineering, there are many nonlinear systems consisting of linear substructures connected by nonlinear connectors.

For this type of nonlinear system, the mode superposition approach provides a very effective numerical model to study the motions of linear substructures (Xing & Price, 1991).

The deflection $Y(\xi,t)$ of the beam is represented by a mode summation form

$$Y(\xi,t) = \boldsymbol{Y}(\xi)\boldsymbol{\Phi}(t), \tag{4.3}$$

where

$$\begin{aligned} &\boldsymbol{Y} = [Y_1 \quad Y_2 \quad \cdots \quad Y_N], \quad \boldsymbol{\Phi} = [\varphi_1 \quad \varphi_2 \quad \cdots \quad \varphi_N]^T, \\ &Y_n(\xi) = \frac{1}{2}\{\frac{cosh(\lambda_n\xi/S)}{cosh\,\lambda_n} + \frac{cos(\lambda_n\xi/S)}{cos\,\lambda_n}\}, \\ &tan\,\lambda_n + tanh\,\lambda_n = 0, \qquad n = 1,2,3,\cdots \end{aligned} \tag{4.4}$$

based on the non-dimensional symmetrical mode functions $Y_n(\xi)$,$(n = 1,2,\ldots,N)$, of the uniform free-free beam. Here, N denotes a number of the retained mode functions $Y_n(\xi)$ and φ_n represents a generalised coordinate corresponding to mode n, which has a length dimension. These mode functions satisfy the following orthogonal relationships,

$$\begin{aligned} &\int_0^S Y_n'' EIY_j''\, d\xi = \begin{cases} 0, & n \neq j, \\ K_{nn}, & n = j, \end{cases} \\ &\int_0^S Y_n \rho Y_j\, d\xi = \begin{cases} 0, & n \neq j, \\ M_{nn}, & n = j, \end{cases} \\ &M_{nn} = \begin{cases} \rho S, & n = 1, \\ \rho S/4, & n \neq 1, \end{cases} \\ &K_{nn} = \begin{cases} 0, & n = 1, \\ \dfrac{\lambda_n^4 \Psi}{4S^3}, & n \neq 1, \end{cases} \\ &\hat{\Omega}_n = \sqrt{K_{nn}/M_{nn}} = \frac{\lambda_n^2}{S^2}\sqrt{\frac{\Psi}{\rho}} \end{aligned} \tag{4.5}$$

The sub-index n indicates the mode number of the free-free beam, $\hat{\Omega}_n$, K_n and M_n represent the n-th natural frequency, generalised stiffness and mass, respectively. For the free-free beam, its first mode is a rigid mode with frequency $\hat{\Omega}_1 = 0$ and mode function $Y_1 = 1$.

Substituting Equation (4.3) into Equation (4.2) and using the orthogonal relationships (4.5), we obtain the following mode equation describing the beam motion

$$\begin{aligned} &\boldsymbol{m}\ddot{\boldsymbol{\Phi}} + \boldsymbol{k}\boldsymbol{\Phi} = \boldsymbol{Y}^T(0) f_{bs} + \boldsymbol{Y}^T(\xi_0) F_0\, cos\,\Omega_0\, t, \\ &\boldsymbol{m} = \mathrm{diag}(M_{nn}), \qquad \boldsymbol{k} = \mathrm{diag}(K_{nn}), \qquad \boldsymbol{\Lambda}^2 = \mathrm{diag}(\hat{\Omega}_n^2) \end{aligned} \tag{4.6}$$

4.2.1.2 Dynamic equilibrium equations of the nonlinear supporting unit

The dynamic equilibrium equation of the nonlinear supporting unit is

$$\boldsymbol{M}\ddot{\boldsymbol{x}} + (\boldsymbol{C} + \boldsymbol{C}_c)\dot{\boldsymbol{x}} + (\boldsymbol{K} + \boldsymbol{K}_k)\boldsymbol{x} = \begin{bmatrix} K_1\Delta_1 \\ f_{sb} \end{bmatrix}, \tag{4.7}$$

where

$$\begin{gathered} \boldsymbol{M} = \begin{bmatrix} m & 0 \\ 0 & M \end{bmatrix}, \quad \boldsymbol{C} = \begin{bmatrix} C_1 & 0 \\ 0 & C \end{bmatrix}, \quad \boldsymbol{C}_c = \frac{c}{\mu^2}\boldsymbol{x}\boldsymbol{x}^T, \quad \boldsymbol{K} = \begin{bmatrix} K_1 + k & 0 \\ 0 & K + k \end{bmatrix}, \\ \boldsymbol{K}_k = -\frac{kl}{\mu}\boldsymbol{I}, \quad \boldsymbol{I} = \begin{bmatrix} 1 & 0 \\ 0 & 1 \end{bmatrix}, \quad \boldsymbol{x} = [x \quad y]^T, \quad \Delta_1 = X_0 - L_1, \\ \mu = \sqrt{x^2 + y^2} \end{gathered} \tag{4.8}$$

Here, Δ_1 represents the static extension of horizontal spring K_1 in the static state defined by Equation (4.1). The force f_{sb} denotes the reaction force from the beam to the lumped mass $2M$. The nonlinearity is given by μ which describes the oblique position of the spring, k and damper, c.

On the interaction section $\xi = 0$ between the beam and the nonlinear suspension unit, a dynamic equilibrium condition and a geometrical constraint condition are required, i.e.

Equilibrium: $$f_{bs} + f_{sb} = 0, \qquad -f_{bs} = f_{sb} = f, \tag{4.9}$$

Geometrical constraint: $$Y(0,t) = y(t), \tag{4.10}$$

which, when Equation (4.3) is used, is written in the mode form

$$\boldsymbol{Y}_0\boldsymbol{\Phi} = y, \qquad \boldsymbol{Y}_0 = \boldsymbol{Y}(0) \tag{4.11}$$

Equation (4.1) to (4.11) give the governing equations describing the dynamics of the integrated interaction system.

4.2.2 Non- dimensional dynamic equations

To derive the non-dimensional equations of the system, the following non-dimensional parameters are introduced

$$\bar{x}=\frac{x}{l},\ \bar{x}_0=\frac{x_0}{l},\ \bar{y}=\frac{y}{l},\ \bar{\Delta}_1=\frac{\Delta_1}{l},\ \bar{\Delta}=\frac{\Delta}{l},\ \bar{t}=\Omega_0 t,\ \bar{Y}=\frac{Y}{l},\ \bar{\xi}=\frac{\xi}{l},\ \bar{S}=\frac{S}{l},$$

$$\omega=\sqrt{(k+K_1)/m},\ \bar{\omega}=\frac{\Omega_0}{\omega},\ E_1=\frac{C_1}{2m\omega},\ \bar{m}=\frac{m}{M},\ \bar{\rho}=\frac{\rho l}{M},\omega=\sqrt{\omega_k^2+\omega_1^2},$$

$$\omega_k=\sqrt{\frac{k}{m}},\ \omega_1=\sqrt{\frac{K_1}{m}},\ \bar{\omega}_k=\frac{\omega_k}{\Omega_0},\ \bar{\omega}_1=\frac{\omega_1}{\Omega_0},\ \widetilde{\omega}_k=\frac{\omega_k}{\omega},\ \ \widetilde{\omega}_1=\frac{\omega_1}{\omega},$$

$$\widetilde{K}_1=\frac{K_1}{k+K_1},\ \bar{K}_1=\bar{m}\widetilde{K}_1\bar{\omega}^2=\frac{K_1\Omega_0^2}{M\omega^4},\ \bar{k}=\tilde{k}_K\bar{\Omega}^2=\bar{m}\tilde{k}_1\bar{\omega}^2=k\Omega_0^2/(M\omega^4),$$

$$\tilde{k}_1=\frac{k}{k+K_1},\tilde{k}_K=\frac{k}{k+K},\widetilde{c}_1=\frac{c}{C_1},\widetilde{c}_K=\frac{c}{C},\ \bar{\varepsilon}=\tilde{c}_K E\bar{\Omega}=\bar{m}\tilde{c}_1E_1\bar{\omega}=\frac{c\Omega_0}{2M\omega^2},\tag{4.12}$$

$$\Omega=\sqrt{(k+K)/M},\ \bar{\Omega}=\frac{\Omega_0}{\Omega},E=\frac{C}{2M\Omega},\bar{g}=\frac{g}{\Omega_0^2 l},\Omega=\sqrt{\Omega_k^2+\Omega_K^2},$$

$$\Omega_k=\sqrt{k/M},\ \Omega_K=\sqrt{K/M},\ \bar{\Omega}_k=\frac{\Omega_k}{\Omega_0},\ \bar{\Omega}_K=\frac{\Omega_K}{\Omega_0},\ \widetilde{\Omega}_k=\frac{\Omega_k}{\Omega},\ \widetilde{\Omega}_K=\Omega_K/\Omega,$$

$$\bar{F}_0=\frac{F_0}{M\Omega^2\ l},\ \bar{f}_1=\bar{K}_1\bar{\Delta}_1,\ \bar{f}=\frac{f_{sb}}{M\Omega^2\ l},\ \bar{\boldsymbol{m}}=\frac{\boldsymbol{m}}{M},\ \bar{\boldsymbol{\Phi}}=\frac{\boldsymbol{\Phi}}{l},\bar{\boldsymbol{\Lambda}}^2=\boldsymbol{\Lambda}^2/\Omega_0^2.$$

The dynamic equilibrium equation and boundary conditions of beam structure are

$$\bar{\boldsymbol{m}}\ddot{\bar{\boldsymbol{\Phi}}}+\bar{\boldsymbol{m}}\bar{\boldsymbol{\Lambda}}^2\bar{\boldsymbol{\Phi}}=\boldsymbol{R}\bar{\boldsymbol{f}}+\bar{\boldsymbol{F}}_0,\tag{4.13}$$

where

$$\boldsymbol{R}=[\boldsymbol{0}\quad -\boldsymbol{Y}_0^T],\bar{\boldsymbol{F}}_0=\boldsymbol{Y}_F^T\bar{F}_0\,\bar{cos}\,t\,,\boldsymbol{Y}_F=\boldsymbol{Y}(\xi_0),\boldsymbol{Y}_0\bar{\boldsymbol{\Phi}}=\bar{y}$$

The dynamic equilibrium equation of the nonlinear supporting unit is

$$\bar{\boldsymbol{M}}\ddot{\boldsymbol{q}}+2[\bar{\boldsymbol{M}}\bar{\boldsymbol{\omega}}\boldsymbol{E}+\boldsymbol{\varepsilon}(\boldsymbol{q})]\dot{\boldsymbol{q}}+[\bar{\boldsymbol{M}}\bar{\boldsymbol{\omega}}^2+\boldsymbol{k}(\boldsymbol{q})+\boldsymbol{k}_1(\boldsymbol{q})]\boldsymbol{q}=\bar{\boldsymbol{f}},\tag{4.14}$$

where

$$\bar{\boldsymbol{M}} = \begin{bmatrix} \bar{m} & 0 \\ 0 & 1 \end{bmatrix}, \bar{\boldsymbol{\omega}} = \begin{bmatrix} \bar{\omega} & 0 \\ 0 & \bar{\Omega} \end{bmatrix}, \boldsymbol{E} = \begin{bmatrix} E_1 & 0 \\ 0 & E \end{bmatrix}, \boldsymbol{I} = \begin{bmatrix} 1 & 0 \\ 0 & 1 \end{bmatrix}, \boldsymbol{I}_1 = \begin{bmatrix} 1 & 0 \\ 0 & 0 \end{bmatrix},$$
$$\boldsymbol{q} = \begin{bmatrix} q_1 \\ q_2 \end{bmatrix} = \begin{bmatrix} \bar{x} \\ \bar{y} \end{bmatrix}, \tag{4.15}$$
$$\boldsymbol{\varepsilon}(\boldsymbol{q}) = \frac{\bar{\varepsilon}}{\bar{\mu}^2}\boldsymbol{q}\boldsymbol{q}^T, \boldsymbol{k}(\boldsymbol{q}) = -\frac{\bar{k}}{\bar{\mu}}\boldsymbol{I}, \bar{\boldsymbol{f}} = \begin{bmatrix} 0 \\ \bar{f} \end{bmatrix}, \boldsymbol{k}_1(\boldsymbol{q}) = -\frac{\bar{f}_1}{q_1}\boldsymbol{I}_1, \bar{\mu} = \sqrt{\boldsymbol{q}^T\boldsymbol{q}}$$

Here, $\boldsymbol{\varepsilon}(\boldsymbol{q})$ and $\boldsymbol{k}(\boldsymbol{q})$ represent a nonlinear damping matrix and a nonlinear stiffness matrix of the system, respectively.

4.2.3 Integrated coupling matrix equation

Combining Equation (4.13) and (4.14), the integrated coupling equation of the system in matrix form is obtained

$$\hat{\boldsymbol{M}}\ddot{\boldsymbol{Q}} + (\hat{\boldsymbol{C}}^L + \hat{\boldsymbol{C}}^N)\dot{\boldsymbol{Q}} + (\hat{\boldsymbol{K}}^L + \hat{\boldsymbol{K}}^N)\boldsymbol{Q} = \hat{\boldsymbol{F}}_0 \tag{4.16}$$

where

$$\boldsymbol{Q} = \begin{bmatrix} q_1 \\ \bar{\boldsymbol{\Phi}} \end{bmatrix}, \boldsymbol{q} = \boldsymbol{T}\boldsymbol{Q}, \hat{\boldsymbol{M}} = \begin{bmatrix} \bar{m} & \boldsymbol{0}^T \\ \boldsymbol{0} & \bar{\boldsymbol{Y}} + \bar{m}\boldsymbol{Y}_0 \end{bmatrix}, \boldsymbol{T} = \begin{bmatrix} 1 & 0 \\ \boldsymbol{0} & \boldsymbol{Y}_0 \end{bmatrix}, \hat{\boldsymbol{F}}_0 = \begin{bmatrix} 0 \\ \bar{\boldsymbol{F}}_0 \end{bmatrix},$$
$$\hat{\boldsymbol{C}}^N = 2\boldsymbol{T}^T\boldsymbol{\varepsilon}(\boldsymbol{q})\boldsymbol{T}, \hat{\boldsymbol{C}}^L = 2\boldsymbol{T}^T\bar{\boldsymbol{M}}\bar{\boldsymbol{\omega}}\boldsymbol{E}\boldsymbol{T} \tag{4.17}$$
$$\hat{\boldsymbol{K}}^L = \{\mathrm{diag}(0, \bar{\mathbf{m}}\bar{\boldsymbol{\Lambda}}^2) + \boldsymbol{T}^T\bar{\boldsymbol{M}}\bar{\boldsymbol{\omega}}^2\boldsymbol{T}\}, \hat{\boldsymbol{K}}^N = \boldsymbol{T}^T[\boldsymbol{k}(\boldsymbol{q}) + \boldsymbol{k}_1(\boldsymbol{q})]\boldsymbol{T}$$

The total degree of freedom of this system is $1+N$ where N is the mode number chosen to describe the beam motion. Equation (4.16) can be rewritten in the state space form

$$\begin{cases} \dot{\boldsymbol{Q}} = \boldsymbol{P} \\ \dot{\boldsymbol{P}} = \hat{\boldsymbol{M}}^{-1}\{\hat{\boldsymbol{F}}_0 - (\hat{\boldsymbol{C}}^L + \hat{\boldsymbol{C}}^N)\boldsymbol{P} - (\hat{\boldsymbol{K}}^L + \hat{\boldsymbol{K}}^N)\boldsymbol{Q}\} \end{cases} \tag{4.18}$$

Here, the super-indices "L" and "N" identify the linear parts and nonlinear parts of the matrices, respectively. The nonlinearity is given by by $\boldsymbol{\varepsilon}(\boldsymbol{q})$ and $\boldsymbol{k}(\boldsymbol{q})$ which represents a nonlinear damping matrix and a nonlinear stiffness matrix as shown in Equation (4.14) and Equation (4.15). The coupling matrix in Equation (4.16) describes the dynamics of the integrated interaction system. Based on this set of equations, we can investigate the coupling mechanism between the elastic beam and the nonlinear suspension unit.

4.3 Nonlinear behaviour of integrated coupling system

4.3.1 Equilibrium points

The static equilibrium points $\boldsymbol{Q}_0 = [q_{10} \quad \bar{\boldsymbol{\Phi}}_0]^T$ and $\bar{\boldsymbol{\Phi}}_0 = [q_{20} \quad \mathbf{0}^T]^T$ of the system can be derived from Equation (4.16) by vanishing velocity $\dot{\boldsymbol{Q}}$, accelerations $\ddot{\boldsymbol{Q}}$ and external force $\hat{\boldsymbol{F}}_0$ of the system, that is

$$\left(\bar{m}\bar{\omega}^2 - \frac{\bar{k}}{\bar{\mu}_0} - \frac{\bar{f}_1}{q_{10}}\right) q_{10} = 0, \;\; \bar{\mu}_0 = \sqrt{q_{10}^2 + q_{20}^2}, \; \eta_1 = cos\vartheta = \frac{q_{10}}{\bar{\mu}_0},$$
$$\eta_2 = sin\vartheta = q_{20}/\bar{\mu}_0, \tag{4.19}$$
$$\left\{ \begin{bmatrix} \bar{M}_{11} & 0 & \cdots & 0 \\ 0 & \bar{M}_{22} & \cdots & 0 \\ \vdots & \vdots & \ddots & \vdots \\ 0 & 0 & \cdots & \bar{M}_{NN} \end{bmatrix} \begin{bmatrix} 0 \\ \bar{\Omega}_2^2 \\ \vdots \\ \bar{\Omega}_N^2 \end{bmatrix} + (\bar{\Omega}^2 - \bar{k}/\bar{\mu}_0) \begin{bmatrix} 1 & Y_{20} & \cdots & Y_{N0} \\ Y_{20} & Y_{20}^2 & \cdots & Y_{20}Y_{N0} \\ \vdots & \vdots & \ddots & \vdots \\ Y_{N0} & Y_{N0}Y_{20} & \cdots & Y_{N0}^2 \end{bmatrix} \right\} \begin{bmatrix} q_{20} \\ 0 \\ \vdots \\ 0 \end{bmatrix} = 0$$

Here, $0 \le \vartheta \le \pi/2$ represents the angle $\angle oBM$ between *o-x* axis and the right inclined spring. A positive value $q_{20} > 0$ or $\eta_2 > 0$ implies the equilibrium point is located on the positive *o-y* axis. This set of equations is nonlinear. In general, an iteration approach is required to obtain its solution. However, as given in Equation (4.2), we have chosen the origin of reference system $o - xy$ at its static equilibrium position with $q_{10} = \bar{x}_0$ and $q_{20} = 0$, which gives the equilibrium point (1). For the case of $q_{20} \neq 0$, the second equation in (4.19) require $\bar{\Omega}^2 - \bar{k}/\bar{\mu}_0 = 0$, which, when substituted into the first equation in (4.19) gives the values of q_{10}. Figure 4.3 illustrates the configuration of the system in 3 different equilibrium positions at their respective equilibrium points and Table 4.1 lists the equilibrium points of the system.

Table 4.1 The equilibrium points (β =1,2,3) of the system

β	Horizontal coordinate		Vertical coordinate		$\bar{\mu}_0^{(\beta)}$
	$q_{10}^{(\beta)}$	$\eta_1^{(\beta)}$	$q_{20}^{(\beta)}$	$\eta_2^{(\beta)}$	
1	$(\bar{f}_1 + \bar{k})/(\bar{m}\bar{\omega}^2) = \tilde{k}_1 + \tilde{K}_1\bar{\Delta}_1$	+1	0	0	$q_{10}^{(1)} = \tilde{k}_1 + \tilde{K}_1\bar{\Delta}_1$
2	$\bar{f}_1/(\bar{m}\bar{\omega}^2 - \bar{\Omega}^2)$	$q_{10}^{(2)}/\bar{\mu}_0^{(2)}$	$+\sqrt{\bar{\mu}_0^{2(2)} - q_{10}^{2(2)}}$	$q_{20}^{(2)}/\bar{\mu}_0^{(2)}$	$\bar{k}/\bar{\Omega}^2 = \tilde{k}_K$
3	$\bar{f}_1/(\bar{m}\bar{\omega}^2 - \bar{\Omega}^2)$	$q_{10}^{(3)}/\bar{\mu}_0^{(3)}$	$-\sqrt{\bar{\mu}_0^{2(3)} - q_{10}^{2(3)}}$	$q_{20}^{(3)}/\bar{\mu}_0^{(3)}$	$\bar{k}/\bar{\Omega}^2 = \tilde{k}_K$

Physically, at an equilibrium point(β), the mass M and m are located at point $q_{20}^{(\beta)}$ on the vertical axis and point $q_{10}^{(\beta)}$ on the horizontal axis, respectively, while the beam is in its static deformation state with its middle point O follows the mass M located at a corresponding position. Figure 4.2 shows the circle governing the equilibrium points (η_1, η_2). Each point (η_1, η_2) on this circle defines an equilibrium point as well as the corresponding parameters of the system. For example, $\eta_2 = 0$ gives point (1) while $\eta_2 \neq 0$ define points (2) and (3).

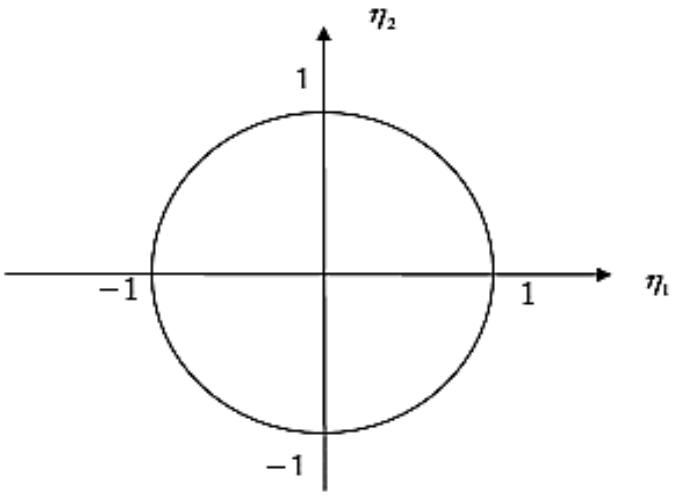

Figure 4.2 The circle governing the static equilibrium points

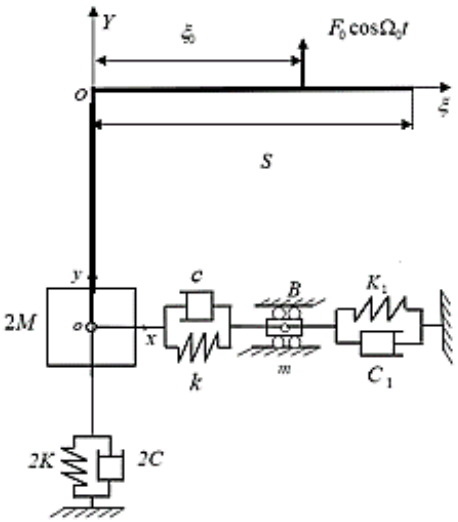

(a)

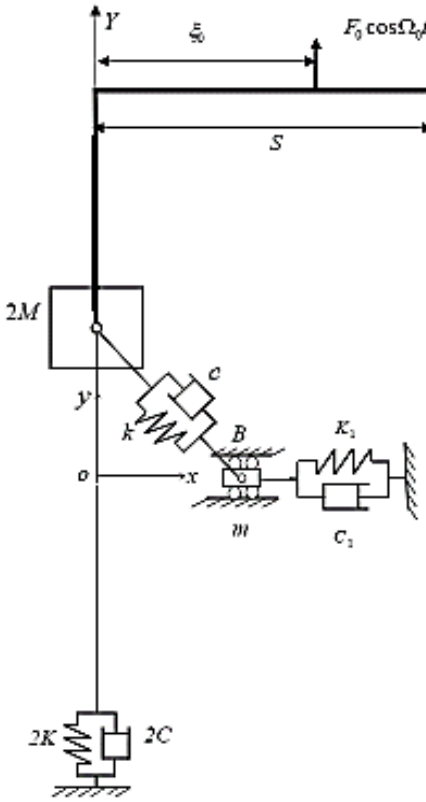

(b)

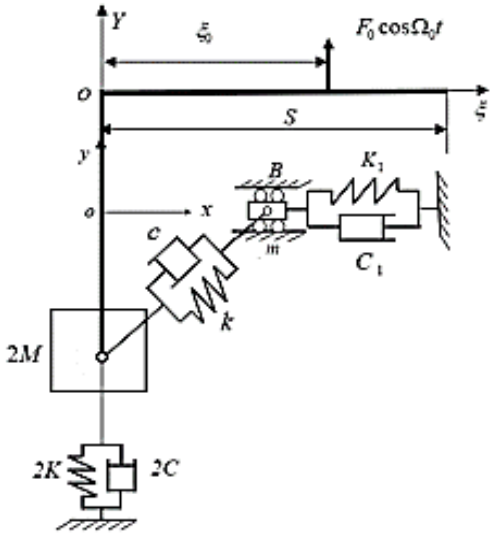

(c)

Figure 4.3 (a) Equilibrium position 1, (b) Equilibrium position 2, (c) Equilibrium position 3 of the system

4.3.2 Stability and frequency of small vibrations about equilibrium points

Designs of suspension systems concern two important requirements. First, the designed system has a stable static equilibrium position in its working environments and second the system has a particular required dynamic stiffness, very high or very low, measured by the supporting frequency of small vibrations of the system about the static equilibrium point. To reveal these characteristics, we must investigate the behaviour about each equilibrium point. To this end, we can examine the eigenvalues κ_I of the Jacobian matrix of the system at each point from Equation (4.18) or the frequencies $i\breve{\Omega}_I = \kappa_I$ of small free vibrations of the system about each point using Equation (4.16). Here, we consider vector $\boldsymbol{Q} = \boldsymbol{Q}_0 + \widetilde{\boldsymbol{Q}}$ in Equation (4.16) to derive a linearized equation at point $\boldsymbol{Q}_0$ to describe small vibrations of the system about this point.

$$\begin{aligned}\hat{\boldsymbol{M}}\ddot{\widetilde{\boldsymbol{Q}}} + \left[\hat{\boldsymbol{C}}^L + \hat{\boldsymbol{C}}^N(\boldsymbol{q}_0)\right]\dot{\widetilde{\boldsymbol{Q}}} + \left[\hat{\boldsymbol{K}}^L + \hat{\boldsymbol{K}}^N(\boldsymbol{q}_0) + \breve{\boldsymbol{K}}(\boldsymbol{q}_0)\right]\widetilde{\boldsymbol{Q}} \\ = \hat{\boldsymbol{F}}_0, \breve{\boldsymbol{K}}(\boldsymbol{q}_0) = \boldsymbol{T}^T\left(\frac{\bar{k}}{\bar{\mu}_0^3}\boldsymbol{q}_0\boldsymbol{q}_0^T + \frac{\bar{f}_1}{q_{10}}\boldsymbol{I}_1\right)\boldsymbol{T}\end{aligned} \tag{4.20}$$

Based on the equilibrium points given in Table 4.1 in association with Equation (4.16) and Equation (4.18), we obtain the following matrices at a point (β)

$$\begin{aligned}\hat{\boldsymbol{K}}^L = \begin{bmatrix}\bar{m}\bar{\omega}^2 & \boldsymbol{0}^T \\ \boldsymbol{0} & \bar{\boldsymbol{m}}\bar{\boldsymbol{\Lambda}}^2 + \bar{\Omega}^2\bar{\boldsymbol{Y}}\end{bmatrix}, \hat{\boldsymbol{K}}^N(\boldsymbol{q}_0) = -\frac{\bar{k}}{\bar{\mu}_0^{(\beta)}}\begin{bmatrix}1 + \dfrac{\bar{f}_1}{\eta_1^{(\beta)}\bar{k}} & 0 \\ 0 & \bar{\boldsymbol{Y}}\end{bmatrix}, \\ \hat{\boldsymbol{C}}^L = 2\begin{bmatrix}\bar{m}\bar{\omega}E_1 & \boldsymbol{0}^T \\ \boldsymbol{0} & \bar{\Omega}E\bar{\boldsymbol{Y}}\end{bmatrix}, \\ \breve{\boldsymbol{K}}(\boldsymbol{q}_0) = \frac{\bar{k}}{\bar{\mu}_0^{(\beta)}}\begin{bmatrix}\eta_1^{(\beta)2} + \dfrac{\bar{f}_1}{\eta_1^{(\beta)}\bar{k}} & \eta_1^{(\beta)}\eta_2^{(\beta)}\boldsymbol{Y}_0 \\ \eta_1^{(\beta)}\eta_2^{(\beta)}\boldsymbol{Y}_0^T & \eta_2^{(\beta)2}\bar{\boldsymbol{Y}}\end{bmatrix}, \\ \hat{\boldsymbol{C}}^N(\boldsymbol{q}_0) = 2\bar{m}\tilde{c}_1E_1\bar{\omega}\begin{bmatrix}\eta_1^{(\beta)2} & \eta_1^{(\beta)}\eta_2^{(\beta)}\boldsymbol{Y}_0 \\ \eta_1^{(\beta)}\eta_2^{(\beta)}\boldsymbol{Y}_0^T & \eta_2^{(\beta)2}\bar{\boldsymbol{Y}}\end{bmatrix}\end{aligned} \tag{4.21}$$

Substituting Equation (4.21) in association with the definition of $\bar{m}E_1\bar{\omega}\tilde{c}_1$ and $\tilde{c}_K$ in Equation (4.12) into Equation (4.20), we obtain an equation describing free vibrations about points (β) as follows

$$\widehat{\boldsymbol{M}}\ddot{\widehat{\boldsymbol{Q}}} + 2\widehat{\boldsymbol{\Pi}}\dot{\widehat{\boldsymbol{Q}}} + \widehat{\boldsymbol{\Lambda}}\widehat{\boldsymbol{Q}} = \boldsymbol{0},$$

$$\widehat{\boldsymbol{\Lambda}} = \begin{bmatrix} \bar{m}\bar{\omega}^2 - \dfrac{(1-\eta_1^2)\bar{k}}{\bar{\mu}_0} & \dfrac{\eta_1\eta_2\bar{k}}{\bar{\mu}_0\boldsymbol{Y}_0} \\ \dfrac{\eta_1\eta_2\bar{k}}{\bar{\mu}_0\boldsymbol{Y}_0^T} & \bar{\boldsymbol{m}}\bar{\boldsymbol{\Lambda}}^2 + \left[\bar{\Omega}^2 - \dfrac{(1-\eta_2^2)\bar{k}}{\bar{\mu}_0}\right]\bar{\boldsymbol{Y}} \end{bmatrix}, \tag{4.22}$$

$$\widehat{\boldsymbol{Q}} = [\tilde{q}_1 \quad \tilde{\boldsymbol{\Phi}}^T], \widehat{\boldsymbol{M}} = \begin{bmatrix} \bar{m} & \boldsymbol{0}^T \\ \boldsymbol{0} & \bar{\boldsymbol{Y}} + \bar{\boldsymbol{m}} \end{bmatrix},$$

$$\widehat{\boldsymbol{\Pi}} = \begin{bmatrix} \bar{m}\bar{\omega}E_1(1+\tilde{c}_1\eta_1^2) & \bar{m}E_1\bar{\omega}\tilde{c}_1\eta_1\eta_2\boldsymbol{Y}_0 \\ \bar{\Omega}E\tilde{c}_K\eta_1\eta_2\boldsymbol{Y}_0^T & \bar{\Omega}E(1+\tilde{c}_K\eta_2^2)\bar{\boldsymbol{Y}} \end{bmatrix}$$

Here, for simplifying the equation expression, we have omitted superscript (β) to identify an equilibrium point listed in Table 4.1, but we need to remember that the values of η_1, η_2 and $\bar{\mu}_0$ are related with (β).

4.3.2.1 Natural vibrations

The natural frequencies of the system are governed by the following real eigenvalue equations of the system

$$\left|\widehat{\boldsymbol{\Lambda}} - \hat{\bar{\Omega}}^2\widehat{\boldsymbol{M}}\right| = 0, \qquad (\widehat{\boldsymbol{\Lambda}} - \hat{\bar{\Omega}}^2\widehat{\boldsymbol{M}})\widehat{\boldsymbol{Q}} = 0, \tag{4.23}$$

from which we can obtain the natural frequencies and corresponding modes of the system in the following matrix form,

$$\widehat{\bar{\boldsymbol{\Lambda}}} = \mathrm{diag}\left(\widehat{\bar{\Omega}}_I\right), \boldsymbol{\Psi} = [\widehat{\boldsymbol{Q}}_1 \quad \widehat{\boldsymbol{Q}}_2 \quad \cdots \quad \widehat{\boldsymbol{Q}}_{N+1}], \boldsymbol{\Psi}^T\widehat{\boldsymbol{M}}\boldsymbol{\Psi} = \boldsymbol{I}, \qquad \boldsymbol{\Psi}^T\widehat{\boldsymbol{\Lambda}}\boldsymbol{\Psi} = \widehat{\bar{\boldsymbol{\Lambda}}}^2 \tag{4.24}$$

For point (1) with $(\eta_1 = 1, \eta_2 = 0)$, so that Equation (4.23) becomes

$$(\bar{m}\bar{\omega}^2 - \hat{\bar{\Omega}}^{(1)2}\bar{m})\tilde{q}_1 = 0, \qquad \hat{\bar{\Omega}}_1^{(1)2} = \bar{\omega}^2, \tag{4.25}$$

$$\{\bar{\boldsymbol{m}}\bar{\boldsymbol{\Lambda}}^2 + [\bar{\Omega}^2 - \bar{k}/\bar{\mu}_0]\bar{\boldsymbol{Y}} - \hat{\bar{\Omega}}^{(1)2}(\bar{\boldsymbol{Y}} + \bar{\boldsymbol{m}})\}\tilde{\boldsymbol{\Phi}} = 0 \tag{4.26}$$

There is no coupling between the vibrations in the horizontal and vertical directions. Equation (4.25) directly gives the natural frequency $\hat{\bar{\Omega}}_1^{(1)}$in the horizontal direction of the system. However, Equation (4.26) still needs to be solved using numerical methods, which will provide

the N natural frequencies $\hat{\bar{\Omega}}_I^{(1)}$, $(I = 2,3,\cdots,N+1)$, of the beam affected by the nonlinear unit. Because of no coupling in Equation (4.25) and (4.26), the corresponding mode vector matrix takes the following form

$$\boldsymbol{\Psi}^{(1,2)} = \begin{bmatrix} \psi_1 & \mathbf{0}^T \\ \mathbf{0} & \widetilde{\boldsymbol{\Psi}} \end{bmatrix}^{(1)}. \tag{4.27}$$

At points (2,3) of ($\eta_2 \neq 0$), the stiffness matrix $\widehat{\boldsymbol{\Lambda}}$ is not diagonal, and there is couplings between the horizontal and vertical directions, so that we have to solve Equation (4.23) numerically for the natural frequencies $\hat{\bar{\Omega}}_I^{(2,3)}$, $(I = 1,2,\cdots,N+1)$, and corresponding mode matrix $\boldsymbol{\Psi}^{(2,3)}$ of the system.

Solving Equation (4.26) and (4.23) numerically, we can obtain the first 5 vertical frequencies and modes at points β = (1), (2, 3).

4.3.2.2 Free vibrations

Both the damping matrix and stiffness matrix in Equation (4.22) are non-diagonal, except for point (1) with $\eta_2 = 0$. For our convenience of theoretical analysis, we may use the mode transformation

$$\widehat{\boldsymbol{Q}} = \boldsymbol{\Psi}^{(\beta)}\breve{\boldsymbol{Q}}, \qquad \breve{\boldsymbol{Q}} = [\breve{q}_1 \quad \breve{\boldsymbol{\Phi}}^T], \qquad (\beta = 1,2,3) \tag{4.28}$$

to transform Equation (4.23) into a form

$$\ddot{\breve{\boldsymbol{Q}}} + 2\breve{\boldsymbol{\Pi}}^{(\beta)}\dot{\breve{\boldsymbol{Q}}} + \widehat{\breve{\boldsymbol{\Lambda}}}^{(\beta)2}\breve{\boldsymbol{Q}} = \mathbf{0}, \qquad \breve{\boldsymbol{\Pi}}^{(\beta)} = \boldsymbol{\Psi}^{(\beta)T}\widehat{\boldsymbol{\Pi}}^{(\beta)}\boldsymbol{\Psi}^{(\beta)} \tag{4.29}$$

in which there is only damping matrix being non-diagonal. The frequencies of free vibrations and corresponding modes are governed by the following complex eigenvalue problem

$$\left|\widehat{\breve{\boldsymbol{\Lambda}}}^{(\beta)2} + 2i\breve{\Omega}^{(\beta)}\breve{\boldsymbol{\Pi}}^{(\beta)} - \breve{\Omega}^{(\beta)2}\boldsymbol{I}\right| = \mathbf{0}, \tag{4.30}$$

$$(\widehat{\breve{\boldsymbol{\Lambda}}}^{(\beta)2} + 2i\breve{\Omega}^{(\beta)}\breve{\boldsymbol{\Pi}}^{(\beta)} - \breve{\Omega}^{(\beta)2}\boldsymbol{I})\breve{\boldsymbol{Q}} = 0$$

Since the damping matrix $\breve{\boldsymbol{\Pi}}^{(\beta)}$is not diagonal, Equation (4.30) needs to be solved by numerical method. As an approximation, we may neglect the non-diagonal terms in the damping matrix to obtain the following approximate complex frequencies

$$\breve{\Omega}_I^{(\beta)} \approx i\breve{E}_I^{(\beta)}\hat{\bar{\Omega}}_I^{(\beta)} \pm \hat{\bar{\Omega}}_I^{(\beta)}\sqrt{1 - \breve{E}_I^{(\beta)2}}, \breve{E}_I^{(\beta)} = \breve{\Pi}_{II}^{(\beta)}/\hat{\bar{\Omega}}_I^{(\beta)}, (I = 1,2,\cdots,N+1) \tag{4.31}$$

For point (1) in association with Equation (4.28), Equation (4.29) reduces to

$$\breve{\boldsymbol{\Pi}}^{(1)}=\begin{bmatrix}\psi_1 & \mathbf{0}^T\\ \mathbf{0} & \tilde{\boldsymbol{\Psi}}^T\end{bmatrix}^{(1)}\begin{bmatrix}\bar{m}\bar{\omega}E_1(1+\tilde{c}_1) & \mathbf{0}^T\\ \mathbf{0} & \bar{\Omega}E\bar{\boldsymbol{Y}}\end{bmatrix}\begin{bmatrix}\psi_1 & \mathbf{0}^T\\ \mathbf{0} & \tilde{\boldsymbol{\Psi}}\end{bmatrix}^{(1)}=\begin{bmatrix}\breve{\Pi}_{11}^{(1)} & \mathbf{0}^T\\ \mathbf{0} & \tilde{\boldsymbol{\Pi}}^{(1)}\end{bmatrix},\tag{4.32}$$

$$\breve{\Pi}_{11}^{(1)}=\bar{m}\bar{\omega}E_1(1+\tilde{c}_1)\psi_1^{(1)2},\qquad \tilde{\boldsymbol{\Pi}}^{(1)}=\bar{\Omega}E\tilde{\boldsymbol{\Psi}}^{(1)T}\bar{\boldsymbol{Y}}\tilde{\boldsymbol{\Psi}}^{(1)}.$$

As a result of this, Equation (4.30) becomes

$$(\hat{\breve{\Omega}}^{(1,2)2}+2i\breve{\Omega}^{(1,2)}\breve{\Pi}_{11}^{(1,2)}-\breve{\Omega}^{(1,2)2})\breve{q}_1=0,\tag{4.33}$$

$$\{\hat{\tilde{\boldsymbol{\Lambda}}}_{\varphi}^{2}+2i\breve{\Omega}^{(1,2)}\tilde{\boldsymbol{\Pi}}^{(1,2)}-\breve{\Omega}^{(1,2)2}\boldsymbol{I}\}\breve{\boldsymbol{\Phi}}=\mathbf{0},\quad \hat{\tilde{\boldsymbol{\Lambda}}}_{\varphi}^{(1,2)}=\mathrm{diag}(\hat{\tilde{\Omega}}_{I=2,3,\cdots,N+1})\tag{4.34}$$

From these equations, we obtain the corresponding complex frequencies of free vibrations about point (1) as

$$\breve{\Omega}_1^{(1)}=i\breve{E}_1^{(1)}\hat{\breve{\Omega}}_1^{(1)}\pm\hat{\breve{\Omega}}_1^{(1)}\sqrt{1-\breve{E}_1^{(1)2}},\qquad \breve{E}_1^{(1)}=\breve{\Pi}_{11}^{(1)}/\hat{\breve{\Omega}}^{(1)}.\tag{4.35}$$

$$\breve{\Omega}_I^{(1)}\approx i\breve{E}_I^{(1)}\hat{\breve{\Omega}}_I^{(1)}\pm\hat{\breve{\Omega}}_I^{(1)}\sqrt{1-\breve{E}_I^{(1)2}},\breve{E}_I^{(1)}=\frac{\tilde{\Pi}_{II}^{(1)}}{\hat{\tilde{\Omega}}_I^{(1)}},\qquad (I=2,\cdots,N+1)\tag{4.36}$$

4.3.2.3 The solution for retaining only rigid mode

As an example for an analytical analysis, we retain only the rigid mode of the beam, so that we have

$$\boldsymbol{Y}_0=1,\quad \bar{\boldsymbol{Y}}=1,\quad \bar{\boldsymbol{m}}=\tilde{\rho}\tilde{S},\quad \bar{\boldsymbol{\Lambda}}^2=\bar{\tilde{\Omega}}_1^2=0,\quad \tilde{\boldsymbol{\Phi}}=\tilde{q}_2,\tag{4.37}$$

to reduce Equation (4.23) to

$$\begin{bmatrix}\bar{m} & 0\\ 0 & \bar{M}\end{bmatrix}\begin{bmatrix}\ddot{\breve{q}}_1\\ \ddot{\tilde{q}}_2\end{bmatrix}+2\begin{bmatrix}\Pi_{11} & \Pi_{12}\\ \Pi_{21} & \Pi_{22}\end{bmatrix}\begin{bmatrix}\dot{\breve{q}}_1\\ \dot{\tilde{q}}_2\end{bmatrix}+\begin{bmatrix}\Lambda_{11} & \Lambda_{12}\\ \Lambda_{21} & \Lambda_{22}\end{bmatrix}\begin{bmatrix}\tilde{q}_1\\ \tilde{q}_2\end{bmatrix}=\begin{bmatrix}0\\ 0\end{bmatrix},\bar{M}=1+\tilde{\rho}\tilde{S},\tag{4.38}$$

$$\Pi_{11}=\bar{m}\bar{\omega}E_1(1+\tilde{c}_1\eta_1^2),\bar{m}E_1\bar{\omega}\tilde{c}_1\eta_1\eta_2=\Pi_{12}=\Pi_{21}=\bar{\Omega}E\tilde{c}_K\eta_1\eta_2,\Pi_{22}=\bar{\Omega}E(1+\tilde{c}_K\eta_2^2),$$

$$\Lambda_{11}=\bar{m}\bar{\omega}^2-(1-\eta_1^2)\bar{k}/\bar{\mu}_0,\Lambda_{12}=\Lambda_{21}=\eta_1\eta_2\bar{k}/\bar{\mu}_0,\Lambda_{22}=\bar{\Omega}^2-(1-\eta_2^2)\bar{k}/\bar{\mu}_0.$$

The two natural frequencies obtained by solving the corresponding Equation (4.24) are as follows

$$\hat{\Omega}^{(\beta)2} = \{(\bar{\Lambda}_{11} + \bar{\Lambda}_{22}) \pm \sqrt{(\bar{\Lambda}_{11} + \bar{\Lambda}_{22})^2 - 4(\bar{\Lambda}_{11}\bar{\Lambda}_{22} - \bar{\Lambda}_{12}^2)}\}/2, \qquad \bar{\Lambda}_{11} = \Lambda_{11}/\bar{m}, \qquad \bar{\Lambda}_{22} = \Lambda_{22}/\bar{M}, \qquad \bar{\Lambda}_{12} = \Lambda_{12}/\sqrt{\bar{M}\bar{m}}. \tag{4.39}$$

Point($\beta = 1$): $\Lambda_{12} = 0 = \bar{\Lambda}_{12}$ due to $\eta_1 = 1, \eta_2 = 0$, we obtain

$$\hat{\Omega}_1^{(1)2} = \bar{\Lambda}_{11} = \Lambda_{11}/\bar{m}, \qquad \hat{\Omega}_1^{(1)} = \sqrt{\Lambda_{11}/\bar{m}}, \qquad \hat{\Omega}_2^{(1)2} = \bar{\Lambda}_{22} = \Lambda_{22}/\bar{M}, \qquad \hat{\Omega}_2^{(1)} = \sqrt{\Lambda_{22}/\bar{M}}, \tag{4.40}$$

which represents the natural frequencies of small vibrations of the system about point (1) in the horizontal and vertical directions, respectively.

Points ($\beta = 2,3$): since$\bar{\Lambda}_{12} > 0$, we have

$$\sqrt{(\bar{\Lambda}_{11} + \bar{\Lambda}_{22})^2 - 4(\bar{\Lambda}_{11}\bar{\Lambda}_{22} - \bar{\Lambda}_{12}^2)} > \sqrt{(\bar{\Lambda}_{11} + \bar{\Lambda}_{22})^2 - 4\bar{\Lambda}_{11}\bar{\Lambda}_{22}} = |\bar{\Lambda}_{11} - \bar{\Lambda}_{22}| \tag{4.41}$$

so that the solutions $\hat{\Omega}^{(\beta)2}$ of Equation (4.39) satisfy the following equation

$$\hat{\Omega}_1^{(2,3)2} < 0.5\{(\bar{\Lambda}_{11} + \bar{\Lambda}_{22}) - \sqrt{(\bar{\Lambda}_{11} - \bar{\Lambda}_{22})^2}\} = \mathrm{Min}(\hat{\Omega}_1^{(1)2}, \hat{\Omega}_2^{(1)2}) \qquad \hat{\Omega}_2^{(2,3)2} > 0.5\{(\bar{\Lambda}_{11} + \bar{\Lambda}_{22}) + \sqrt{(\bar{\Lambda}_{11} - \bar{\Lambda}_{22})^2}\} = \mathrm{Max}(\hat{\Omega}_1^{(1)2}, \hat{\Omega}_2^{(1)2}) \tag{4.42}$$

This implies that the lowest natural frequency about points ($\beta = 2,3$) is smaller than the lowest natural frequency about point (1) but the highest natural frequency about points ($\beta = 2,3$) is larger than the highest natural frequency about point (1).

4.3.2.4 Stability

The eigenvalues κ_I of the Jacobian matrix of Equation (4.18) at a point (β) are given by

$$\hat{\kappa}_I^{(\beta)} = i\hat{\Omega}_I^{(\beta)}, \qquad \breve{\kappa}_I^{(\beta)} = i\breve{\Omega}_I^{(\beta)}, \tag{4.43}$$

for natural vibrations and free vibrations, respectively. From Equation (4.31), we obtain the approximate eigenvalues

$$\breve{\kappa}_I^{(\beta)} \approx -\breve{E}_I^{(\beta)}\hat{\Omega}_I^{(\beta)} \pm i\hat{\Omega}_I^{(\beta)}\sqrt{1 - \breve{E}_I^{(\beta)2}}, \breve{E}_I^{(\beta)} = \breve{\Pi}_{II}^{(\beta)}/\hat{\Omega}_I^{(\beta)}, (I = 1,2,\cdots,N+1) \tag{4.44}$$

Based on the stability theory for nonlinear dynamical systems, we obtain the following conclusions. The eigenvalues in Equation (4.44) have only negative real parts confirm that the system is stable at point (β). If there is at least one eigenvalue with zero real part, the

corresponding equilibrium point (β) becomes a non-hyperbolic point, and any positive real number of eigenvalues cause unstability of the point (β). The characteristic of eigenvalues in Equation (4.44) depends on the natural frequency $\hat{\Omega}_I^{(\beta)}$ and damping $\breve{E}_I^{(\beta)}$ which are determined by parameters in Equation (4.23). For majority of engineering systems, there are a real natural frequency $\hat{\Omega}_I^{(\beta)}$ and small positive damping $\breve{E}_I^{(\beta)} < 1$, so that the free vibrations of the system about point (β) are stable damped vibrations. Figure 4.4 shows the free vibration of the system in time history and phase orbit. It can be seen that the response tends to equilibrium position.

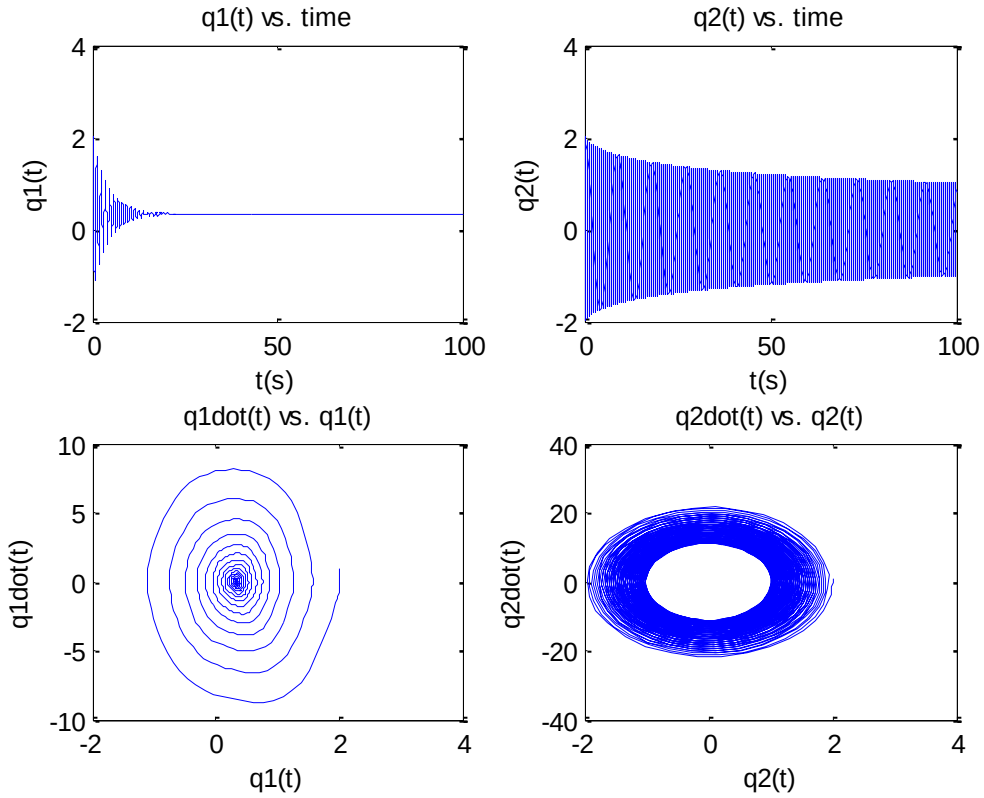

Figure 4.4 Free vibration time series and phase plots

4.3.3 Bifurcation

As an initial start for the bifurcation analysis of the system, the time series and phase plots of the system is first obtained.

From Equations (4.16) and (4.17) of the integrated coupling equation of the system, and retaining only the rigid mode of the beam with the condition as shown in Equation (4.37), we obtain

$$\ddot{q}_1 = \frac{\bar{f}_1}{\bar{m}} - \frac{2\bar{\varepsilon}}{\bar{m}\bar{\mu}} q_1 q_2 \dot{q}_2 - 2\bar{\omega} E_1 \dot{q}_1 - \frac{2\bar{\varepsilon}}{\bar{m}\bar{\mu}} q_1^2 \dot{q}_1 - \bar{\omega}^2 q_1 + \frac{\bar{k}}{\bar{m}\bar{\mu}} q_1 \tag{4.45}$$

$$\ddot{q}_2 = \frac{\bar{F}_0}{1+\bar{m}} - \frac{2\bar{\varepsilon}}{(1+\bar{m})\bar{\mu}} q_1 q_2 \dot{q}_1 - \frac{2\bar{\Omega} E q_2}{(1+\bar{m})} - \frac{2\bar{\varepsilon}}{(1+\bar{m})\bar{\mu}} q_2^2 \dot{q}_2 - \frac{\bar{\Omega}^2 q_2}{(1+\bar{m})} + \frac{\bar{k}}{(1+\bar{m})\bar{\mu}} q_2 \tag{4.46}$$

Equations (4.45) and (4.46) are inserted into Matlab using the 'ODE45' function (Matlab ODE solver based on a Runge-Kutta method) to obtain the time series and phase plots of the system.

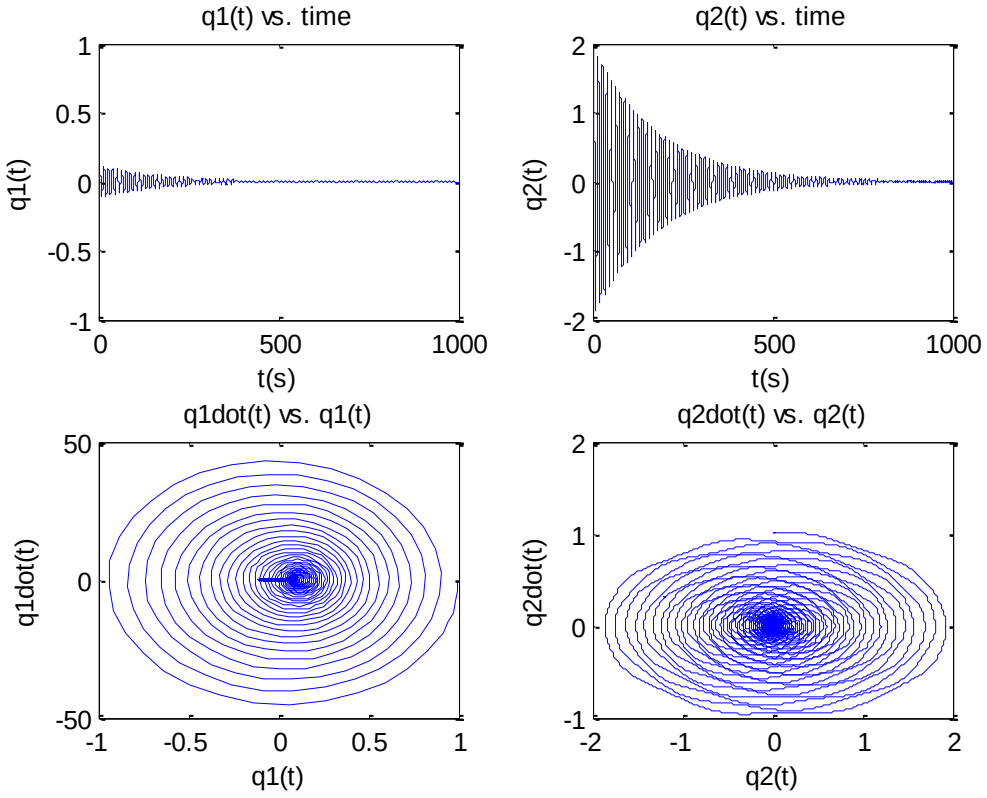

Figure 4.5 Time series and phase plots of the system using ODE45 function

From Figure 4.5, the phase plot of q_2 which illustrates the displacement against velocity of mass *M* across the y-axis is seen to split into two parts. This depicts the occurrence of period doubling bifurcations.

A 4th order Runge-Kutta (RK4) code (with fixed time step) has been developed also and compared with the results of the ODE45 obtained in Figure 4.5. Figure 4.6 to Figure 4.8 shows the time series and phase plots of the system using the RK4 method with time steps of 0.01,0.001 and 0.0001.

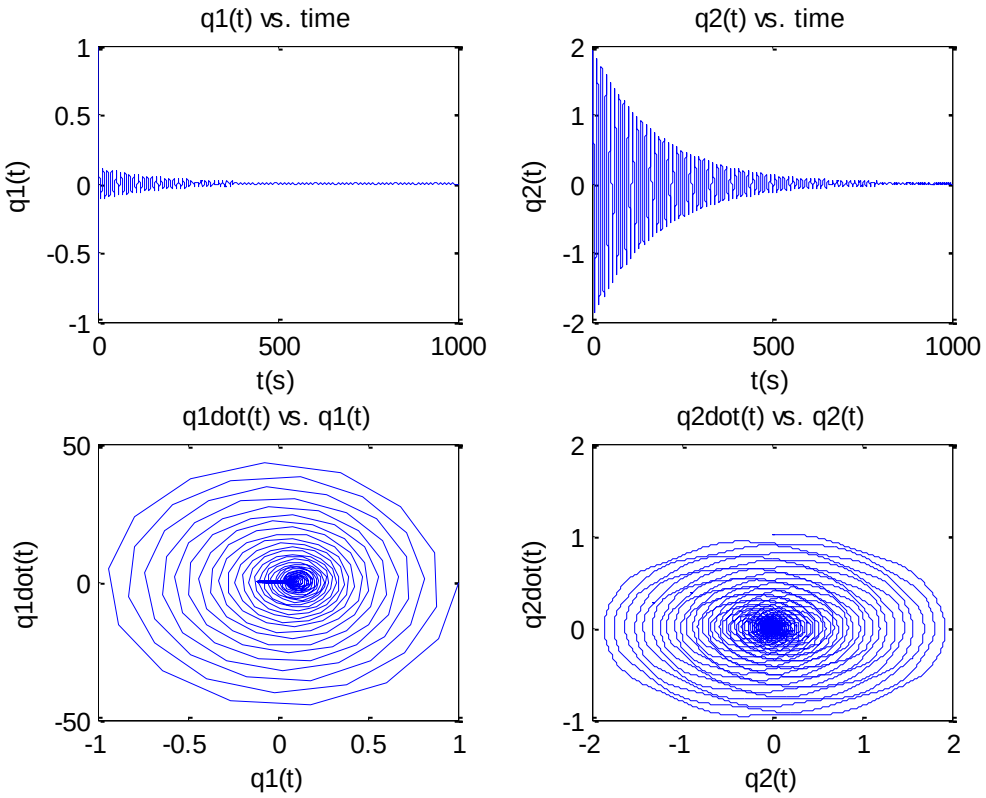

Figure 4.6 Time series and phase plots of the system using RK4 with time step, h= 0.01

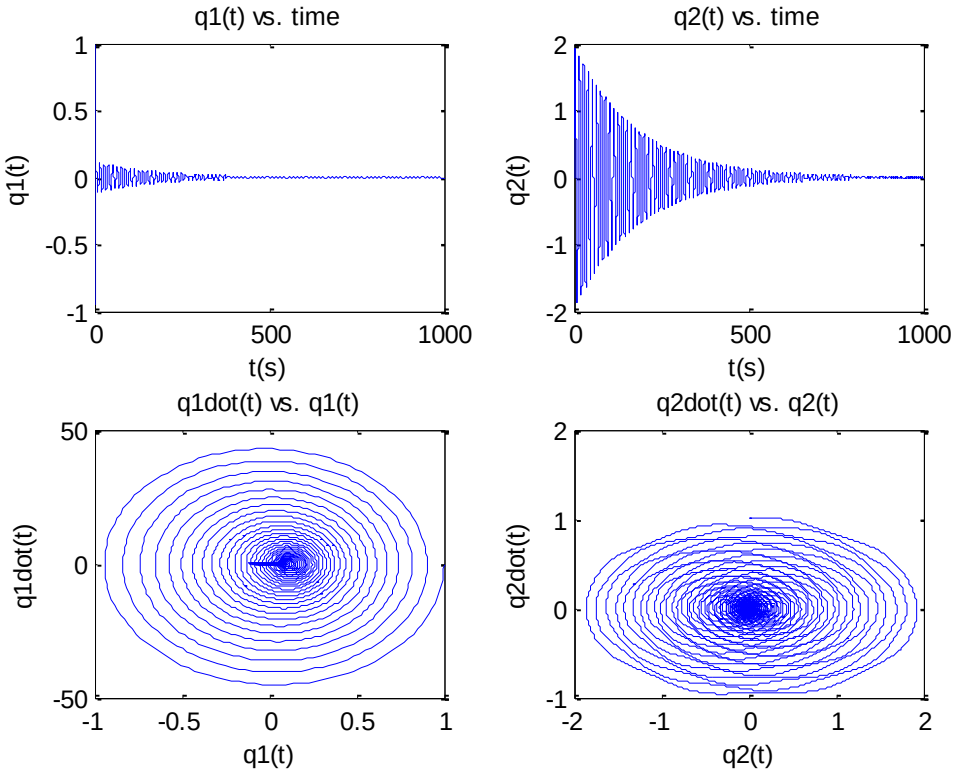

Figure 4.7 Time series and phase plots of the system using RK4 with time step, h=0.001

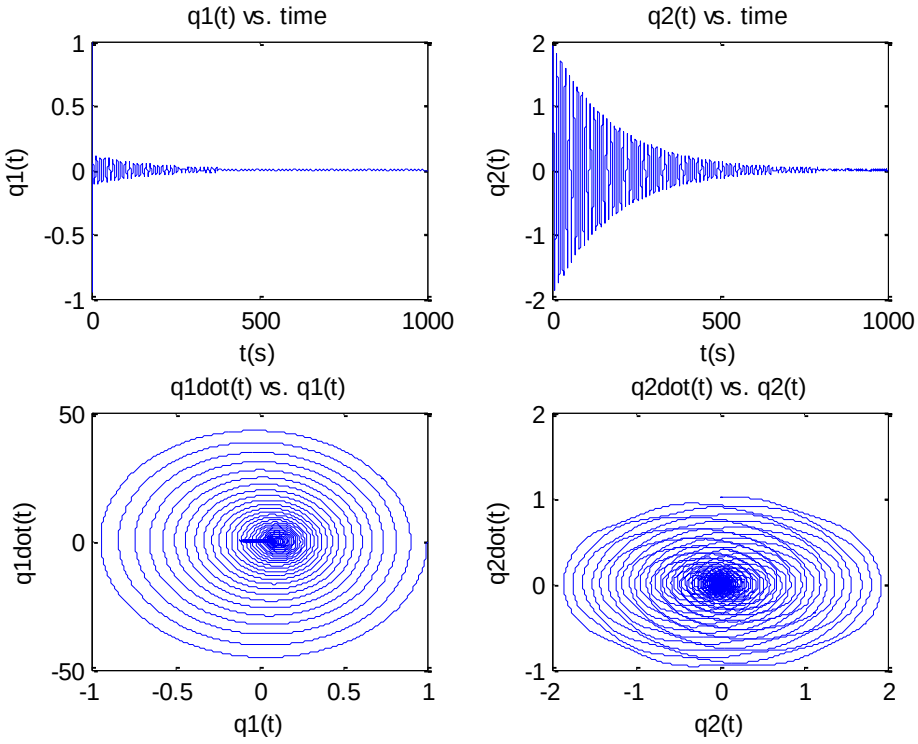

Figure 4.8 Time series and phase plots of the system using RK4 with time step, h=0.0001

From Figure 4.6, Figure 4.7 and Figure 4.8, it can be seen that as the time step is decreased, the results agree with the one obtained using ODE45 in Figure 4.5. For time step of 0.00001 the RK4 method takes a long time to run and uses up too much memory resulting in an error during simulation. Comparing the RK4 method to ODE45, the ODE45 method is faster and more accurate. This is because it uses a variable step and also uses both 4th and 5th order Runge-Kutta methods to obtain error estimates in each step. Therefore, ODE45 (variable time step) is used for the remaining of the thesis, as the method performs better than RK4 (fixed time step).

4.4 Interaction analysis

To derive the equations to reveal the influence of beam motions on the nonlinear suspension unit or vice versa, we can separately investigate the governing equation of the nonlinear unit or the beam by incorporating the effect of another side, the beam or the nonlinear unit. The interaction conditions in Equations (4.9) to (4.11) provide a bridge to obtain these equations as follows.

4.4.1 Equation governing the influence of beam motions on nonlinear suspension system

From Equation (4.13), it follows that

$$\ddot{\bar{\boldsymbol{\Phi}}} + \bar{\boldsymbol{\Lambda}}^2\bar{\boldsymbol{\Phi}} = \bar{\boldsymbol{m}}^{-1}\boldsymbol{R}\bar{\boldsymbol{f}} + \bar{\boldsymbol{m}}^{-1}\bar{\boldsymbol{F}}_0, \quad \boldsymbol{R} = [\boldsymbol{0} \quad -\boldsymbol{Y}_0^T], \tag{4.47}$$

which, when pre-multiplied by $\boldsymbol{Y}_0$, gives

$$\begin{aligned}\boldsymbol{Y}_0\ddot{\bar{\boldsymbol{\Phi}}} + \boldsymbol{Y}_0\bar{\boldsymbol{\Lambda}}^2\bar{\boldsymbol{\Phi}} &= \boldsymbol{Y}_0\bar{\boldsymbol{m}}^{-1}\boldsymbol{R}\bar{\boldsymbol{f}} + \boldsymbol{Y}_0\bar{\boldsymbol{m}}^{-1}\bar{\boldsymbol{F}}_0 \\ &= -m_b^{-1}\bar{f} + \boldsymbol{Y}_0\bar{\boldsymbol{m}}^{-1}\bar{\boldsymbol{F}}_0, \qquad m_b^{-1} = \boldsymbol{Y}_0\bar{\boldsymbol{m}}^{-1}\boldsymbol{Y}_0^T\end{aligned} \tag{4.48}$$

Since

$$m_b^{-1} = \boldsymbol{Y}_0\bar{\boldsymbol{m}}^{-1}\boldsymbol{Y}_0^T = \sum_{n=1}^{N}\bar{M}_{nn}^{-1}\,Y_{n0}^2 > 0, \tag{4.49}$$

we have

$$\begin{aligned}\bar{f} &= f_b\bar{F}_0\,\bar{cos}\,t - m_b\boldsymbol{Y}_0\ddot{\bar{\boldsymbol{\Phi}}} - m_b\boldsymbol{Y}_0\bar{\boldsymbol{\Lambda}}^2\bar{\boldsymbol{\Phi}} \\ &= f_b\bar{F}_0\,\bar{cos}\,t - m_b\ddot{\bar{y}} - k_b(\bar{\boldsymbol{\Phi}})\bar{y},\end{aligned} \tag{4.50}$$

where

$$k_b(\bar{\boldsymbol{\Phi}}) = m_b \frac{\boldsymbol{Y}_0 \bar{\boldsymbol{\Lambda}}^2 \bar{\boldsymbol{\Phi}}}{\boldsymbol{Y}_0 \bar{\boldsymbol{\Phi}}} = \frac{m_b \sum_{n=1}^{N} Y_{n0} \bar{\Omega}_n^2 \bar{\varphi}_n}{\sum_{n=1}^{N} Y_{n0} \bar{\varphi}_n}, f_b = m_b \boldsymbol{Y}_0 \bar{\boldsymbol{m}}^{-1} \boldsymbol{Y}_F^T. \tag{4.51}$$

Substituting Equation (4.50) into Equation (4.14), we obtain

$$\begin{gathered}(\bar{\boldsymbol{M}} + \boldsymbol{m}_b)\ddot{\boldsymbol{q}} + 2[\bar{\boldsymbol{M}}\bar{\boldsymbol{\omega}}\boldsymbol{E} + \boldsymbol{\varepsilon}(\boldsymbol{q})]\dot{\boldsymbol{q}} + \{\boldsymbol{k}_b + [\bar{\boldsymbol{M}}\bar{\boldsymbol{\omega}}^2 + \boldsymbol{k}(\boldsymbol{q}) + \boldsymbol{k}_1(\boldsymbol{q})]\}\boldsymbol{q} = \boldsymbol{f}_b, \\ \boldsymbol{m}_b = \text{diag}(0, m_b), \quad \boldsymbol{k}_b = \text{diag}(0, k_b), \quad \boldsymbol{f}_b = [0 \quad f_b]^T \bar{F}_0 \cos t.\end{gathered} \tag{4.52}$$

Here, m_b, k_b represent an additional dynamic mass and stiffness, respectively, which are added to the nonlinear suspension system by the beam due to their dynamic interactions. f_b defines a force factor at which the excitation force is added to the lumped mass. The values of these added parameters depend on the retained mode number of the beam. The added stiffness k_b also involves the dynamic response $\bar{\boldsymbol{\Phi}}$ of the beam. For a unit dynamic response of mode *n,* i.e. $\bar{\boldsymbol{\Phi}}^T = [0 \quad \cdots \quad 0 \quad \bar{\varphi}_n \quad 0 \quad \cdots \quad 0]^T$, the added mass and stiffness are respectively obtained by Equation (4.53) and (4.54)

$$m_b = \bar{M}_{nn} Y_{n0}^{-2}, \tag{4.53}$$

$$k_b(\bar{\varphi}_n) = m_b \bar{\Omega}_n^2 = \bar{M}_{nn} Y_{n0}^{-2} \bar{K}_{nn} / \bar{M}_{nn} = Y_{n0}^{-2} \bar{K}_{nn}. \tag{4.54}$$

Table 4.2 lists the added parameters affected by the number *N*=1∼5 of retained modes. Table 4.3 lists the added parameters affected by a unit dynamic response mode *n* = 1, 2, 3, 4, 5.

Table 4.2 The values of added parameters affected by retained mode number of the beam on the nonlinear suspension unit ($\bar{m}_b = \frac{m_b}{\bar{M}_{11}}, \xi_0 = 1$)

N	1	2	3	4	5
$\bar{m}_b$	1.0000	0.4036	0.2222	0.1538	0.1176
f_b	1.0000	-0.5776	0.3140	-0.2176	0.1664

Table 4.3 The values of added parameters affected by a unit dynamic response mode *n* of the beam on the nonlinear suspension unit

n	1	2	3	4	5
$m_b(\varphi_n)$	1.0000	0.6767	0.4943	0.5003	0.5000
$k_b(\varphi_n)$	0	67.67	1443	8908	30787

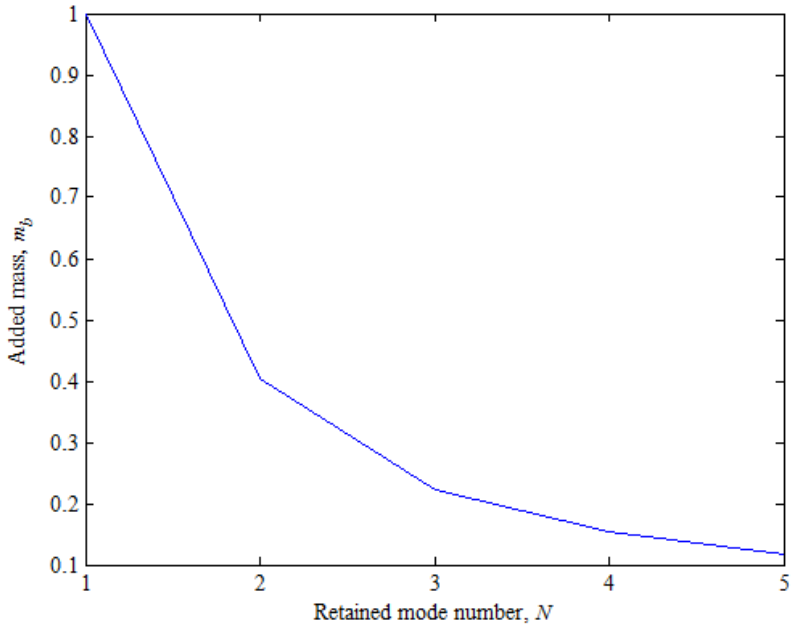

Figure 4.9 Graph of additional mass $\bar{m}_b$ with respect to retained mode number

From Figure 4.9, it can be seen that the additional dynamic mass, $\bar{m}_b$ decreases as the number of retained mode N increases. Each mode has a natural frequency associated with it. The natural frequency of the structure depends on the mass and stiffness distributions in the structure.

The equation of natural frequency is

$$\hat{\Omega}_n = \sqrt{\frac{K_{nn}}{M_{nn}}} \tag{4.55}$$

As the natural frequency increases, the mass decreases and vice versa. The value of force factor at which the excitation force is added to the lumped mass greatly depends on the point, ξ_0, at which the excitation force is applied to on the beam. From Figure 4.10, at $\xi_0 = 1$, the force factor is a positive value at odd numbers of retained modes and negative at even numbers of retained modes. The positive value defines a pulling force while the negative value implies a compressed force.

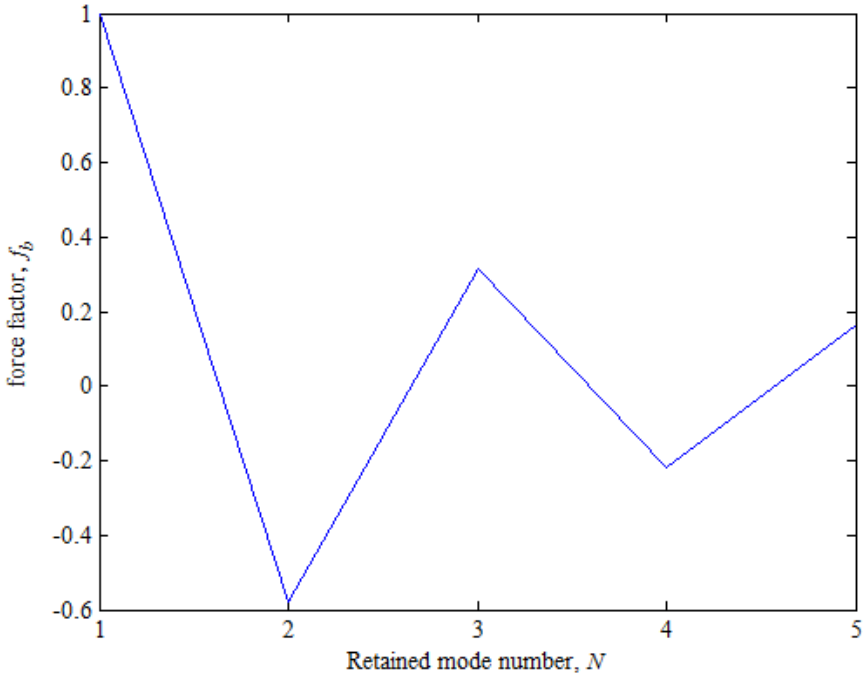

Figure 4.10 Graph of force factor with respect to retained mode number

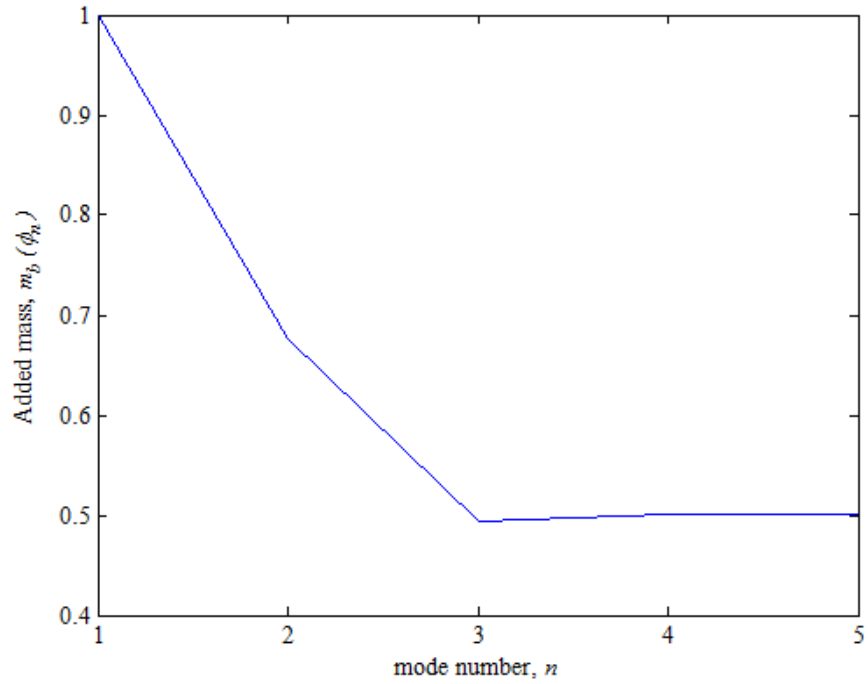

Figure 4.11 Graph of added mass for a unit dynamic response with respect to mode number

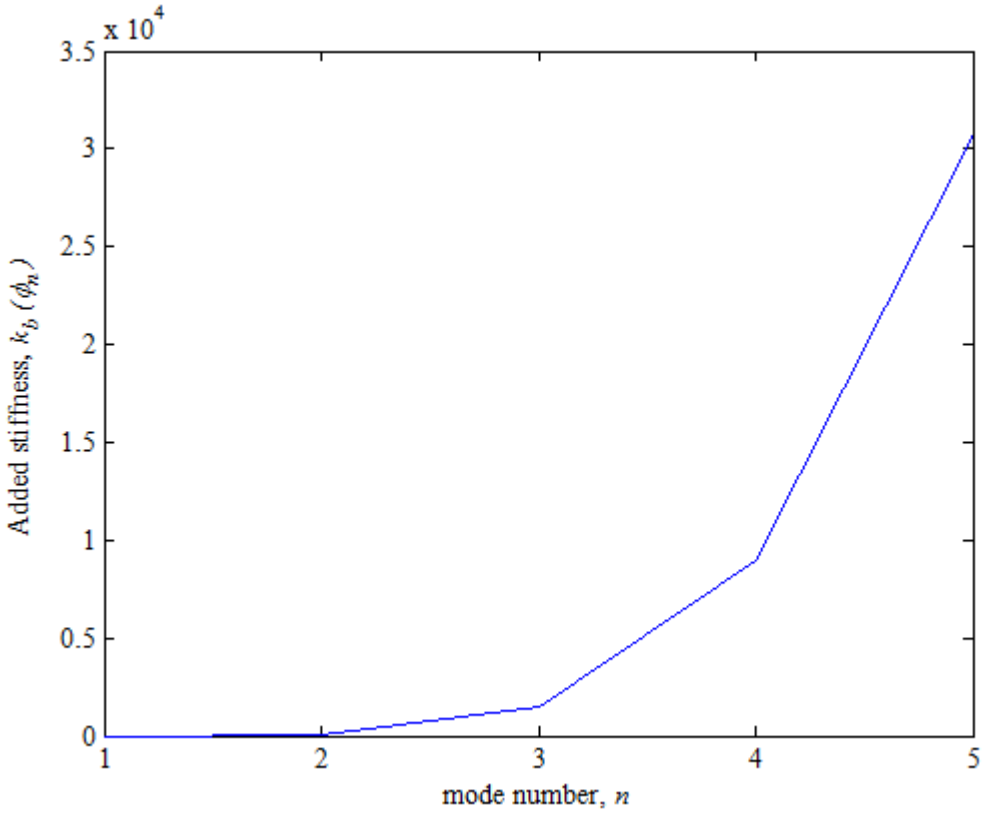

Figure 4.12 Graph of added stiffness for a unit dynamic response with respect to mode number.

Figure 4.11 and Figure 4.12 show graphs of dynamic response of mode n for the added mass and stiffness. From Figure 4.11, it can be seen that the additional mass, $m_b(\varphi_n)$ decreases as the mode number increases. However, the value of additional mass for mode numbers n = 3, 4, and 5 continue to have a similar value which is approximately 0.5. From Figure 4.12, it can be seen that the additional dynamic stiffness, $k_b(\varphi_n)$ added to the nonlinear suspension system by the beam increases as the mode number increases. The increase in additional stiffness is very large from 67 at n =2 to 30787 at n =5. Referring to Equation (4.55), increase in mode number means increase in the natural frequency, thus increase in the stiffness of the structure.

Here, we consider $N = 1$ implying that only one rigid mode $Y_1 = 1$ with $\bar{\Omega}_1^2 = 0$ in Equation (4.3) is retained, so that $\boldsymbol{Y}_0 = 1$, and therefore we have

$$\bar{\boldsymbol{m}} = \bar{M}_{11} = \bar{\rho}\bar{S}, \qquad m_b = \bar{M}_{11}, \qquad k_b = 0, \qquad f_b = 1 \tag{4.56}$$

Physically, m_b in Equation (4.27) is the total mass of the beam. Since the beam is considered rigid and there is no elastic deformation, the added stiffness $k_b = 0$, and the force factor $f_b = 1$.

The two components of stiffness forces are

$$\boldsymbol{F}_R = \{\boldsymbol{k}_b + [\bar{\boldsymbol{M}}\bar{\boldsymbol{\omega}}^2 + \boldsymbol{k}(\boldsymbol{q}) + \boldsymbol{k}_1(\boldsymbol{q})]\}\boldsymbol{q} \tag{4.57}$$

of which the horizontal component is not affected by the beam motion while the vertical component is affected by the additional added stiffness of the beam onto the nonlinear supporting unit. We choose the static position $\boldsymbol{q}_0 = [q_{10} \quad 0]^T$ satisfying Equation (4.1) as a zero point of the potential energy, that is

$$\Pi[\boldsymbol{q}_0] = \bar{m}\bar{\omega}^2 q_{10}^2 - \bar{k}q_{10} - \bar{f}_1 q_{10} = 0 \tag{4.58}$$

The potential energy at position **q** of the system is

$$\begin{aligned}\Pi[\boldsymbol{q}] = \int_{\boldsymbol{q}_0}^{\boldsymbol{q}} d\boldsymbol{q}^T &= \left[\frac{1}{2}\boldsymbol{q}^T(\boldsymbol{k}_b + \bar{\boldsymbol{M}}\bar{\boldsymbol{\omega}}^2)\boldsymbol{q}\right]_{\boldsymbol{q}_0}^{\boldsymbol{q}} - \frac{1}{2}\int_{\boldsymbol{q}_0}^{\boldsymbol{q}} \bar{k}(\boldsymbol{q}^T\boldsymbol{q})^{-\frac{1}{2}} d(\boldsymbol{q}^T\boldsymbol{q}) - \bar{f}_1(q_1 - q_{10}) \\ &= \frac{1}{2}[\bar{m}\bar{\omega}^2(q_1^2 - q_{10}^2) + \bar{\Omega}^2 q_2^2 + k_b q_2^2] - \bar{k}(\boldsymbol{q}^T\boldsymbol{q})^{1/2} + \bar{k}q_{10} - \bar{f}_1 q_1 \\ &\quad + \bar{f}_1 q_{10} \\ &= \frac{1}{2}[\bar{m}\bar{\omega}^2(q_1^2 + q_{10}^2) + \bar{\Omega}^2 q_2^2 + k_b q_2^2] - \bar{k}\sqrt{q_1^2 + q_2^2} - \bar{f}_1 q_1.\end{aligned} \tag{4.59}$$

In this equation, the term $k_b q_2^2/2$ represents the elastic energy of the beam, which vanishes if only the beam rigid mode is retained.

The graphs in Figure 4.13 to Figure 4.18 show the nonlinear stiffness force affected by k_b.

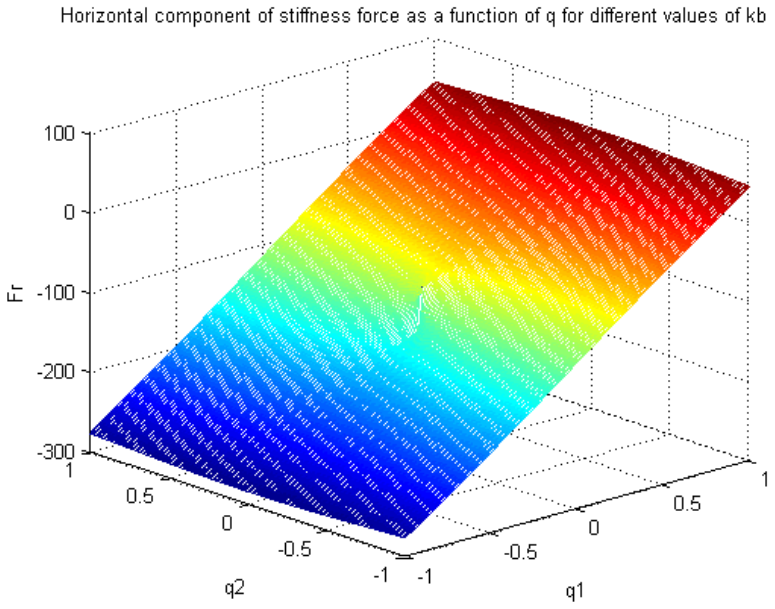

Figure 4.13 Horizontal nonlinear stiffness force affected by k_b

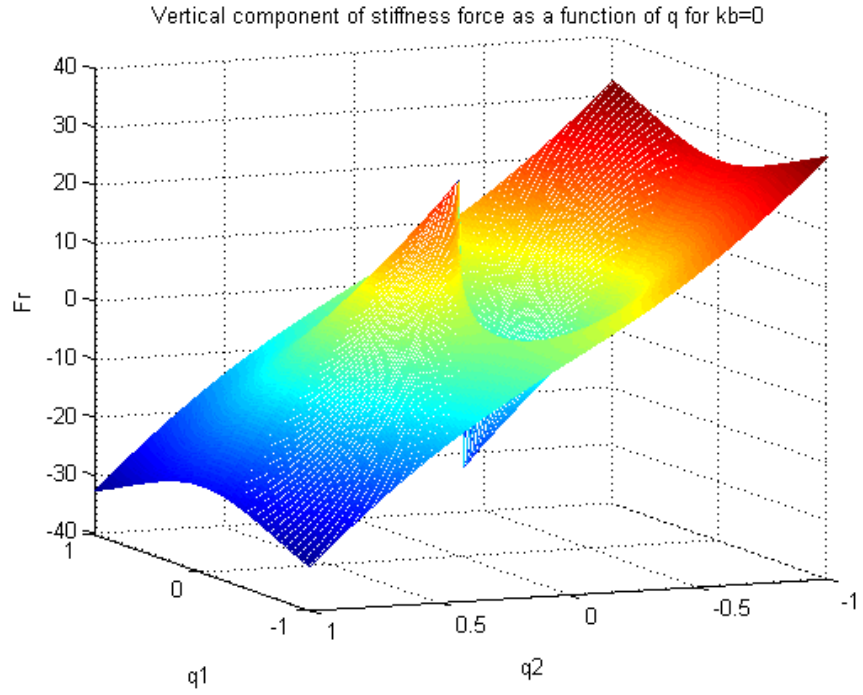

Figure 4.14 Vertical nonlinear stiffness force when k_b = 0

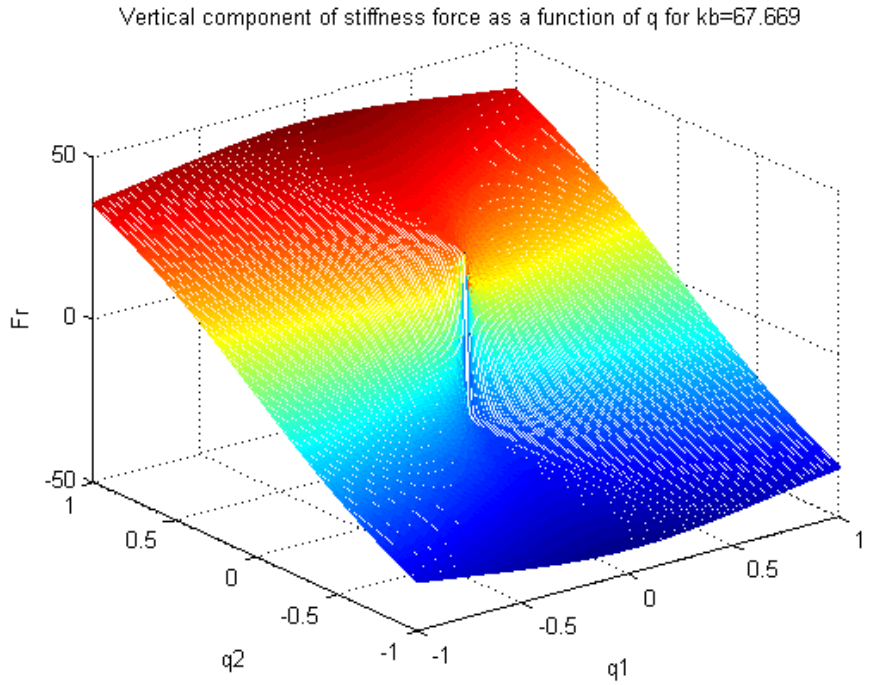

Figure 4.15 Vertical nonlinear stiffness force when k_b = 67.99

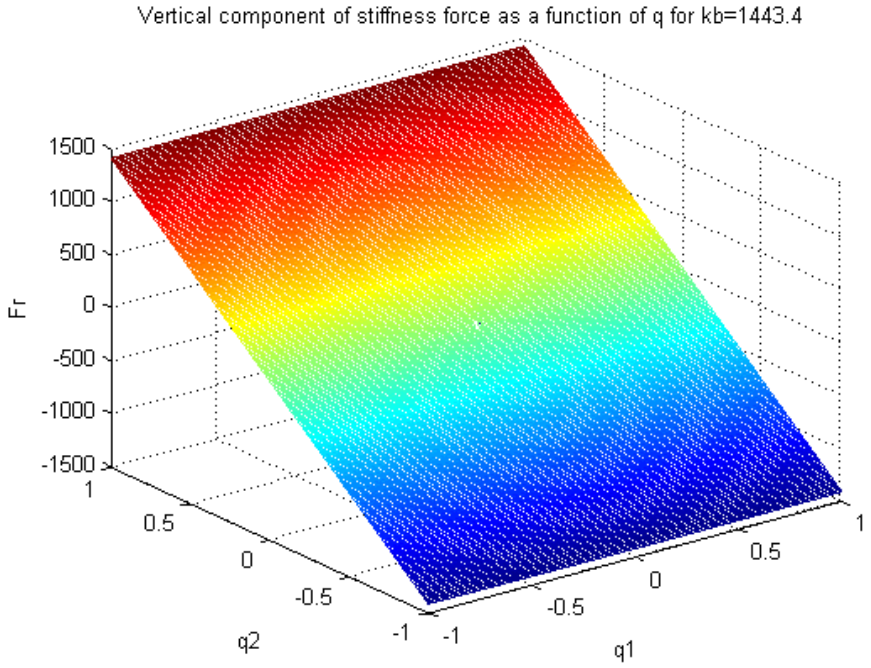

Figure 4.16 Vertical nonlinear stiffness force when k_b = 1443.4

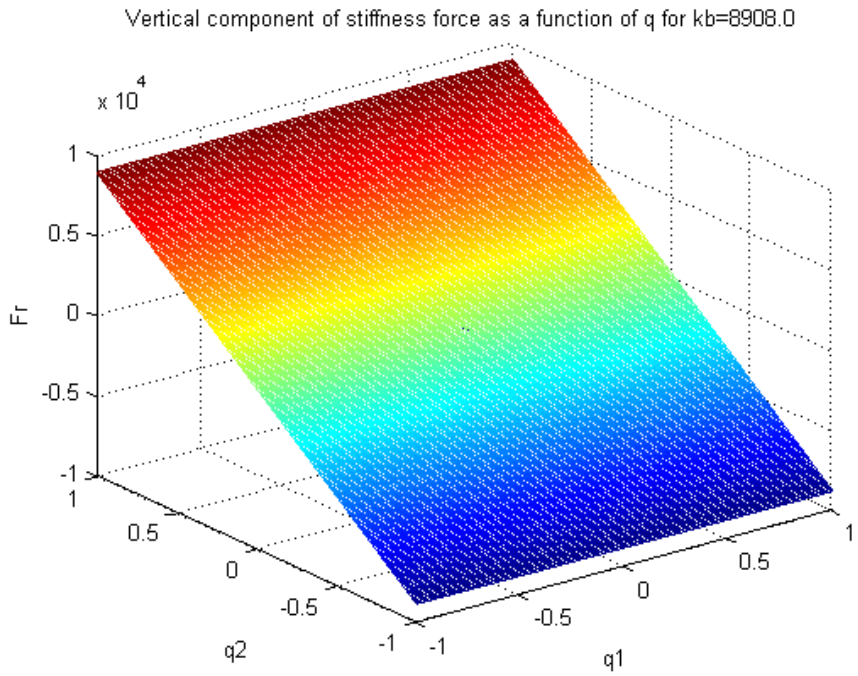

Figure 4.17 Vertical nonlinear stiffness force when k_b = 8908

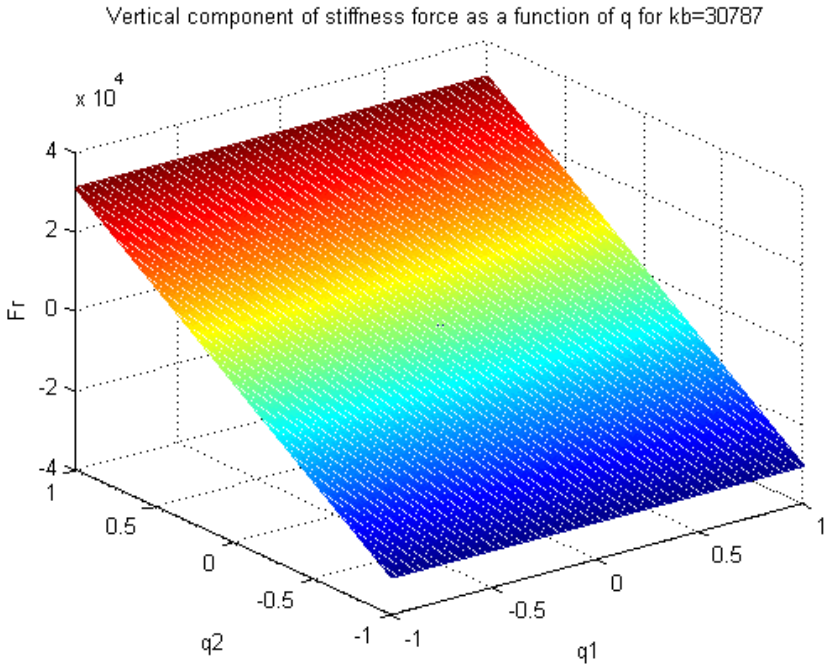

Figure 4.18 Vertical nonlinear stiffness force when k_b = 30787

From Equation (4.57) the horizontal stiffness force F_{R1} and the vertical stiffness force F_{R2} of the beam and nonlinear suspension unit can be derived. From here, the parameters that affect the stiffness forces can be identified.

Inserting the values of $\boldsymbol{k}_b$,$\bar{\boldsymbol{M}}$, $\bar{\boldsymbol{\omega}}^2$, $\boldsymbol{k}(\boldsymbol{q})$, $\boldsymbol{k}_1(\boldsymbol{q})$ and $\boldsymbol{q}$ from Equation (4.15) and (4.52) we obtain

$$\boldsymbol{F}_R = \left[\boldsymbol{k}_b + \left(\begin{bmatrix}\bar{m} & 0\\ 0 & 1\end{bmatrix}\begin{bmatrix}\bar{\omega}^2 & 0\\ 0 & \bar{\Omega}^2\end{bmatrix} + -\frac{\bar{k}}{\bar{\mu}}\boldsymbol{I} + -\frac{\bar{f}_1}{q_1}\boldsymbol{I}_1\right)\right]\begin{bmatrix}q_1\\ q_2\end{bmatrix}$$

$$\begin{bmatrix}F_{R1}\\ F_{R2}\end{bmatrix} = \begin{bmatrix}\left(\bar{m}\bar{\omega}^2 - \dfrac{\bar{k}}{\sqrt{q_1^2+q_2^2}} - \dfrac{\bar{f}_1}{q_1}\right)q_1\\ \left(k_b + \bar{\Omega}^2 - \dfrac{\bar{k}}{\sqrt{q_1^2+q_2^2}}\right)q_2\end{bmatrix} \qquad (4.60)$$

It can be seen in Figure 4.13 that the value of k_b does not affect the horizontal component of stiffness force. The graphs overlap each other even though different values of k_b are used. This

is also proven from Equation (4.60), whereby there is no k_b term in the equation for the horizontal stiffness force F_{r2}.

In Figure 4.14 to Figure 4.18, the values of k_b is seen to affect the vertical stiffness force. When the value of k_b= 0 and k_b= 67.99, the graphs illustrate a nonlinear behaviour, but for larger values of k_b , the graph becomes a linear graph. This is because, larger values of k_b result in k_b being dominant over all the other terms (including the nonlinear term) in the vertical stiffness force equation.

There is a potential energy associated with the stiffness force, which can be found by integrating the force with displacement. The potential energy at position **q** of the system is given by Equation (4.59).

Figure 4.19 to Figure 4.23 show the potential energy at position **q** (static equilibrium position) of the system with different values of k_b.

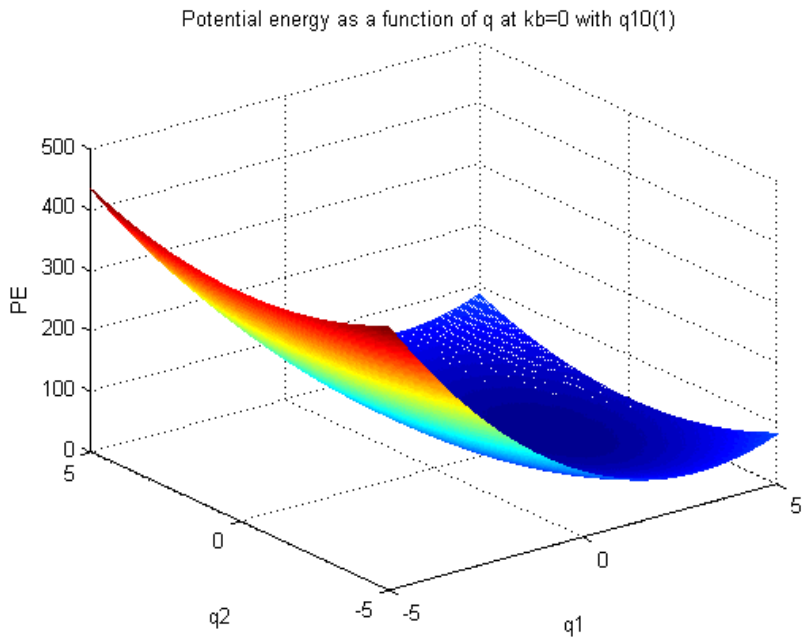

Figure 4.19 Potential energy for position q at the static position q_{10} = 0.6471

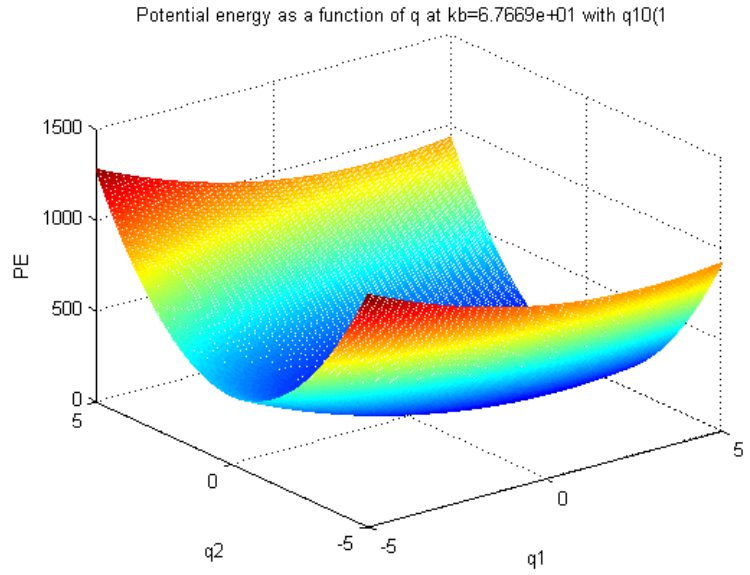

Figure 4.20 Potential energy for position q at the static position q_{10} = 0.6471.

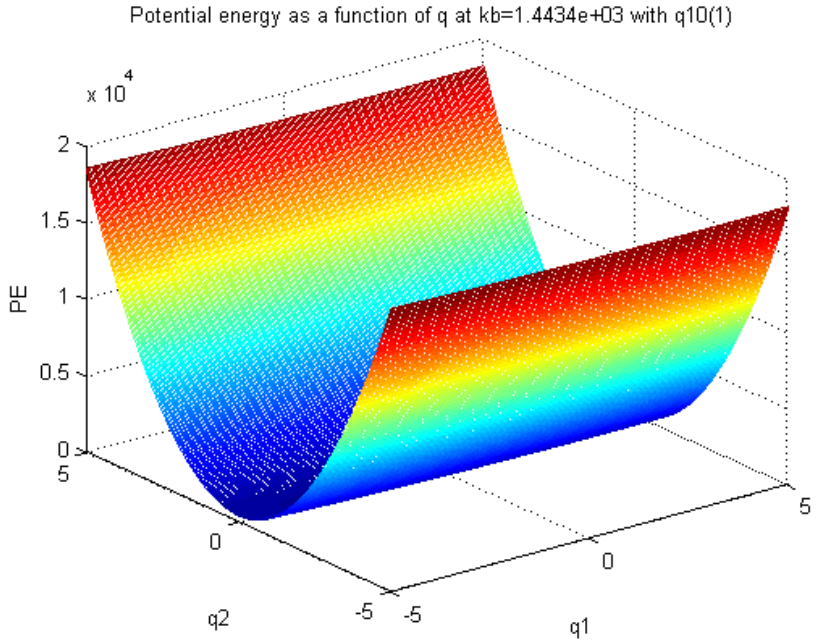

Figure 4.21 Potential energy for position q at the static position q_{10} = 0.6471.

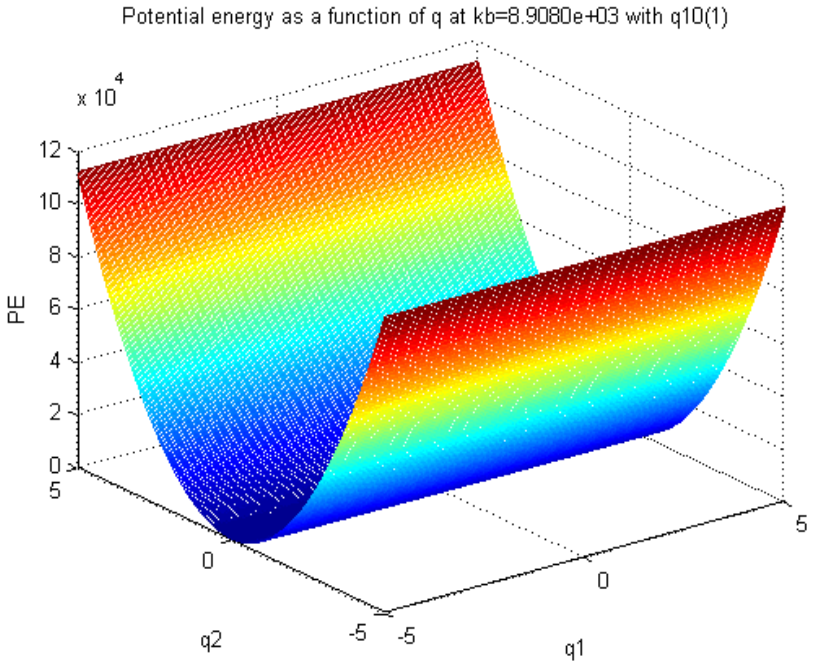

Figure 4.22 Potential energy for position q at the static position q_{10} = 0.6471.

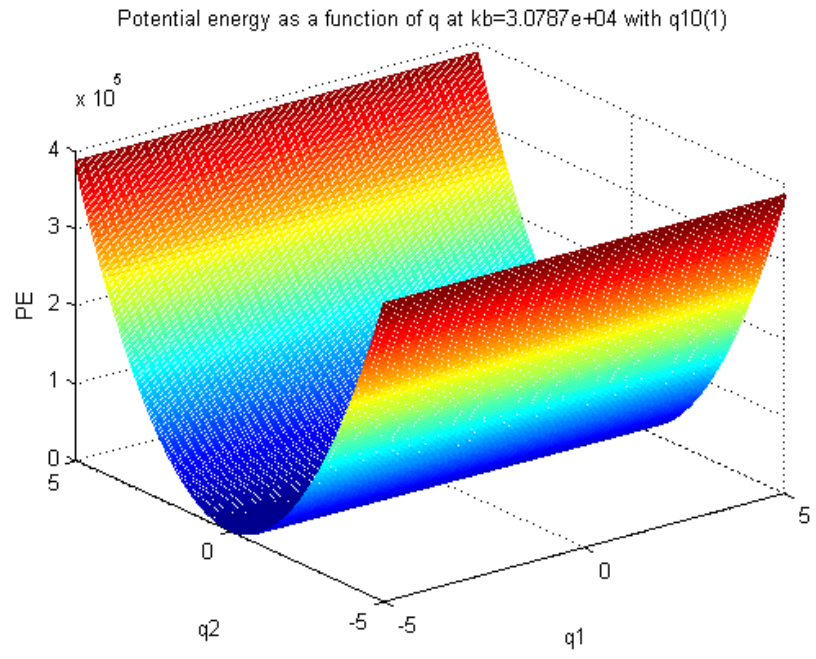

Figure 4.23 Potential energy for position q at the static position q_{10} = 0.6471.

When k_b is zero, which means there is no elastic energy in the beam, and the beam is in its rigid mode, the graph of potential energy varies across q_1 (x-axis). When there is a value of k_b the

graph varies across q_2 (y-axis). This is in line with the equation of stiffness forces whereby k_b only affects the y-axis. As k_b increases, so does the value of potential energy.

The kinetic energy at position $\boldsymbol{q}$ of the system is

$$T[\boldsymbol{q}] = \frac{1}{2}\dot{\boldsymbol{q}}^T(\bar{\boldsymbol{M}} + \boldsymbol{m}_b)\dot{\boldsymbol{q}} = \frac{1}{2}[\bar{m}\dot{q}_1^2 + (1 + m_b)\dot{q}_2^2] \tag{4.61}$$

The total mechanical energy of undamped system in a solution is a constant, so that we have

$$T[\boldsymbol{q}] + \Pi[\boldsymbol{q}] = C. \tag{4.62}$$

4.4.2 Phase trajectories of nonlinear isolator

A phase trajectory is a geometric representation of the trajectories of a dynamical system in the phase plane. Here, the dynamical system is the beam connected to the isolation unit and the phase plane is in terms of q_1 and q_2. The undamped and damped phase trajectories of the system are shown in Figure 4.24 and Figure 4.25.

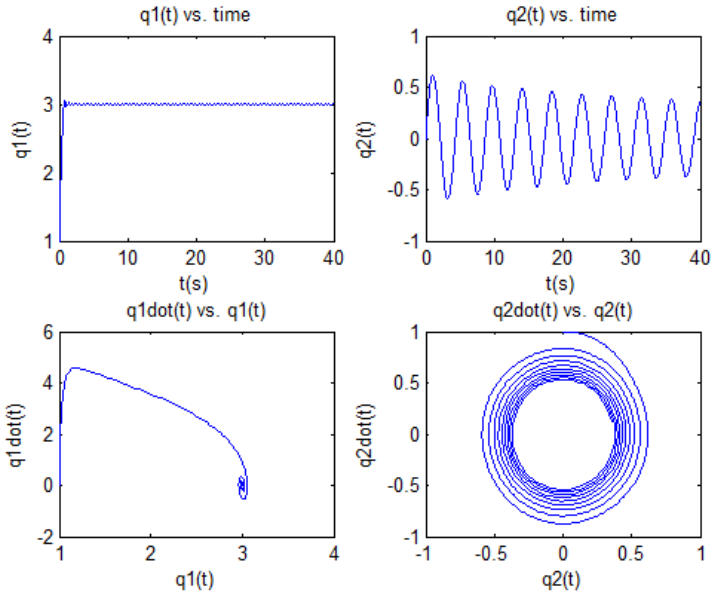

Figure 4.24 Undamped phase trajectories of the nonlinear unit affected by elastic beam

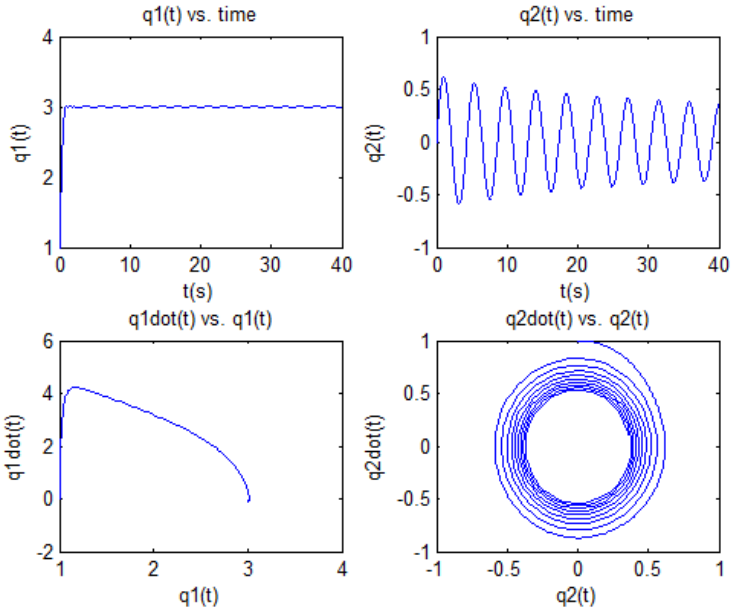

Figure 4.25 Damped phase trajectories of the nonlinear unit affected by elastic beam with c1=0.01, c=0.2.

From the graphs in Figure 4.24 and Figure 4.25 it can be seen that the trajectories spiral into the origin and all the points accumulate into the origin. When there is damping in the system, the trajectory of q_1 approaches the origin much faster compared to without damping.

4.4.3 Equation governing the influence of nonlinear suspension unit on beam motions

Combining Equation (4.13) and (4.14) and eliminating the interaction force vector $\bar{\boldsymbol{f}}$, we obtain the governing equation of nonlinear suspension unit on beam motions

$$(\bar{\boldsymbol{m}} + \boldsymbol{m}_N)\ddot{\bar{\boldsymbol{\Phi}}} + \boldsymbol{c}_N\dot{\bar{\boldsymbol{\Phi}}} + [\bar{\boldsymbol{m}}\bar{\boldsymbol{\Lambda}}^2 + \boldsymbol{k}_N]\bar{\boldsymbol{\Phi}} = \boldsymbol{c}_{N1}\dot{q}_1 + \bar{\boldsymbol{F}}_0, \tag{4.63}$$

where

$$\boldsymbol{m}_N = \bar{\boldsymbol{Y}}, \boldsymbol{k}_N = \bar{\Omega}^2(1 - \bar{k}/\bar{\mu})\bar{\boldsymbol{Y}}, \boldsymbol{c}_N = 2(E\bar{\Omega} + \bar{\varepsilon}q_2^2/\bar{\mu}^2)\bar{\boldsymbol{Y}}, \boldsymbol{c}_{N1} = -2\bar{\varepsilon}q_2q_1/\bar{\mu}^2\boldsymbol{Y}_0^T \tag{4.64}$$

This matrix equation describes the beam dynamics influenced by the nonlinear suspension unit. Here, $\boldsymbol{m}_N$, $\boldsymbol{k}_N$, $\boldsymbol{c}_N$ and $\boldsymbol{c}_{N1}$ denote an additional mass, stiffness and damping matrix added to the beam by the nonlinear suspension unit, respectively. Due to these added parameters, the dynamic behaviour of the beam are as follows.

i. The original linear beam system now behaves nonlinearities provided by nonlinear stiffness $\boldsymbol{k}_N$ and damping $\boldsymbol{c}_N$ and $\boldsymbol{c}_{N1}$.

ii. The couplings between the normalised mode coordinates of the beam are generated by the additional mass, stiffness and damping matrices.

iii. The natural vibration frequencies of the beam about an equilibrium point are affected as discussed in section 4.3.2.1.

4.5 Beam-nonlinear isolator design

The beam-nonlinear isolator design for particular low stiffness support and high stiffness support will be discussed in this section.

4.5.1 Low stiffness support

We consider Figure 4.1 as a simplified model for ground vibration tests of large full-scale aircrafts. The central mass is considered as the mass of the fuselage and the two beams connected on to the central mass are the two wings of the aircraft. Aircrafts flying in the air are in a free-free state without any mechanical supports. However, in tests, the aircraft is supported on the ground so the supporting system must have an affect on the aircraft's dynamic characteristics. For a reliable test result, the effect of supporting system should be as less as possible. It has been demonstrated that the effect of supporting system on the aircraft could be neglected if the frequency of an assumed rigid aircraft Ω_{SA}, on the supporting system is less than one third of the first elastic natural frequency of the free-free aircraft Ω_{EA} (Molyneux 1958; Xing 1975), i.e.

$$\Omega_{SA} \leq \Omega_{EA}/3. \tag{4.65}$$

For small aircrafts, their first elastic natural frequency is high enough and there is no difficulty to design a supporting system satisfying Equation (4.65). However, for very large aircrafts, the first natural frequency, usually the first-order bending frequency of aircraft wings is lower than 1Hz. Therefore, the supporting frequency for large aircraft tests should be less than 0.3 Hz. Due to a very large weight of the aircraft supported in the static state, the static stiffness of the supporting system must be sufficiently large to balance the heavy weight. As a result, it is very difficult to design a supporting system with less than 0.3Hz supporting frequency for large aircrafts by means of normal supporting designs, such as air spring system etc. (Molyneux 1958; Xing 1975). Nonlinear supporting system provides an effective approach to design this type of supporting systems.

To support the airplane on the ground, Point β=3 is chosen as the static equilibrium state of the aircraft on the ground. Based on Equation (4.1), $\Delta = Y_0 - L$, from which we can choose a suitable height Y_0 according to the initial length L of the vertical spring, so that a negative parameter $\bar{\Delta}$ and the vertical stiffness $\bar{K}$ are determined by

$$\bar{K} = (1 + \bar{\rho}\bar{S})\bar{g}/|\bar{\Delta}|, \qquad K = M\Omega_0^2\bar{K}. \tag{4.66}$$

Because the total mass of the large airplane is huge, the stiffness of the vertical spring is very large. If there are no two inclined springs, the supporting frequency of the aircraft and the static compression of the vertical spring are required to satisfy the conditions

$$\Omega_{SA} = \sqrt{\bar{K}/(1 + \bar{\rho}\bar{S})} = \sqrt{\bar{g}/|\bar{\Delta}|} \le \Omega_{EA}/3, \qquad |\bar{\Delta}| \ge 9\bar{g}/\Omega_{EA}^2. \tag{4.67}$$

A limited space of test site does not allow these conditions to be realised only using linear supporting systems. From Equation (4.40) and Table 4.1, we have the natural frequency

$$\Omega_{NSA} = \hat{\bar{\Omega}}_2^{(1)} = \sqrt{(1 - \bar{k}\bar{\Omega}^{-2}/\bar{\mu}_0^{(1)})/(1 + \tilde{\rho}\tilde{S})}\bar{\Omega}, \bar{\mu}_0^{(1)} = \tilde{k}_1 + \tilde{K}_1\bar{\Delta}_1. \tag{4.68}$$

Based on Equations (4.8) and (4.12), we obtain

$$\bar{\Delta}_1 = (X_0 - L_1)/l, \qquad \bar{\mu}_0^{(1)} = \tilde{K}_1(k/K_1 + \bar{\Delta}_1), \tag{4.69}$$

so that to reduce the supporting frequency Equation (4.68) we must choose point (3) to design the system satisfying

$$1 \ge \bar{k}\bar{\Omega}^{-2}/\bar{\mu}_0^{(1)} > 0, \qquad \tilde{k}_1 + \tilde{K}_1\bar{\Delta}_1 > 0. \tag{4.70}$$

This design condition is easily realised. In this design, the nonlinear stiffness term $\bar{k}\bar{\Omega}^{-2}/\bar{\mu}_0^{(1)}$ plays a negative stiffness in Equation (4.68) to reduce the supporting frequency. Theoretically, from Equation (4.70), we may choose the value of $\bar{k}\bar{\Omega}^{-2}/\bar{\mu}_0^{(1)}$ near to 1 to realise the standard $\Omega_{NSA} < \Omega_{EA}/3$. Equation (4.38) confirms that for the system with two dampers in Figure 4.1, the damping factors are positive, and the system is stable. Therefore, during ground vibration tests involving small vibrations of the aircraft about point (3), any small disturbance of the system from the equilibrium state can be damped.

4.5.1.1 Choosing suitable parameters

The suitable parameters are first chosen to satisfy Equation (4.70).

The values of stiffness K and K_1 can be found from Equation (4.1). The value of stiffness k is chosen to be the same as K.

$$K = \frac{-g(M+\rho s)}{\Delta}, \qquad \Delta = Y_0 - L$$
$$K_1 = \frac{k(l-x_0)}{x_0 - \Delta_1}, \qquad \Delta_1 = X_0 - L_1 \tag{4.71}$$

Table 4.4 list the parameter values that satisfy Equation (4.70).

Table 4.4 Parameter values for low stiffness support

Parameters	Values
M	1
X_0	0.7
L_1	0.6
l	1
Y_0	1
L	10.3
ρ	100
S	1
x_0	0.5

4.5.1.2 Linear analysis

Linear analysis is done by applying small vibration about the chosen equilibrium point (3) to find the natural frequencies and modes of the system which will be compared with the natural frequencies and modes of the free-free beam.

At equilibrium point (3), using the eigenvalue equation in (4.23), the eigenvalues and eigenvectors of the beam affected by the nonlinear isolator are found. The eigenvalues are the natural frequencies of the beam supported on the nonlinear isolator and is shown in Table 4.5. The eigenvectors are the generalised coordinates which is used to find the mode shapes of the beam supported on the nonlinear isolator. Using the mode summation equation in (4.3), the normalised mode shapes are found as shown in Figure 4.26. The natural frequencies and modes of the free-free beam are shown in Table 4.6 and Figure 4.27. By comparing Table 4.5 with Table 4.6, the natural frequencies at equilibrium point (3) are a little lower than the corresponding one of the free - free beam. This is caused by the lumped mass M of the supporting isolator which does not exist in the free - free beam. At $N = 1$ (rigid mode in the vertical direction), the natural frequency of the beam supported on the nonlinear support is 6.7435e-7 which is less than one third of the first elastic natural frequency ($N = 2$) of the free-free beam. This satisfies the requirement of Equation (4.70).

Table 4.5 Natural frequencies of beam supported on the nonlinear support at equilibrium point (3)

n	1	2	3	4	5
Frequency	6.7435e-7	1	5.3902	13.3146	24.7658

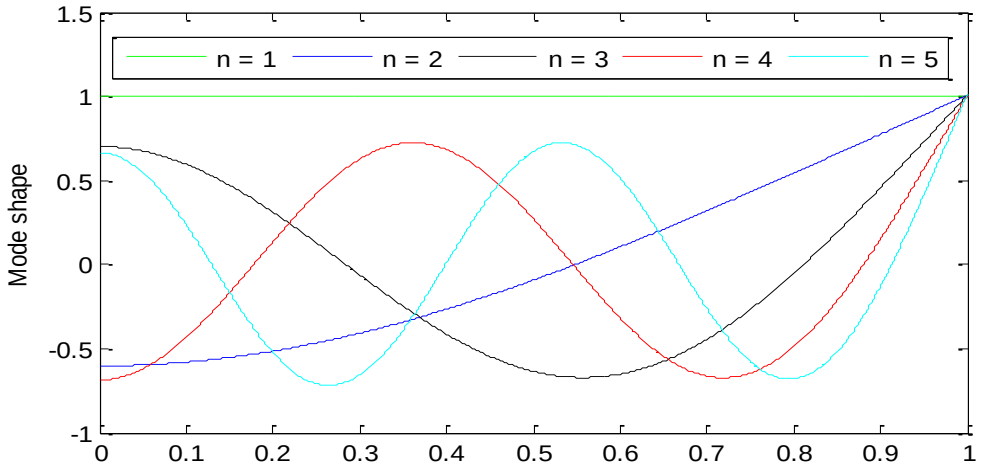

Figure 4.26 Mode shapes of the beam affected by the nonlinear isolator at equilibrium point (3) for mode, n=1 to 5

Table 4.6 Natural frequency of the free-free beam

N	1	2	3	4	5
Frequency	0	1	5.4039	13.3443	24.8139

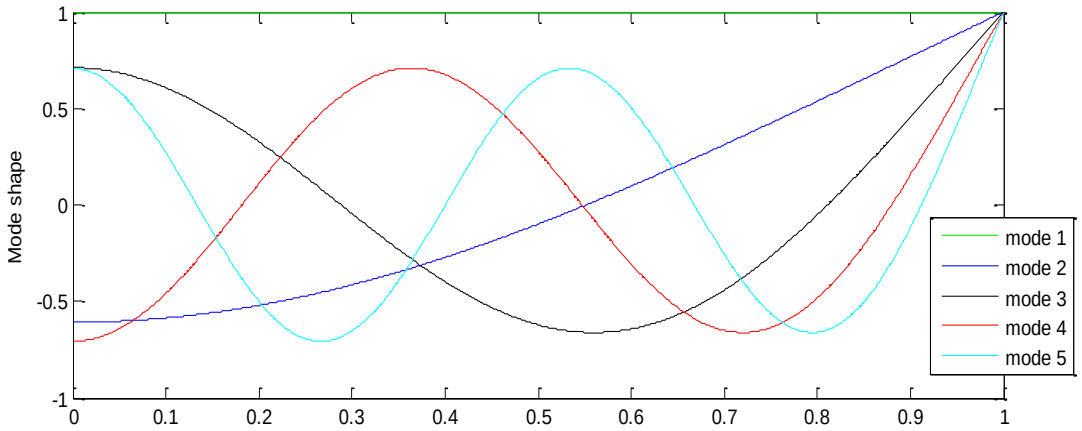

Figure 4.27 Mode shapes of the free-free beam

The mode shapes of the beam supported on the nonlinear isolator in Figure 4.26 are compared to the mode shapes of the free free beam in Figure 4.27, and it can be seen that the mode shapes of the beam on the nonlinear isolator is similar to mode shapes of the free free beam.

The error between the theoretical value (free - free beam) of natural frequency and the calculated value (beam - nonlinear isolator) is found according to Equation (4.72).

$$\text{Natural frequency error} = |\text{Theoretical value} - \text{Calculated value}| \tag{4.72}$$

The mode shape error between the theoretical (free - free beam) shape and calculated (beam - nonlinear isolator) shape is found from Equation (4.73) . For each mode shape, 10 points along the beam were chosen to be compared.

$$\text{Mode shape error} = \sqrt{\sum_{I=1}^{10} (theoretical - calculation)_I{}^2 / 10} \tag{4.73}$$

where I : point on the beam

Table 4.7 Natural frequency error for modes n =1...5

n	1	2	3	4	5
Error	6.7435e-7	0	0.0137	0.0297	0.0481

Table 4.8 Mode shape error for modes, n =1...5

n	1	2	3	4	5
Error	1.9279e-12	0.0060	0.0107	0.0152	0.0177

4.5.1.3 Effect of supporting system to the structure

The parameters k and Ω_0 were varied to stay in the limits of Equation (4.70) and the change in frequency of the beam is observed and shown in Figure 4.28 and Figure 4.29.

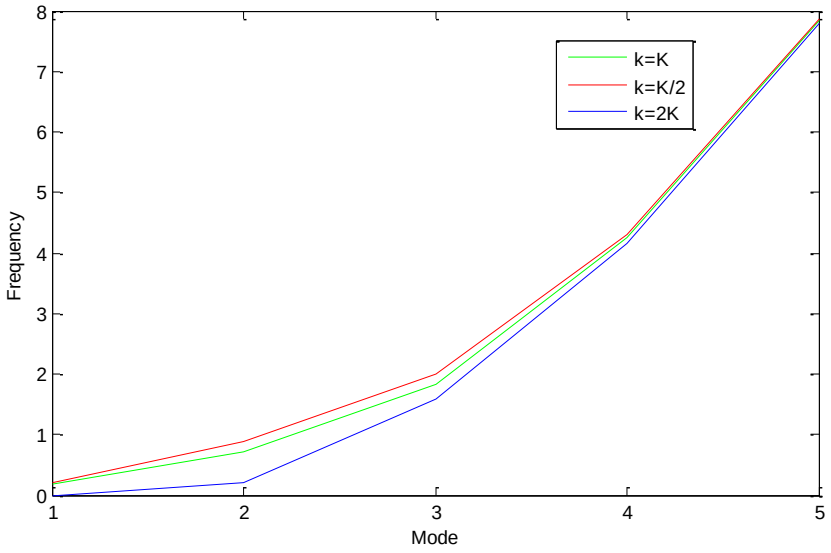

Figure 4.28 Change in frequency when *k* is varied

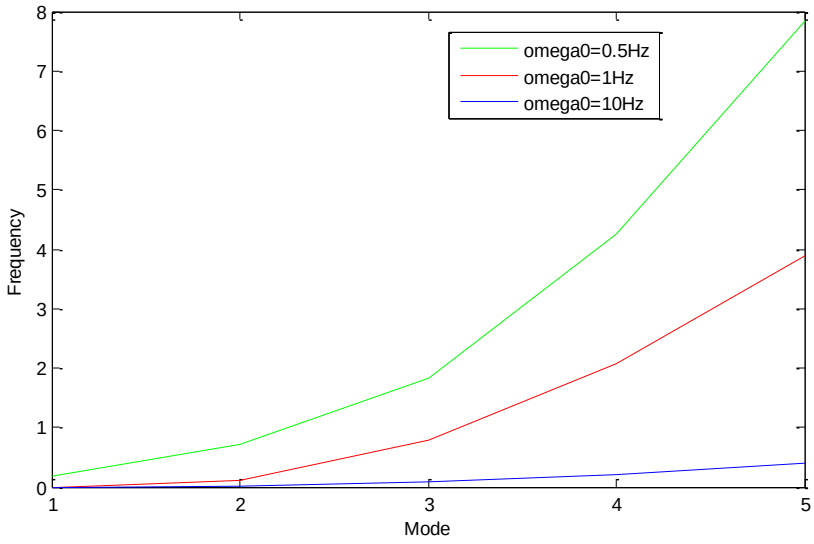

Figure 4.29 Change in frequency when Ω_0 is varied

From Figure 4.28 it can be seen that the larger the value of stiffness *k,* the smaller the frequency of the beam. From Figure 4.29 it is observed that the larger the value of small excitation frequency Ω_0 given to the system, the smaller the frequency of the beam.

4.5.1.4 Dynamic response

The dynamic response of the system is analysed by applying two sinusoidal excitation force to the beam. Equation (4.18) of the integrated coupling equation of the system in state space form was inserted into the Simulink Differential Equation Editor block as shown in Figure 4.30 and

the parameters in Matlab m-file was defined. Because the system is a nonlinear system, it will exhibit nonlinear behaviour, thus chaos and bifurcation will be involved and studied.

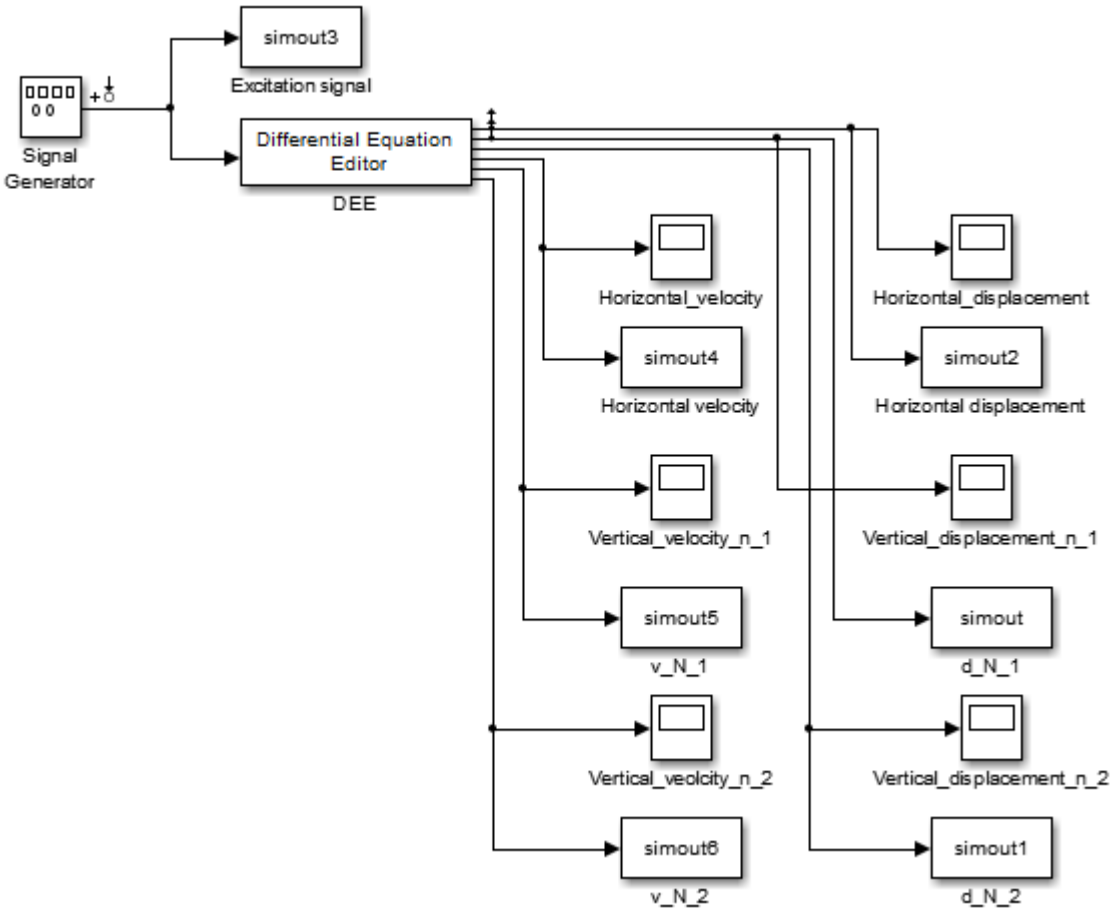

Figure 4.30 Simulink programme using the Differential Equation Editor block

To observe the nonlinear dynamical behaviour of bifurcation and chaos, the phase plane plot of velocity vs displacement for the vertical motion of the beam at n=1 is shown in Figure 4.31 to Figure 4.35.

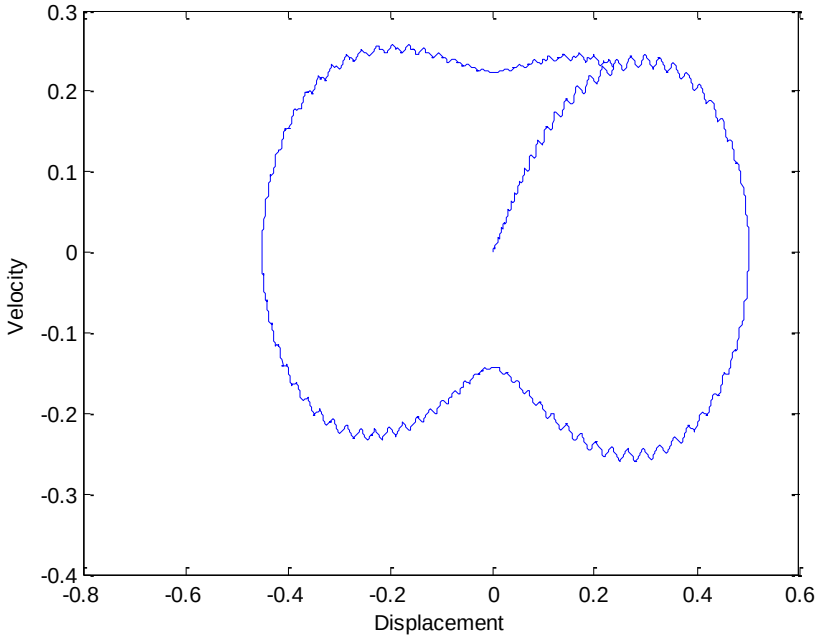

Figure 4.31 Phase plane plot when $F_0 = 0.01$, Ω_0=0.5

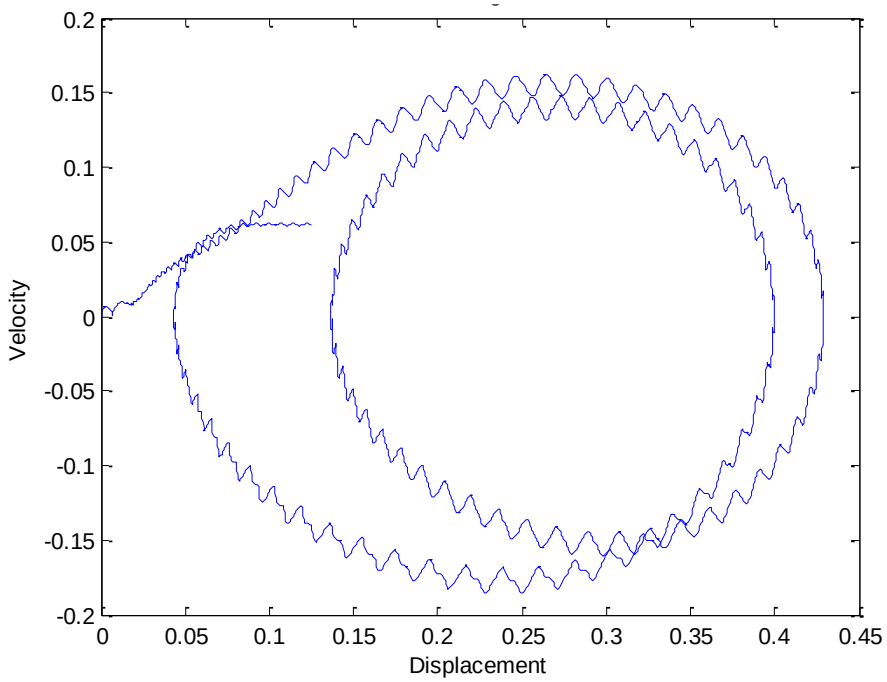

Figure 4.32 Phase plane plot when $F_0 = 1$,Ω_0=0.5

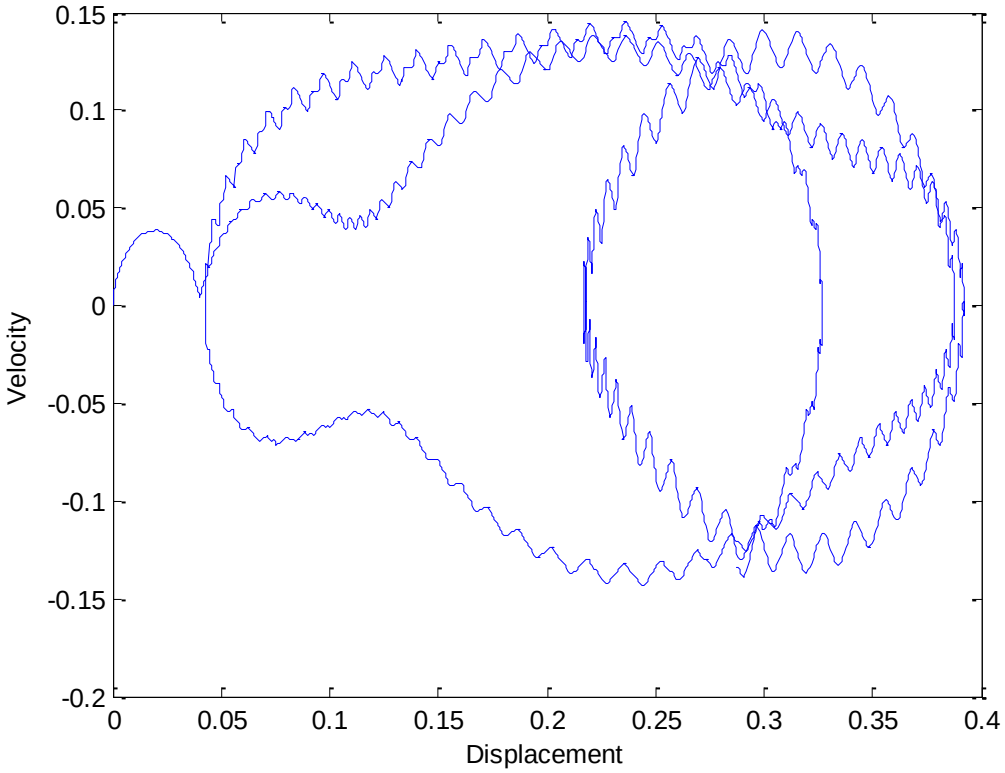

Figure 4.33 Phase plane plot when $F_0 = 6$,Ω_0=0.5

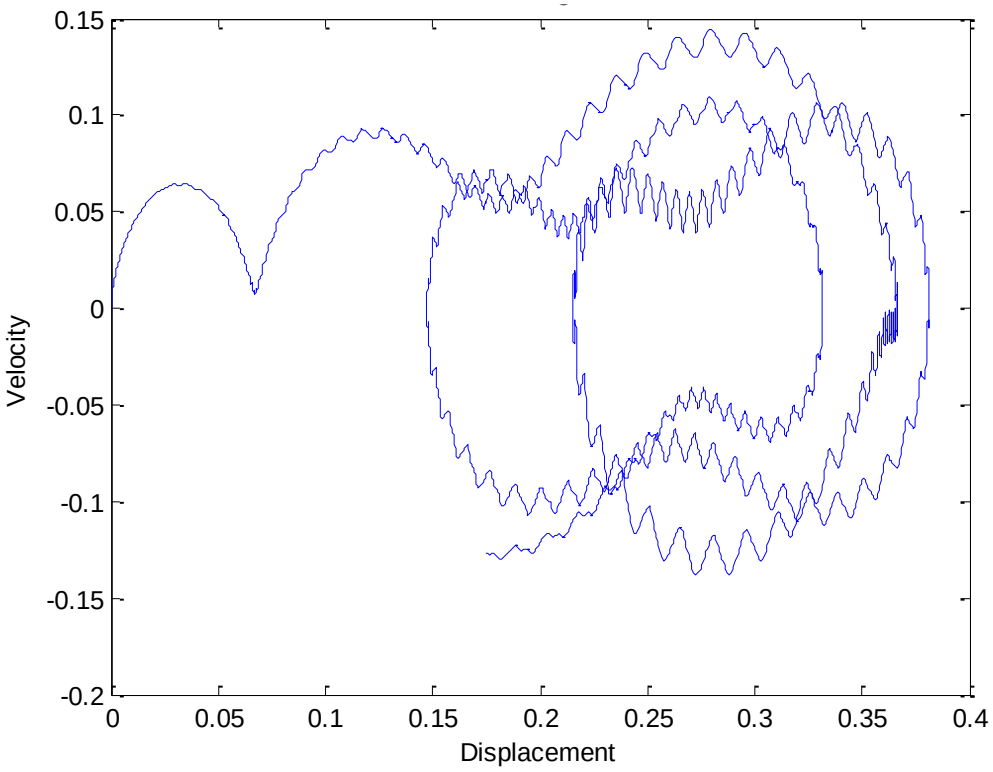

Figure 4.34 Phase plane plot when $F_0 = 12$,Ω_0=0.5

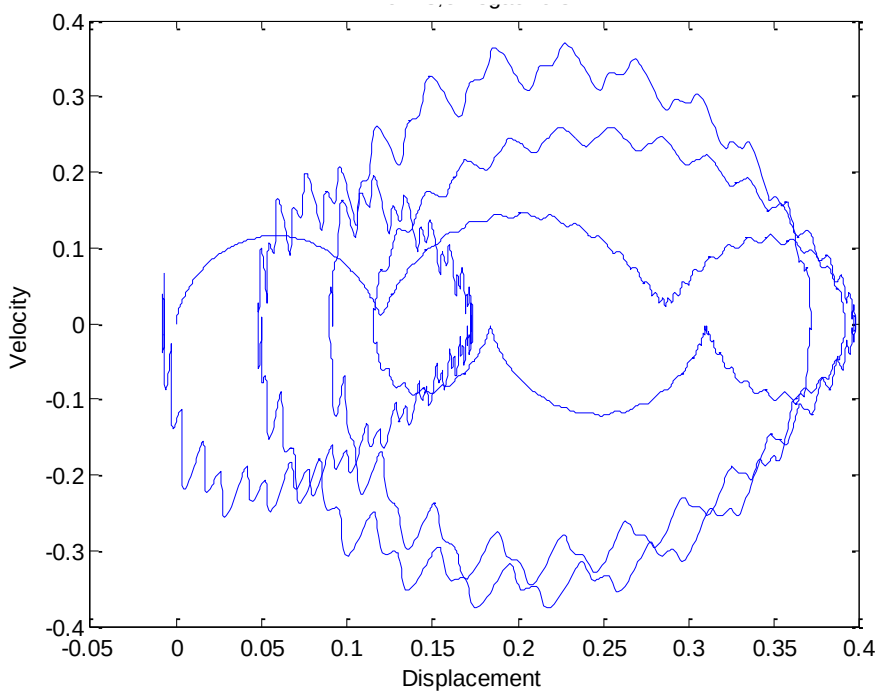

Figure 4.35 Phase plane plot when $F_0 = 18$,Ω_0=0.5

Fixing the value of excitation frequency Ω_0 =0.5, F_0 is varied to observe the condition for bifurcation and chaos. From Figure 4.31, when $F_0 = 0.01$, the response is a 1 period motion. When $F_0 = 1$, period doubling bifurcation starts to happen as shown in Figure 4.32. When $F_0 = 6$ and $F_0 = 12$ a 4 period motion can be observed as shown in Figure 4.33 and Figure 4.34. Increasing the value of excitation force to $F_0 = 18$, a 8 period motion is observed in Figure 4.35.

Increasing the excitation force $F_0 = 20$ and varying the excitation frequency Ω_0 from 0.1Hz to 100Hz, Poincare' maps where plotted in Figure 4.36 to observe the behaviour of the system.

The Poincaré section method provides a means for viewing the phase space diagram so that the motion is observed periodically. To do this, the trajectory is sectioned at regular intervals. Chaotic trajectories and regular trajectories differ in a significant manner, with chaotic trajectories fill out an area in phase space while regular trajectories fill out curves. From Figure 4.36, it can be seen that the Poincaré maps all form closed loops and no chaotic orbit is observed, and they show quasiperiodic behaviour of the integrated interaction system, with moderate order to full order depending on the frequency.

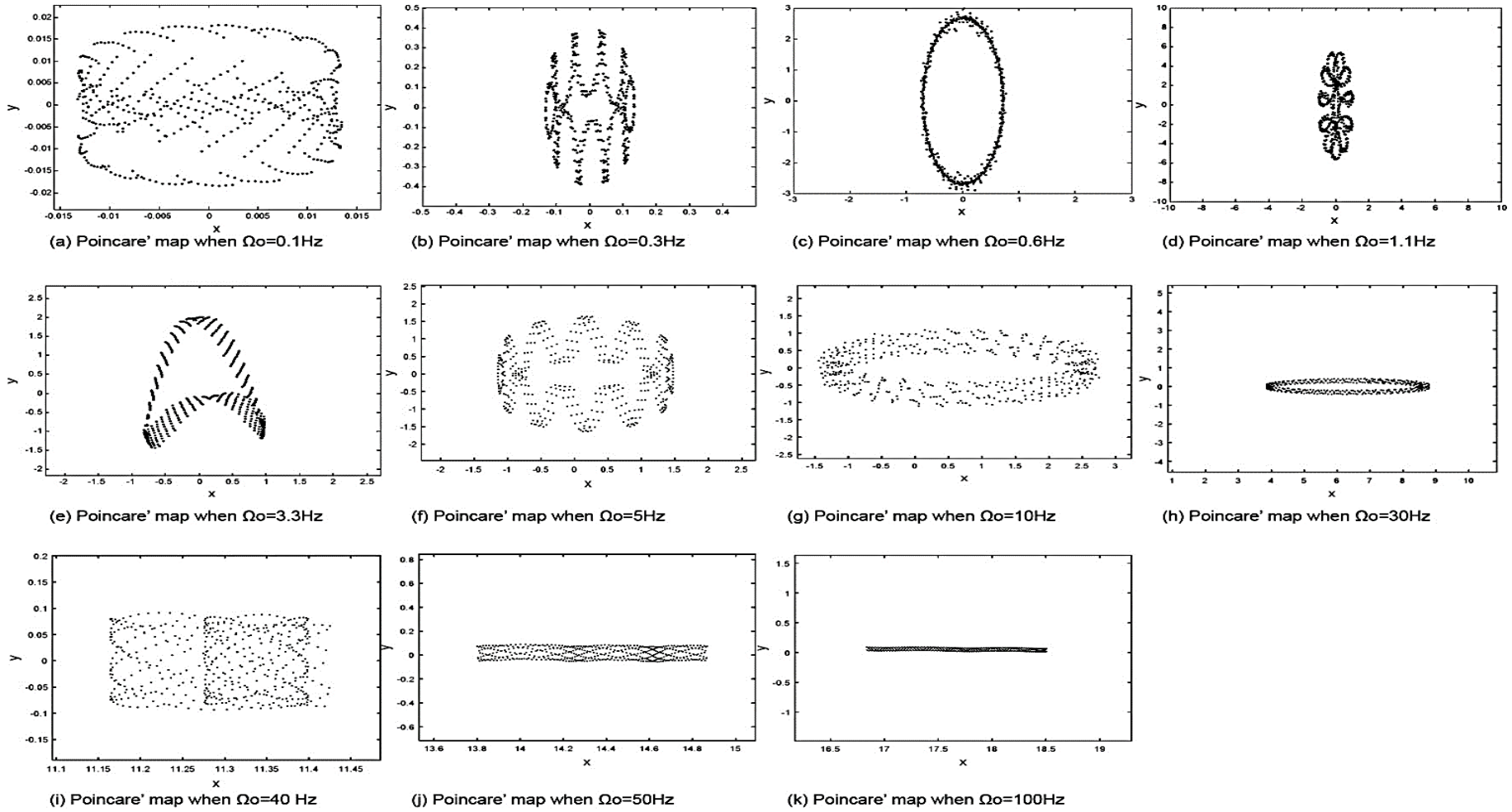

Figure 4.36 Poincare' maps of the system when $F_0 = 20$ and (a)Ω_0=0.1Hz,(b)Ω_0=0.3Hz,(c)Ω_0=0.6Hz,(d)Ω_0=1.1Hz, (e)Ω_0=3.3Hz,(f)Ω_0=5Hz,(g)Ω_0=10Hz,(h)Ω_0=30Hz, (i)Ω_0=40Hz,(j)Ω_0=50Hz,(k)Ω_0=100Hz

4.5.2 High stiffness support

Now we consider the system shown in Figure 4.1 as a model of laboratory dynamic tests. In this test, a beam that is to be tested is symmetrically fixed at a platform of mass supported by the nonlinear isolation unit. We wish to have the beam fixed on the "rigid" foundation. This implies that the supported unit should have an extremely large supporting stiffness and frequency. We also choose point (1) as our static equilibrium state of the system. We have known that this system with the dampers is stable about point (1), therefore, we directly discuss how to obtain an extremely high supporting frequency.

The supporting frequency given in Equation (4.68) is still valid. From Equation (4.69), to obtain an extremely high frequency, it is necessary to choose point (1) in the left half part of the symmetrical system satisfying

$$\bar{k}\bar{\Omega}^{-2}/\bar{\mu}_0^{(1)} < 0, \qquad \tilde{k}_1 + \tilde{K}_1\bar{\Delta}_1 < 0. \tag{4.74}$$

In this design, the nonlinear stiffness term $\bar{k}\bar{\Omega}^{-2}/\bar{\mu}_0^{(1)}$ plays a positive stiffness in Equation (4.68) to increase the supporting frequency. Theoretically, choosing a very small negative value of $\tilde{k}_1 + \tilde{K}_1\bar{\Delta}_1$ satisfying Equation (4.74), we can obtain a sufficiently large supporting frequency to treat the supporting foundation as "rigid".

The fixed –free beam is used as a theoretical model for studying the high stiffness support. The parameters used to produce a high stiffness support is shown in Table 4.9.

Table 4.9 List of parameters used for high stiffness support

Parameters	Values
M	1
X_0	1
L_1	0.6
l	1
Y_0	0.467
L	0.5
ρ	0.01
s	1
x_0	-0.9
k	3.0025+6

Table 4.10 Natural frequencies of fixed- free beam

N	1	2	3	4	5
Frequency	∞	62.854	393.9279	1.1031e+3	2.1617e+3

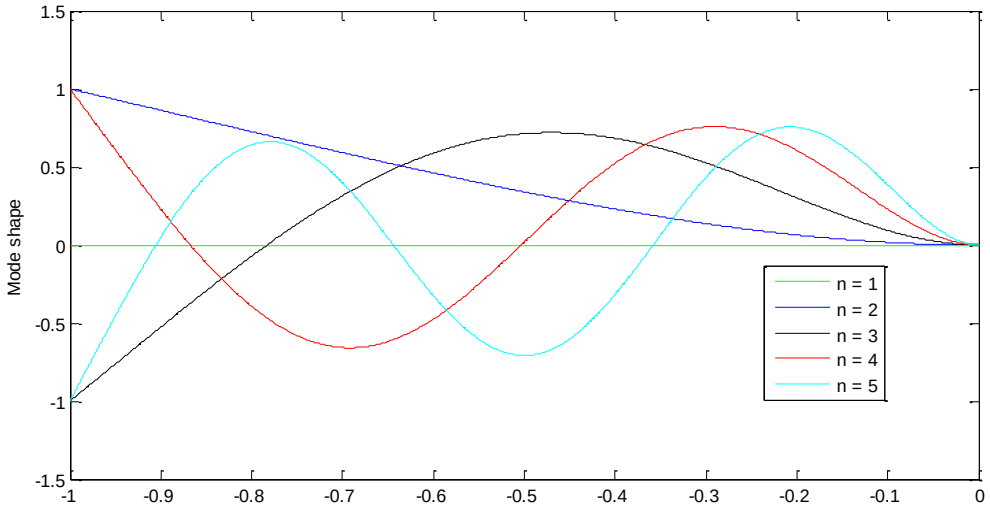

Figure 4.37 Mode shapes of the fixed-free beam

Table 4.11 Natural frequencies of beam on nonlinear vibration isolator with high stiffness support

N	1	2	3	4	5
Frequency	3.0821+3	76.9839	484.2000	1.3651e+3	2.7081e+3

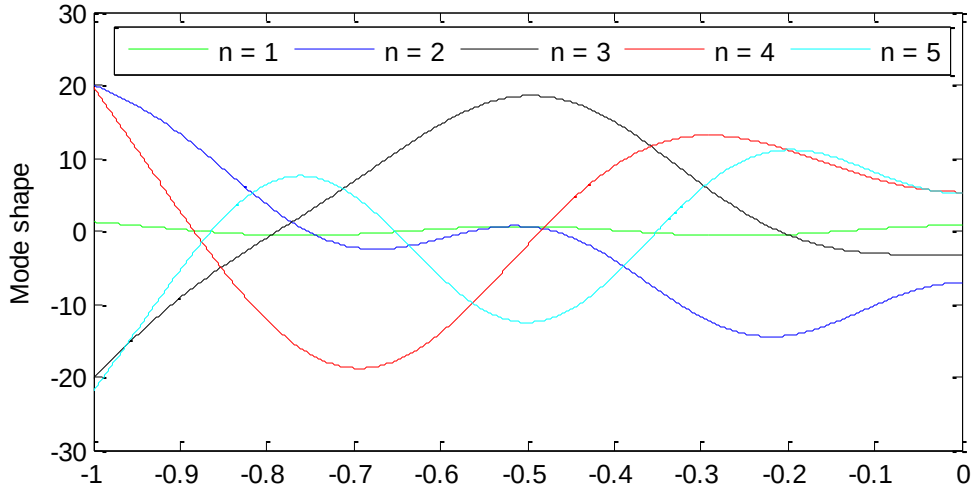

Figure 4.38 Mode shapes of beam on nonlinear isolator for modes n=1 to 5

The eigenvalue equation in (4.23) was solved numerically using Matlab and the eigenvalues and eigenfunctions of the beam supported on the nonlinear isolator for high stiffness support were found. The eigenvalues are the natural frequencies of the beam for mode n = 1 to 5 and is shown in Table 4.11. At the first mode, a very high natural frequency of 3.0821e+3 has been obtained. When compared to the natural frequencies of the fixed - free beam in Table 4.10, it can be seen that the first frequency is much lower than the theoretical one (infinity), while the other frequencies (at mode n=2,3,4,5) are higher than the theoretical one. The natural frequency error between the theoretical (fixed - free beam) and the calculated (beam - nonlinear isolator with high stiffness support) is shown in Table 4.12. The eigenfunctions are the generalised coordinates of the beam which is used in the mode summation equation in (4.3) to find the mode shapes of the beam supported on the nonlinear isolator as shown in Figure 4.38. The mode shape error between the theoretical (fixed - free beam) and calculated (beam - nonlinear isolator with high stiffness support) is shown in Table 4.13.

Table 4.12 Error between natural frequency of fixed - free beam to beam on nonlinear isolator with high stiffness support for modes, n= 1...5

N	1	2	3	4	5
Error	∞	14.1299	90.2721	262.00	546.4

Table 4.13 Error between mode shape of fixed - free beam to beam on nonlinear isolator with high stiffness support for modes, n= 1...5

N	1	2	3	4	5
Error	0.5714	10.5635	3.3855	3.0589	3.4969

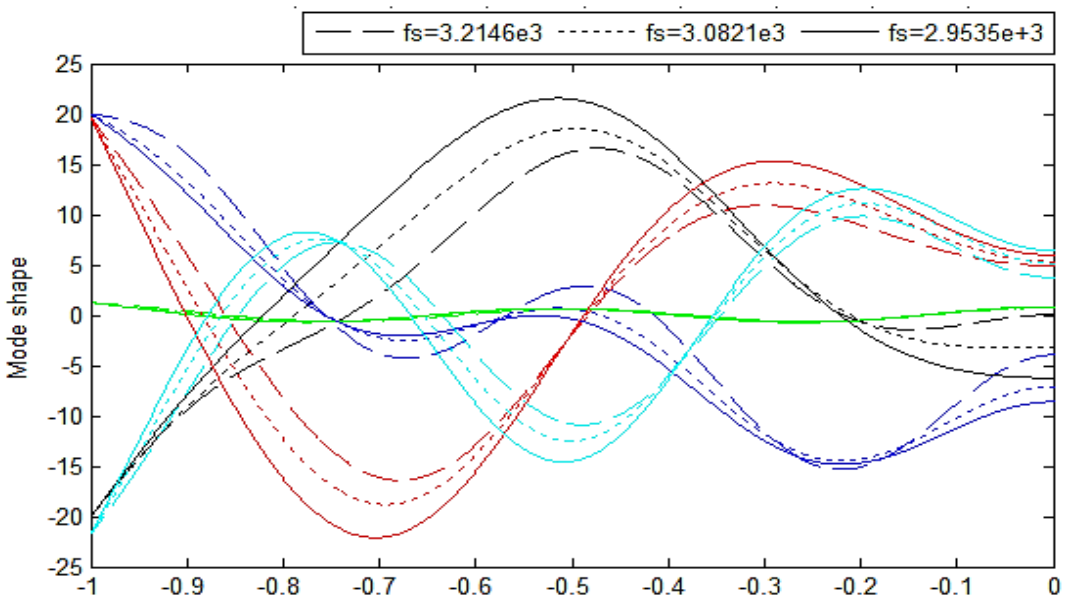

Figure 4.39 Mode shapes with varying supporting frequency, fs

To show that the motion at the middle point can be reduced with increasing supporting stiffness, a graph of the mode shapes with different supporting frequency is plotted. From Figure 4.39, it can be seen that the higher the supporting frequency, thus higher supporting siffness, the lower the motion at the middle point.

4.6 Special cases of the generalised interaction system

As mentioned earlier in Section 4.2, the generalised nonlinear suspension unit as shown in Figure 4.1 can be reduced to several simplified systems as reported in available references. Here, three special cases (simplified systems) of the generalised interaction system are presented.

4.6.1 Case I: A rigid mass supported by a nonlinear suspension unit.

Many engineering analysis only concern the supporting frequency of the structure treated as a rigid body supported by a nonlinear suspension unit, so that the elasticity of the structure can be omitted. For this case, mode set (4.2) includes only one rigid mode. From Equation (4.56), it follows

$$\boldsymbol{Y} = Y_1 = 1, m_b = \rho S/M,\ k_b = 0,\ G_b = \rho Sg/(M\Omega_0^2 l). \tag{4.75}$$

Here, m_b and G_b are the non-dimensional mass and static gravity of the beam, respectively. The additional stiffness k_b of the beam vanishes due to no elastic deformations involved. This

simplified system can be represented by a modified Figure 4.1 in which the beam is now deleted and the lumped mass $2M$ replaced by $2(M+\rho S)$ including the beam mass.

4.6.2 Case II: Simplified nonlinear suspension unit with fixed points A and B

If we consider a design with an infinite stiffness K_1 implying the two carts A and B are fixed at its original position $x=\hat{x}$, so that $\dot{x}=0=\ddot{x}$, the system in Figure 4.1 can be reduced to a simplified system as the one reported by Hao & Cao (2014) and shown in Figure 2.9 (b). The dynamic equilibrium equation for this simpified system is derived by letting $K_1 \to \infty$ and $x=\widehat{x}$ in Equation (4.7), i.e.

$$\begin{aligned} &M\ddot{y}+C\dot{y}+cy^2\dot{y}/\mu_{\hat{x}}^2+K(y+\Delta)+ky(1-l/\mu_{\hat{x}})=f+F_0\cos\Omega t-Mg,\\ &\hat{x}=\Delta_1,\quad \mu_{\hat{x}}=\sqrt{\hat{x}^2+y^2} \end{aligned} \tag{4.76}$$

By letting $\bar{K}_1 \to \infty$, $\gamma_K \to 0$, $\gamma_K \to 1$ and $\bar{\omega}^2 \to \infty$ in Equation (4.14), we obtain

$$\begin{gathered} \ddot{\bar{y}}+2\bar{\Omega}E\left(1+\frac{X_c}{\mu_{\mathrm{II}}^2}\bar{y}^2\right)\dot{\bar{y}}+\bar{\Omega}^2\left[\Gamma_K+\left(1-\frac{1}{\mu_{\mathrm{II}}}\right)\Gamma_k\right]\bar{y}=\bar{f}+\bar{F}_0\,\bar{cos}\,t-\bar{g}-\bar{F},\bar{\hat{x}}=\bar{\Delta}_1, \\ \mu_{\mathrm{II}}^2=\bar{\hat{x}}^2+\bar{y}^2. \end{gathered} \tag{4.77}$$

Furthermore, letting the vertical stiffness $K \to 0$, damper $C \to 0$ and $c \to 0$, we can further reduce the nonlinear suspension unit to a proposed nonlinear spring system for aircraft ground vibration tests (Molyneux 1958; Xing 1975) or an oscillator of which the nonlinear dynamical characteristics on stabilities, bifurcations and chaos has been reported (Cao *et al* 2008a,b). The dynamics of this further reduced suspesnsion unit is now governed by one of the following equations

$$\begin{aligned} M\ddot{y}+ky\left(1-\frac{l}{\mu_{\hat{x}}}\right)&=f+F_0\cos\Omega_0 t-Mg, \\ \ddot{\bar{y}}+\bar{\Omega}^2\,(1-1/\mu_{\mathrm{II}})\bar{y}&=\bar{f}+\bar{F}_0\,\bar{cos}\,t-\bar{g}. \end{aligned} \tag{4.78}$$

4.6.3 Case III: Simplified nonlinear suspension unit with two rigid springs k.

Assuming the two springs k are two rigid rods with damping $c=0$, we have a geometric relationship

$$x^2+y^2=l^2 \tag{4.79}$$

Considering this and stiffness $k \to \infty$, we introduce a finite spring force $T = k(\mu_x - l)$ into Equation (4.7) and obtain

$$\begin{aligned} m\ddot{x} + C_1\dot{x} + \frac{Tx}{l} + K_1(x - \Delta_1) = 0, \\ M\ddot{y} + C\dot{y} + K(y + \Delta) + Ty/l = f + F_0 \cos\Omega_0 t - Mg. \end{aligned} \tag{4.80}$$

Eliminating coordinate x and force T in Equation (4.8) we obtain the dynamic equilibrium equation of the simpified system. A further simplication can be done by neglecting the mass m and the damper C_1, which gives

$$\begin{aligned} M\ddot{y} + C\dot{y} + K(y + \Delta) + K_1(\Delta_1 - \sqrt{l^2 - y^2})y/\sqrt{l^2 - y^2} \\ = f + F_0 \cos\Omega_0 t - Mg. \end{aligned} \tag{4.81}$$

Furthermore, we can assume that the horizontal spring force $K_1\left(\Delta_1 - \sqrt{l^2 - y^2}\right) = K_1(\Delta_1 - x) = \widehat{F}$ applied at the points *A* and *B* is a constant (Platus 1992; Liu *et al* 2010). This design can be realised by using a gas spring K_1 of which the gas pressure change with *x* variations can be neglected. The positive value of the force $\hat{F}$ defines a pulling force while the negative one implies a compressed force. Now, Equation (4.81) reduces to

$$M\ddot{y} + C\dot{y} + K(y + \Delta) + \hat{F}\bar{y}/\mu_{\text{III}} = f + F_0 \cos\Omega_0 t - Mg, \mu_{\text{III}} = \sqrt{1 - \bar{y}^2}, \tag{4.82}$$

which has its nondimensional form

$$\ddot{\bar{y}} + 2\bar{\Omega}E\dot{\bar{y}} + (\bar{\Omega}^2 + \bar{\hat{F}}/\mu_{\text{III}})\bar{y} = \bar{f} + \bar{F}_0 \cos t - \bar{g} - \bar{F} \quad , \bar{\hat{F}} = \hat{F}/(M\Omega_0^2 l) \tag{4.83}$$

4.7 Performance Analysis

To evaluate the performance of the nonlinear isolator, a performance analysis was done by looking at the force transmissibility of the nonlinear isolator. Transmissibility is a measure of the reduction of vibration transmitted from a source to a receiver, in other words, it is an index of the performance of an isolator (Carella, 2008). Force transmissibility is the ratio between the magnitude of transmitted force (receiver) over magnitude of excitation force (source). In this section, the force transmissibility of the nonlinear isolator is investigated. A harmonic excitation force is acted upon the nonlinear isolator in Equation (4.14). The force transmissibility was found numerically using Matlab's ode45 solver with a given excitation force of F_0=0.6, and varying the excitation frequency, Ω_0 from 0 to 100Hz. An excitation force of F_0=0.6 was used so that the magnitude of transmissibility at 0 frequency ratio, Ω_0/Ω is 0dB. This means that the transmitted force is the same as the excitation force at Ω_0/Ω=0. The force transmissibility of the nonlinear isolator is compared to the force transmissibility of a linear

isolator as shown in Figure 4.40, using values of damping ratio of vertical damper, E= 6.15e-4, stiffness of oblique spring, k=K (stiffness of vertical spring) and initial condition y0=[0.5 0 7 0]. The initial condition is defined by y0=[q_1 $\dot{q}_1$ q_2 $\dot{q}_2$] where q_1: displacement of mass,m in the horizontal direction, $\dot{q}_1$: velocity of mass, m in the horizontal direction, q_2: displacement of mass, M in the vertical direction, $\dot{q}_2$: velocity of mass, M in the vertical direction. The initial condition used, y0=[0.5 0 7 0] means that the initial displacement of mass m is at 0.5 and the initial displacement of mass M is at 7. This also defines the position of the oblique spring. Figure 4.40 shows the transmissibility plot in decibel (dB) scale for the nonlinear isolator and linear isolator. The linear isolator consists of a mass with a vertical spring and damper. The effectiveness of a vibration isolator can be measured by looking at the bandwidth of the isolation region and peak transmissibility (Carella, 2008). Isolation region is the frequency region within which the transmitted force becomes smaller than the excitation force, that is when the transmissibility is less than 1, or 0dB. Peak transmissibility is the maximum amplitude of the transmitted force for a given amplitude of input force. It can be seen from Figure 4.40 that the transmissibility of the nonlinear isolator has a wider isolation region and a lower peak transmissibility compared to the linear isolator. This shows that the nonlinear isolator performs better than a linear isolator.

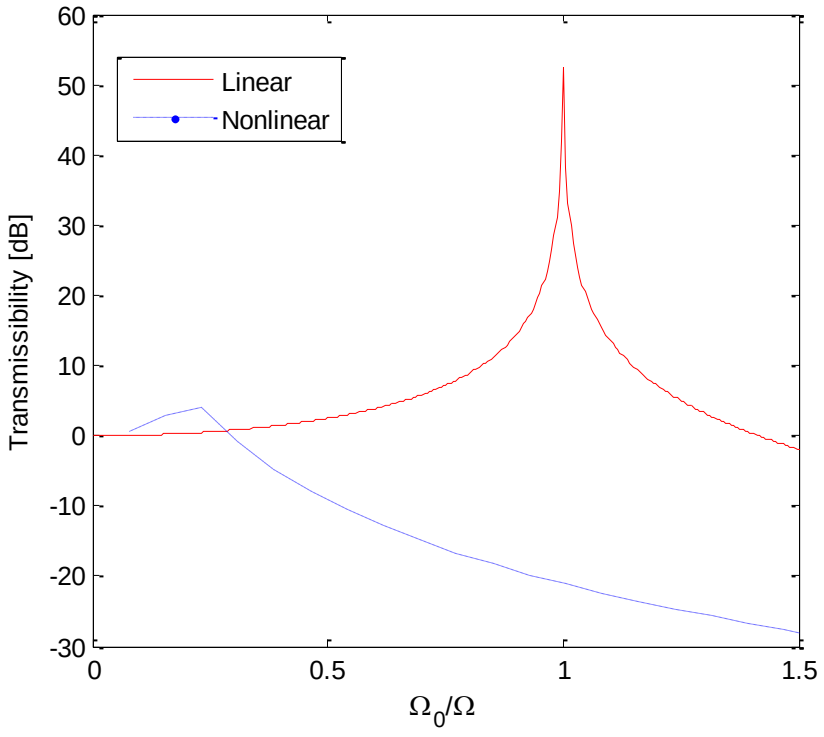

Figure 4.40 Force transmissibility of nonlinear isolator compared to a linear isolator

To observe the effect of changing the position of the oblique spring, the initial condition y0 was varied and the force transmissibility of the nonlinear isolator is shown in Figure 4.41. It is shown that the isolation region is wider as the initial displacement of the mass in the vertical direction is increased. Therefore, it is better to have a higher value of initial displacement of the mass in the vertical direction. Figure 4.42 shows the force transmissibility of the nonlinear isolator when the damping coefficient is varied. It can be seen that the peak transmissibility decreases as the damping coefficient increases. A reasonable amount of damping can therefore decrease the peak transmissibility which is beneficial for the performance of the nonlinear isolator. The force transmissibility of the nonlinear isolator with varying stiffness of the oblique spring is shown in Figure 4.43. It can be observed that as the stiffness increases, the beginning value of transmissibility increases and peak transmissibility also increases. Therefore, it is advised that a lower stiffness of the vertical spring is to be used to obtain a better performance for the nonlinear isolator. Finally, the force transmissibility of the nonlinear isolator is compared to the force transmissibility of a hardening HSLDS mount (Carella, 2008) as shown in Figure 4.44. It can be seen that the nonlinear isolator has a lower peak transmissibility and a wider isolation region and therefore has a better performance compared to the HSLDS mount.

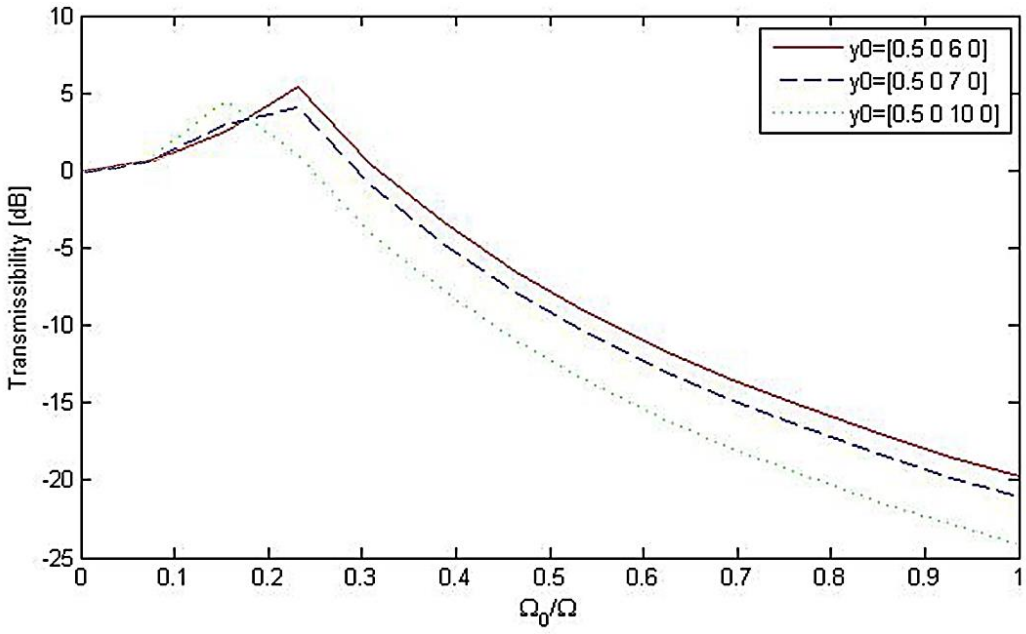

Figure 4.41 Force transmissibility of nonlinear isolator with different initial conditions

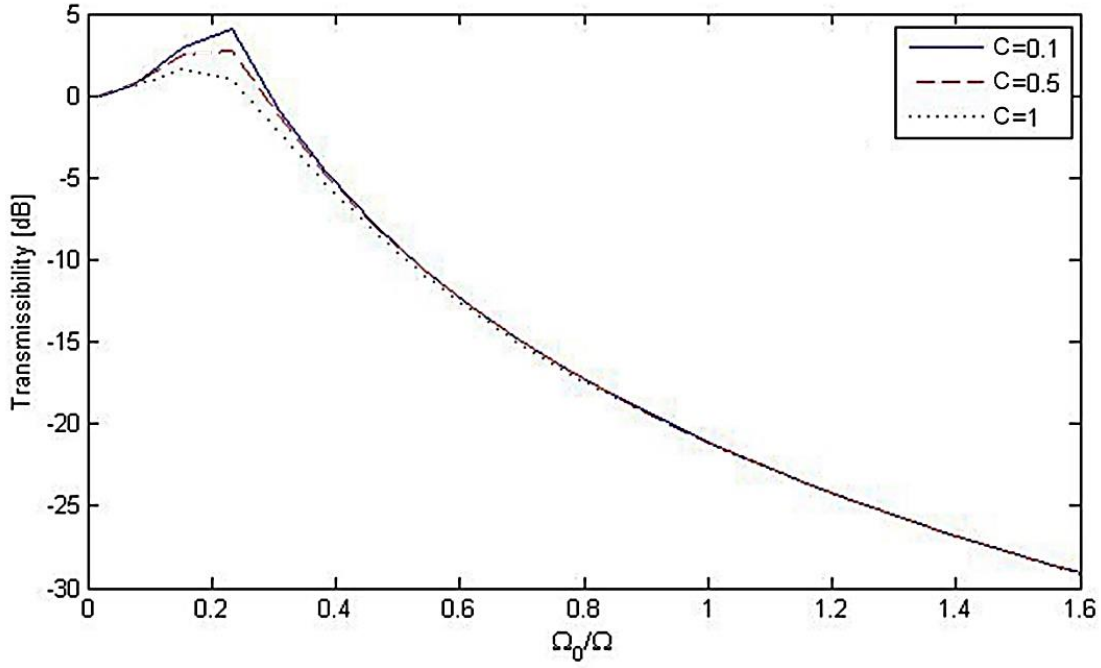

Figure 4.42 Force transmissibility of nonlinear isolator with varying damping coefficients

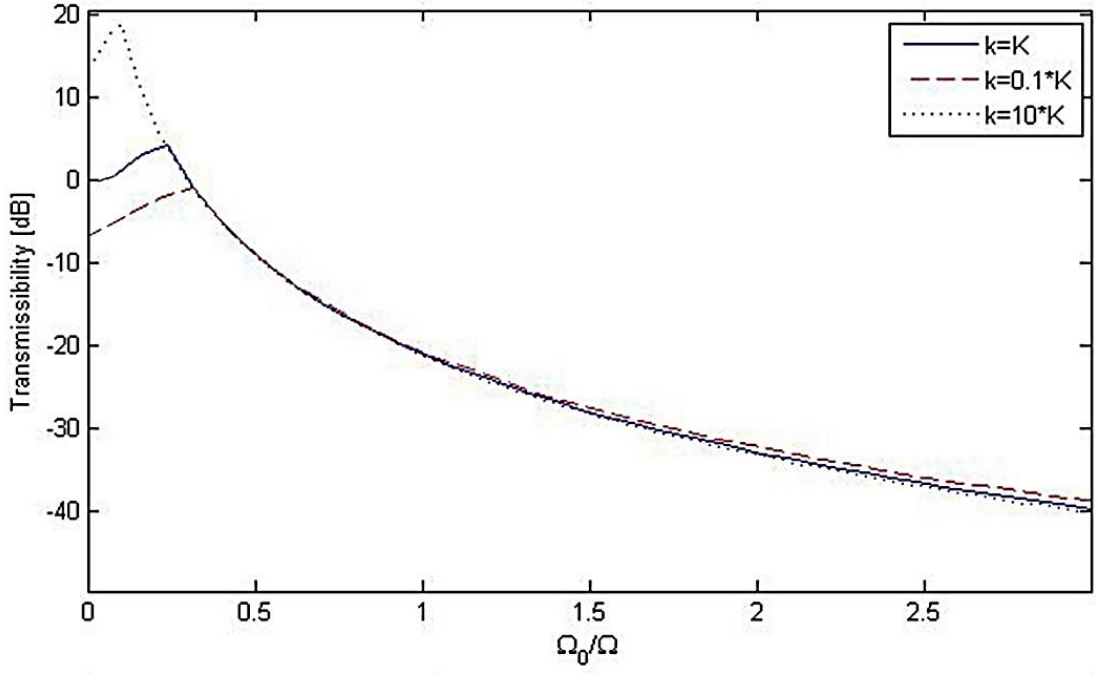

Figure 4.43 Force transmissibility of nonlinear isolator with varying stiffness

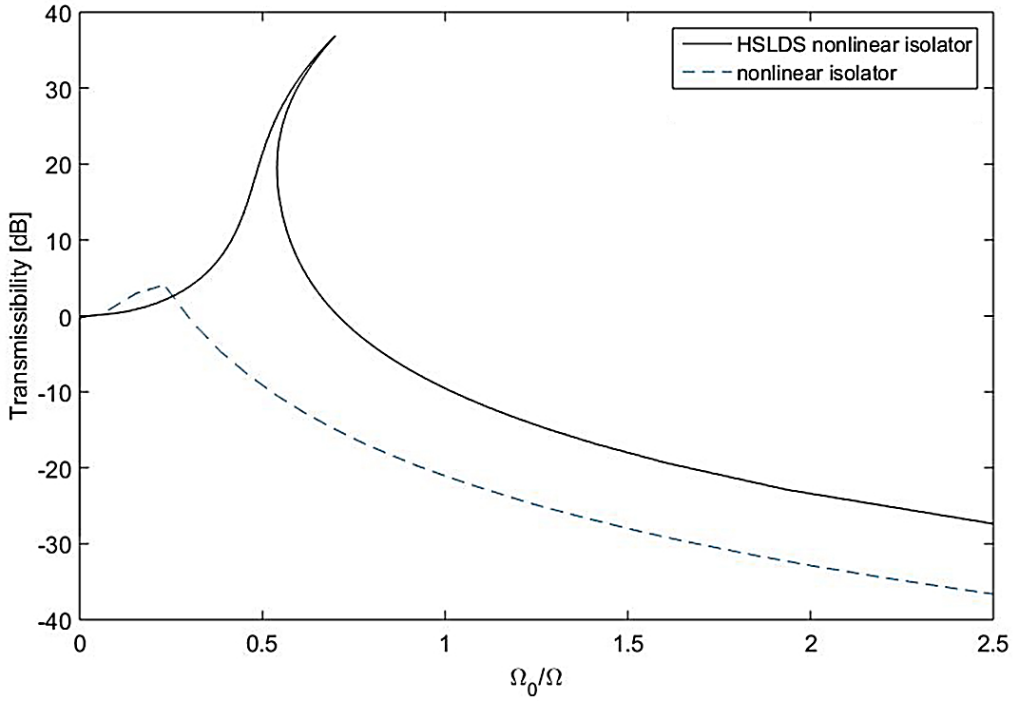

Figure 4.44 Force transmissibility of nonlinear isolator compared with HSLDS isolator

4.8 Summary

In summary, first the mathematical model of a beam and nonlinear isolator has been established. Then, nonlinear behaviour of the coupled system is studied. The equilibrium points are found and stability of small vibrations at the equilibrium points are analysed. The possible occurrence of bifurcation is depicted from the phase plot. Then, an analysis of the interaction between the beam and the nonlinear isolator has been done. The beam is shown to provide additional mass, stiffness and force to the isolator. Following this, the horizontal and vertical stiffness force of the nonlinear isolator affected by the additional dynamic stiffness of the beam has been studied. It is found that only the vertical stiffness force is affected by the added stiffness. The higher the value of added stiffness k_b, the higher the value of vertical stiffness force. Furthermore, the potential energy at a particular position on the nonlinear isolator with and without k_b is found, and it is observed that as k_b increases, the potential energy also increases. The undamped and damped phase trajectories of the nonlinear unit affected by the beam are found to be stable. Then, the beam nonlinear isolator design for low frequency support was discussed to find suitable values of parameters K, k and K_1. Linear analysis was done and the natural frequencies and mode shapes of the beam supported by the nonlinear isolator at modes n=1 to n=5 was found to be similar to the free-free beam natural frequencies and mode shapes. The frequency obtained at n=1 (rigid mode) of the beam is

6.7435e-7 which is less than one third of the first elastic natural frequency (n=2) of the free-free beam which has a value of 1. This satisfies the requirement to perform ground vibration test. The dynamic response of the system was analysed and the phase plots were found, and period doubling bifurcation is seen to occur when $F_0 = 1$ and Ω_0=0.5Hz. Poincare' maps were plotted and the system showed closed loop and no chaos was observed. The beam nonlinear isolator design for high frequency support was then discussed. Linear analysis was done to find the natural frequencies and mode shape for modes n=1 to n=5 . The results were compared with the fixed free beam and the error between the theoretical and calculated values were found. Three special cases for the generalised interaction system is then presented. Finally, performance analysis was done by looking at the force transmissibility of the nonlinear isolator. The effect of changing the position of the oblique spring, the damping coefficient and stiffness coefficient has been observed. The force transmissibility of the nonlinear isolator is also seen to perform better than a linear isolator and also performs better than a HSLDS mount.

Chapter 5: Beam- active vibration isolator interaction

5.1 Introduction

In this chapter, the beam-active isolator with low suspension frequency and high suspension frequency will be discussed. First, a mathematical model was developed, and its corresponding equations were derived. Then, interaction between the beam and the active isolator was analysed by considering the influence of beam motions on the active isolator. Following this, a suitable negative feedback gain for the beam-active isolator that can provide a low suspension frequency and a high suspension frequency was obtained and inserted into the system to observe its response. Then, the dynamic response of the beam-active isolator system with low suspension frequency and high suspension frequency is found by applying two sinusoidal forces to the beam to see the effect of the supporting system on to the beam.

5.2 Beam-active isolator with low suspension frequency

The active isolation unit was designed referring to the work of Xing et al. (2005) where they illustrated several design strategies that can produce zero or infinite-dynamic modulus. A beam is attached on top of the active isolator to analyse the beam active-isolator interaction.

5.2.1 Mathematical model of an integrated active isolator-structure interaction

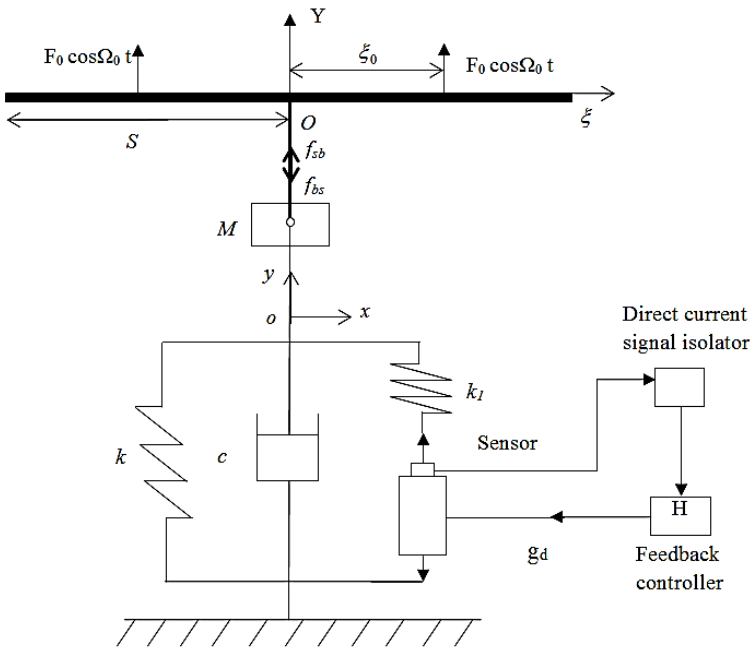

Figure 5.1 An integrated system consisting of an elastic beam and an active isolator unit.

Figure 5.1 shows an integrated interaction system in which an elastic structure is supported by an active vibration isolation unit. To simplify the mathematical analysis and maintain the essential characteristics of the problem, the structure is considered as a uniform elastic free-free beam subject to two harmonic forces $F_0\, cos\, \Omega_0\, t$ applied symmetrically at point $\xi_0$under the beam coordinate system$O - \xi Y$fixed at the middle point O of the beam. There is a lumped mass M connected at point O by a rigid rod of which the mass is included into$M$. The beam is of span length $2S$, mass density ρ per unit length and bending stiffness $\Psi = EI$. Since the beam is elastic, its deflection $Y(\xi, t)$ is a function of beam material point ξ and time t. The lumped mass $M$is supported by an active isolation system and it moves in the y direction only.

The active isolation system consists of k and c which denote the stiffness and damping coefficients of the mechanical device supporting the static weight of the elastic structure. A spring of small stiffness k_1 is connected in series with an active displacement feedback controller. The feedback control system provides a dynamic force f_c=$g_d y$ proportional to the displacement. A direct current signal isolator is used to isolate the signal produced by static deflections caused by the weight of the aircraft so that the feedback system produces only alternating forces acting on the mass. Therefore, the feedback system does not affect the static stiffness of the supporting system.

5.2.1.1 Dynamic equilibrium equation and boundary conditions of beam structure

Referring to Section 4.2.1.1 in Chapter 4, the mode equation describing the beam motion is

$$\begin{aligned} &\boldsymbol{m}\ddot{\boldsymbol{\Phi}} + \boldsymbol{k}\boldsymbol{\Phi} = \boldsymbol{Y}^T(0)f_{bs} + \boldsymbol{Y}^T(\xi_0)F_0\cos\Omega_0 t, \\ &\boldsymbol{m} = \mathrm{diag}(M_{nn}), \qquad \boldsymbol{k} = \mathrm{diag}(K_{nn}), \qquad \boldsymbol{\Lambda}^2 = \mathrm{diag}(\widehat{\Omega}_n^2) \end{aligned} \tag{5.1}$$

5.2.1.2 Dynamic equilibrium equation of the active suspension system

The dynamic equilibrium equation of the active suspension system is described by

$$M\ddot{y} + c\dot{y} + \left(k + \frac{k_1 g_d}{k_1 + g_d}\right)y = f_{\mathrm{sb}} \tag{5.2}$$

Here, the force f_{sb} denotes the reaction force from the beam to the lumped mass M.

5.2.1.3 Interaction conditions between the beam structure and the active suspension unit

On the interaction section $\xi = 0$ between the beam and the active suspension unit, a dynamic equilibrium condition and a geometrical constraint condition are required, as shown in Chapter 4 in Equation (4.9) and Equation (4.10) which is written in the mode form as

$$\boldsymbol{Y}_0\boldsymbol{\Phi} = y, \qquad \boldsymbol{Y}_0 = \boldsymbol{Y}(0) \tag{5.3}$$

5.2.2 Interaction analysis of beam-active isolator with low suspension frequency

5.2.2.1 Equation governing the influence of beam motions on active suspension unit

To design an accurate active isolator, the influence of the beam onto the isolator should be considered.

From Equation (5.1), we have

$$\begin{aligned} &\boldsymbol{m}\ddot{\boldsymbol{\Phi}} + m\Lambda^2\boldsymbol{\Phi} = \boldsymbol{Y}_0^T f_{bs} + \boldsymbol{Y}_F^T F_0\cos\Omega_0 t, \qquad Y_F = Y(\xi_0) \\ &\ddot{\boldsymbol{\Phi}} + \Lambda^2\boldsymbol{\Phi} = m^{-1}\boldsymbol{Y}_0^T f_{bs} + m^{-1}\boldsymbol{Y}_F^T F_0\cos\Omega_0 t \end{aligned} \tag{5.4}$$

which when pre-multiplied by $\boldsymbol{Y}_0$, gives

$$\begin{aligned} &\boldsymbol{Y_0}\ddot{\boldsymbol{\Phi}} + \boldsymbol{Y_0}\Lambda^2\boldsymbol{\Phi} = \boldsymbol{Y_0}\boldsymbol{m^{-1}}\boldsymbol{Y}_0^T f_{bs} + \boldsymbol{Y_0}\boldsymbol{m^{-1}}\boldsymbol{Y}_F^T F_0\cos\Omega_0 t \\ &= m_b^{-1} f_{bs} + \boldsymbol{Y_0}\boldsymbol{m^{-1}}\boldsymbol{Y}_F^T F_0\cos\Omega_0 t, \qquad m_b^{-1} = \boldsymbol{Y_0}\boldsymbol{m^{-1}}\boldsymbol{Y}_0^T \end{aligned} \tag{5.5}$$

Since

$$m_b^{-1} = \boldsymbol{Y_0 m^{-1} Y_0^T} = \sum_{n=1}^{N} M_{nn}^{-1} Y_{n0}^2 > 0, \tag{5.6}$$

$$m_b = \frac{1}{\sum_{n=1}^{N} \frac{Y_{n0}^2}{M_{nn}}} \tag{5.7}$$

we have

$$\begin{aligned} f_{bs} &= m_b \boldsymbol{Y_0 \ddot{\Phi}} + m_b \boldsymbol{Y_0 \bar{\Lambda}^2 \Phi} - m_b \boldsymbol{Y_0 m^{-1} Y_F^T} F_0 \cos \Omega_0 t \\ &= m_b \ddot{Y} + k_b(\boldsymbol{\Phi}) Y - f_b F_0 \cos \Omega_0 t \end{aligned} \tag{5.8}$$

where

$$k_b(\boldsymbol{\Phi}) = m_b \frac{\boldsymbol{Y_0 \Lambda^2 \Phi}}{\boldsymbol{Y_0 \Phi}} = \frac{m_b \sum_{n=1}^{N} Y_{n0} \hat{\Omega}_n^2 \varphi_n}{\sum_{n=1}^{N} Y_{n0} \varphi_n}, f_b = m_b \boldsymbol{Y_0 m^{-1} Y_F^T} \tag{5.9}$$

Since, from Equation (4.9) in Chapter 4

$$-f_{bs} = f_{sb}$$

we have

$$f_{sb} = -m_b \ddot{y} - k_b(\boldsymbol{\Phi}) y + f_b F_0 \cos \Omega_0 t \tag{5.10}$$

Substitute Equation (5.10) into Equation (5.2), we obtain

$$\begin{aligned} M\ddot{y} + c\dot{y} + \left(k + \frac{k_1 g_d}{k_1 + g_d}\right) y &= -m_b \ddot{y} - k_b(\boldsymbol{\Phi}) y + f_b F_0 \cos \Omega_0 t \\ (M + m_b)\ddot{y} + c\dot{y} + \left(k + \frac{k_1 g_d}{k_1 + g_d} + k_b(\boldsymbol{\Phi})\right) y &= f_b F_0 \cos \Omega_0 t \end{aligned} \tag{5.11}$$

Here, m_b, k_b represent an additional dynamic mass and stiffness, respectively, which are added to the active suspension system by the beam due to their dynamic interactions. f_b defines a force factor at which the excitation force is added to the lumped mass. The values of these added parameters depend on the retained mode number of the beam. The added stiffness k_b also involves the dynamic response Φ of the beam. For a unit dynamic response of mode *n,* i.e. $\Phi^T = [0 \quad \cdots \quad 0 \quad \varphi_n \quad 0 \quad \cdots \quad 0]^T$, the added mass and stiffness are respectively obtained by Equations (5.12) and (5.13),

$$m_b(\varphi_n) = M_{nn} Y_{n0}^{-2}, \tag{5.12}$$

$$k_b(\varphi_n) = m_b \hat{\Omega}_n^2 = M_{nn} Y_{n0}^{-2} K_{nn} / M_{nn} = Y_{n0}^{-2} K_{nn}. \tag{5.13}$$

Here, we consider $N = 1$ implying that only one rigid mode $Y_1 = 1$ with $\hat{\Omega}_1^2 = 0$ in Equation (5.1) is retained, so that $\boldsymbol{Y}_0 = 1$, and therefore we have

$$m = M_{11} = \rho S, \qquad m_b = M_{11}, \qquad k_b = 0, \qquad f_b = 1 \tag{5.14}$$

Physically, m_b in Equation (5.14) is the total mass of the beam. Since the beam is considered rigid and there is no elastic deformation, the added stiffness $k_b = 0$, and the force factor $f_b = 1$.

Table 5.1 and Table 5.2 show the values of the added parameters affected by retained mode number, *N* and values of the added parameters affected by a unit dynamic response mode, *n*.

Table 5.1 The values of added parameters affected by retained mode number *N* of the beam on the active suspension unit, ($\xi_0 = 1$).

N	1	2	3	4	5
m_b	100	167.6685	217.0955	267.1206	317.1223
f_b	1.000	-0.9685	0.6986	-0.7075	0.7071

Table 5.2 The values of added parameters affected by a unit dynamic response mode *n* of the beam on the active suspension unit.

n	1	2	3	4	5
$m_b(\varphi_n)$	100	67.67	49.43	50.03	50.00
$k_b(\varphi_n)$	0	68	1443	8908	30787

The values from Table 5.1 and Table 5.2 were plotted in Figure 5.2 to Figure 5.5 to further illustrate the results. It can be seen from Figure 5.2 that the additional mass, m_b increases as the number of retained mode, *N* increases. Figure 5.3 shows the graph of force factor f_b at $\xi_0 = 1$ versus retained mode number. The value of force factor is seen to be positive at odd numbers of retained modes and negative at even numbers of retained modes. The positive value of force factor defines a pulling force and a negative value implies a compressed force.

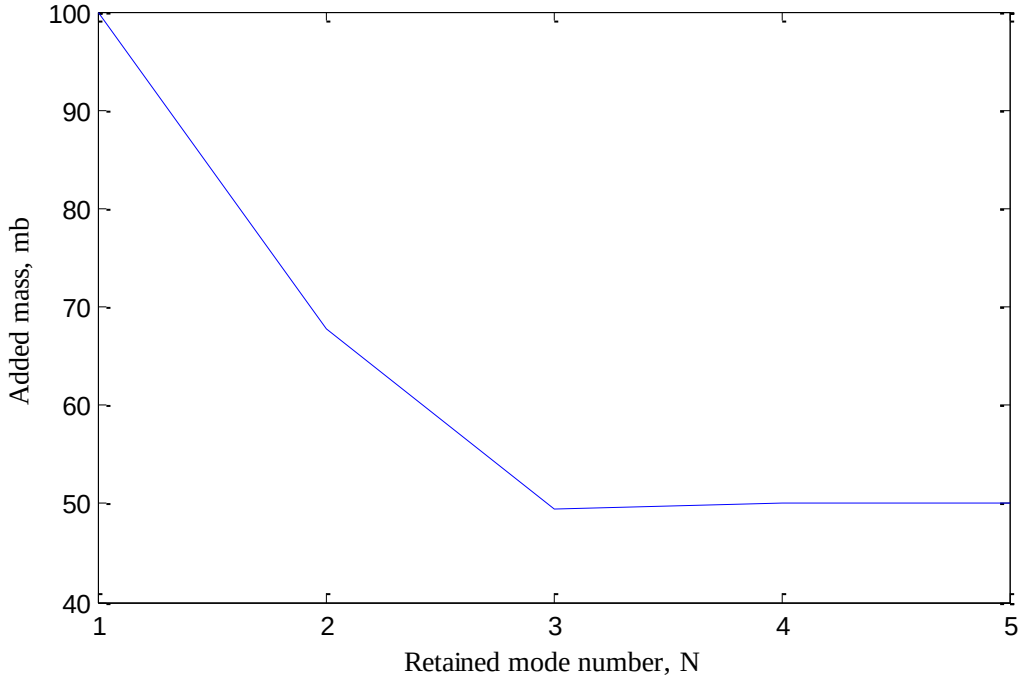

Figure 5.2 Graph of additional mass with respect to retained mode number

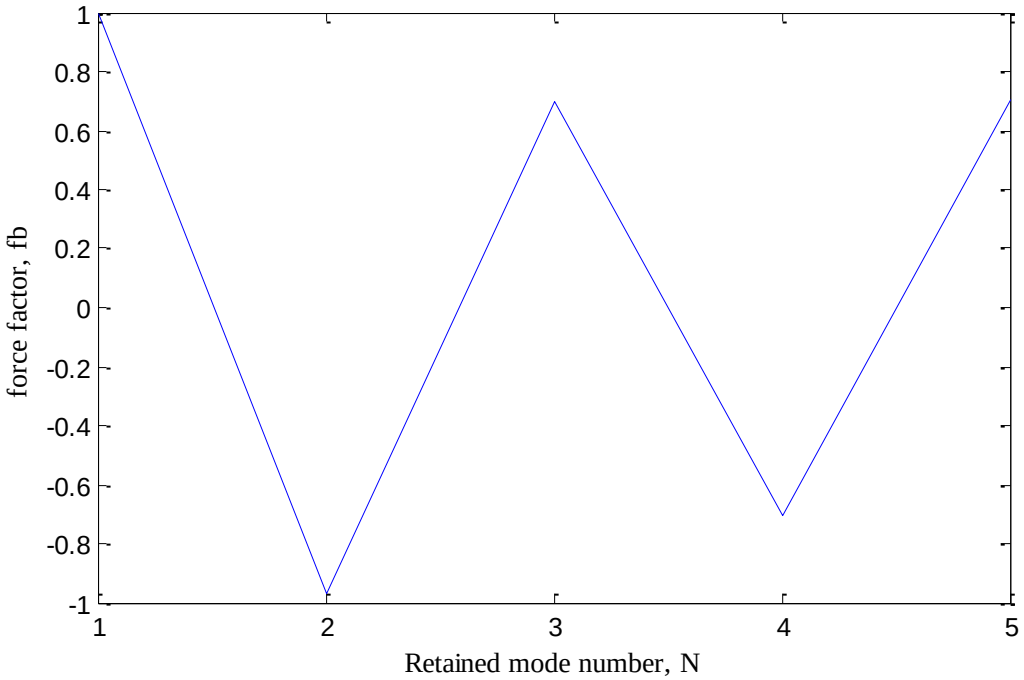

Figure 5.3 Graph of force factor with respect to retained mode number

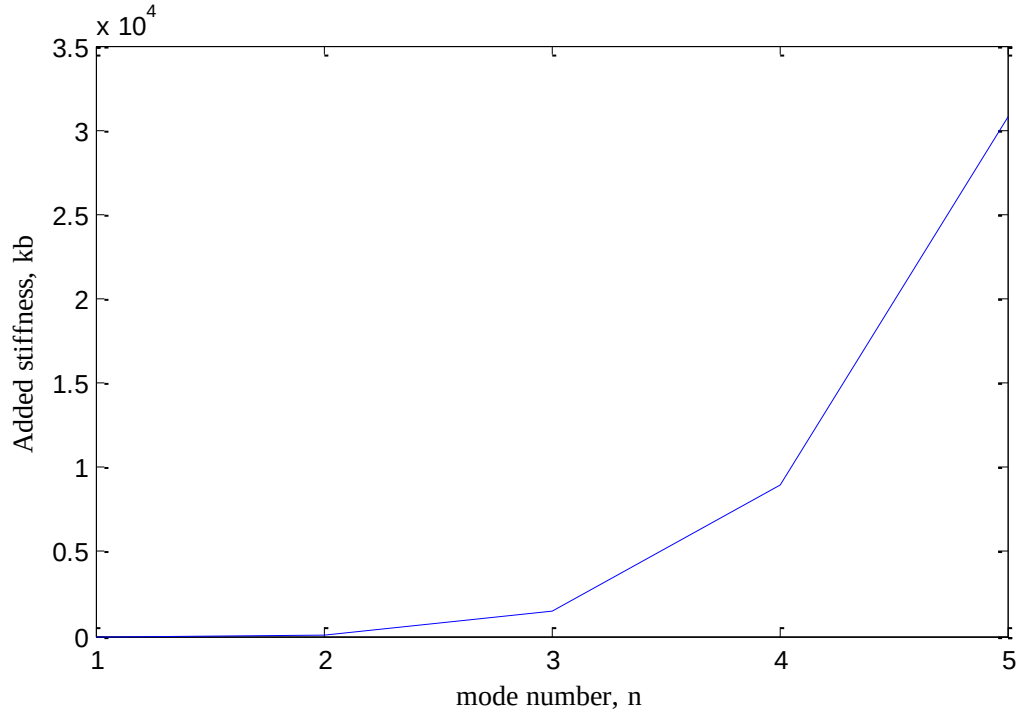

Figure 5.4 Graph of added stiffness for a unit dynamic response with respect to mode number

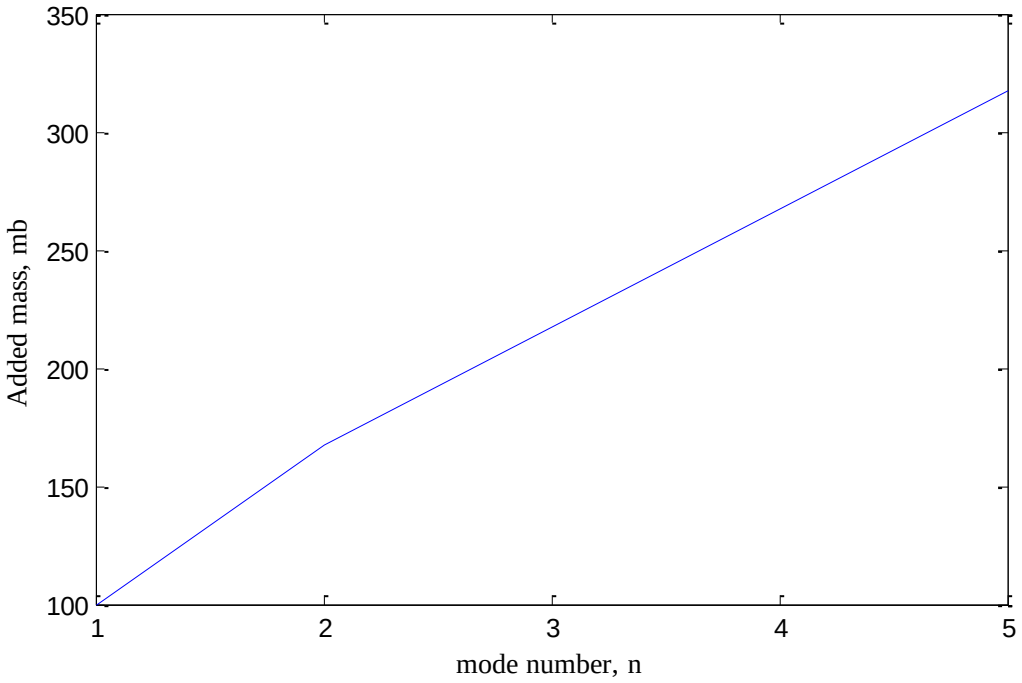

Figure 5.5 Graph of added mass for a unit dynamic response with respect to mode number

Figure 5.4 and Figure 5.5 illustrate the graph of added mass, $m_b(\varphi_n)$ and added stiffness, $k_b(\varphi_n)$ for a unit dynamic response versus mode number, n**.** It can be seen that the added mass and stiffness increases as the mode number increases.

5.3 Controller design for beam-active isolator with low suspension frequency

5.3.1 Suitable negative feedback for a low suspension frequency

In the first instance, it is considered that *M* is the mass of the fuselage of an airplane, and the beam is the wing. The total mass of the airplane is *M* + total mass of the wing. This can be used to find a suitable spring stiffness, *k* for the static case.

The static equilibrium equation describing the system at its static position is given by

$$(M + \rho S)g = k\delta \tag{5.15}$$

where

g : acceleration of gravity

δ : static compression deformation of the mechanical spring

Therefore, the static stiffness, *k* is given by

$$k = \frac{(M + \rho S)g}{\delta} \tag{5.16}$$

The supporting frequency in static equilibrium is described by

$$\Omega_s = \sqrt{\frac{k}{(M + \rho S)}} \tag{5.17}$$

From Equation (5.11), the frequency of the supporting system for a unit dynamic response mode *n* is given by

$$\Omega_n = \sqrt{\frac{k + \frac{k_1 g_d}{k_1 + g_d} + k_b(\varphi_n)}{M + m_b(\varphi_n)}} = \sqrt{\frac{k - \frac{k_1 |g_d|}{k_1 - |g_d|} + k_b(\varphi_n)}{M + m_b(\varphi_n)}} \tag{5.18}$$

where

$$\left(k - \frac{k_1|g_d|}{k_1 - |g_d|} + k_b(\varphi_n)\right): \text{ dynamic stiffness}$$

k_1 : stiffness of spring connected in series with the active controller

g_d : negative feedback gain

$k_b(\varphi_n)$: additional dynamic stiffness added by the beam

$m_b(\varphi_n)$: additional dynamic mass added by the beam

A suitably chosen negative feedback gain, g_d satisfying the condition

$$-\left(\frac{k_1(k + k_b(\varphi_n))}{k_1 + k + k_b(\varphi_n)}\right) < g_d < 0 \tag{5.19}$$

allows a reduced frequency to be achieved as indicated by Equation (5.18).

Here, three cases for the beam-active isolator with low suspension frequency were studied:

1. The first case is when there is no support and no feedback control, so the beam is in free free state. The natural frequencies and mode shapes of the free free beam are shown in Table 4.6 and Figure 4.27 in Chapter 4.

2. The second case is when there is support but no feedback control as shown in Table 5.3.

Table 5.3 Beam frequency at modes 1 to 5 when there is support but no feedback control

N	1	2	3	4	5
Frequency	4.4075	5.4371	8.2170	14.5949	25.3404

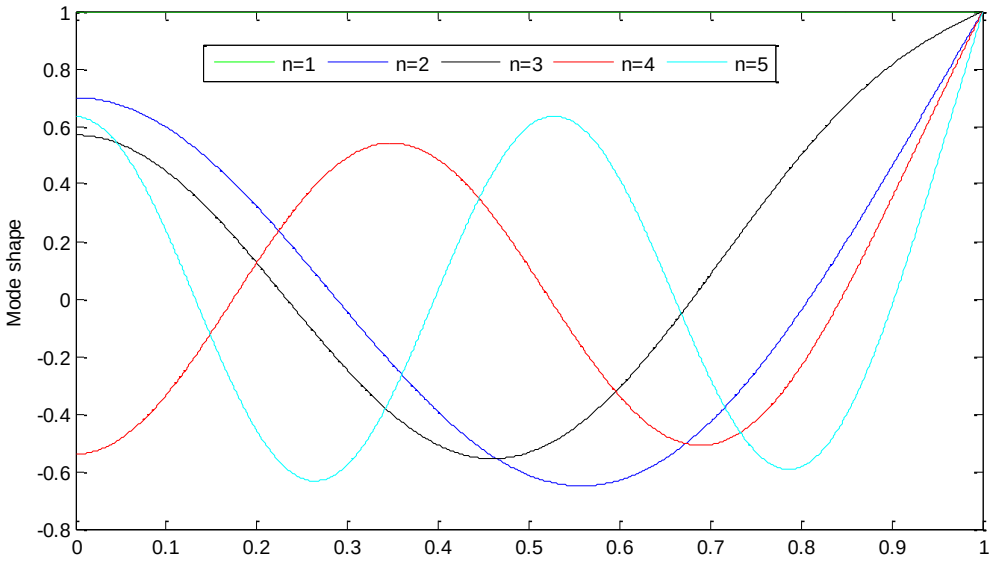

Figure 5.6 Mode shapes of beam when there is support but no feedback control

The natural frequencies of the beam in Table 5.3 are higher then the natural frequencies of the free free beam. This is due to the effect of the mass M and the stiffnes k at the isolator. The mode shape in Figure 5.6 for modes n=2 and n =3 differ from the mode shapes of the free free beam due to the difference in natural frequency.

3. The third case is when there is support and with the presence of feedback control.

For the third case, as shown in Equation (5.18), the feedback control which uses the negative feedback gain, g_d is related to the dynamic stiffness. In the region of the static equilibrium position of the whole system, the dynamic stiffness is adjusted to produce a supporting system of very low frequency.

Using the Matlab 'fmincon' function, the minimum value of the dynamic stiffness is found and the value of k_1 and g_d that contribute to the minimum value is shown in Table 5.4.

Table 5.4 Value of g_d and k_1 that produces a minimum dynamic stiffness

Mode	k_1	g_d	Dynamic stiffness (minimum)	Suspension frequency
1	132.56	-124.17	0.1436	0.0377

Using the value of k_1 and g_d from Table 5.4, the frequency and mode shapes of the beam at modes 1 to 5 are found as shown in Table 5.5 and Figure 5.7. It can be seen that the natural frequencies at modes 2,3,4 and 5 are slightly lower than the corresponding modes of the free free beam. This is due to the lumped mass which does not exist in the free free beam state. The

mode shapes in Figure 5.7 are very similar to the mode shapes of the free- free beam in Figure 4.27 in Chapter 4.

The rigid mode at n=1 is the supporting frequency of the system and the second mode, n=2 corresponds to the beam first bending frequency in free-free state. Due to the effect of the isolation support, the frequency of the second mode will be higher than the first mode. Comparing

Table 5.3 and Table 5.5, for the beam first elastic frequency at n=2, without support, its natural frequency is 1. When there is support but no feedback control, its frequency increases to 5.4371. When there is support, and feedback control is applied, the suspension frequency at n=1 is 0.0377 which is less than one third of the first elastic natural frequency. This satisfies the requirement to perform ground vibration test.

The error between the theoretical (free-free beam) values and calculated values are compared in Table 5.6 and Table 5.7.

Table 5.5 Beam frequency at modes 1 to 5 when there is support and feedback control

n	1	2	3	4	5
Frequency	0.0377	0.9962	5.3495	13.2124	24.5697

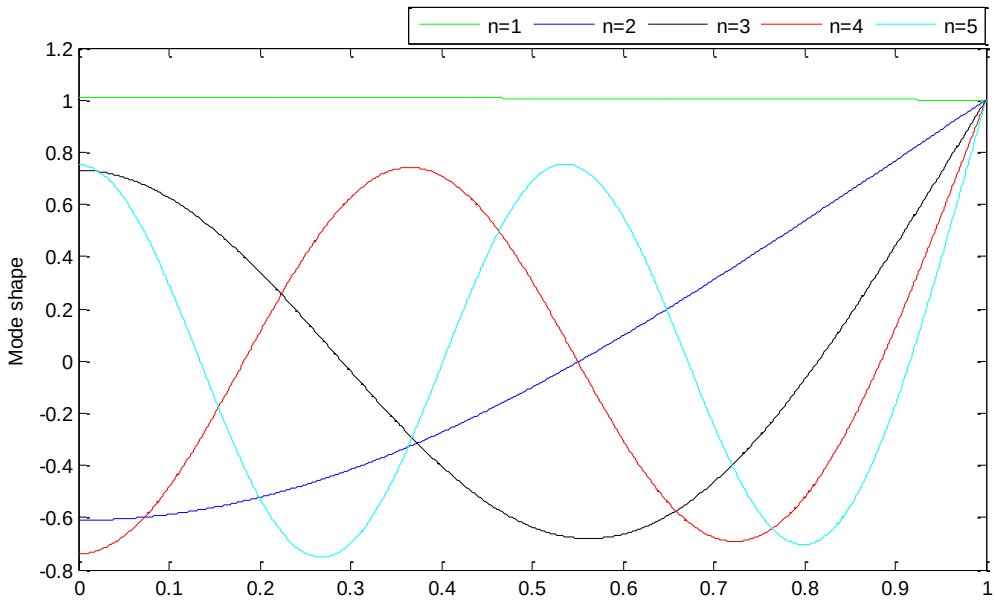

Figure 5.7 Mode shapes of beam when there is support and feedback control is applied

Table 5.6 Error between natural frequency of free - free beam to beam on active isolator with low stiffness support for modes, *n*= 1...5

N	1	2	3	4	5
Error	0.0377	0.0038	0.0544	0.1319	0.2442

Table 5.7 Error between mode shape of free - free beam to beam on active isolator with low stiffness support for modes, *n*= 1...5

N	1	2	3	4	5
Error	0.0063	0.0020	0.0154	0.0248	0.0345

From Equation (5.19), introducing α, where

$$\begin{aligned} & g_d = -\left(\frac{k_1(k+k_b(\varphi_n)}{k_1+k+k_b(\varphi_n)}\right)+\alpha > -\left(\frac{k_1(k+k_b(\varphi_n)}{k_1+k+k_b(\varphi_n)}\right) \\ & \longrightarrow \alpha > 0 \\ & -\left(\frac{k_1(k+k_b(\varphi_n)}{k_1+k+k_b(\varphi_n)}\right)+\alpha < 0 \\ & \longrightarrow \alpha < \left(\frac{k_1(k+k_b(\varphi_n)}{k_1+k+k_b(\varphi_n)}\right) \\ & 0 < \alpha < \left(\frac{k_1(k+k_b(\varphi_n)}{k_1+k+k_b(\varphi_n)}\right) \\ & 0 < \alpha < G \end{aligned} \tag{5.20}$$

where

$$G = \left(\frac{k_1(k+k_b(\varphi_n)}{k_1+k+k_b(\varphi_n)}\right) \tag{5.21}$$

Varying the value of α according to the range in Equation (5.20) and inserting it into the equation of suspension frequency (5.18) will give the graph in Figure 5.8. It is found that the lower the value of α, the lower the suspension frequency.

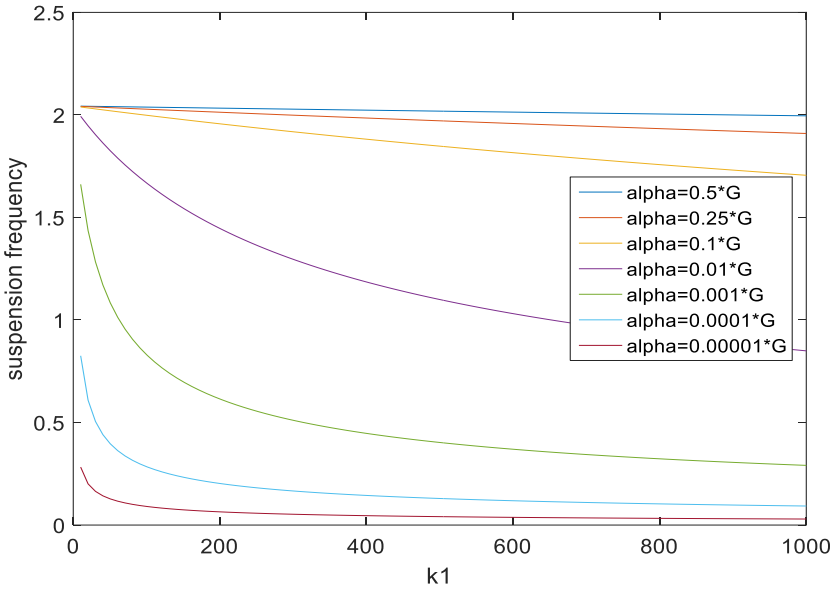

Figure 5.8 Effect of α on the suspension frequency using k=19620 and k_1=0 to 1000

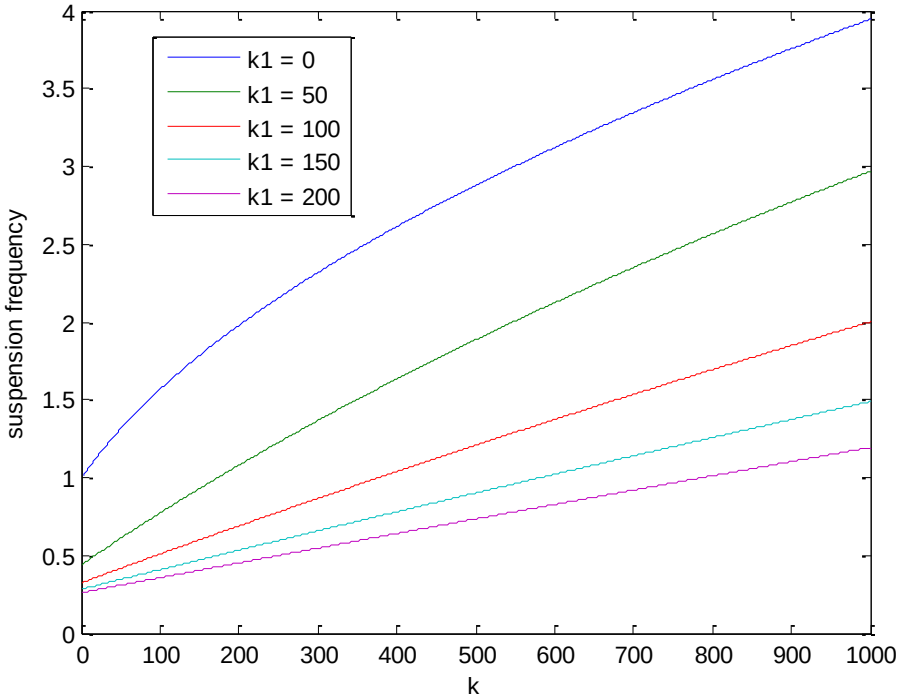

Figure 5.9 Suspension frequency VS k with different values of k_1

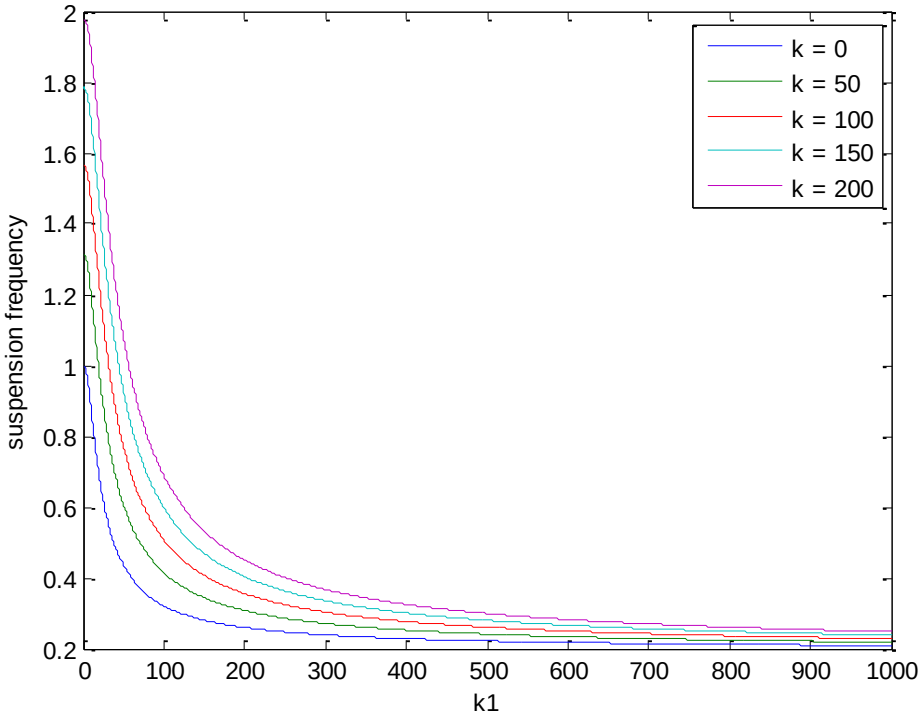

Figure 5.10 Suspension frequency VS k1 with different values of k

Figure 5.9 shows the graph of suspension frequency with respect to stiffness, k using different values of stiffness, k_1. It can be seen that the suspension frequency increases as k increases, however, the smaller the value of k_1 used, the lower the value of suspension frequency. Figure 5.10 illustrates the graph of suspension frequency with respect to stiffness k_1 using different values of k. It is shown that as k_1 increases the suspension frequency decreases, but the higher the value of k, the higher the suspension frequency.

5.3.2 Applying active control

The response of linear time-invariant models expressed in the standard state space equation form is

$$\begin{aligned} \dot{x} &= Ax + Bu \\ y &= Cx + Du \end{aligned} \tag{5.22}$$

that is, as a set of coupled, first-order differential equations. The solution proceeds in two steps; first the state-variable response $x(t)$ is found by solving the set of first-order state equations (the first equation in (5.22)), and then the state response is substituted into the algebraic output equations (the second equation in (5.22)) in order to compute $y(t)$.

Based on the equation of motion of the beam and equation of motion of the active suspension unit in Equations (5.1) and (5.2), the state space representation of the proposed suspension system is

$$\begin{bmatrix}\dot{x}_1\\ \dot{x}_2\end{bmatrix} = \underbrace{\begin{bmatrix} 0 & 1 \\ -\frac{1}{M+m_b(\varphi_n)}\left(k+\frac{k_1 g_d}{k_1+g_d}+k_b(\varphi_n)\right) & -\frac{c}{M+m_b(\varphi_n)}\end{bmatrix}}_{A}\begin{bmatrix}x_1\\ x_2\end{bmatrix} + \underbrace{\begin{bmatrix}0\\ \frac{1}{M+m_b(\varphi_n)}\end{bmatrix}}_{B} f_b F_0 \cos\Omega_0 t \tag{5.23}$$

$$y = \underbrace{[1 \quad 0]}_{C}\begin{bmatrix}x_1\\ x_2\end{bmatrix} + \underbrace{[0]}_{D} f_b F_0 \cos\Omega_0 t$$

Inserting the values of matrices *A, B, C* and *D* from Equation (5.23) into the Simulink block diagram as shown in Figure 5.11 and Matlab m-file, and varying the value of negative feedback gain, we can observe the displacement of the mass and the beam ($M + m_b(\varphi_n)$) as shown in Figure 5.12.

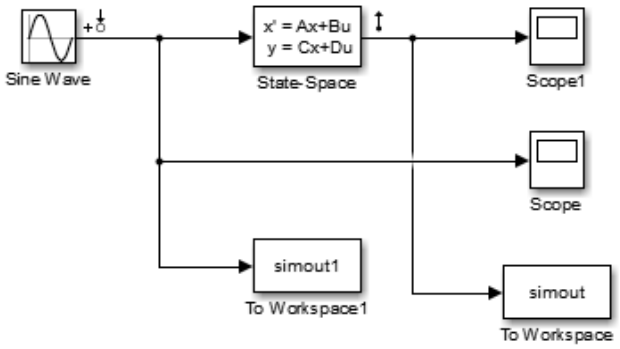

Figure 5.11 Simulink block diagram of the active suspension system

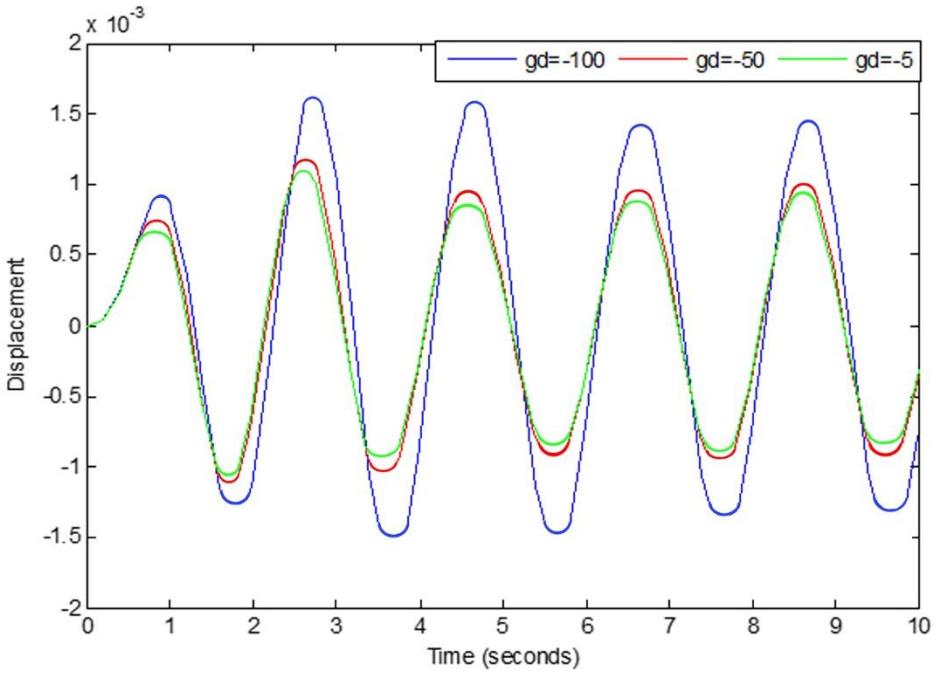

Figure 5.12 Displacement of mass and beam $(M + m_b(\varphi_n))$ using different values of g_d

From Figure 5.12, it is observed that the displacement of the mass and beam decreases as the value of negative feedback gain g_d increases.

5.4 Beam-active isolator with high suspension frequency

5.4.1 Mathematical model and governing equations

Figure 5.13 shows a suspension system with a high supporting stiffness which is similar to the suspension system with a low supporting stiffness as shown in Figure 5.1, except that it does not have a direct current signal isolator. The direct current signal isolator is used to isolate direct current signals, such as signals produced by static deflections caused by the weight of the aircraft. Therefore, it is only required for low suspension frequency support that has a high static low dynamic stiffness whereas for high suspension frequency support that has a high static high dynamic stiffness the use of direct current signal isolator is unnecessary.

A study by Mizuno et.al (2007) showed how a mechanical spring connected in series to an active negative spring produces a suspension system with a very high suspension stiffness. The active negative spring for this system consists of a sensor, feedback controller and actuator as shown in Figure 5.13.

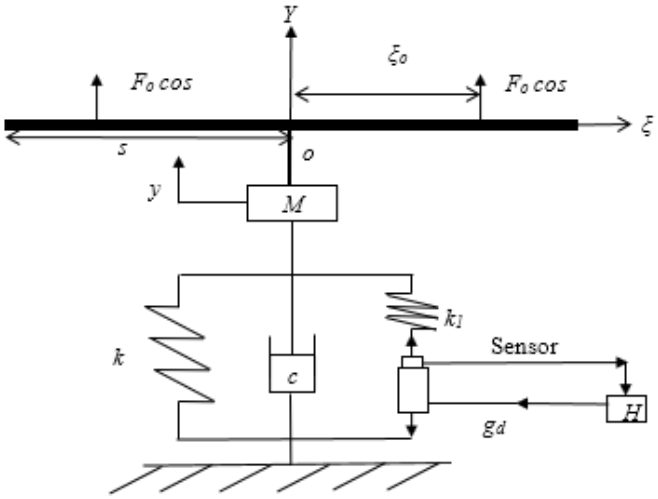

Figure 5.13 A suspension system with a high suspension stiffness (Xing et al., 2005)

5.4.2 Dynamic equilibrium equation of the active suspension system

The dynamic equilibrium equation of the active suspension system is

$$M(\ddot{y} + g) + c\dot{y} + k + \frac{k_1 g_d}{k_1 + g_d}(y - \delta) = f_{sb}, \tag{5.24}$$

Where k is a strong mechanical spring used to support part of the weight M, δ represents the static compression deformation of the supporting system, g is the acceleration of gravity and y denotes the upward dynamic displacement of the system from the static equilibrium position. Here, the forcef_{sb} denotes the reaction force from the beam to the lumped mass M.

5.4.3 Interaction analysis of beam-active isolator with high suspension frequency

The interaction analysis of beam- active isolator with high suspension frequency is similar to the interaction analysis with low suspension frequency except that the value of mass density per unit length ρ used is 0.01. Therefore, the added mass affected by a unit dynamic response mode shown in Table 5.8 and the added mass affected by retained mode number shown in Table 5.9 is different from those of the low suspension frequency. The added dynamic stiffness and force factor is the same as those for the low suspension frequency and is shown in Section 5.2.2.

Table 5.8 The values of added parameters affected by a unit dynamic response mode *n* of the beam on the active suspension unit

n	1	2	3	4	5
$m_b(\varphi_n)$	100	67.67	49.43	50.03	50.00

Table 5.9 The values of added parameters affected by retained mode number *N* of the beam on the active suspension unit

N	1	2	3	4	5
m_b	100	167.6685	217.0955	267.1206	317.1223

5.5 Controller design for beam-active isolator with high suspension frequency

5.5.1 Suitable negative feedback gains for a high suspension frequency

A suitably chosen feedback gain $g_d$satisfying the condition

$$g_d \leq -k_1 \tag{5.25}$$

provides a suspension system with a very high supporting stiffness and support frequency in Equation (5.26).

$$\Omega_n = \sqrt{\frac{k + \frac{k_1 g_d}{k_1 + g_d} + k_b(\varphi_n)}{M + m_b(\varphi_n)}} = \sqrt{\frac{k + \frac{k_1 |g_d|}{|g_d| - k_1} + k_b(\varphi_n)}{M + m_b(\varphi_n)}} \tag{5.26}$$

where

$k + \frac{k_1|g_d|}{|g_d|-k_1} + k_b(\varphi_n)$ is the dynamic stiffness

For the beam- active isolator with high suspension frequency, the frequency of the first mode (rigid mode) at $n = 1$ which is the supporting frequency is required to be as high as possible. The maximum value of dynamic stiffness is found using the 'fmincon' command in Matlab by minimizing the negative of the function. Using value of k_1 in the range of 2 to 1000 and g_d in

the range of -5000 to -1, the maximum value of dynamic stiffness at the first mode is found as shown in Table 5.10.

Table 5.10 Values of g_d and k_1 that produces a maximum dynamic stiffness at the rigid mode

k_1	g_d	Dynamic stiffness	Frequency
550.89	-550.89	1.625e+8	1.2684e+4

From Equation (5.25), introducing α, where

$$\begin{aligned} g_d &= -k_1 + \alpha \\ -k_1 + \alpha &\leq -k_1 \\ \alpha &\leq 0 \end{aligned} \tag{5.27}$$

Varying the value of α according to the range in Equation (5.27) and inserting it into the equation of suspension frequency (5.26) will give the graph in Figure 5.14. It can be seen that the lower the value of α, the higher the suspension frequency.

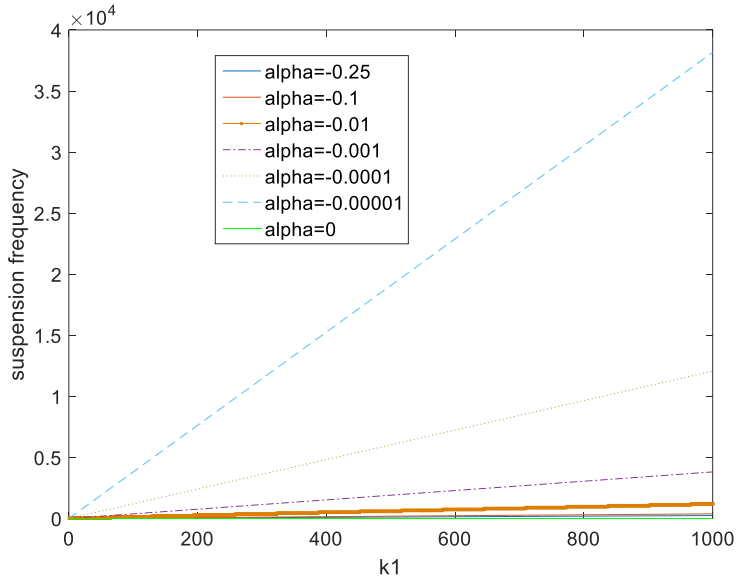

Figure 5.14 Effect of α on the suspension frequency using k=200 and k_1=0 to 1000

5.5.2 Applying active control

Based on the equation of motion of the active suspension unit and the equation of motion of the beam in Equations (5.24) and (5.1), the state space representation of the proposed suspension system is:

$$\begin{bmatrix}\dot{x}_1\\ \dot{x}_2\end{bmatrix}=\underbrace{\begin{bmatrix}0 & 1\\ -\dfrac{1}{M+m_b(\phi_n)}\left(k+\dfrac{k_1 g_d}{k_1+g_d}+k_b(\phi_n)\right) & -\dfrac{c}{M+m_b(\phi_n)}\end{bmatrix}}_{A}\begin{bmatrix}x_1\\ x_2\end{bmatrix}+$$

$$\underbrace{\begin{bmatrix}0\\ \dfrac{f_b}{M+m_b(\phi_n)}\end{bmatrix}}_{B}\left(F_0\cos\Omega_0 t+\frac{\left(k+\dfrac{k_1 g_d}{k_1+g_d}\right)\delta}{f_b}+\frac{Mg}{f_b}\right) \tag{5.28}$$

$$y=\underbrace{\begin{bmatrix}1 & 0\end{bmatrix}}_{C}\begin{bmatrix}x_1\\ x_2\end{bmatrix}+\underbrace{[0]}_{D}\left(F_0\cos\Omega_0 t+\frac{\left(k+\dfrac{k_1 g_d}{k_1+g_d}\right)\delta}{f_b}+\frac{Mg}{f_b}\right)$$

Inserting the values of matrices *A, B, C* and *D* from Equation (5.28) and values of k_1=550.89 and g_d = -560 into the Simulink block diagram as shown in Figure 5.15 and Matlab m-file, by giving an excitation signal with frequency Ω_0 = 0.05 as shown in Figure 5.16, we can observe the displacement of the mass *M* and beam ($M + m_b(\varphi_n)$) with a value of 0.1648 as shown in Figure 5.17. The value of $g_d$is chosen according to the range in Equation (5.25).

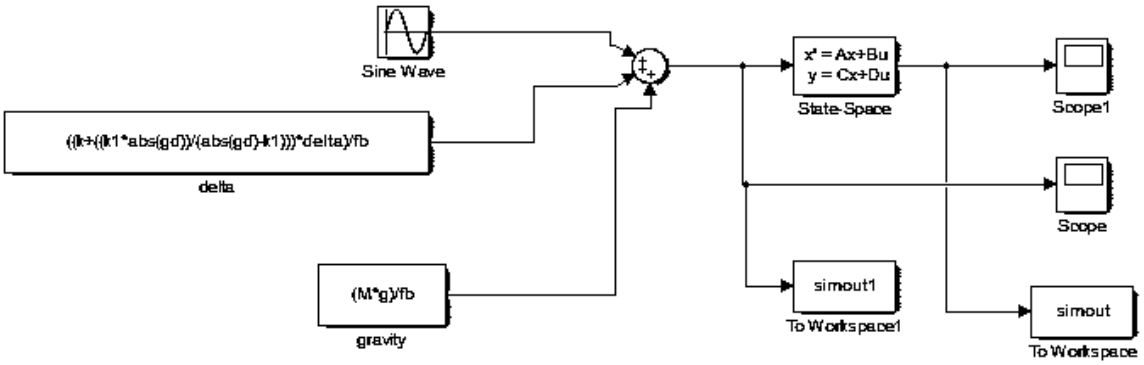

Figure 5.15 Simulink block diagram of the active suspension system

The effect of varying the value of displacement feedback gain, g_d can be seen in Figure 5.18. It is observed that the higher the feedback gain, the lower the displacement of ($M + m_b(\varphi_n)$). This shows the effect of the support system on to the beam.

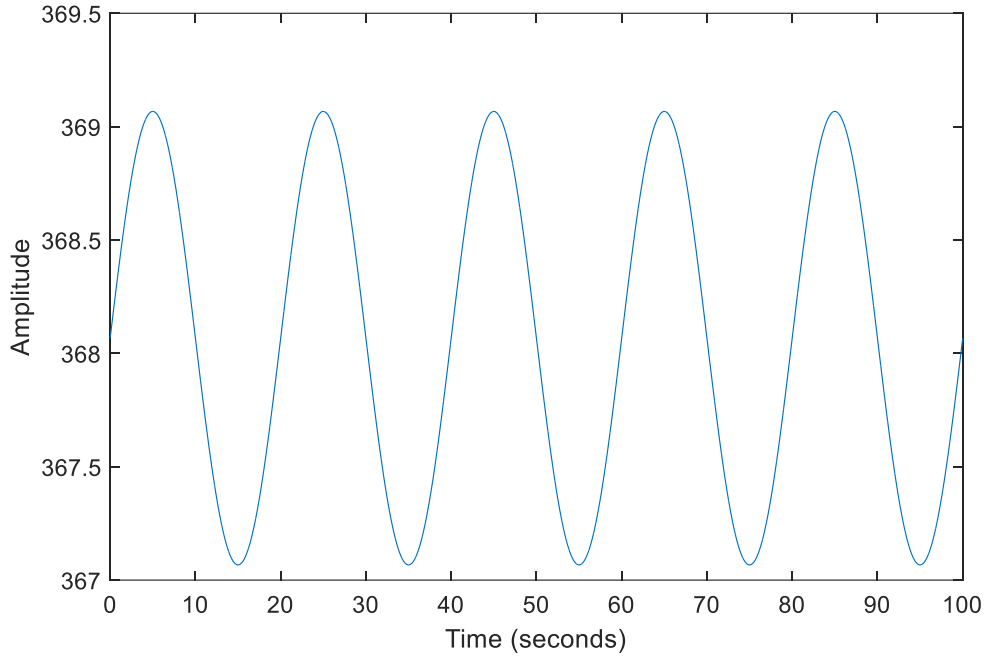

Figure 5.16 Excitation signal given to the system

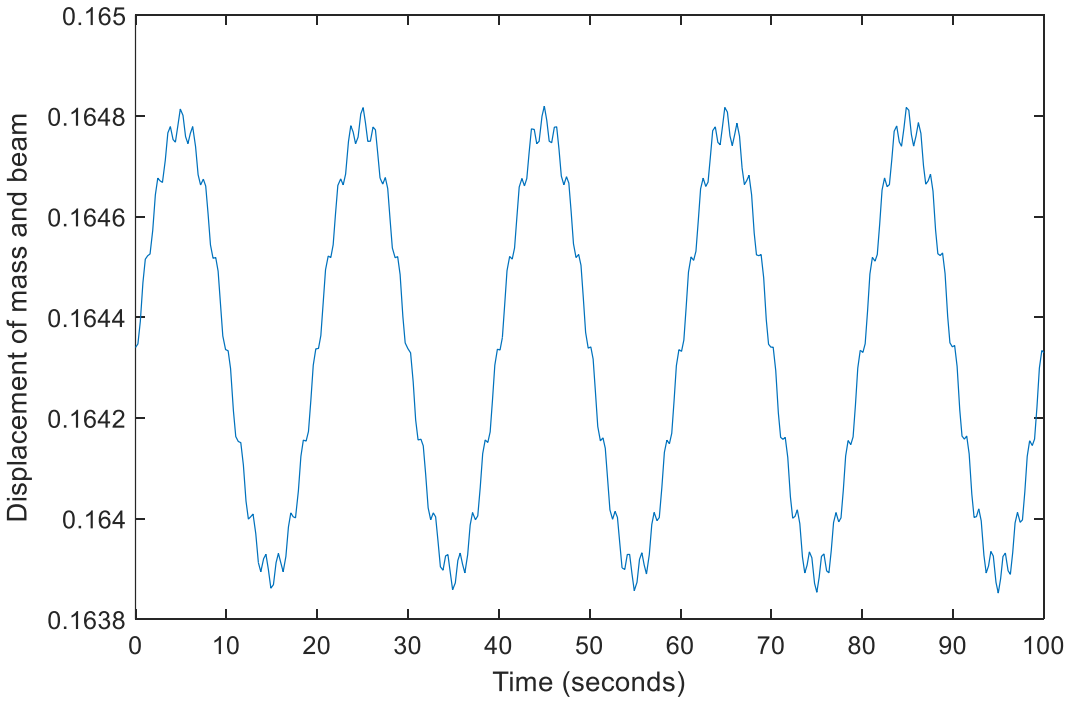

Figure 5.17 Displacement of mass and beam for high support frequency using g_d = -560

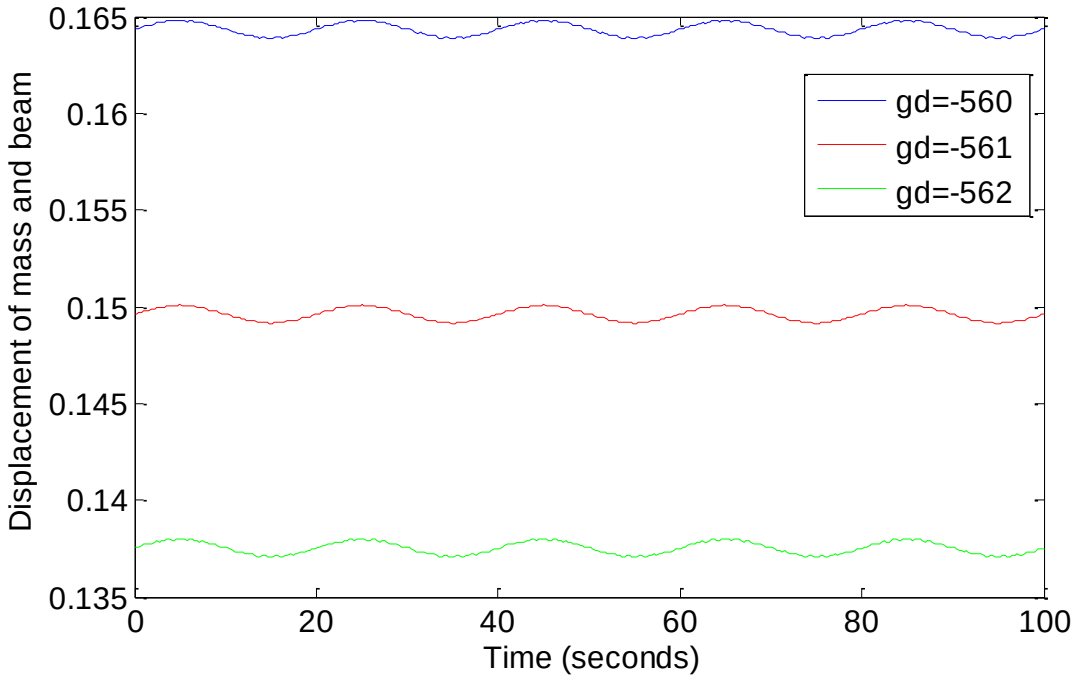

Figure 5.18 Displacement of mass and beam using different values of g_d

5.6 Summary

In this chapter, first, an analysis of the interaction between a beam and an active isolator with a low and a high suspension frequency has been studied. It was founded that the beam provides additional mass, stiffness and force to the active isolator. For the low suspension frequency design, first, suitable values of stiffness k_1 and negative feedback gain g_d that contribute to a low suspension frequency are found. Three cases for the beam-active isolator with low suspension frequency were studied; (i) when there is no support, no feedback control, (ii) when there is support but no feedback control, (iii) when there is support and with the presence of feedback control. Using the values of k_1=132.56 and g_d=-124.17, the suspension frequency at n=1 is 0.0377 which is less than one third of the first elastic natural frequency which has a value of 1. This satisfies the requirement to perform ground vibration test. For modes n= 2, 3, 4 and 5, the natural frequencies and mode shapes are very similar to the natural frequencies and mode shapes of the free free beam and the error between them have been found. Then, the displacement of the mass and beam was observed when different values of $g_d$was used . The effect of the supporting system to the structure is that as g_d increases, the displacement of mass and beam decreases. The analysis of the interaction between a beam and an active isolator with a high suspension frequency was then studied. By choosing a suitable value of g_d= -550.89 and k_1=550.89, the maximum dynamic stiffness at the rigid mode was

found which produces a suspension frequency of 1.625e8 which is very large. The dynamic response of the system was then studied. Using a displacement feedback gain g_d= -560, the displacement of mass and beam is found to be 0.1648. The displacement of the mass and beam using three different values of feedback gains are observed and it is found that the higher the value of feedback gain the lower the displacement of the mass and beam.

Chapter 6: Beam-active vibration isolator design for low and high suspension frequency

6.1 Introduction

In this chapter, a whole design of a beam -active vibration isolator is presented. First, a conceptual design of a beam- active isolator that allows adjustable supporting stiffness for low frequency and high frequency support is proposed. Then a detailed design including the electrical system equation is discussed. Following this, the design is then put into Simulink software using the Simscape software package to simulate for real application. From here, the dynamic response of the system is observed by looking at the effects of changing the negative feedback gains for both low frequency support and high frequency support.

6.2 Conceptual design of beam-active isolator for low and high frequency support

By referring to the work of Xing et al. (2005), the beam- active isolator for low frequency support shown in Figure 5.1 in Chapter 5 can also be used as a beam-active isolator with adjustable supporting stiffness that allows for both low frequency and high frequency support.

The dynamic equation of the system as shown in Equation (5.2) in Chapter 5 provides a dynamic supporting stiffness

$$\tilde{k} = \left(k + \frac{k_1 g_d}{k_1 + g_d} + k_b(\varphi_n) \right) \tag{6.1}$$

$$= \begin{cases} \text{for high stiffness,} & g_d \leq -k_1 \\ \text{for low stiffness,} & -\left(\frac{k_1 (k + k_b(\varphi_n)}{k_1 + k + k_b(\varphi_n)} \right) < g_d < 0 \end{cases}$$

The suspension frequency for a unit dynamic response is shown in Equation (5.18) in Chapter 5 which is

$$\Omega_n = \sqrt{\frac{k + \frac{k_1 g_d}{k_1 + g_d} + k_b(\varphi_n)}{M + m_b(\varphi_n)}} \tag{6.2}$$

6.3 Design of active isolation system

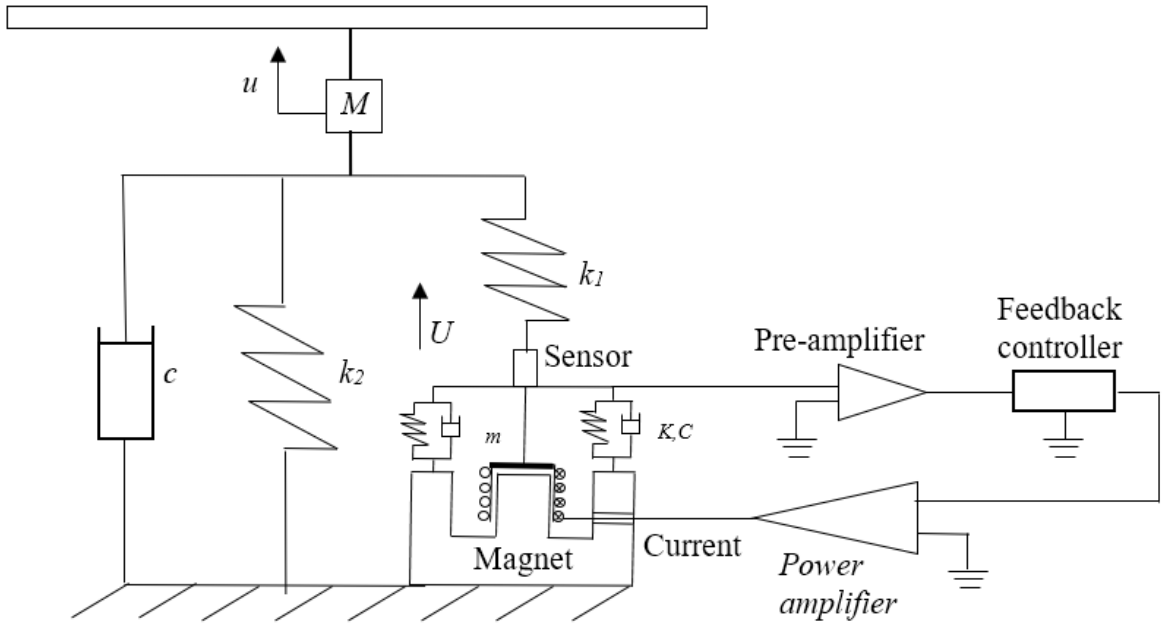

Figure 6.1 An active vibration isolation system including a mass-spring-damper unit modelling a practical actuator (Xing et al., 2005)

The conceptual design in Figure 5.1 in Chapter 5 is drawn in more detail in Figure 6.1 showing the mechanical and electrical parts of the active vibration isolation system to realise the theoretical work into real engineering applications so that experimental work can be done in the future. Here, M represents the mass of a structure where a beam is attached on top of it by a rigid rod, c is the supporting damping coefficient, k_2 is the stiffness of the spring supporting the static weight of the beam, k_1 is the stiffness of the spring connecting the structure and the moving coil of an electromagnetic actuator. The moving parts of the actuator and the sensor have a mass m that is supported by a spring K and a damper C to a magnet fixed on the base. Here, the spring K and the damper C may include other supporting stiffness and damping in parallel with the coil

supporting elements, which depends on different requirements of practical applications. The sensor detects the dynamic signals U of the moving coil and passes it through a pre –amplifier, a feedback gains control unit, and a power amplifier to produce a resultant control current supplied into the moving coil surrounded by the magnetic field to obtain the expected feedback force.

6.3.1 Electric system equation

An electrodynamic transducer can be used as an actuator for the active vibration isolation system. This actuator is constructed similar to loudspeakers whereby an electrical current is converted into a mechanical force. The actuator's voice coil is attached to a suspended aluminum support and test article attachment structure called the "armature". The actuator's armature is guided allowing it to easily move in the direction of the generated force and have the highest stiffness possible in all other directions. Actuators are primarily unidirectional vibration devices. It is essential for the suspension of the armature to be stiff in all transverse directions to minimize any lateral deflections caused by load attachment.

An electromagnetic actuator is also known as electrodynamic shaker and is a type of force generator. Electrical current flowing in the armature coil interacts with the strong DC magnetic field of the shaker's magnet structure (body) to produce physical force. This force can be taken as being generated between the armature coil and the shaker's body. Since the armature is free to move relative to the body in the direction of the force, both the shaker's armature (and its attached test article) and the shaker's body are subjected to the generated force. If the armature coil current is varied, as in alternating vibration excitation, both the armature and the shaker body will be accelerated in response to this force and will each respond according to their inherent mass, with vibratory motion, each independent of the other.

Force generated by the interaction of the armature coil is proportional to the current flowing in the coil and the strength of the magnetic field. Based on Lorentz force law, the generated force F can be found from the following equation (Wildi, 2006)

$$F = B\, l\, i \tag{6.3}$$

where B is flux density of the field [T], l is the active length of the conductor [m] and i is the current flowing in the conductor [A]. For simplification it is assumed that B has constant value due to the small change in coil position. Thus, the force generated by the actuator is proportional

to the current, i In the electric sub-system, an electric model as shown in Figure 6.2 can be used to derive the relation between current (i) and control voltage (u).

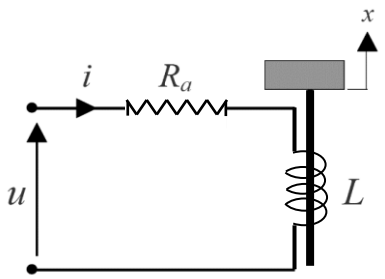

Figure 6.2 Equivalent diagram of the electric circuit of the electromagnetic actuator

By applying Kirchhoff's voltage law (KVL) to the electromagnetic actuator:

$$R_a i + L\frac{di}{dt} = u - \varepsilon_{emf} \tag{6.4}$$

$$\varepsilon_{emf} = i\frac{dL}{dx}\frac{dx}{dt} \tag{6.5}$$

where R_a, L, u are actuator resistance (Ω), actuator inductance (H), and voltage input (V) respectively. To linearize the model, some assumptions are made. First, the inductance impedance, L, is normally a lot smaller than resistance, R_a, thus it can be neglected. Second, dL/dx can also be neglected because the displacement, x of vibration is very small. Finally, from Equations (6.4) and (6.5) it can be found that the relation between voltage input and the generated force from the actuator is,

$$\left(\frac{B\ l}{R_a}\right) u = F \tag{6.6}$$

6.4 Active vibration isolation design in Simulink

To realize the system for real application, the design of active vibration isolation system in Figure 6.1 is built in Simulink using Simscape blocks as shown in Figure 6.4. By using Simscape blocks, a system model is built the same way a physical system is assembled. Simscape automatically constructs from the model, equations that characterize the system behaviour which is then integrated with the rest of the Simulink model (Esfandiari & Lu, 2014).

Figure 6.4 of the Simulink model is designed according to the real design of the active vibration isolator as shown in Figure 6.1. The sine wave block is inserted into the system which acts as the excitation signal. It is passed through a Simulink-PS converter block which converts a simulink signal to a physical sign. al. The Ideal Translational Motion Sensor 1 measures the displacement of the mass. The Translational Spring is the spring k_2, the Translational Damper is the damper $c$and the Translational Spring 1 is the spring k_1 . The Ideal Motion Sensor is the sensor between k_1 and the actuator and measures the displacement of the actuator's armature. This signal is passed to the PS Gain which is the Feedback Controller. From here, the signal is passed to the Generic Linear Actuator which is the actuator that provides the feedback force. The Pre-amplifier and Power amplifier are neglected because the signals in Simulink are suffiecient enough to run the actuator. The components in Simulink have an ideal characteristic thus no loss of power occurs.

6.4.1 Supporting system with low supporting frequency

Inserting value of k=1962, c=1000, k_1=132.565 and g_d=-124.17 (taken from Table 5.4 in Chapter 5) into the Simulink Simscape block diagram in Figure 6.4, the dynamic response of the rigid mode is found. The dynamic response found using Simulink Simscape is compared to the dynamic response found using the Simulink block diagram in Figure 5.11 in Chapter 5 and is plotted in Figure 6.3. This comparison is done to verify the result obtained from the simulation work using Simulink with the simulation done using Simscape blocks in Simulink by calculating the percent difference.

The equation used to find the percent difference is

$$\% \text{ Difference} = \frac{\text{Simscape result} - \text{Simulink result}}{\text{Simscape result}} \times 100 \tag{6.7}$$

From Figure 6.3, it can be seen that the graph of displacement of mass and beam for the first mode obtained using the Simscape block is similar to the the graph of displacement of mass and beam using Simulink. Using Simscape, the displacement of mass and beam is 6.455 x 10^{-4} . Using Simulink, the displacement of mass and beam is 6.162 x 10^{-4} . The percent difference between the displacement obtained using Simulink against the displacement obtained using Simscape is 4.539.

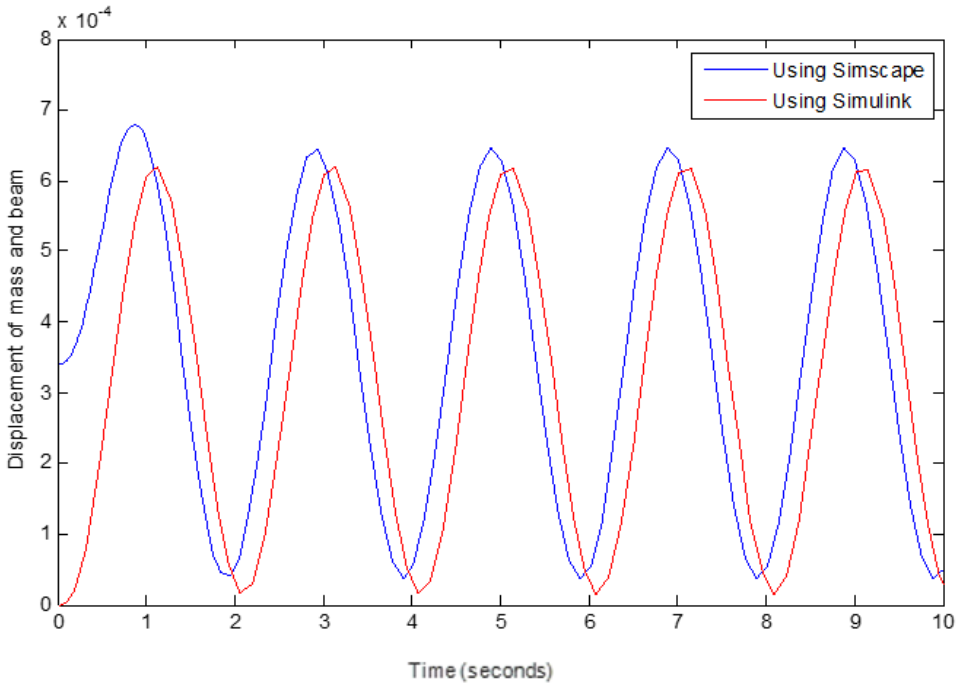

Figure 6.3 Displacement of $(M + m_b(\varphi_n))$ using Simulink and using Simscape

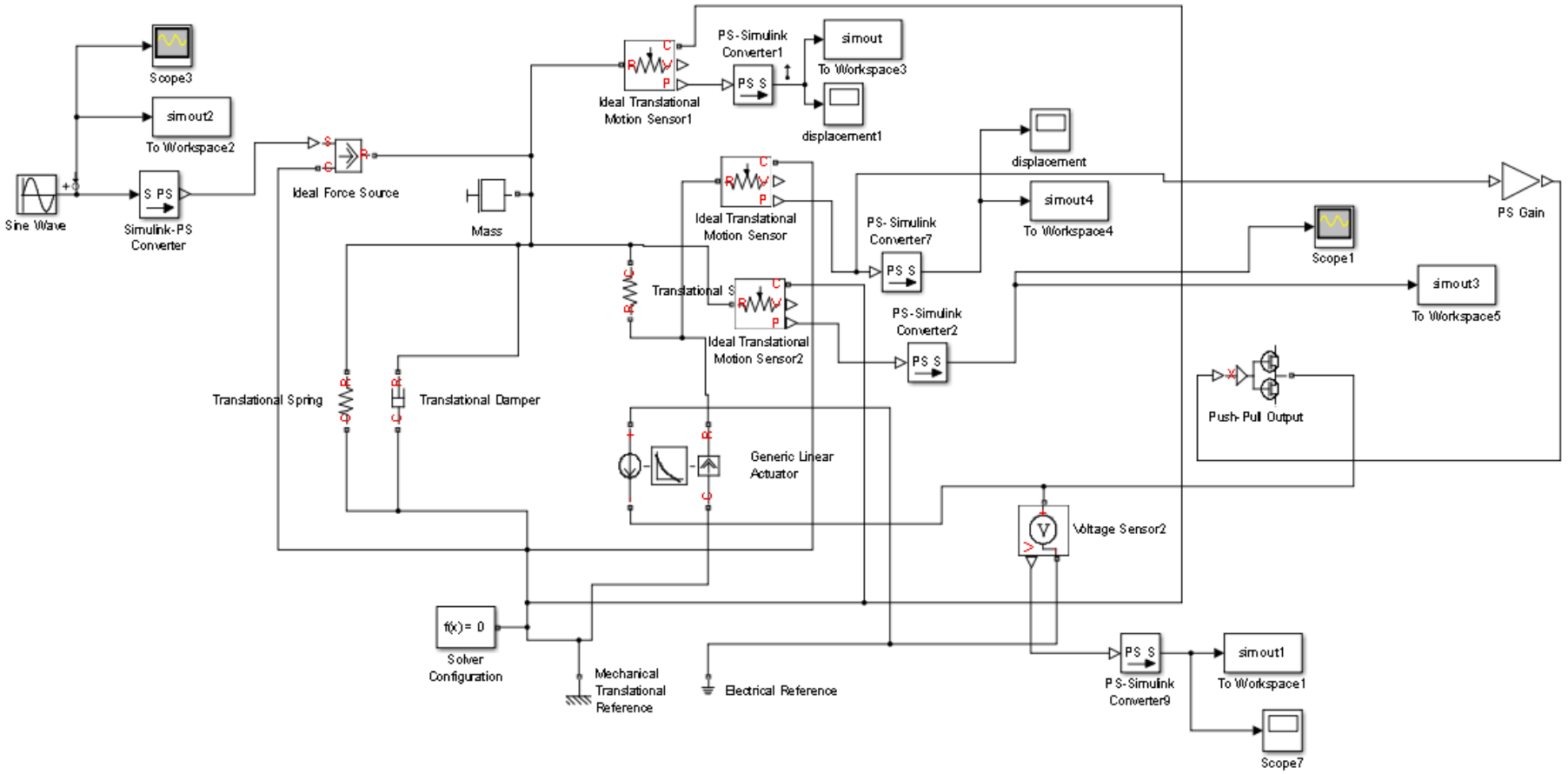

Figure 6.4 Design of active isolator in Simulink using the Simcape blockset for low suspension frequency

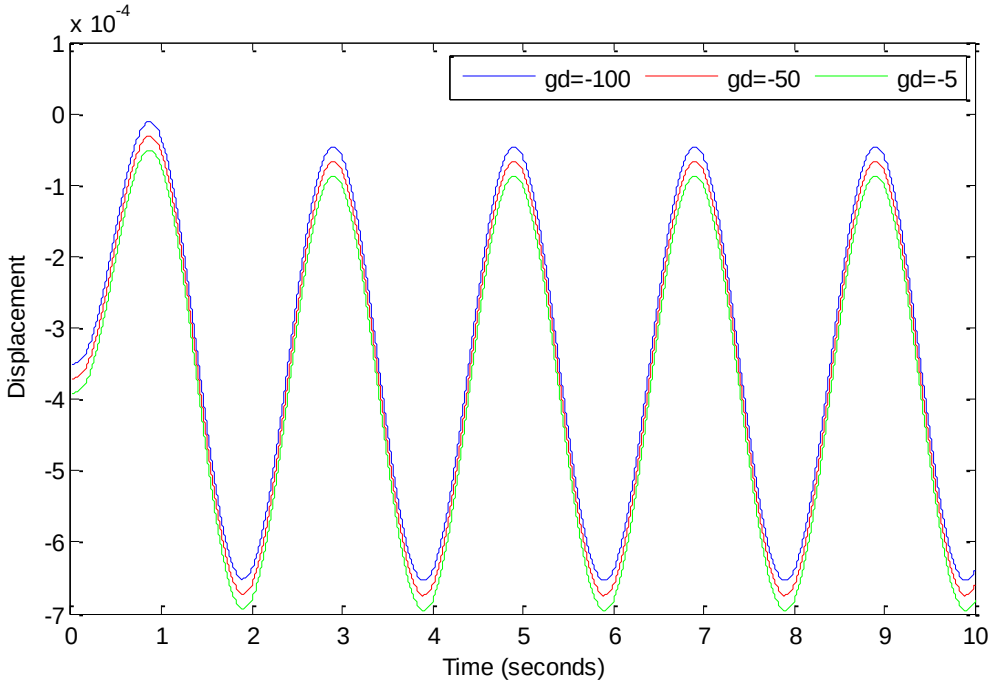

Figure 6.5 Displacement of mass and beam using different values of g_d

The negative feedback gain was varied to observe the displacement of the beam as shown in Figure 6.5. It can be seen that the higher the negative feedback gain, the smaller the displacement of mass and beam. This is the same as the result found from Section 5.3.2 in Chapter 5, whereby it has been found that the effect of the supporting system to the structure is that as the negative feedback gain, g_d increases, the displacement of mass and beam decreases.

6.4.2 Suspension system with high suspension frequency

The value of k_1 =550.89 and g_d=-560 that contributes to a high suspension frequency is inserted into the Simulink Simscape block in Figure 6.8 which is similar to Figure 6.4, except that there are some additional components (gravity and static compression deformation) added to the excitation signal. Figure 6.6 shows the dynamic response obtained using Simscape blok diagram that gives a value of 0.18814 and is compared with the dynamic response obtained using the Simulink block diagram (in Figure 5.15 in Chapter 5) that gives a value of 0.1648. The percent difference between the displacement found using Simulink Simscape simulation against the displacement found using Simulink alone is 12.41 . In Figure 6.7 , the feedback gain was varied to observe its effect on the displacement of mass and beam. It is found that as the feedback gain increases, the displacement of mass and beam decreases. This is the

same as the result in Section 5.5.2 in Chapter 5 where it has been found that the higher the feedback gain the lower the displacement of the mass and beam.

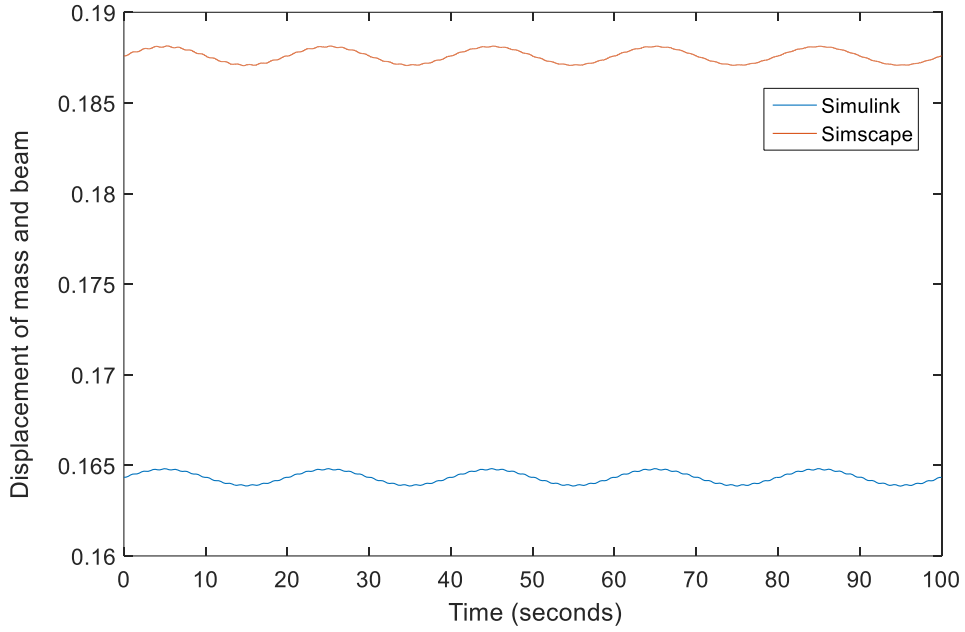

Figure 6.6 Dynamic response for high suspension frequency using Simscape and Simulink

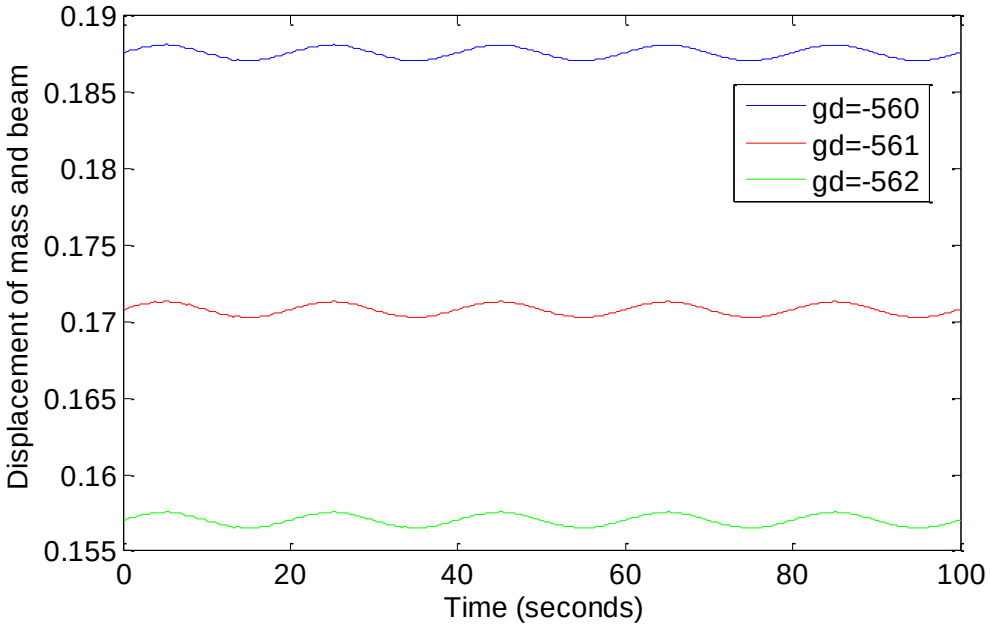

Figure 6.7 Dynamic response for high suspension frequency with varying g_d

6.5 Summary

In this chapter, a design of the beam- active isolator with a low and high suspension frequency has been studied. From the conceptual design, a real design of the isolator was put into Simulink using the Simscape blocks and the dynamic response of the low and high frequency support were found. For low frequency support, the dynamic response obtained using the Simulink Simscape block diagram is compared with the dynamic response obtained using Simulink simulation in Section 5.3.2 in Chapter 5. For the first mode, the percentage difference between the result found using Simscape against the result found using Simulink is 4.539. Furthermore, it has been found that the higher the value of negative feedback gain, the smaller the displacement of mass and beam. This is the same as the result found using Simulink in Figure 5.12 in Chapter 5 . For high frequency support, the dynamic response for the first mode using Simscape is compared with the dynamic response using Simulink and the percentage difference found is 12.41. It has been found that as the value of feedback gain increases, the displacement of mass and beam decreases. These results match the results obtained using Simulink in Figure 5.18 in Chapter 5, where it has been found that the effect of the supporting system to the structure is that as g_d increases the displacement of mass and beam decreases.

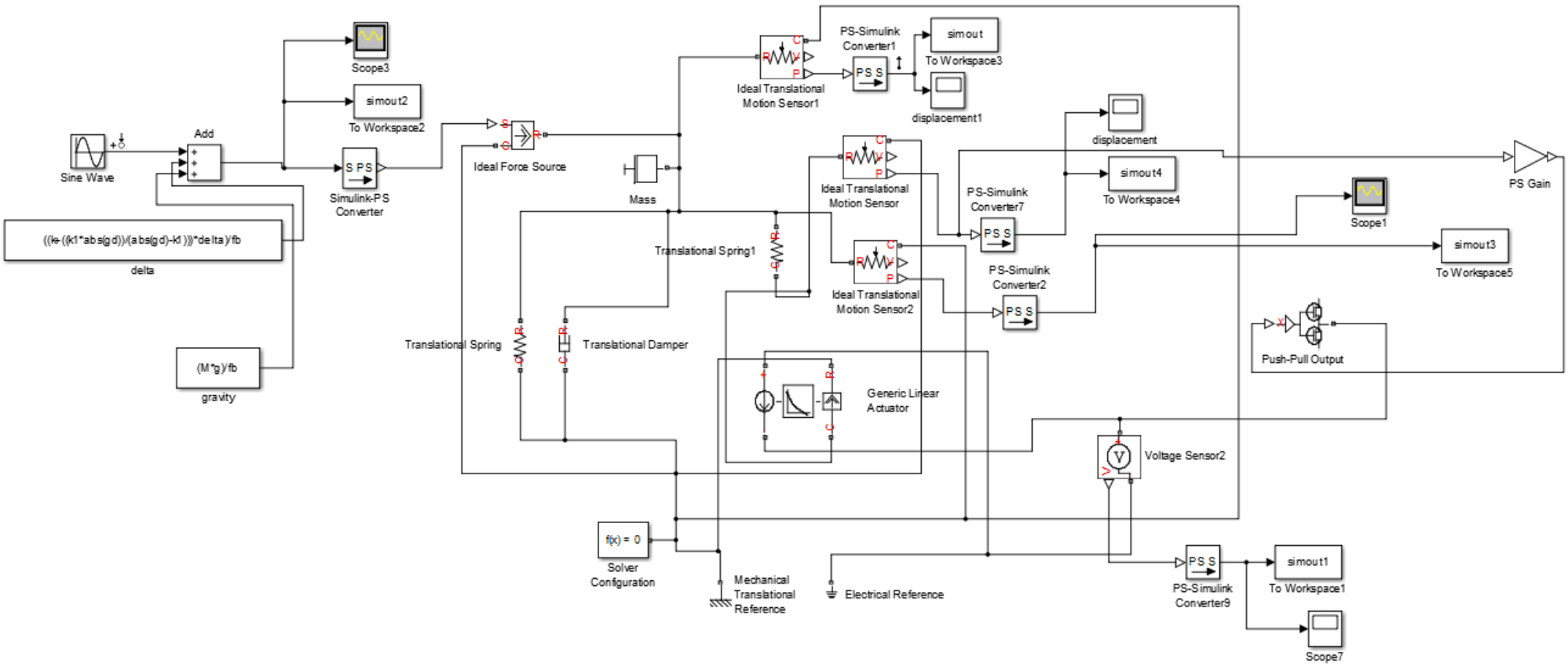

Figure 6.8 Design of active isolator in Simulink using the Simcape blockset for high suspension frequency

Chapter 7: Conclusion and recommendation

7.1 Conclusion

To achieve a particular low and high supporting stiffness of a system, it is necessary to use nonlinear isolator or active isolator. However, there exists an interaction between a structure and the isolator, therefore it is important to analyse this interaction so that accurate and improved performance of applying either nonlinear isolator or active isolator can be realised. In this thesis, the mathematical model of the integrated beam-nonlinear isolator and beam-active isolator were first established. Then, the equilibrium points were found and stabilities about the equilibrium points of the integrated nonlinear system and the dynamic response were analysed and possible nonlinear phenomena such as bifurcation and chaos were observed. A numerical study of the natural frequencies in small vibration of the system around the chosen equilibrium point was then performed and the interaction characteristics of the integrated nonlinear system was revealed. Performance analysis for the nonlinear isolator was done by observing the force transmissibility. For the beam-active isolator, a control system was designed using Simulink and the dynamic response for the beam -active isolator for low and high stiffness support were found. Finally, the beam-active isolator system that can provide a low and a high stiffness support has been designed and analysed using the Simulink Simscape blockset. In brief, the main results and conclusion of this study are stated below:

1. The interaction analysis of the beam-nonlinear isolator and beam-active isolator has shown that the beam provides additional mass, stiffness and force to the isolator. For the beam-nonlinear isolator, the added stiffness is seen to affect the vertical stiffness force only, and as the added stiffness increases, the vertical stiffness force also increases. The added stiffness has also been found to affect the potential energy, as the added stiffness increases, the potential energy also increases.

2. For the beam-nonlinear isolator with low stiffness support, the requirement to perform ground vibration test whereby the rigid mode of the beam must be less than one third of the first elastic natural frequency of the free-free beam has been satisfied. The frequency obtained at n=1 (rigid mode) of the beam supported on the nonlinear support is 6.7435e-7 which is less than one third of the first elastic natural frequency

(n=2) of the free-free beam which has a value of 1. The mode shapes of the beam on the nonlinear isolator is found to be similar to the mode shapes of the free - free beam. It has been found that the effect of the nonlinear isolator onto the beam is, the larger the value of stiffness k (the main element with nonlinear geometric characteristics that adjust the dynamic supporting stiffness), the smaller the frequency of the beam. Also, the larger the value of excitation frequency Ω_0 given to the system, the smaller the frequency of the beam. The dynamic response of the system was then observed, and the phase plots were found. Period doubling bifurcation is seen to occur when $F_0 = 1$ and Ω_0=0.5Hz. Poincare maps also showed that the system forms closed loop and no chaotic behaviour has been observed. For the beam-nonlinear isolator with high stiffness support, the natural frequencies of the beam and the mode shapes at modes 1 to 5 are compared with that of a fixed - free beam. At the first mode, a very high natural frequency of 3.0821e+3 has been obtained. Performance analysis in terms of force transmissbility of the nonlinear isolator reveals that the nonlinear isolator performs better than a linear isolator and also performs better than a hardening HSLDS mount.

3. For the beam- active isolator with low suspension frequency, when there is support, and feedback control is applied, the suspension frequency at mode n=1 (rigid mode) is 0.0377. This satisfies the requirement to perform ground vibration test, as mentioned in point number (2). The effect of supporting system to the structure is that as the value of negative feedback gain g_d increases, the displacement of the mass and beam decreases. For the beam- active isolator with high suspension frequency, the frequency of the first mode (rigid mode) at n=1 which is the supporting frequency is required to be as high as possible. The highest value of frequency is found to be 1.625e8 Hz when k_1 is 550.89 and g_d is -550.89. The effect of placing a spring in series with the active negative spring is that the higher the stiffness of the spring the higher the suspension stiffness of the system. The effect of feedback gain onto the frequency of the beam is that the higher the feedback gain, the lower the frequency of the beam.

4. A conceptual design of the beam-active isolator for low and high frequency support has been built using the Simscape blocks in Simulink. The dynamic response for low frequency support and high frequency support obtained using Simulink has been compared with the dynamic response found using Simscape. For low frequency support, the percentage difference between the result found using Simscape against the result found using Simulink for the first (rigid) mode is 4.539. It has also been found

that the higher the value of negative feedback gain, the smaller the displacement of mass and beam. For high frequency support, the percentage difference between the dynamic response found using Simscape and the dynamic response found using Simulink is 12.41. It has also been found that the displacement of mass and beam decreases with increasing feedback gain.

7.2 Recommendation

Recommendation for future work of this research are listed as follows:

1. **Setup the experiment according to the conceptual design of beam-active isolator to verify the simulation results obtained from this study**
   The simulation study of the beam-active isolator using Simulink and Simscape blockset have been discussed in this thesis. However, the experimental work has yet to be done. Therefore, to further verify the simulation results obtained, it is recommended that a physical experiment is to be conducted according to the conceptual design discussed in Chapter 6. The experimental setup would consist of the beam, a DC power supply, an exciter (which could be an electromagnetic shaker), accelerometers, an electromagnetic actuator, a pre-amplifier and power amplifier, a data acquisition hardware and a computer.

2. **Study the interaction between the active control system and the structure**
   In this thesis, for the beam- active isolator, the displacement of mass and beam depends only on the stiffness and damper of the system, the negative feedback gain and additional mass and stiffness added by the beam to the active isolator with omission of the effects of the actuator dynamics. The active isolator can also be called as an active control system is made up of sensors, an actuator, power amplifier, pre- amplifier and a controller. According to Xing et al. (2009), an active control system is a physical system that consists of several units involving various mechanical, electrical, magnetic or hydraulic physical processes, connected to a structure whereby the motion and characteristics of the structure are controlled by the control system and vice versa. The control efficiency is affected by the dynamic motion of the structure. This phenomenon describes a control–structure interaction (CSI). Therefore, to design an accurate beam-

active isolator, the interaction between the active control system and the beam (structure) must be considered.

3. **Extend the study of beam-nonlinear isolator interaction to plate-nonlinear isolator interaction and general structure- nonlinear isolator interaction**

   The numerical simulations for the interaction between beam and nonlinear isolator has been studied in this thesis using MATLAB sotware. For future research, this can be extended to numerical simulations for the interaction between a plate with 3 or 4 nonlinear passive isolators. From here, the work can then be extended to numerical simulations for the interaction between a general structure (e.g., an aircraft wing) and a nonlinear passive isolator which could be done using ANSYS software.

List of References

Abolfathi, A. (2012). *Nonlinear vibration isolators with asymmetric stiffness*. University of Southampton. Faculty of Engineering and the Environment, Doctoral Thesis, 237pp.

Ahn, H.-J. (2008). Performance limit of a passive vertical isolator using a negative stiffness mechanism. *Journal of Mechanical Science and Technology*, *22*, 2357–2364.

Alabuzhev, P., Gritchin, A., Kim, L., Migirenko, G., Chon, V., & Stepanov, V. (1989). *vibration protecting and measuring systems with quasi zero stiffness*. New York: Hemisphere Publishing.

Araki, Y., Asai, T., Kimura, K., Maezawa, K., & Masui, T. (2013). Nonlinear vibration isolator with adjustable restoring force. *Journal of Sound and Vibration*, *332*(23), 6063–6077. Retrieved from http://linkinghub.elsevier.com/retrieve/pii/S0022460X13005701

Bai, X.-X., Wereley, N. M., & Hu, W. (2015). Maximizing semi-active vibration isolation utilizing a magnetorheological damper with an inner bypass configuration. *Journal of Applied Physics*, *117*(17). Retrieved from http://scitation.aip.org/content/aip/journal/jap/117/17/10.1063/1.4908302

Cao, Q., Wiercigroch, M., Pavlovskaia, E. E., Grebogi, C., & T. Thompson, J. M. (2006). Archetypal oscillator for smooth and discontinuous dynamics. *Physical Review E*, *74*(4), 046218.

Cao, Q., Wiercigroch, M., Pavlovskaia, E. E., Grebogi, C., & Thompson, J. M. T. (2008a). The limit case response of the archetypal oscillator for smooth and discontinuous dynamics. *International Journal of Non-Linear Mechanics*, *43*(6), 462–473. Retrieved from http://www.sciencedirect.com/science/article/pii/S0020746208000176

Cao, Q., Wiercigroch, M., Pavlovskaia, E. E., Thompson, J. M. T., & Grebogi, C. (2008b). Piecewise linear approach to an archetypal oscillator for smooth and discontinuous dynamics. *Philosophical Transactions. Series A, Mathematical, Physical, and Engineering Sciences*, *366*(1865), 635–652. Retrieved from http://www.ncbi.nlm.nih.gov/pubmed/17698466

Carne, T. G., Griffith, D. T., & Casias, M. E. (2007). Support Conditions for Experimental Modal Analysis. *Sound and Vibration*, 11–15. Retrieved from http://www.sandv.com/downloads/0706carn.pdf

Carrella, a., Brennan, M. J., & Waters, T. P. (2007). Static analysis of a passive vibration isolator with quasi-zero-stiffness characteristic. *Journal of Sound and Vibration*, *301*(3–5), 678–689. Retrieved from http://linkinghub.elsevier.com/retrieve/pii/S0022460X06007954

Carrella, A., Brennan, M. J., Waters, T. P., & Shin, K. (2008). On the design of a high-static-low-dynamic stiffness isolator using linear mechanical springs and magnets. *Journal of Sound and Vibration*, *315*, 712–720.

Carrella, Alessandro. (2008). *Passive vibration isolators with high-static-low-dynamic-stiffness*.University of Southampton. Institute of Sound and Vibration Research, Doctoral Thesis, 226pp.

Chapra, S. C., & Canale, R. P. (2015). *Numerical Methods for Engineers* (Seventh). McGraw-Hill Education.

Chu, C.-L., Wu, B.-S., & Lin, Y.-H. (2006). Active vibration control of a flexible beam mounted on an elastic base. *Finite Elements in Analysis and Design*, *43*(1), 59–67. Retrieved from http://www.sciencedirect.com/science/article/pii/S0168874X06001144

Crede, C. E., & Ruzicka, J. . (1976). Theory of Vibration Isolation. In C.M. Harris (Ed.), *Shock and Vibration Handbook* (2nd editio). McGraw-Hill, Inc., New York,.

Cveticanin, L. (2014). *Strongly Nonlinear Oscillators: Analytical Solutions*. Springer.

El-Sinawi, A. H. (2004). Active vibration isolation of a flexible structure mounted on a vibrating elastic base. *Journal of Sound and Vibration*, *271*(1–2), 323–337. Retrieved from http://www.sciencedirect.com/science/article/pii/S0022460X03007715

Esfandiari, R. S., & Lu, B. (2014). *Modeling and analysis of dynamic systems* (Second). CRC Press.

Friswell, M. I., Flores, E. I. S., & Xia, Y. (2012). Vibration isolation using nonlinear springs. *ISMA2012-USD2012*, 2333–2342. Retrieved from http://michael.friswell.com/PDF_Files/C324.pdf

Fuller, C. R., Elliott, S. J., & Nelson, P. A. (1996). Active Control of Vibration. In *Active Control of Vibration*. Elsevier.

Funakubo. (1991). *Actuators for Control*. CRC Press.

Green, G. S. (1945). The effect of flexible ground supports on the pitching vibrations of an aircraf. *R&M*, *2291*.

Han, S. (1998). Analysis on the beam-exciter interaction in modal testing. *16th International Modal Analysis Conference*, 1656–1661. Retrieved from http://sem-proceedings.com/16i/sem.org-IMAC-XVI-16th-Int-164904-Analysis-Beam-exciter-Interaction-Modal-Testing.pdf

Hansen, C., Snyder, S., Qiu, X., Brooks, L., & Moreau, D. (2012). *Active Control of Noise and Vibration, Second Edition* (Vol. 2). CRC Press.

Hao, Z. (2016). *Research on Dynamics and Vibration Control based upon High-Performance Low- frequency Isolator*. Harbin Institute of Technology. School of Astronautics, Doctoral thesis, 134pp.

Hao, Z., & Cao, Q. (2014). A novel dynamical model for GVT nonlinear supporting system with stable-quasi-zero-stiffness. *Journal of Theoretical and Applied Mechanics*, *52*(1), 199–213.

Harris, Cyril M, & Crede, C. E. (1976). Shock and vibration handbook. In *McGraw-Hill handbooks*.

Hartog, J. P. Den. (1985). *Mechanical Vibrations*. Courier Dover Publications.

Heiland, K. P. (1992). Recent advancements in passive and active vibration control systems. *Proceedings of SPIE - The International Society for Optical Engineering*, *1619*, 22–33. Retrieved from http://www.scopus.com/inward/record.url?eid=2-s2.0-0026743868&partnerID=tZOtx3y1

Hilborn, R. C. (2000). *Chaos and Nonlinear Dynamics: An Introduction for Scientists and Engineers* (Second). OUP Oxford.

Ho, C., Lang, Z., & Billings, S. A. (2012). The benefits of nonlinear cubic viscous damping on the force transmissibility of a Duffing-type vibration isolator. *UKACC International Conference on Control 2012*, 479–484.

Holterman, J. (2002). *Vibration Control of High-precision Machines with Active Structural Elements*. Enschede (The Netherlands): Twente University Press (TUP).

Hosseinloo, A. H. (2011). A new passive vibration isolator design for random base excitations in zero and non-zero G-loading situations. *2011 Defense Science Research Conference and Expo (DSR)*, 1–4. Retrieved from http://ieeexplore.ieee.org/lpdocs/epic03/wrapper.htm?arnumber=6026843

Huang, X., Liu, X., & Hua, H. (2014). On the characteristics of an ultra-low frequency nonlinear isolator using sliding beam as negative stiffness. *Journal of Mechanical Science and Technology*, *28*(3), 813–822. Retrieved from http://link.springer.com/10.1007/s12206-013-1205-5

Huang, X., Liu, X., Sun, J., Zhang, Z., & Hua, H. (2014). Vibration isolation characteristics of a nonlinear isolator using Euler buckled beam as negative stiffness corrector: A theoretical and experimental study. *Journal of Sound and Vibration*, *333*(4), 1132–1148. Retrieved from http://www.sciencedirect.com/science/article/pii/S0022460X13008997

Ibrahim, R. A. (2008). Recent advances in nonlinear passive vibration isolators. *Journal of Sound and Vibration*, *314*(3–5), 371–452. Retrieved from http://www.sciencedirect.com/science/article/pii/S0022460X08000436?via%3Dihub

Inman, D. J. (2007). *Engineering Vibration* (Third). Prentice Hall.

Kletz, B. T., & Melcher, J. (2013). Simultaneous supply of infinite and infinitesimal stiffness of active isolation systems that are exposed to multiple vibration sources. In H. Sodano (Ed.), *SPIE Smart Structures and Materials + Nondestructive Evaluation and Health Monitoring*. Retrieved from http://proceedings.spiedigitallibrary.org/proceeding.aspx?articleid=1675190&resultClick=1

Kovacic, I., Brennan, M. J., & Waters, T. P. (2008). A study of a nonlinear vibration isolator with a quasi-zero stiffness characteristic. *Journal of Sound and Vibration*, *315*(3), 700–711. Retrieved from http://linkinghub.elsevier.com/retrieve/pii/S0022460X07009960

Lee, J., & Clark, W. W. (1999). Semi-Active Control of Flexural Vibrations with an MR Fluid Actuator. In T. T. Hyde (Ed.), *1999 Symposium on Smart Structures and Materials* (pp. 167–174). Retrieved from http://proceedings.spiedigitallibrary.org/proceeding.aspx?articleid=982748

Liu, J., Li, Y., Zhang, Y., Gao, Q., & Zuo, B. (2014). Dynamics and control of a parallel mechanism for active vibration isolation in space station. *Nonlinear Dynamics*, *76*(3), 1737–1751. Retrieved from http://link.springer.com/10.1007/s11071-014-1242-3

Liu Yan-bin, Yu-shu, C., & Qing-jie, C. (2012). Bifurcations of resonance in an irrational system. *Vibration and Shock*, *31*, 151–154. Retrieved from http://en.cnki.com.cn/Article_en/CJFDTOTAL-ZDCJ201202031.htm

Lu, Z., Brennan, M. J., Yang, T., Li, X., & Liu, Z. (2013). An investigation of a two-stage nonlinear vibration isolation system. *Journal of Sound and Vibration*, *332*(6), 1456–1464. Retrieved from http://www.sciencedirect.com/science/article/pii/S0022460X12009133

Meirovitch, L. (1975). *Elements of vibration analysis.* Mc-Graw Hill

Mizuno, T., Takasaki, M., Kishita, D., & Hirakawa, K. (2007). Vibration isolation system combining zero-power magnetic suspension with springs. *Control Engineering Practice*, *15*(2), 187–196. Retrieved from http://www.sciencedirect.com/science/article/pii/S0967066106001183

Moheimani, S. O. R., & Fleming, A. J. (2006). *Piezoelectric Transducers for Vibration Control and Damping*. Springer Science & Business Media.

Molyneux, W. G. (1958). The Support of an Aircraft for Ground Resonance Tests. *Aircraft Engineering and Aerospace Technology*, *30*(6), 160–166.

Nayfeh, A. H., & Balachandran, B. (1995). *Applied nonlinear dynamics : analytical, computational, and experimental methods*. Wiley.

Nayfeh, A. H., & Mook, D. T. (2004). *Nonlinear Oscillations*. WILEY-VCH Verlag GinbH & Co. KGaA, Weinheiin.

Peng, Z. K., Lang, Z. Q., Jing, X. J., Billings, S. A., Tomlinson, G. R., & Guo, L. Z. (2008). The transmissibility of vibration isolators with a nonlinear anti-symmetric damping characteristic. *Journal of Vibration and Acoustics*, *132*(1), 014501-014501–014507. Retrieved from http://eprints.whiterose.ac.uk/74641/1/985.pdf

Platus, D. L. (1992). Negative-stiffness-mechanism vibration isolation systems. *Proc. SPIE 3786, Optomechanical Engineering and Vibration Control*.

Preumont, A., & Seto, K. (2008). *Active Control of Structures* (First). Wiley-Blackwell.

Rao, S. S. (2011). Mechanical Vibrations. In *Prentice Hall* (Fifth). Prentice Hall.

Ravindra, B., & Mallik, A. K. (1995). Chaotic response of a harmonically excited mass on an isolator with non-linear stiffness and damping characteristics. *Journal of Sound and Vibration*, *182*(3), 345–353. Retrieved from http://www.sciencedirect.com/science/article/pii/S0022460X85702039

Rivin, E. (2003). Passive Vibration Isolation. In *ASME Press*.

Robertson, W. S., Kidner, M. R. F., Cazzolato, B. S., & Zander, A. C. (2009). Theoretical design parameters for a quasi-zero stiffness magnetic spring for vibration isolation. *Journal of Sound and Vibration*, *326*(1–2), 88–103. Retrieved from http://www.sciencedirect.com/science/article/pii/S0022460X09003423

Seon Mi Han, & Haym Benaroya. (2002). *Nonlinear and Stochastic Dynamics of Compliant Offshore Structures*. Springer Netherlands.

Silva, C. W. de. (2006). *Vibration: Fundamentals and Practice, Second Edition* (second). CRC Press.

Strogatz, S. H. (1994). Nonlinear Dynamics and Chaos with Applications to Physics, Biology, Chemistry, and Engineering. In *Book* (1st edition, pp. 1–505). Westview Press.

Tang, B., Zhou, L., Xiong, Z., Wang, J., & Zhan, M. (2014). A programmable broadband low frequency active vibration isolation system for atom interferometry. *The Review of Scientific Instruments*, *85*(9). Retrieved from http://scitation.aip.org/content/aip/journal/rsi/85/9/10.1063/1.4895911

Thomson, W. (1996). *Theory of Vibration with Applications*. CRC Press.

Tjepkema, D., van Dijk, J., & Soemers, H. M. J. R. (2012). Sensor fusion for active vibration isolation in precision equipment. *Journal of Sound and Vibration*, *331*(4), 735–749. Retrieved from http://www.sciencedirect.com/science/article/pii/S0022460X11007656

Tsuji, Y., Sasaki, T., Waters, T. P., Fujito, K., & Wang, D. (2014). A nonlinear vibration isolator based on a post-buckled inverted L-shaped beam. *6th World Conference on Structural Control and Monitoring (WCSCM)*. Retrieved from http://eprints.soton.ac.uk/368076/

Unsal, M. (2006). *Semi-active vibration control of a parallel platform mechanism using magnetorheological damping*. University of Florida. Doctoral dissertation. 197pp. Retrieved from http://cimar.mae.ufl.edu/CIMAR/pages/thesis/unsal_m.pdf

Varoto, P. S., Oliveira, D., & L P R. (2001). On the interaction between the vibration exciter and the structure under test in vibration testing. *Of SPIE the International Society For*, *1*, 640–647. Retrieved from http://www.scopus.com/inward/record.url?eid=2-s2.0-0035049976&partnerID=40&md5=1908c9dccc86fad7bc7f63fbb963c69b

Wagg, D., & Nield, S. (2010). *Nonlinear Vibration with Control*. Springer.

Wang, B., Yan, J., & Cheng, G. (2011). Optimal structure design with low thermal directional expansion and high stiffness. *Engineering Optimization*, *43*(6), 581–595. Retrieved from http://www.tandfonline.com/doi/abs/10.1080/0305215X.2010.499941

Wang, H., Xing, J. T., Price, W. G., & Li, W. (2008). An investigation of an active landing gear system to reduce aircraft vibrations caused by landing impacts and runway excitations. *Journal of Sound and Vibration*, *317*(1–2), 50–66. Retrieved from http://linkinghub.elsevier.com/retrieve/pii/S0022460X08002563

Wildi, T. (2006). *Electrical machines, drives, and power systems*. Pearson Prentice Hall.

Winterflood, J. (2001). *High performance vibration isolation for gravitational wave detection*. University of Western Australia. Department of Physics, Doctoral thesis, 286pp.

Winterflood, J., Blair, D. ., & Slagmolen, B. (2002). High performance vibration isolation using springs in Euler column buckling mode. *Physics Letters A*, *300*(2–3), 122–130. Retrieved from http://www.sciencedirect.com/science/article/pii/S037596010200258X

Xing, J.-T., & Price, W. G. (1991). A mixed finite element method for the dynamic analysis of coupled fluid-solid interaction problems. *Proceedings of the Royal Society: Mathematical and Physical Science*.

Xing, J. T., Xiong, Y. P., & Price, W. G. (2009). A generalised mathematical model and analysis for integrated multi-channel vibration structure-control interaction systems. *Journal of Sound and Vibration*, *320*(3), 584–616.

Xing, J.T., Xiong, Y. P., & Price, W. G. (2005). Passive–active vibration isolation systems to produce zero or infinite dynamic modulus: theoretical and conceptual design strategies. *Journal of Sound and Vibration*, *286*(3), 615–636. Retrieved from

http://linkinghub.elsevier.com/retrieve/pii/S0022460X04008405

Xing, Jing Tang. (1975). Theory and techniques on mode vibration experiments of aircraft structures. In *Theory and techniques on mode vibration experiments of aircraft structures*. NAI press.

Xing, Jing Tang. (2013). *Integrated interaction analysis of a generalised nonlinear suspension system and supporting beam structures*. Unpublished Manuscript.

Xing, Jing Tang. (2015). *Energy Flow Theory of Nonlinear Dynamical Systems with Applications*. Springer International Publishing Switzerland.

Xiong, Y. P., Xing, J. T., & Price, W. G. (2005). Interactive power flow characteristics of an integrated equipment—nonlinear isolator—travelling flexible ship excited by sea waves. *Journal of Sound and Vibration*, *287*(1–2), 245–276.

Xu, D., Zhang, Y., Zhou, J., & Lou, J. (2013). On the analytical and experimental assessment of the performance of a quasi-zero-stiffness isolator. *Journal of Vibration and Control*, *20*(15), 2314–2325. Retrieved from http://jvc.sagepub.com/content/20/15/2314

Yang, C., Yuan, X., Wu, J., & Yang, B. (2012). The research of passive vibration isolation system with broad frequency field. *Journal of Vibration and Control*, *19*(9), 1348–1356. Retrieved from http://jvc.sagepub.com/content/19/9/1348.short

Yang, J., Xiong, Y. P., & Xing, J. T. (2013). Dynamics and power flow behaviour of a nonlinear vibration isolation system with a negative stiffness mechanism. *Journal of Sound and Vibration*, *332*(1), 167–183. Retrieved from http://linkinghub.elsevier.com/retrieve/pii/S0022460X12006311

Yilmaz, C., & Kikuchi, N. (2006). Analysis and design of passive band-stop filter-type vibration isolators for low-frequency applications. *Journal of Sound and Vibration*, *291*(3–5), 1004–1028. Retrieved from http://linkinghub.elsevier.com/retrieve/pii/S0022460X05004797

Yu, L., Rao, C., & Du, L. (2009). An active control method for vibration isolation of precision equipments. *2009 ISECS International Colloquium on Computing, Communication, Control, and Management*, *3*, 368–371. Retrieved from http://ieeexplore.ieee.org/lpdocs/epic03/wrapper.htm?arnumber=5267916

Yu, X., Zhu, S.-J., & Liu, S.-Y. (2008). Bifurcation and chaos in multi-degree-of-freedom nonlinear vibration isolation system. *Chaos, Solitons & Fractals*, *38*(5), 1498–1504. Retrieved from http://www.sciencedirect.com/science/article/pii/S0960077907002755

Zhang, H., Kou, B., Jin, Y., & Zhang, H. (2015). A new implementation method of low stiffness for magnetic levitation gravity compensator. *2015 IEEE Magnetics Conference (INTERMAG)*, 1–1. Retrieved from http://ieeexplore.ieee.org/document/7156895/

Zhang, J. Z., Li, D., Chen, M. J., & Dong, S. (2004). An Ultra-Low Frequency Parallel Connection Nonlinear Isolator for Precision Instruments. *Key Engineering Materials*, *257–258*, 231–238.

Papers and conferences

Turahim, K. K., Djidjeli, K., & Xing, J. T. (2016). An investigation on the effect of active vibration isolator on to a structure for low stiffness support. At 23*rd International Congress on Sound and Vibration (ICSV* 23*), Greece*. 10 - 14 *Jul* 2016*.* 7 pp.

Turahim, K. K., Djidjeli, K., & Xing, J. T. (2017). An investigation on the interaction analysis of beam- active isolator with low suspension frequency. At 12*th ICBEN congress on Noise as a Public Health Problem, Switzerland*. 18 - 22 *June* 2017*.* 10 pp.

Xing, J. T., Xiong, Y. P., Djidjeli, K., & Turahim, K. K. (2017). A Generalised Nonlinear Isolator-Elastic Beam Interaction Analysis for Extremely Low or High Supporting Frequency. At 9*th European Nonlinear Dynamics Conference (ENOC* 2017*), Hungary*. 25 - 30 *June* 2017*.* 10 pp.

Turahim, K. K., Djidjeli, K., & Xing, J. T. (2019) An investigation on the interaction analysis of beam- nonlinear isolator with low and high stiffness support, *Journal of Engineering and Technology*, 10(2), 1-25.